Development and Characterization of Microwave Processed Cavitation Erosion Resistant Cladding

A Thesis submitted in the fulfilment of the requirements for the degree of

Doctor of Philosophy
in
Mechanical Engineering

Submitted by

Sandeep Bansal

Registration No.: 901708016

Under the Supervision of

Dr. Dheeraj Gupta
Professor
MED,TIET, Patiala

Dr. Vivek Jain
Associate Professor
MED, TIET, Patiala

THAPAR INSTITUTE
OF ENGINEERING & TECHNOLOGY
(Deemed to be University)

DEPARTMENT OF MECHANICAL ENGINEERING
THAPAR INSTITUTE OF ENGINEERING &TECHNOLOGY,
PATIALA-147004, INDIA

September, 2022

Dedicated to The Lord, My Beloved Family, Respected Teachers, and God-gifted Friends……

CONTENTS

Declaration

I hereby declare that the thesis entitled "**Development and Characterization of Microwave Processed Cavitation Erosion Resistant Cladding**" submitted to the **Department of Mechanical Engineering** at **Thapar Institute of Engineering & Technology, Patiala** for the award of the degree of **Doctor of Philosophy in Mechanical Engineering** is a record of original bonafide research work carried out by me under the supervision of **Dr. Dheeraj Gupta and Dr. Vivek Jain.** All the requirements for the submission of this thesis have been fulfilled as per institute norms. No part of the matter embodied in this report has been submitted to any other university or institute for the award of any degree.

Bansal

Sandeep Bansal

Date: 08-09-2022

It is certified that the above statement made by the student is correct to the best of our knowledge and belief.

08/9/2022

Dr. Dheeraj Gupta
Professor
Mechanical Engineering Department
TIET, Patiala-147004, India
dheeraj.gupta@thapar.edu

08/09/2022

Dr. Vivek Jain
Associate Professor
Mechanical Engineering Department
TIET, Patiala-147004, India
vivek.jain@thapar.edu

Acknowledgement

I take this opportunity to express special appreciation and gratitude to my thesis supervisors, **Dr. Dheeraj Gupta** and **Dr. Vivek Jain**, for their continuous support (both technical and moral), motivation, knowledge and belief in me during the course of my Ph.D. work. I am thankful for the positive suggestions and meticulous guidance that helped me to improve my scientific writing and carry out the new research. I feel motivated and honoured to work under their supervision throughout my entire Ph.D. thesis.

I gratefully acknowledge the funding for this work through the **Science & Engineering Research Board (SERB), India**, under the project titled "**Development of Microwave Processed Cavitation Erosion Resistant Cladding**" File no.: EMR/2016/007964.

I wholeheartedly thank the doctoral committee members **Dr. T. K. Bera** (Chairman, Board of Studies), **Dr. Somendru Jana, Dr. Anant Kumar Singh, Dr. Satish Kumar Sharma, Dr. Dheeraj Gupta and Dr. Vivek Jain** for the feedback and reviews that were given on my research proposal and progress monitoring presentations. Their guidance was beneficial for me to improve my research work. I am also thankful to **Dr. Tarun Nanda** and **Dr. Anu Mittal**, our Ph.D. coordinators, for their approachability and keeping me informed with all the relevant communication throughout E-mails.

A special thanks to the office of the Mechanical Engineering Department for providing all the facilities required for research work. Thanks to all my lab mates, seniors, and friends for their support and a very special and sincere thanks to Dr. Sarbjit Kaushal, Mr. Rajat Kumar, Mr. Jonty Mago, Mr. Pushpinder Kumar, Mr. Rahul Gupta, Mrs. Anuradha, Mr. Deepak Sharma, Mr. Kunal Arora and Mr. Khalid Bashir, who had helped me a lot during my research work.

A huge thanks go to the whole family, who always encouraged me and stood by me. I thank all my family and relatives who had supported and cared for me during my research work. I am grateful to all those who have helped me directly or indirectly in this journey of my life.

Finally, I bow and thank the **Almighty, Mata Naina Devi Ji and Bihari Ji**, without whom I could not have completed this journey of completing my research work for the highest degree in the engineering discipline

Sandeep Bansal

Abstract

Hydroelectric power plants are experiencing huge revenue losses due to the failure of various components caused by cavitation erosion wear. The turbine is the primary components of any hydroelectric power plant and it fails catastrophically due to severe damage caused by cavitation erosion wear. The some of the well-established/ ongoing developments in the advanced surface engineering techniques have provided an effective solution to enhance the cavitation erosion resistance for the cavitation prone components. However, the improvement in wear resistance of the functional surfaces through coating/cladding with suitable overlaying material would be one of the most straightforward and economical solution. The conventional coating/cladding processes have many drawbacks such as excessive substrate deformation, high porosity, lower deposition efficiency, weak adhesion strength, poor fracture toughness, higher costs, and production of toxic gasses. Therefore, the coating/cladding by a novel method, that can overcome the drawbacks of existing methods, is needed. Microwave cladding process has the potential to overcome the maximum limitations of the conventional surface processing techniques.

Hence, in the present study, the microwave processed composite clads of Ni-based (EWAC) as matrix material with variable weight percentage of reinforcements such as Cr_3C_2, WC10Co2Ni and Al_2O_3 on SS-316 substrate were developed. For this purpose, a domestic microwave oven with 2.45 GHz frequency and variable power from 180 W to 900 W was used. The charcoal powder was used as susceptor material. The percentage of reinforcements were varied from 0-30% (by wt%) for Cr_3C_2 and WC10Co2Ni with an increase of 10% step; and 0-15% (by wt%) for $Al_2O_3$with an increase of 5% step. The cladding process parameters such as microwave power and exposure time influences the quality of clads. Therefore, prior to the development of the clads the parameters for defect free and good metallurgical bonded clads were optimized.

The prepared clads were examined for microstructure, phase quality and quantity, porosity, microhardness, flexural strength (bonding strength) and cavitation erosion resistance at different parametric conditions. The probe sonicator-vibratory ultrasonic apparatus was used for indirect acoustic cavitation erosion testing.

The optimization of process parameters revealed that an increase in power level significantly decreases the required processing time. The minimum exposure microwave power 900 W is required to melt the powder material system and partial amount of substrate material to cause the dilution for development of metallurgical bonded clads. The processing time required for the metallurgical bonded clads varies from 390 s to 590 s, for metallurgical characterization specimens, for different ceramic/cermets based composites. The least processing time of 390 s for Ni based-30Cr_3C_2 and highest processing time of 590 s for Ni based-15Al_2O_3 were required. Similarly, for the same compositions, the processing time required for tribological characterization specimens was 700 s and 790 s; and for flexural studies specimens was varied from 1200 s and 1445 s. The microstructure analysis reveals that all the developed composite clads are almost free from all types of cracks (interfacial and solidification cracks) and the potential of the process for clads thickness varies from 520 µm to 1090 µm. The highest and least thickness was achieved for Ni based-15Al_2O_3 and Ni based-10 WC10Co2Ni clads, respectively. The results of porosity analysis show that the developed composite clads possess significantly less porosity as compared to conventionally used cladding/coatings processes. The XRD analysis confirms the presence of Cr_2Ni_3, $Cr_{23}C_6$, Cr_7C_3, CrSi, $CrSi_2$, SiO_2, NiC, SiC, Cr_3Ni_2SiC phases in the Ni-based and Cr_3C_2 reinforced composite clads; and phases $NiCo_2O_4$, Ni_2W_4C, Ni_2Si, $NiAl_2O_4$, W_2C, Ni_3Si, Cr_3C_2, and FeNi in Ni-based and WC10Co2Ni reinforced composite clads; and phases: Intermetallics (Ni_3Si, $FeNi_3$, and Fe_7Ni_3), Carbides (Fe_5C_2) and Oxides (Al_2O_3 and SiO_2) in Ni-based and Al_2O_3 reinforced composite clads are developed. The formation of various carbides, silicides and

intermetallics during microwave hybrid heating led to higher average microhardness of the developed composite clads. The average microhardness of the developed Ni-based/30 WC10Co2Ni composite clad comes out to be highest (925±57 HV) among all the developed clads, which is almost 4.91 times higher than that of the substrate (SS-316). The presence of high strength carbides and intermetallics in the composite clads also resulted in the higher flexural strength of these clads. The value of flexural strength in case of Ni-based-15 Al_2O_3 composite clad was highest and it is of 854±16 MPa.

The functional characterization results, in terms of vibratory cavitation erosion testing at varying test parameters (stand-off distance, vibration amplitude and horn immersion depth) revealed that cavitation erosion resistance (CER) of all selected composition developed composite clads is higher than the SS-316 substrate. The Ni-based-30 WC10Co2Ni composite clad shows highest CER among all the developed clads, which is almost 12.78 times higher than the substrate. The ANNOVA results revealed that all the three test parameters were significant for cavitation erosion wear. The stand-off distance (SOD) comes out to be the most influential test parameter followed by vibration amplitude (AMP) and horn immersion depth (IMD). The maximum cavitation erosion wear occurs at 0.5 mm SOD, 60 AMP and 80 mm IMD. The overall results led to the conclusions that the microwave energy proved its successful utilization to develop clads of various materials that can resist the cavitation erosion wear successfully. Hence, the microwave processed composite clads can be successfully used in hydroelectric power plant applications.

Keywords*:* Microwave Cladding; Composite Clads; Characterization; Cavitation Erosion Resistance; Fractographic Analysis; Taguchi L9 orthogonal array

List of Figures

List of Tables

List of Abbreviations

Abbreviations		Full-Form
Al_2O_3	=	Alumina
AMP	=	Amplitude
ASTM	=	American Society for Testing & Material
BCC	=	Body Centre Cubic
BSE	=	Backscatter Image
CER	=	Cavitation Erosion Rate
CI	=	Cavitation Inducer
CML	=	Cumulative Mass Loss
Cr_3C_2	=	Chromium Carbide
CVD	=	Cathodic Vapour Deposition
CVL	=	Cumulative Volume Loss
DC	=	Direct Current
EDS	=	Energy Dispersive Spectroscopy
EM	=	Electromagnetic
FCC	=	Face Centre Cubic
FGM	=	Functionally Graded Materials
HEA	=	High Energy Entropy Alloy
HT	=	Heat Transfer
HVOF	=	High-Velocity Oxy-Fuel
IBT	=	Incubation Time
IEA	=	International Energy Agency
IMD	=	Immersion Depth
ISO	=	International Standards Organization
JCPDS	=	Joint Committee on Powder Diffraction Standards
MDE	=	Mean Depth for Erosion
MDER	=	Mean Erosion Rate
MHH	=	Microwave Hybrid Heating
MMC	=	Metal Matrix Composites
Mo	=	Molybdenum

MSS	=	Martensitic Stainless Steel
MW	=	Microwaves
NaCl	=	Sodium Chloride
NCER	=	Normalised Cavitation Erosion Rate
NIR	=	Normalised Intensity Ratio
OM	=	Optical Microscopy
PPM		Part Per Million
PTA	=	Plasma Tungsten Arc
PVD	=	Physical vapour Deposition
PH	=	Pouvoir Hydrogene
SEM	=	Scanning Electron Microscopy
SEI	=	Secondary Electron Image
SMAW	=	Submerged Arc Welding
SOD	=	Standoff Distance
SPE	=	Solid Particle Erosion
SS	=	Stainless Steel
TEM	=	Transmission Electron Microscopy
TIG	=	Tungsten Inert Gas
TMP	=	Thermo Mechanical Processing
UTM	=	Universal Testing Machine
WC	=	Tungsten Carbide
XRD	=	X-ray Diffraction

List of Symbols

Symbol		Meaning
°	=	Degree
°C	=	Degree Centigrade
μ'	=	Magnetic Constant
μ_0	=	Magnetic Permeability
μm	=	Micrometre
μ_r	=	Relative Permeability
A	=	Ampere
cm	=	Centimetre
D_p	=	Depth of Penetration
D_s	=	Skin Depth
f	=	Frequency
g/cm^3	=	Grams Per Centimetre Cube
GHz	=	Giga-Hertz
GPa	=	Giga-Pascal
GW	=	Giga-Watt
HV	=	Vickers Hardness
j	=	Polarization
K	=	Kelvin
kg/m^3	=	Kilogram Per Metre Cube
kHz	=	Kilo-Hertz
kV	=	Kilo-Volt
kW	=	Kilo-Watt
l/h	=	Litre Per Hour
l/min	=	Litre Per Min
m	=	Metre
m/s	=	Metre Per Min

m^3/h	=	Metre Cube Per Hour
mg/h	=	Milligram Per Hour
MHz	=	Mega-Hertz
mm	=	Millimetres
mm/min	=	Millimetres Per Min
mm/s	=	Millimetres Per Seconds
MPa	=	Mega Pascal
N	=	Newton
nm	=	Nanometre
Pa	=	Pascal
rpm	=	Revolution Per Min
S^{-1}	=	Per Seconds
$tan\delta$	=	Tangent Loss
µm/h	=	Micrometre Per Hours
V	=	Voltage
W	=	Watt
W/m K	=	Watt Per Metre Kelvin
ε'	=	Electrical Permittivity
ε''	=	Dielectric Loss Factor
ε_o	=	Electric Permittivity
ω	=	Angular Frequency
λ_o	=	Wavelength

CHAPTER 1
INTRODUCTION AND OVERVIEW

1. Origin of the Current Research Problem

1.1 Climate Change and Renewable Energy

Since the start of human civilization, energy plays a fateful role in social and economic development. It is considered as backbone of economy of a country. Any hindrance in its supply can causes severe effect on the functionality of a country. Over the last few decades, in response to meet the great increase in demand of electricity due to the increase in population and technological advancements globally, the fossil energy sources have been tapped comprehensively, which leads to rapid depletion of them. The exorbitant use of remaining fossil energy sources must be discontinued immediately, not only because they are being depleted, but also, the key concern of severe environmental pollution caused by the combustion of fossil energy sources.

In the year 2018, an increase of 50% in CO2 emissions by 2030 was estimated by the International Energy Agency, world outlook agency [1]. In response to this status, global warming and the threat of climate change is forcing the industries to use energy sources more efficaciously, while energy-related greenhouse gas (GHG) emissions have become the most discussed issue of the current decade. In this respect, efforts in the field of research and development of renewable energy technologies are needed that can provide solutions to these environmental challenges by offering clean and reliable energy sources. The renewable energy shares, among the other energy sources in the world, have increased in recent years, and are projected to grow in near future [2]. The hydropower has the greatest potential to be an emission-reducing sustainable system, which makes it an important asset in the global renewable energy supply. The various available renewable sources utilization and dependency of the leading six countries for producing electricity is as presented in Figure 1.1.

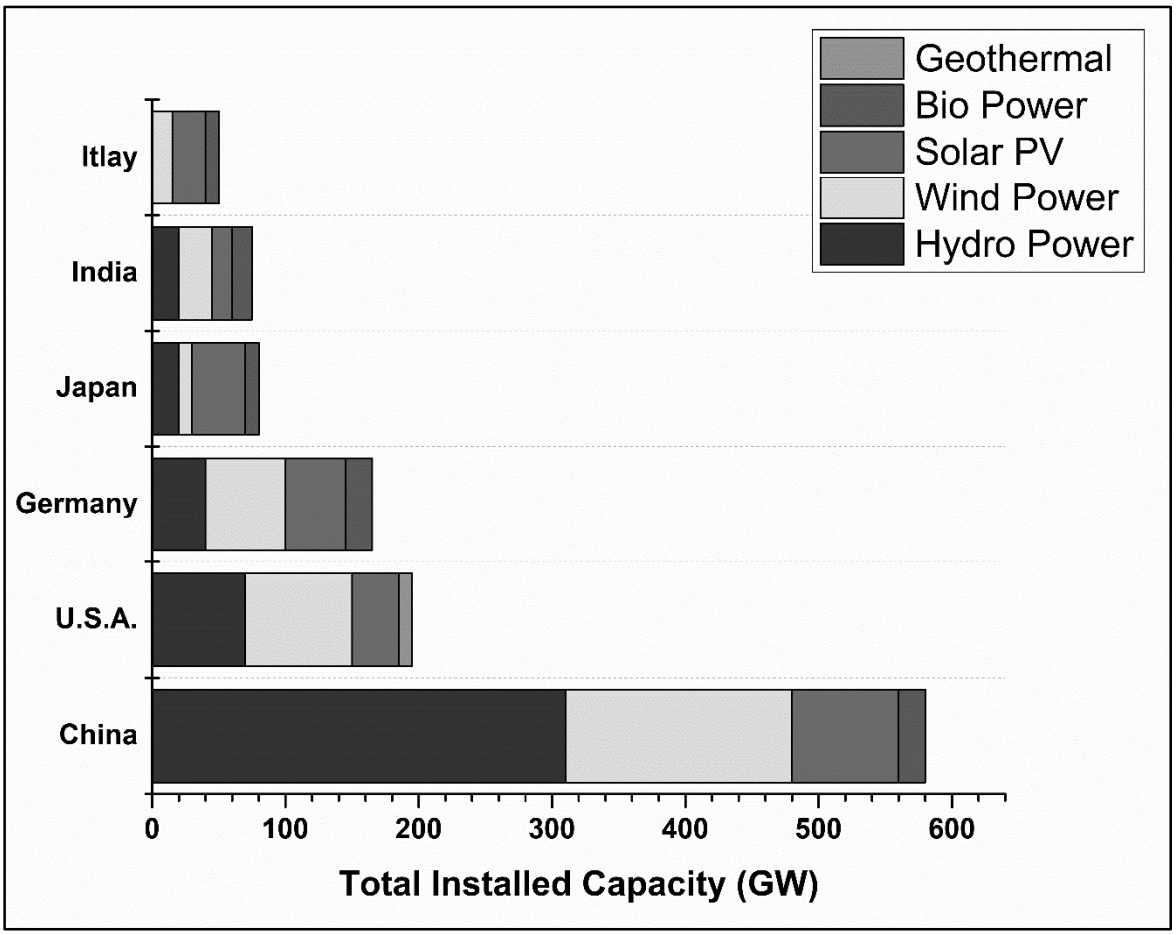

Figure 1.1: Leading countries using renewable sources to produce electricity [3]

The study shows, India has now overtaken Japan and become 5th largest hydroelectric power producer globally and still has a huge potential for generation of hydropower [3]. The Indian power sector highly depends on hydropower and it holds second position. The importance of hydropower for production of electricity, when compared with all other renewable and non-renewable methods, like wind, solar, biomass, waste, coal, diesel, gas, is confirmed from Figures 1.2 and 1.3.

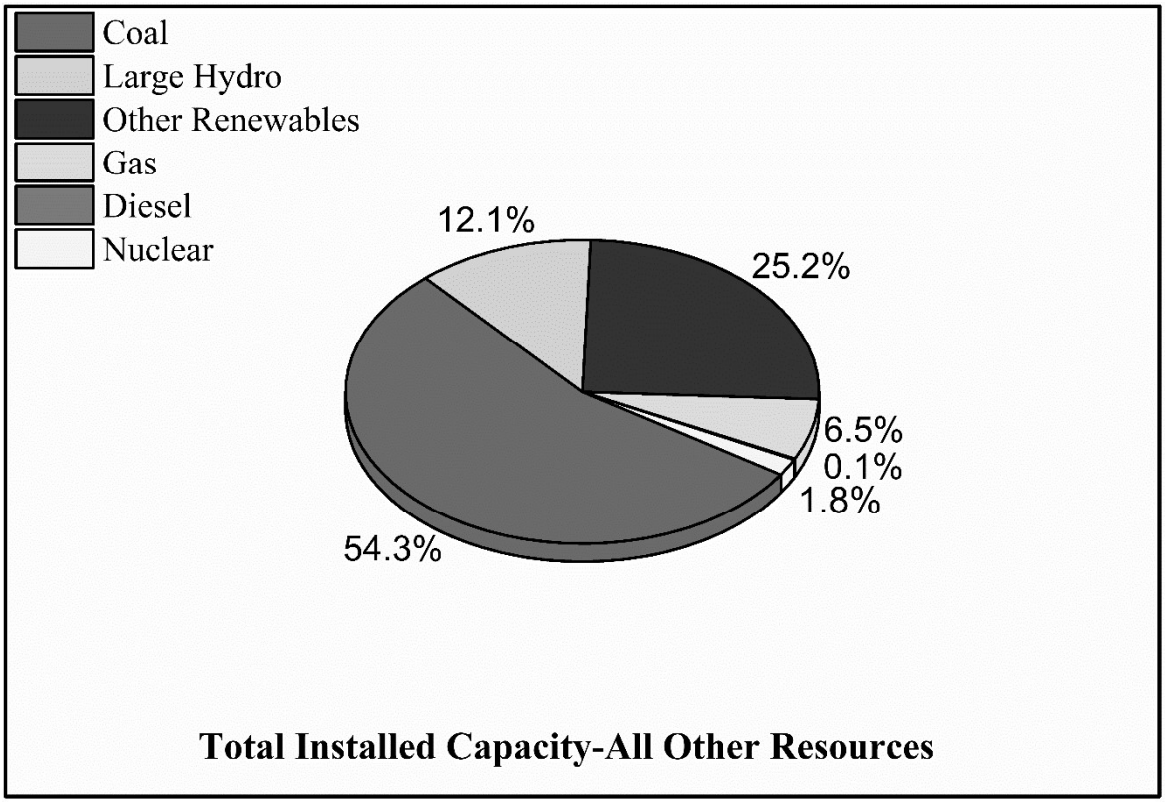

Figure 1.2: Contribution of all the resources in installed grid power capacity in INDIA [4] (Ministry of power statistics)

However, despite of all these advantages, hydropower plant comes across numerous constructional, operational and maintenance issues, that may severely affect the electricity generation capacity of plant. Additionally, the burden of huge revenue losses to the power plant may arise because of the increase in downtime due to several teething problems. The performance and workability of the plant highly depends upon the satisfactory working of the hydro turbine and its associated components. These may be severally damaged due to one or all of the following reasons:

i. Cavitation erosion

ii. Sediment erosion

iii. Fatigue

iv. Material defect

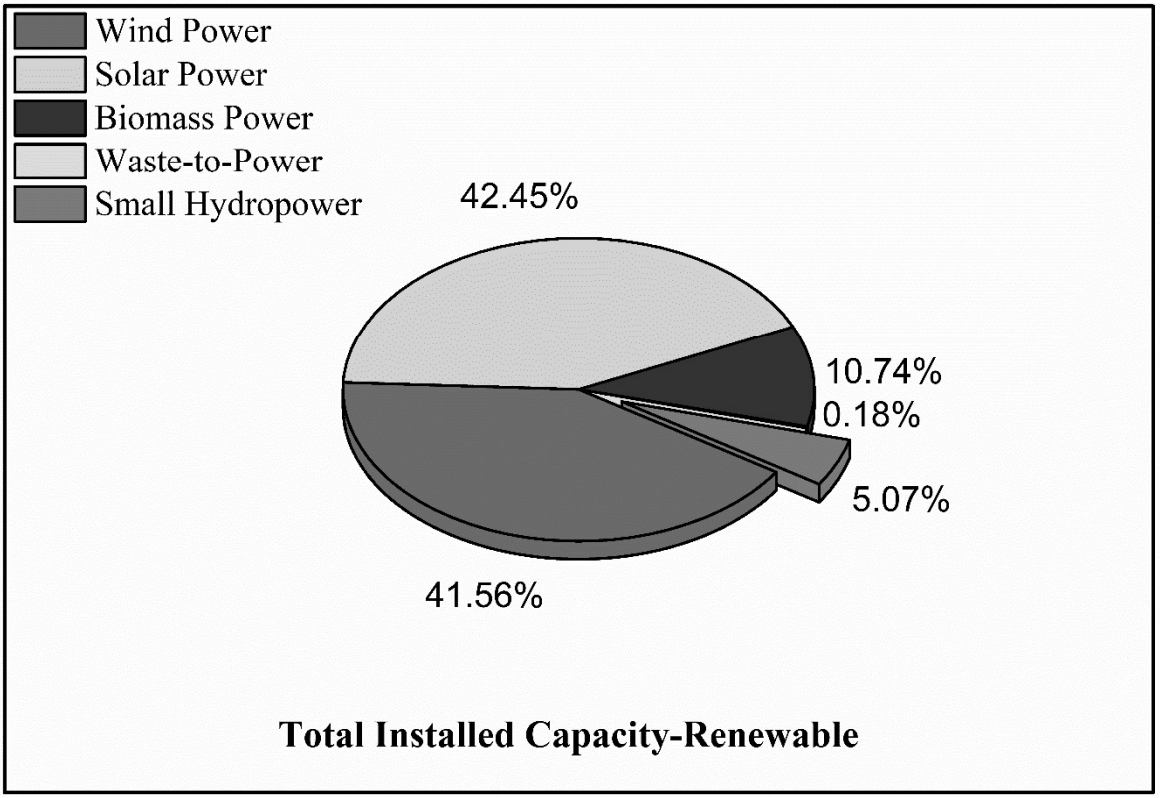

Figure 1.3: Contribution of the renewable resources in installed grid power capacity in INDIA [5] (Ministry of Renewable energy statistics)

i. Cavitation erosion: Cavitation erosion (CE) is a leading cause of material degradation in the different fields related to liquid transportation. This occurs when there is a pressure fluctuation within the flowing liquid inside the turbomachines. This severally affected the satisfactory workability of the machinery and results into noise, extreme vibration and loss in efficiency. The damage to a Kaplan turbine blade caused by cavitation erosion is as illustrated in Figure 1.4. The severity of the cavitation erosion is well described by an article "*Tiny Bubble Challenges Giant Turbines: Three Gorges Puzzle*" published in The Royal society in 2015 [6]. "Three gorges" is world's largest hydropower project situated in China. The turbine blades of this hydropower plant severally damaged in the next year of its commissioning, due to cavitation erosion. However, the turbine blades were manufactured by leading manufacturing companies.

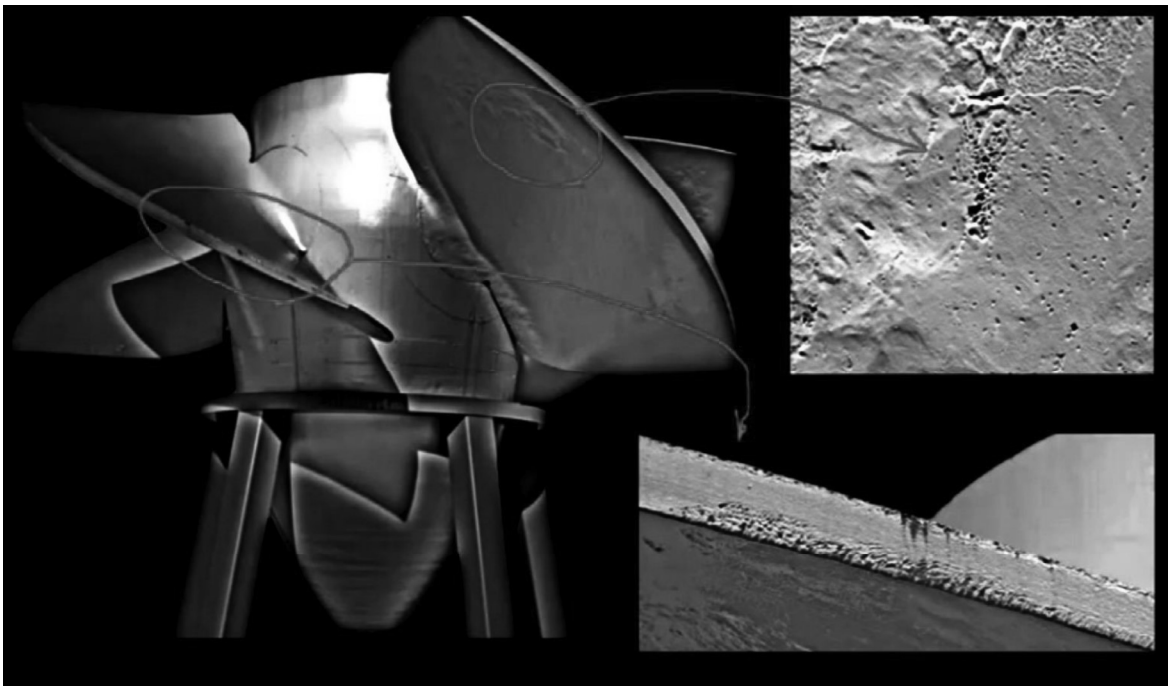

Figure 1.4: The damage to Kaplan turbine blade resulting from pitting action of cavitation erosion [7]

ii. Sediment erosion: Sediment erosion in hydro-turbine parts is occurred due to continuous striking of sand or sediment particles that are present in water. These hard particles, striking with high velocity, gradually remove the material by cutting action and repeated deformation [8]. This type of wear destructs the oxide film on the surfaces that guide the flow and make them irregular, which may also offer favourable initiation spots for cavitation erosion. This results in noise and extreme vibration, which, further leads to both a releasing and contributing reason for power plant damages. The rate of erosion depends upon numerous properties of sediments such as their size, shape and concentration. Sediment erosion is a major problem for small hydro power plants, situated in steep hilly terrains, particularly in the countries of south Asia that belong to Himalayan region like India, China and Nepal. During monsoon season, the high amount of sediment is present and it becomes challenging to resist these sediments to pass through the turbines. The main constituent of this silt (Fe_2O_3, Al_2O_3, SiO_2, CaO, and MgO) is quartz (70-98%). This is extremely hard (In Moh's scale hardness 7), and it can cause severe damage to turbine parts.

iii. Fatigue: Fatigue is another cause of failure of hydro turbine. Cracks may develop in the hydro-turbine parts which are subjected to continuous cycling loading. The growth of these cracks up to boundaries, overtime, may gradually fail the hydro-turbine parts. The failure of any one component of hydro-turbine leads to complete failure of hydro-turbine, as it is

assembly of numerous components. Some studies [9] reveal the formation of eddy current as major cause for vibration and stress generation.

iv. Material defect: The available literature on failure of hydro-turbine reports that material defect is not frequent failure mechanism for hydro-turbines [6], because most of the material defects are controlled during manufacturing phase. However, during installation, the generation of material defects can result into failure of components. Therefore, it is mandatory to strictly follow the required design configuration, during assembly of all components, in hydro power plants. However, some defects like sensitization of steels, due to the heating effect of collapsing cavitation bubbles, is also reported [10].

It is found that cavitation and silt erosion are most frequent reasons for failure of hydro-turbine. Thus, emphasis on sediment and cavitation erosion is paramount for the countries belong to south Asia region, because most of the hydro energy of this region is extracted mainly from Himalayan rivers.

1.2 Cavitation Phenomenon

Cavitation erosion (CE) is a leading cause of material degradation in components of hydro-power plants. Cavitation phenomenon generally occurs, when there is a fluctuation of the pressure within the flowing liquid inside the hydro-machines. Whenever pressure in the flowing liquid falls below its vapour pressure at a particular instant or location that gives rise to nucleation of cavities (vapour bubbles) [11]. These vapour cavities travel with the flow. However, when the pressure starts rising and reaches a higher value, these vapour cavities start collapsing violently. The ensuing collapse of these cavities generates micro-jets and high-pressure shock waves, which result in the extreme generation of stress into material. If the resultant pressure of these shock waves is greater than the mechanical strength of the material, a small hollow indentation has been formed which is known as pit. When these pits have been accumulated in a very narrow area then material finally gets eroded. The step wise mechanism of pit formation is illustrated in Figure 1.5.

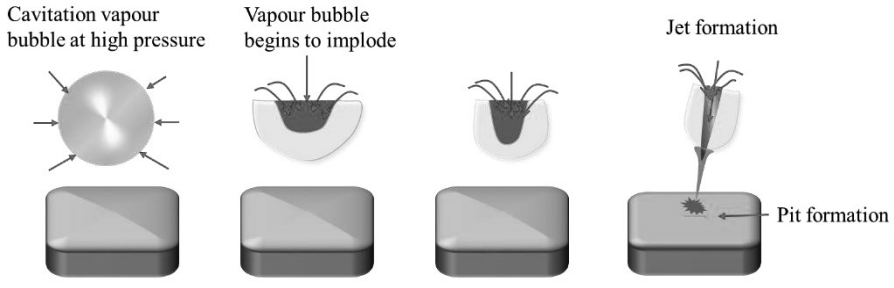

Figure 1.5: Step wise representation of cavitation phenomenon

The various parts of hydro-turbines which are more likely to lose their satisfactory functionality, due to cavitation and sediment erosion are listed in Table 1.1.

Table1.1: The components of turbine which are highly susceptible to cavitation erosion

Classification of Hydraulic Turbines	**Type of Turbine**	**Parts Prone to Cavitation Damage**
Reaction	Francis	1.The Trailing edge of the blade 2. The leading edge of the blade 3.Wicket gates guide vanes 4. Draft tubes
	Kaplan	Guide vanes, Blades
Impulse	Pelton	Bucket
	Bulb	Blades

1.3 Methods to Prevent or Control Damage due to Cavitation Erosion

An insight of literature review indicates that it is not possible to avoid cavitation phenomenon completely. However, their effect can be minimised, either by completely eliminated the load fluctuation or reduced it to minimum. The studies on cavitation [12] also suggest that this problem may be avoided completely, at the design level, by using the following approaches;

i. Designing the turbine in such a way that in the draft tube it operates with forward whirl

ii. Improving the pressure distribution at back side of the blades of turbine

iii. Changing the blade profile to make it forward edge shape

Apart from this, on the operational level, the effect of cavitation and sediment erosion damage to the hydro-turbine parts can be minimised by using following methods [13] (Figure 1.6):

i. Online vibration monitoring

ii. Use of cavitation resistant materials

iii. Injection of air into the draft tube

iv. Tailoring the surface properties of the bulk component

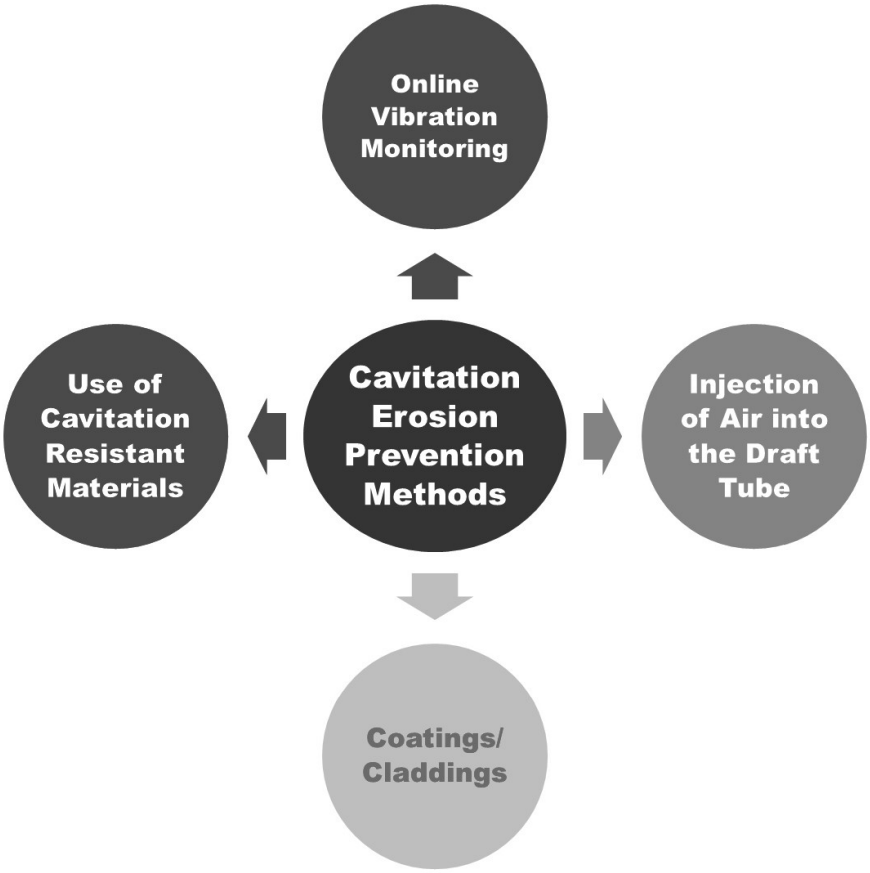

Figure 1.6: Cavitation erosion prevention methods

i. Online vibration monitoring: This is the most common and effective method used to control the cavitation in hydro-power plants. In this method, vibration monitoring devices are used which can detect the abnormal vibrations. The abnormal vibrations are induced to machine by the section which is experiencing cavitation. These values of abnormal vibrations are compared with the standard permissible limits of vibrations. If any value of abnormal vibrations beyond the permissible limit is noticed, the machine control system commands to discontinue the operation and shut down the machine immediately. This ensures not only the prevention of further damage; but also, the safety of the plant officials.

ii. Use of cavitation erosion resistant materials: The wise choice of turbine material and fabrication method can prevent damages due to cavitation. The cavitation incubation time and rate are greatly affected by the material properties. The cavitation erosion rate of the materials, which have higher cavitation incubation rate, will be higher. It is reported that harder materials are more resistive to cavitation damages because higher microhardness results into logarithmically increase into cavitation incubation time. However, ductility and toughness also play important role to enhance cavitation erosion resistance by increase the ability of material to absorb cavitation energy [14]. But, the resistance to fracture of any material is affected

differently by properties like hardness, toughness and ductility. The failure possibility of material due to cavitation erosion wear can be reduced by increasing the hardness and toughness of materials simultaneously. But, this is a problematic task to increase both these properties simultaneously in any material system. Therefore, the use of composite material might help to tackle this problem.

iii. Injection of air into the draft tube: The draft tube experiences the problem of cavitation due to the separation of flow at the exit of the blades of turbine. This separation of flow induces high amplitude vibration to the machine components, which causes unfavourable effects to the turbine assembly. The studies[15] also show that vibrations were dampened and also flow were stabilized by injection of air into the draft tube. Therefore, these days, the draft tube for Kaplan and Francis turbines are submerged completely into the water.

iv. Tailoring the surface properties of the bulk component: Surface Engineering is one of the most common methods used these days to prevent turbines damage. Where, in this approach user can tailor the properties of the bulk surface component for enhancement of the cavitation erosion resistance[16]–[18]. It has been found from literature that both bulk and surface modification are used to enhance cavitation and sediment erosion properties of the components [8]. Since, wear is a surface phenomenon, therefore, instead of modification of the entire bulk component, the modification of surface without altering the major properties of bulk is economical and better option. The various surface modification methods are in used, while coatings/claddings methods have been used by researchers more commonly. In this surface of the bulk is to coat/clad against various cavitation and sediment erosion wear and it can yield better tailored properties with enhanced wear resistance [19], [20].

1.4 Methods to Prevent or Control Damage due to Sediment Erosion

Sediment erosion, in hydro-power plants, causes severe issues by increasing the maintenance shut down time and huge economic losses due to damage and low productivity. The impact of sediment erosion can be reduced to acceptable level with the help of following well accepted methods (Figure 1.7):

i. The construction of civil structures (de-silt chambers and dams)

ii. The proper monitoring of sediment concentration to power house

iii. Coatings/claddings

iv. Selection of materials

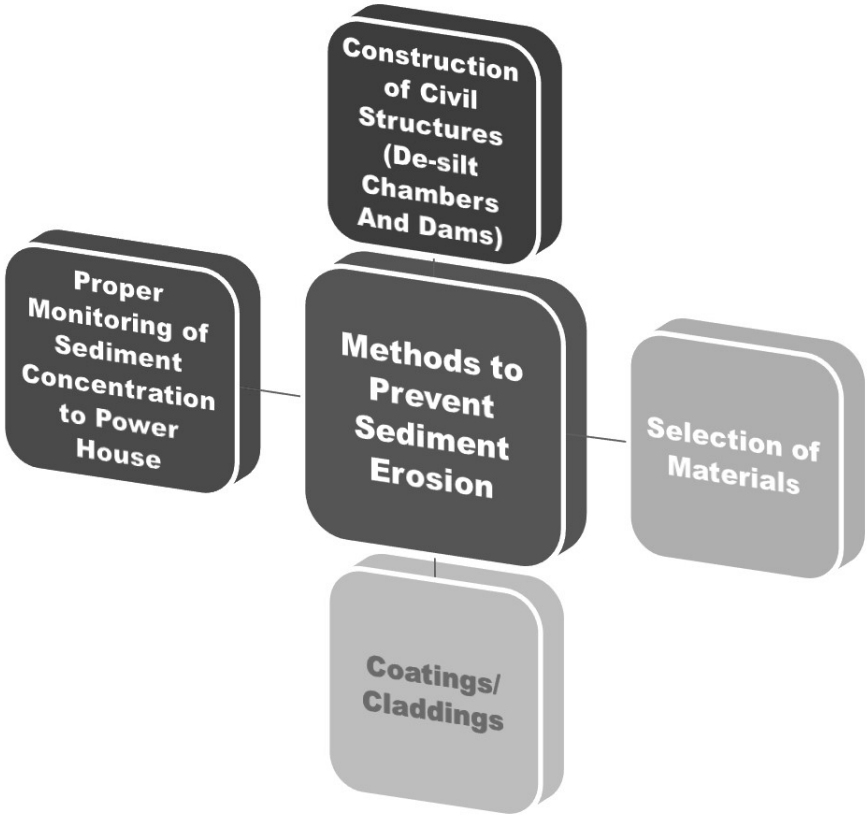

Figure 1.7: Sediment erosion prevention methods

i. The construction of civil structures (de-silt chambers and dams): The civil structures such as dams are constructed across the direction of river flow to store water, and later use for various purposes. Mostly, the dams are constructed to store water for irrigation, electricity generation, flood control and also to reduce flow velocity in order to settle down the sediments into reservoir. Thus, erosive sediments flow may be prevented to enter, at an acceptable level, into power house. The de-silt chambers are also civil structures which are constructed in line to the dam in order to prevent the flow of finer erosive particles to enter into the power house by reducing the flow velocity [21]. As a result, after crossing the de-silt chamber, only clean water is supplied to power house, which helps to minimise the damage causes due to sediment erosion.

ii. The proper monitoring of sediment concentration to power house: This is another method that is used to prevent the damage due to sediment erosion. In this method, the content of silt is measured in the river, in part per million (PPM), by an online silt measuring device. If value of silt content limit is found greater than the permissible limit, the sensor commands to discontinue the operation and shut down the machine immediately.

iii. Coatings/claddings: In this, bulk's exposed surface is coated/cladded with another hard facing material to make it able to resist the sediment erosion. This method is extensively used to prevent damage to machines by both cavitation and sediment erosion [19], [22].

iv. Selection of materials: The wise selection of sediment erosion resistant material is also helpful to combat sediment erosion up to some extent. The hardened stainless steels are most commonly used for this purpose [23]. The turbine parts are generally fabricated or cast from these stainless steel. Further, these parts are heat treated to enhance the sediment erosion resistance.

On the basis of above discussions, it has been observed that, although, the online monitoring of cavitation and silt erosion is helpful to prevent damage due to cavitation and sediment erosion, but, the shutdown time results into low efficiency. Also, complete submergence of draft tube, constructing dam and de-silt chambers; particularly to combat cavitation and sediment erosion does not provide plausible solution. Therefore, bulk or surface modification may provide the best solution to combat both cavitation and sediment erosion. Moreover, the degradation of materials starts from surface, therefore, modification of surface instead of designing of suitable bulk material is always economical and the most realistic method to resist wears.

1.5 Surface Engineering

Surface engineering may be defined as a method to tailor the properties of surface of constituents (metallic/ non-metallic), to improve the functionality and service life, to be used for decorative or functional purposes. Surface engineering is broadly termed as sub-discipline of materials science. It mainly deals with the surface of bulk. It is the spectrum of all the applications of engineering and most commonly used method to enhance resistance against wear, oxidation and frictional energy losses. Most of the engineering components experience degradation of material which initiates from surface, because surfaces are exposed to surrounding environment. As a result, surfaces experience degradation overtime. Hence, the improvement of surface is major concern in most of the engineering applications. The major properties that are required by any engineering component to function satisfactory for long period are:

i. Resistance against wear

ii. Resistance against corrosion

iii. Minimum energy losses due to friction

iv. Resistance against oxidation at elevated temperatures

v. Better thermal properties

vi. Better electrical properties

The modification of surface can be done by different methods which are illustrated in Figure 1.8.

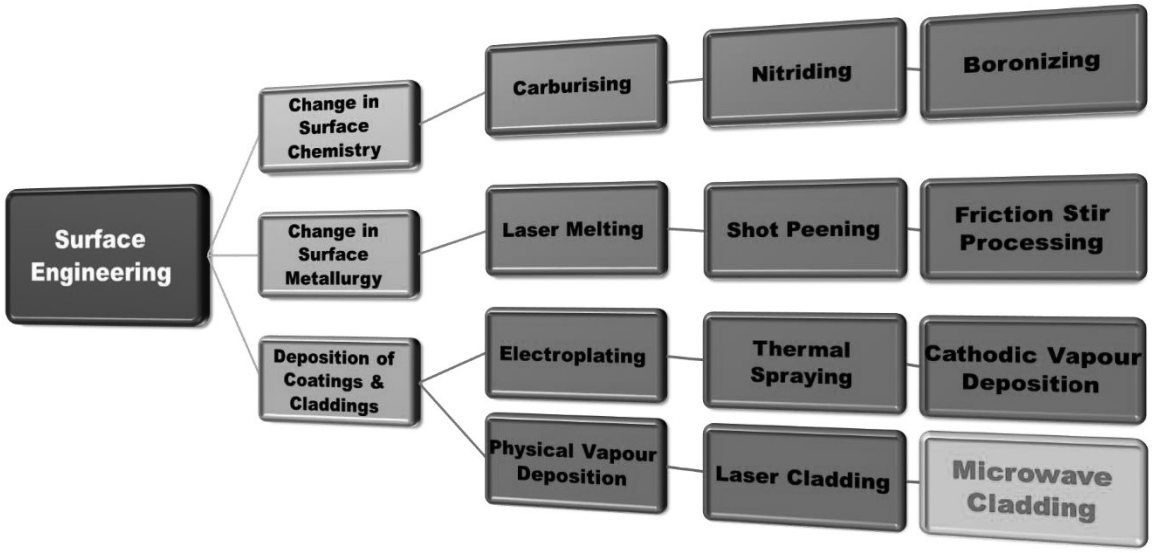

Figure 1.8: Different types of surface engineering methods

The most common surface engineering technologies applied to steel alloys, mainly used in hydropower plant, include transformation hardening, surface melting, conventional carburization, conventional nitriding, coating/cladding, and plating [24], [25]. Surface hardening of stainless steels for improved wear resistance while maintaining corrosion resistance and ductility has historically been very difficult. One of the most realistic and economical approach to improve wear resistance, by overcoming above mentioned problems, could be overlaying the functional surface with layer of hard and wear-resistant material i.e. coating/cladding. Most of the techniques shown in Figure 1.8 are well developed and used extensively by the industries. A brief comparison based on some important parameters of different coating/cladding processes is shown in Table 1.2.

Table1.2: Comparison of distinguished methods used for claddings/coatings [26]

Process Characteristics	Gaseous State Processes		Solution Process	Molten or Semi-Molten State Processes		
	PVD	CVD	Electroplating	Laser Cladding	Thermal Spraying	Welding
Deposition Rate (Kg/h)	Up to 0.5 Per Source	Up to 1 Per Source	0.1-0.5	0.1	0.1-10	3.0-50
Coating Thickness (μm)	0.1-1000	0.5-2000	10-500	50-2000	50-1000	1000-100000
Substrate Deposition or Treatment Temperature (°C)	50-500	150-12000	25-100	200-2000	100-800	500-1200
Uniformity of Coating	Good	Very Good	Fair/Good	Fair	Variable	Variable
Bonding Mechanism	Atomic	Atomic	-	Metallurgical	Mechanical	Metallurgical

The tribological coating/claddings are commonly developed through the thermal spray, laser and conventional welding processes [27]. The thermal spraying is a broadly used technique considering its low cost and remarkable wear resistance [28] [29].

However, this process has some major limitations like absence and/or poor metallurgical bonding with the substrate, the presence of hard spots, high porosity, and chemical inhomogeneity in the coating. Hence, the performance of the coating in aggressive tribological loading (pinpoint) and environment can be poor due to poor adhesion strength of coating with the substrate [30], [31]. In contrast, the conventional welding processes ensure good adhesion strength of deposits with substrate due to metallurgical bonding. However, the substrate deforms severely due to excessive dilution. To encounter the above mentioned problems, the electromagnetic energy, like a laser, is extensively used to deposit clad on the surface of steel [32]–[35]. Laser cladding is well known for better control over dilution and it gives finer microstructure [36], [37]. In spite of these facts, it has some limitations like high

thermal stress developed during process owing to high-temperature gradient during superfast cooling associated and that causes solidification cracks in clads[38]. Apart from this, distortion, porosity and residual stresses are also a major concern in laser cladding [39], [40]. The cladding of different thermal expansion materials may get delaminated from the substrate due to arises of the solidification cracks. The defects associated in clad arises due to the high thermal gradient which causes rapid solidification. The laser cladding is also not advantageous for processing large areas due to lower deposition rate [41]. The brief comparison of the different coating/cladding process along with their limitations is presented in Table 1.3.

Table1.3: Different surface modification techniques with their limitations [42]

S.no	Surface coating techniques	Limitations
1	CVD and PVD	➢ Physical Vapor Deposition and Chemical Vapor Deposition processes operate at high vacuums and temperatures which requires skilled operators. ➢ The rate at which the coating is deposited is usually quite slow. In addition to these, an appropriate cooling system is also required as the process involves a large amount of heat.
2	Electroless deposition	➢ Coating thickness limits up to 1-100 μm.
3	Electrolytic deposition	➢ A conducting substrate is required. ➢ DC power supply is generally required.
4	Thermal spraying	➢ It does not produce metallurgically bonded coatings. ➢ There are various hard spots left in the coating layer which leads to high abrasion. ➢ The problems such as inhomogeneous microstructure, unbound or unmelted particles and high porosity are associated with spray coating.

5	Laser surface treatment	➢ High initial setup cost and high power requirements. ➢ The laser is an intense heat source, which might cause confined thermal distortion and induced residual and thermal stresses on the substrate during cladding. ➢ The laser cladding is not advantageous for processing large areas due to lower deposition rate. ➢ Defects like porosity are high in this process. ➢ Development of cracks on the surface due to high cooling rate.

In summary, during coating/cladding formation, the problems arise due to the heating source (laser beam in laser cladding, flame/arc in spraying and conventional welding). In general, the heat energy transferred from heating source to material through conventional mode (radiation, conduction and convection) of heat transferred and hence, rise in temperature to the melting or sub molten region is achieved. This causes deposition of the coating/cladding with a high thermal gradient. Where, the kinetics of heat transfer mainly depends on physical properties (thermal conductivity, thermal diffusivity, specific heat, convective heat transfer coefficient etc.) of material system used, which governed the quality of clads. Therefore, the community of the researchers should look into the solutions for the above discussed issues highlighted in well accepted practices used for the development of the coating/claddings. The novel material processing technology is required to use which can overcome the limitations of current material processing technologies, and also capable of producing cladding with better microstructure and properties. However, the processes need to prove their significance as a faster and cost-effective process before welcomed by industries.

1.6 Factors of Efficient Material Processing

The prime concern of academicians and industries is to develop a technique which can overcome, not only, the limitations of existing methods to produce coatings/claddings, but also, capable to cope up with the growing energy demand. It should also be environment friendly,

effective, sustainable and efficient. The selection of the processing method is critical and the following parameters are to be considered while selecting.

1. Initial setup cost
2. Quality of finished product
3. Structure-property Correlations
4. Power requirement
5. Processing time per unit product
6. Maintenance Cost
7. Safe working environment

Recently, microwave processing of materials has gained popularity, as a surface modification technique, to fulfil almost all the requirements of efficient material processing [43]–[46]. Microwave cladding covers almost all the limitations of the conventional surface processing techniques. It leads to uniform bulk heating which reduces the residual stresses, thermal gradient and thermal distortion of the target material and it also helps to attain metallurgically bonded surface layer without any cracks. So, this novel technique has a promising future [47], [48] as it has many advantages over the other surface coating techniques.

1.7 Introduction to Microwaves

Microwaves are consisting of magnetic and electric waves which propagate perpendicular to each other and having wavelengths varying from 30 cm to 1 mm in the air as shown in Figure 1.9. These wavelengths belong to an electromagnetic spectrum having a frequency range of 300 MHz to 300 GHz [49]. Microwaves are used in many applications including food

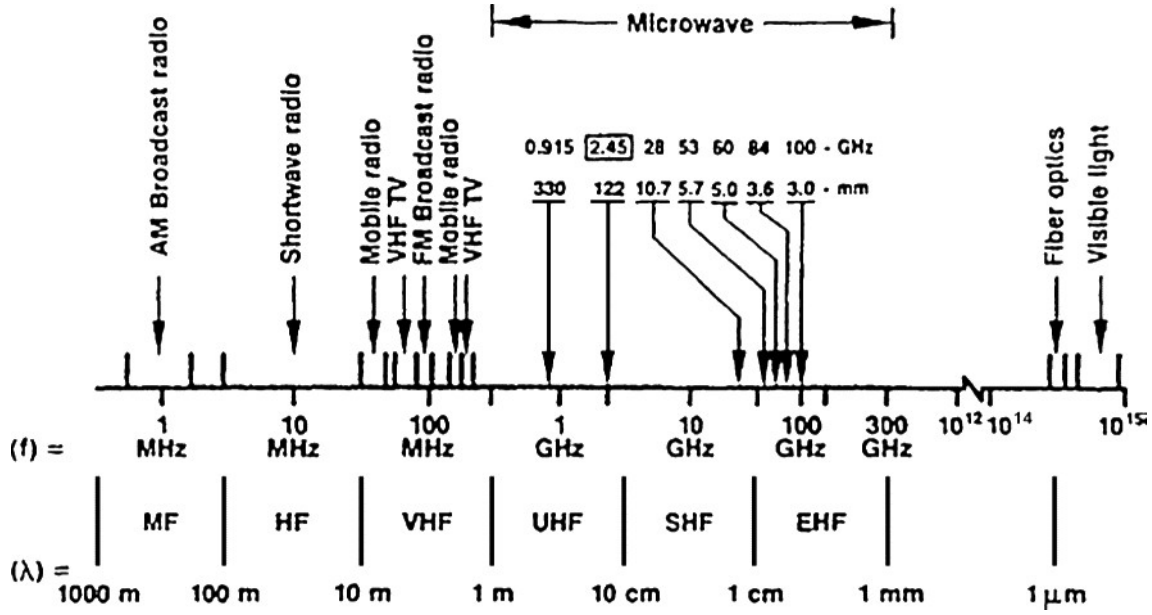

Figure 1.9: Electro-magnetic spectrum displaying wavelengths and frequencies of microwaves [23]

processing, medical purposes, and communication systems, industrial heating and material processing etc. due to these ranges of frequencies. In India, the frequency range allocated for microwaves is 2.45 GHz; however various frequencies are utilized for microwave heating furnaces ranging from 915 MHz-18 GHz [50], [51]. Earlier, the microwaves applications were limited to communications systems including satellite communications, radar and televisions broadcasting. In the year 1945, American physicist and inventor, Percy Spencer [52] investigated heating effects of microwave radiations and patented the technology used for the heating purposes, which is known as a microwave oven.

The applications of microwaves in the domain of heating were further explored by researchers [53], [54] in the area of material processing like vulcanization of rubber, steel making, processing of ceramics and metallic materials, alternative sources of energy recovery [55] etc. The main characteristics of microwave radiations as a heating source during material processing using are illustrated in Figure 1.10.

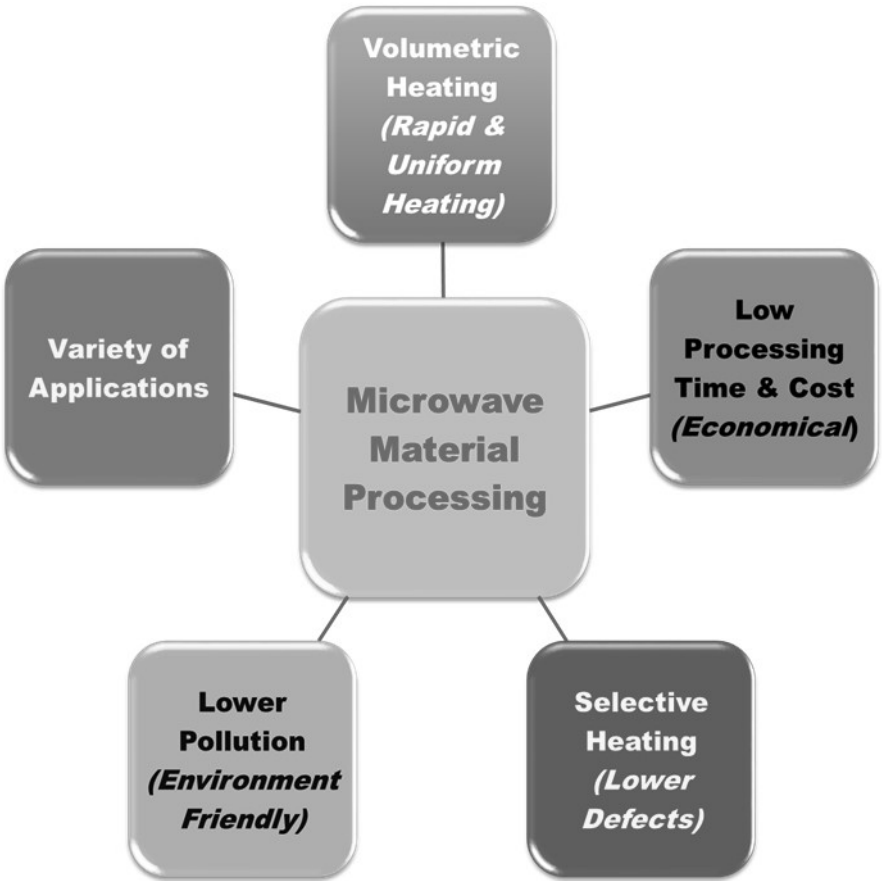

Figure 1.10: Characteristics that favours the materials processing through microwave radiations [56]

1.8 Fundamentals of Microwave Interaction with Material

The interaction of microwave, like any other electromagnetic radiation, with material governs by the certain properties of electromagnetic radiation particularly amplitude, both electric and magnetic field components, phase angle and rate of transfer of energy from one point to another point; that is ability to propagate through material [57]. During expose to microwaves, electric and magnetic properties of material such as tangent loss, dielectric constant and resistivity also plays decisive role in interaction of material with electromagnetic radiation to produce heat in some of them. Based on the response of the materials with microwave irradiation, the materials can be categorised in following ways [58]:

i. Transparent materials: The materials, with low dielectric loss factor, allow the microwaves to penetrate and transmit through them completely without absorption of any energy component is termed as transparent materials or low -loss insulators materials. Materials like alumina (Al_2O_3), teflon, glass, thermosetting plastics and quartz are some examples of these class of materials. The response of the transparent material to incident microwave irradiation is as illustrated in Figure 1.11(a).

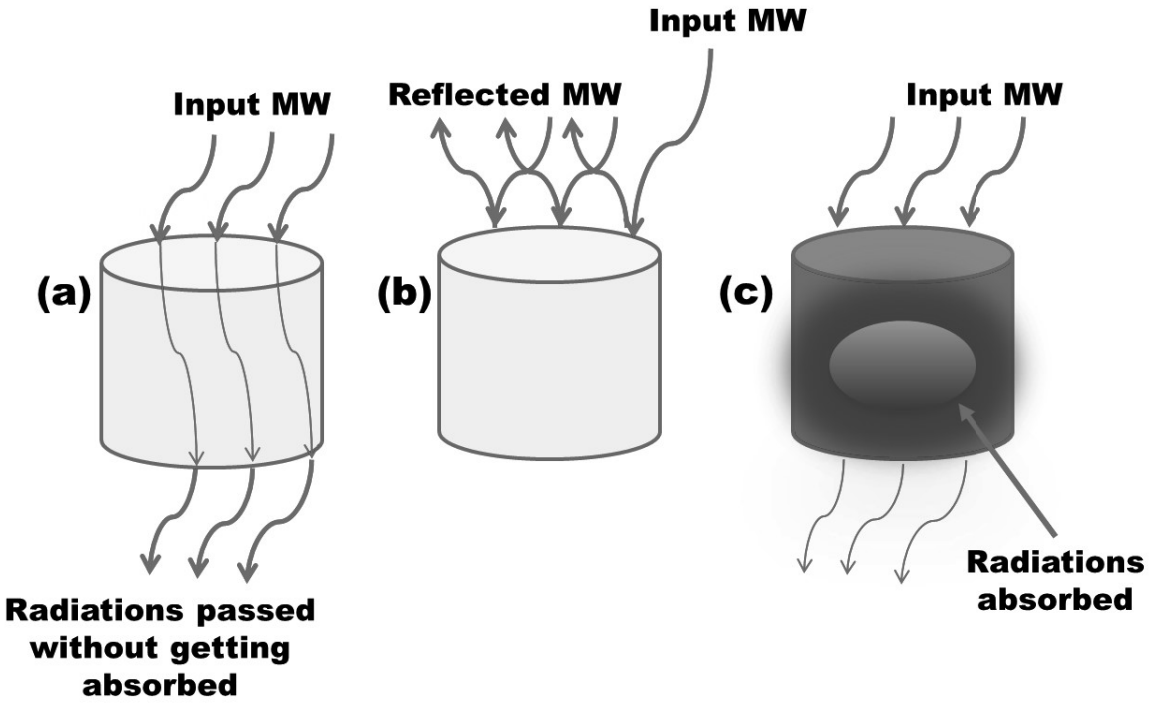

Figure 1.11: Response of distinguished materials when exposed to microwave irradiation a) transparent material b) opaque material c) absorbent material

ii. Opaque materials: The materials, with high dielectric loss factor, reflect the microwaves completely, without absorption of any energy component, or allow negligible penetration are termed as opaque materials or conductors. In general, all metals are conductors at room

temperature and come under this category. The response to incident microwave irradiation by the opaque material is illustrated in Figure 1.11 (b).

iii. Absorbent materials: The materials, with mixed properties in range from conductors to insulators, absorb microwaves readily and convert this absorbed electromagnetic energy into heat; are termed as absorbent materials or lossy dielectrics. Materials like charcoal and ceramics are some examples of these types of materials. The response to incident microwave irradiation by the absorbent material is illustrated in Figure 1.11(c).

iv. Mixed absorbers: The advanced materials, which have mixed or multi-phase and in which one phase acts as high loss insulator and other as low loss insulator, are termed as mixed absorbers. Some materials are transparent to microwaves such as alumina, glass and silica, but start absorbing microwaves after heated to a critical temperature. On the other hand, some materials, such as silicon carbide, absorb microwaves effectively even at ambient temperature [57]. Therefore, in materials, that are transparent to microwaves, a microwave absorbing second phase is added intentionally in order to absorb microwave energy effectively even at room temperature. Polymer matrix composite and ceramic matrixes composite are some of the examples of these types of materials.

1.9 Microwave Heating Mechanism

The heating mechanism as a result of transfer of energy during the interaction of microwave radiation with the absorbing material is complex. When the material is exposed to microwave radiation for processing, the movement of free electrons, electron spin, domain wall and dipoles are disturbed by the electric and magnetic component of microwave [57]. The response to exposed radiation depends upon the material. One mechanism or a combination of several mechanisms can occur simultaneously, during interaction. The material can further be characterized into magnetic and non-magnetic in the context of microwave heating mechanism, which is different for magnetic and non-magnetic materials.

1.9.1 Heating mechanisms in non-magnetic materials

These materials do not affect by magnetic field component of microwave. Basically, dipolar losses and conduction losses are two main loss mechanisms for these type of materials [59]. The highly conductive and metallic materials are mainly dominated by conduction losses, on the other hand, dielectric insulators are dominated by dipolar losses.

i. **Dipolar loss:** This loss plays a significant role in the dielectric insulator materials such as food products, water, ceramics, CMC and PMC [60]. The dipoles are generated in these materials, during exposure to external electric field. The disturbance is created in these

molecular dipoles by the oscillating electric field. The molecular dipoles try to be in phase, by reorienting themselves, with this oscillating electric field. While, these frequent changes in the molecules orientation is resisted by molecular interaction, frictional, elastic and inertial forces. Consequently, increase in kinetic energy of molecules results in volumetric heating. Hence, the temperature of the material increases rapidly due to increase in kinetic energy of all dipoles in the material.

ii. Conduction loss: This loss plays a significant role in pure metals, materials based on metals and semiconductors such as Al, Cu, Ni, Fe, Si and metal matrix composite (MMC) [61], [62]. The free electrons of these materials start movement towards the applied external electric field. The significantly high conductivity of these materials results into rapid attenuation of field inside the material which further induces large current. This leads to development of an induced magnetic field inside the material against the direction of external magnetic field. The force generated by this induced magnetic field faces restriction from molecular interaction, frictional, elastic and inertial forces. The rapid repetition of this phenomenon by oscillating electric field results into uniform and volumetric heating inside the material.

1.9.2 Heating mechanisms in magnetic materials

These materials are affected by both the components (electric and magnetic) of microwave. The magnetic field affects the orientation of domains, electron spin and domain wall, while the motion to free electrons is imparted by the electric field. The conduction loss in addition to magnetic losses like magnetic resonance (electron spin and domain wall resonance), hysteresis and eddy current are exhibited in these materials.

i. Eddy current loss: In this heating mechanism, when any conductor is exposed to changing external magnetic field, eddy currents are induced on all magnetic domains that are present at the surface layer, in the form of close loops [60], [62]. Any change in external magnetic field is opposed by these eddy currents. The density of the eddy current can be expressed as equation 1.1 [61].

$$\boldsymbol{J = \sigma E} \tag{1.1}$$

Where σ is electrical conductivity

E is the electric field induced by the altering magnetic field

Hence, the electric resistivity of the material is key factor and plays a decisive role in eddy current losses.

ii. Hysteresis losses: The magnetic materials experience these losses, which are caused by the irreversible magnetization process, when exposed to alternating magnetic field. The change

in polar orientation of magnetic poles, in every cycle, causes oscillation in magnetic dipoles. This rapid oscillating moment is the cause of significant friction and results into heating inside the material. This heating mechanism is known as hysteresis loss. Hysteresis loss is the prime cause of heating of ferrous magnetic materials when exposed to an alternating magnetic field [60], [62].

iii. Resonance losses: Apart from the hysteresis and eddy current losses, magnetic resonance losses are main cause of microwave heating of few metal oxides like ferrites [63]. Domain wall and electron spin resonance contributes a lot to induce magnetic resonance losses.

Available literature indicates that residual losses are also contributor of the losses that originate from several magnetic resonances and relaxations [59]. These occur mainly due to rotational and domain wall resonance.

1.10 Historical Developments in Microwave Processing

The historical or chronological developments in the field of microwave heating and processing of materials are as shown in Figure 1.12. The microwave applications were earlier based on lower temperature applications, which were further explored for higher temperature applications like in the field of processing of mostly ceramic materials [64], [65]. The ceramic materials are readily coupled with microwave radiations of frequency 2.45 GHz.

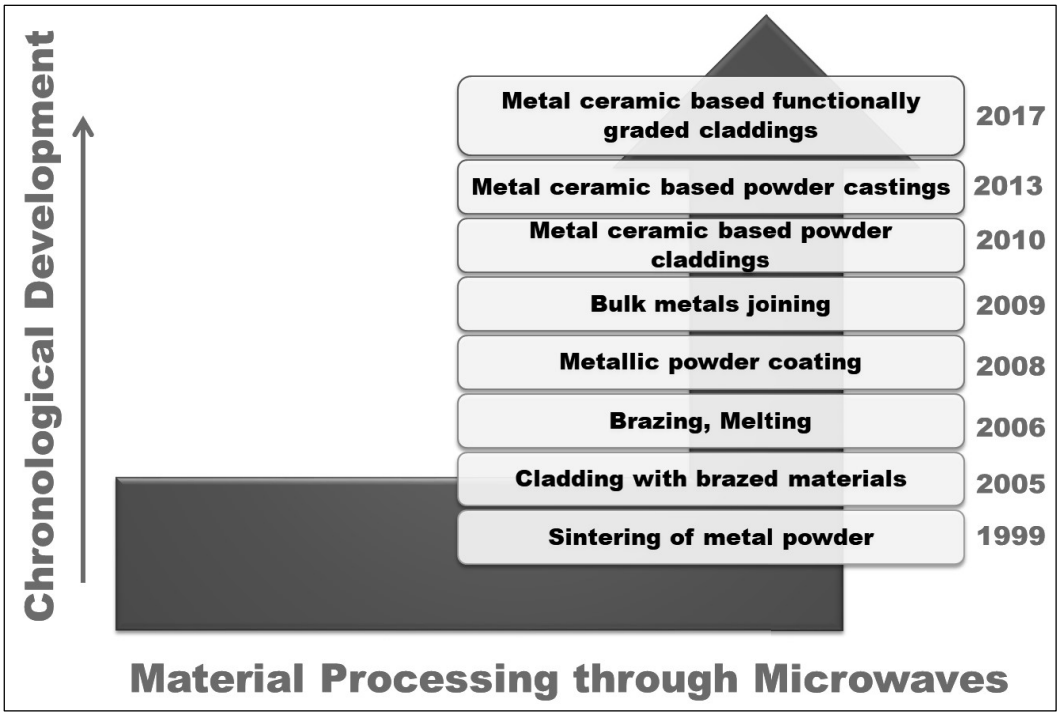

Figure 1.12: Chronological developments in microwave processing of metallic materials

However, bulk metallic materials reflected back the microwave radiations of low frequency of 2.45 GHz at room temperature. The perception among the researchers or scientific community

was to process such materials difficult at room temperature of low frequency microwave radiations. Further, researchers carried out many trials and in the year-1999, Roy et al. [66] reported the successful sintering of metallic powder, which further explored the possibility of coupling of microwaves with metallic materials in the form of fine powders of few microns. The outcome of this research has changed the mind-set of the scientific community and forced to them to re-think upon the processing of metallic powders by using microwave radiations [67]–[69]; which were successfully achieved afterwards. The various active research groups of worldwide have carried out the work in different capacities to expand the horizon (Figure 1.12) of microwave metal processing. The group of IIT Roorkee, India, Sharma et al. [70] in 2009 successfully processed the bulk material and joined the bulk metallic materials by microwave in a domestic microwave oven. This work resulted in the utility of microwaves in the field of higher temperature applications. In the year 2010, Gupta and Sharma [71] extended this work for producing claddings of various materials on a metallic substrate using a domestic microwave oven. The applications of attaining high temperature by microwaves were explored in recent years and amount of work has been carried out in the field of material claddings/coatings and joining areas. The possibilities of Functionally Graded Materials development through microwave hybrid heating are also recently explored and results obtained by authors are very much attractive (Kaushal et al. [72]–[74].

1.11 Conventional /Microwave Hybrid Heating

In the case of microwave heating, the heating profile is inverted i.e. heating starts from the core of material and moves towards outward direction. However, in the case of conventional heating, heat is supplied at the outer surface and transferred to the material core by conduction, convection and radiation modes of heat transfer. Due to the direct absorption of microwaves in the case of microwave heating, heating is done at the molecular level. In the case of conventional heating, there is a significant thermal gradient at the surfaces, which leads to poor microstructures of the surface [75]. However, in the case of microwave heating, the presence of thermal runways in the core leads to microstructure distortion and cracking [76]. To overcome this differential heating phenomenon at core and surface, the theory of microwave hybrid heating has been proposed by the researchers. In the case of MHH, both conventional heating and microwave heating are utilized. Hence, heating can be done in both the directions in order to lower the thermal gradient between the core and surface. Bulk metallic materials are opaque (reflect microwaves) to microwave radiations under normal conditions of 2.45 GHz frequency. But at an elevated temperature, these materials start absorbing microwave radiations

[77]. In the case of MHH suitable susceptor like charcoal powder, silicon carbide material is used to facilitate the interaction of microwave radiations of low frequency to such materials first and hence it causes to raise their temperature. This heated susceptor material transferred heat to metallic materials by conventional mode of heat transfer and reaches the temperature of metallic materials to the elevated temperature. The metallic materials at such high temperature started to interact directly to incident microwave radiations and further heating is taking place by absorption of these radiations only. The materials processed through MHH technique gives better microstructures like reduced grain size, reduced porosity etc. This is only possible due to the uniform and rapid heating associated in MHH, and also results into huge savings in the energy consumptions and processing times. The comparisons of the different heating phenomenon are shown in Figure 1.13.

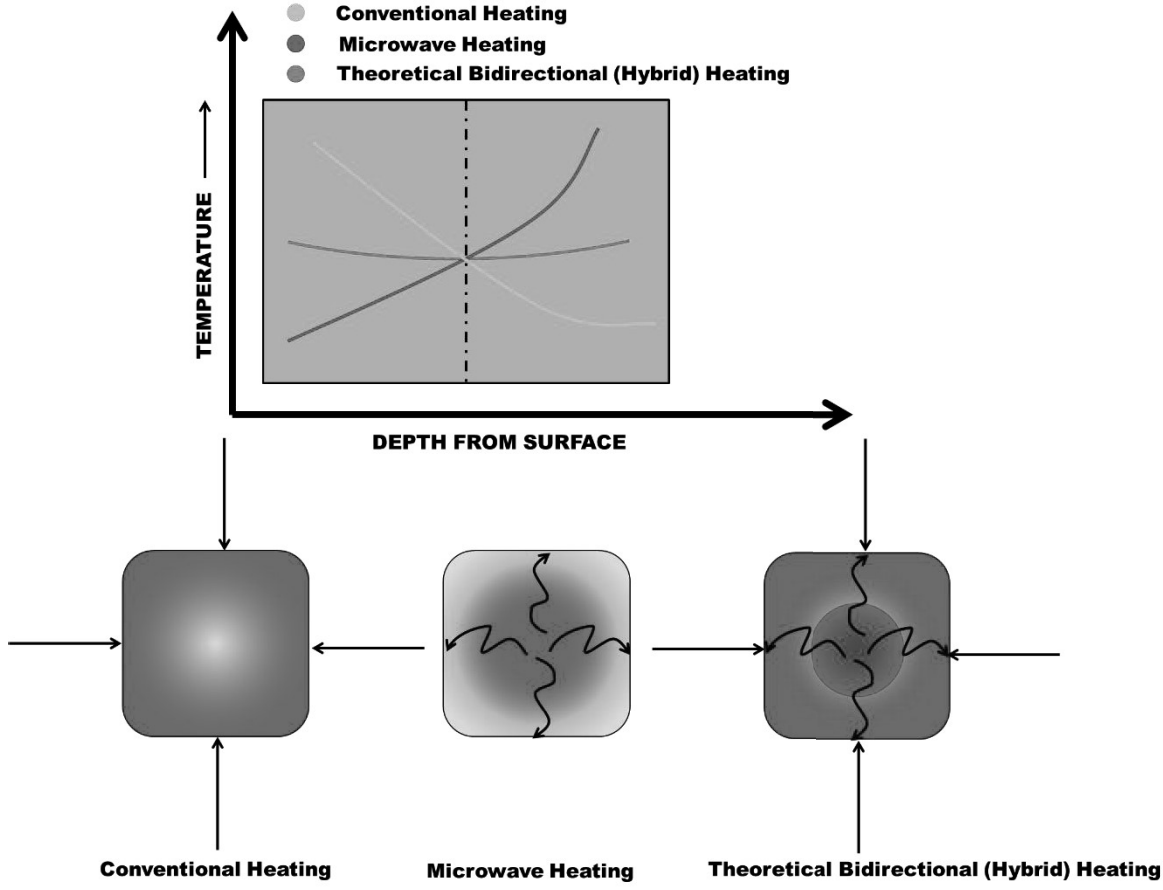

Figure 1.13: Heating profile distribution in conventional, microwave and microwave hybrid heating (MHH) modes

1.12 Advantages of Microwave Processing of Materials

The main advantages of microwave material processing are associated with its characteristics of a higher heating rate of target materials coupled with lower energy consumptions and lower processing times (Figure 1.14). Comparatively, better microstructures, higher efficiency with

reduced energy consumptions, lower defect formation and lower cost of heating are involved in microwave processing of material than conventional heating.

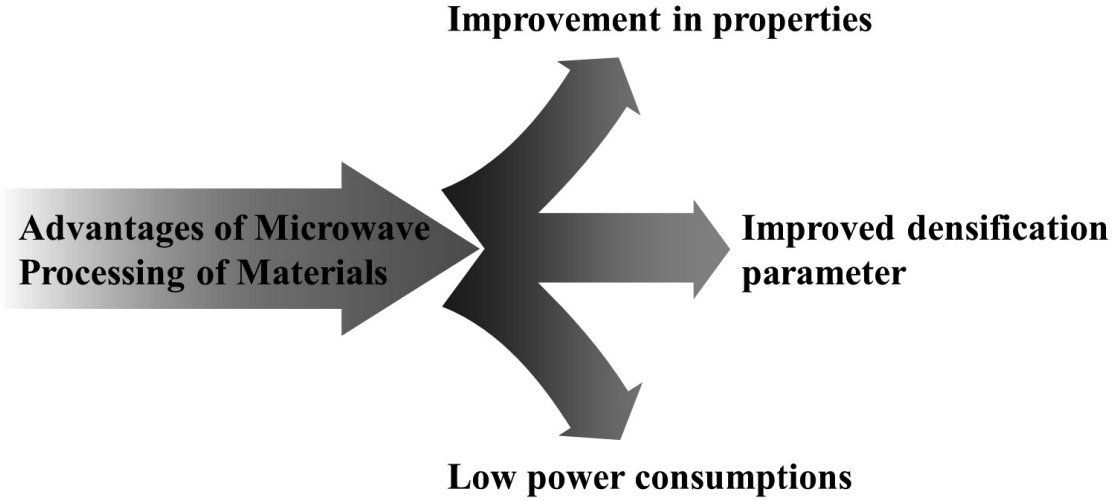

Figure 1.14: Advantages of microwave processing of materials

1.13 Limitations of Microwave Processing of Materials

The utilization of microwave energy to process the materials has gained the attention of researchers in the last decade because of its promising features. However, some challenges are also associated with this technique, which can attract the researchers to explore this field further. Some challenges that are faced during the use of microwave as a heating source to process the materials are listed following:

i. The problem of poor interaction of microwave irradiation with metallic materials at room temperature.
ii. The control of temperature inside the microwave cavity during processing is difficult.
iii. The parts with intricate and complex geometries are difficult to process using microwave irradiation.
iv. The leakage of microwave radiation may harm the humans involved in the process.

1.14 Thesis Overview

The current thesis work has been divided into the following chapters:

Chapter 1: In this chapter, the origin of the research problem and its global impact has been discussed in detail. The various methods used to combat with the cavitation erosion wear are explored. The viability of surface engineering in the significant reduction of surface wear loss has been discussed. The efficient utilization of electromagnetic energy in the form of microwaves in different fields and their limitations are also presented. The motivation behind the work has been outlined.

Chapter 2: A brief literature review of well-established surface modification techniques which are commonly used in industries for solving the issue on cavitation erosion has been discussed. A literature review of materials processing using microwave heating has been presented and discussed. The gaps were identified during the detailed literature review, and the problem has been defined for the current research work. As a result, the objectives for the current work have been identified and defined logically.

Chapter 3: In this chapter, the basis for the selection of the substrate, matrix material and reinforcement material has been presented and discussed. The detailed characterization like their shape, size, compositions, phases of selected raw materials (substrate, matrix powdered material and reinforcement powdered material) by using suitable available techniques has been presented and discussed in detail. The specifications and operation of the apparatus and equipment used for mechanical, metallurgical, and tribological characterization has been also presented and discussed.

Chapter 4: The current chapter presents the details about the development of composite clads by using a novel microwave hybrid heating (MHH) technique. Prior to clad development, the primary sample preparation is also discussed in this chapter.

Chapter 5: In this chapter, the results of metallurgical and mechanical characterization for the so developed clads of Ni-based (EWAC)-Cr_3C_2, Ni-based (EWAC)-WC10Co2Ni and Ni-based (EWAC)-Al_2O_3 are discussed. The results obtained by using suitable techniques and standards to get the microstructure, crystal structure or phases formation, porosity, microhardness, and flexural strength are presented and discussed in detailed.

Chapter 6: This chapter focused on the results obtained from the tribological characterizations of developed clads. The parametric studies of weight loss results of cavitation erosion of SS-316, EWAC/xCr_3C_2, EWAC/xWC10Co2Ni, and EWAC/xAl_2O_3 are presented. Following that, the effect of the parameters such as stand-off distance, amplitude, and immersion depth on the cavitation erosion wear behaviour of developed clads is thoroughly discussed. The fractographic analysis of worn surfaces to determine the possible wear mechanism has been reported. Finally, the confirmatory experiments at optimized process parameters have been discussed.

Chapter 7: The conclusions of the findings from the present research work have been discussed. The major outcomes of the present work and future scope have been highlighted.

CHAPTER 2

LITERATURE REVIEW AND PROBLEM FORMULATION

Surface degradation of hydraulic turbine parts due to cavitation erosion phenomenon is a major concern. Surface engineering can be a straightforward solution for protecting the components against cavitation erosion wear. The use of microwave radiations as a heating source has established solutions for problems existing in surface modification techniques. This source of energy is the fastest and economical way for processing ranges of materials. In the current chapter, brief literature surveys of well-established surface modification techniques, which are widely used these days in industries facing challenges of cavitation erosion, have been discussed. The literature survey also carried on use of microwave radiations for processing range of materials (especially metals) for different purposes is discussed here in this chapter. The gaps in literature have been identified and problem is formulated for carrying out the work for present doctoral thesis. Hence, accordingly, the research objectives for the current work have been framed.

2.1 Stainless Steel

Stainless steel is used in almost every industry around the world. In 2019, despite of the decline in the production from 3.9 MT to 3.2 MT, India was still ranked second in the world for stainless steel production, trailing only China [78]. Austenitic stainless steels, which were invented in Essen, Germany at the beginning of the twentieth century, now account for roughly two-thirds of total stainless steel world production. Austenitic stainless steel is extensively used in various turbomachines and their components because of its lower cost, easy machinability, and excellent corrosion resistance [9], [79]. The SS-316 grade of austenitic stainless steel possesses slightly better properties than most commonly used 300 series family members, i.e., SS-304. The SS-316 contains molybdenum, generally 2 to 3% (as per ASTM-276), making it suitable for working in a highly corrosive environment and thus widely used for making hydro power plant components [80]. The components of the hydropower plant, such as pumps, hydro turbines, and propellers, produces noise and extreme vibrations and often get seriously damaged due to the cavitation erosion [21]. The damage to these parts causes chronic failure of hydraulic machinery [9], resulting in significant economic losses.

However, researchers have implemented various design approaches to reduce the effects of cavitation erosion [12]. But, low efficiency of these design approaches reduces their

use in preventing cavitation erosion [13]. Thus, in recent years, the use of advanced materials or surface modification to mitigate cavitation erosion has attracted attention as better solutions [81]. The surface modification provides easier and cost-effective solutions to combat the cavitation erosion wear [82]. Therefore, many researchers around the world are focusing their efforts on addressing this issue through surface engineering. Many techniques have been developed and used to improve CER as shown in Figure 2.1.

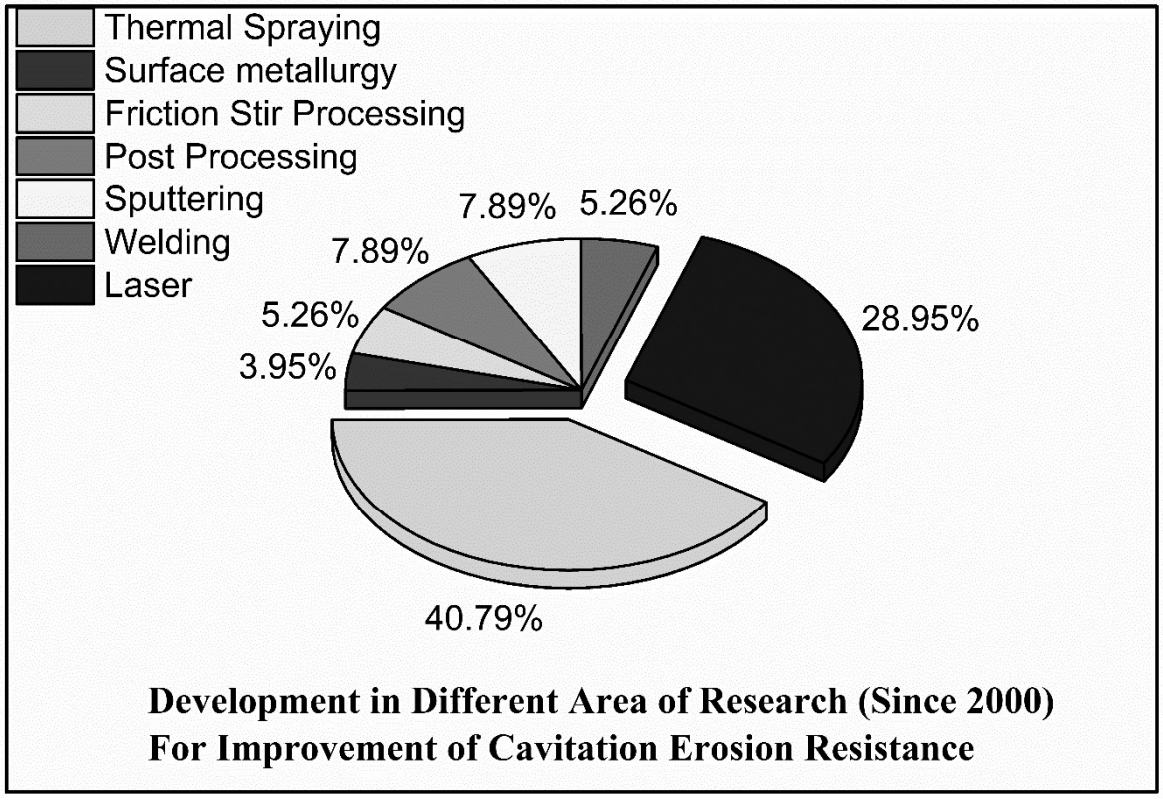

Figure 2.1: The chart showing the percentage of research carried out in different areas or energy used in surface modification for improvement of cavitation erosion resistance

It is clear from the pie chart that almost 70% of total work done since 2000, in the field of using surface engineering techniques to improve CER, is coatings/claddings with the use of thermal spraying (HVOF) and laser processing. Therefore, an extensive literature survey of these well-matured techniques has been carried out.

2.2 Literature Survey of Available Well-Matured Methods for Improvement of Cavitation Erosion Resistance

2.2.1 Cavitation erosion resistance coatings by using high velocity oxy-fuel technique

The versatility and higher output of thermal spraying make it the most popular surface modification technique.

Lin et al. in 2021 [83] deposited coatings of WC-10Ni and WC-10Co-4Cr using thermal spraying technique (HVOF). This work was focused on the investigation of cavitation erosion

resistance of deposited coatings, which contains distinguished binder phase. The deposited coatings were tested using seawater (3.5 wt% NaCl) as liquid medium. The effect of flow velocity on cavitation erosion resistance was also checked. The WC-10Ni coatings were less porous with higher hardness (H) and modulus of elasticity (E) than WC-10Co-4Cr. The volume loss and volume loss rate of WC-10Ni coatings were also less at all level of flow velocities. The low value of porosity; and higher value of H/E and H^3/E^2 were identified as main cause for higher CER of WC-10Ni coatings. The H/E ratio characterizes the resistance of the material to elastic deformation. The H^3/E^2 ratio allows to estimate the ability of material to dissipate energy at plastic deformation during loading. Higher H^3/E^2 indicates that material can strongly withstand against plastic deformation. The increase in flow velocity influences the volume loss rate directly in 3.5 wt% NaCl medium. The debonding of WC particles and cracks propagation from defects such as cracks and pits were found main cause for failure of both the coatings.

Hong et al. in 2020 [84] investigated the microstructure and flow velocity relationship with cavitation erosion behaviour by depositing the Cr_3C_2-NiCr and WC-CoCr ceramic-metal coatings through HVOF on steel substrate. They also discussed the possible cavitation erosion wear mechanisms at different flow velocities using rotating disk rig facility and distilled water as test liquid. Their experimental results showed the significantly higher microhardness and slightly lower porosity of WC-CoCr coatings, in comparison with Cr_3C_2-NiCr coatings. Both the coatings were well combined with substrate and showed the increase in volume loss rate with increase in value of flow velocities. However, the WC-CoCr coatings show less volume loss rate than Cr_3C_2-NiCr coatings at each value of flow velocity. The higher microhardness and lower porosity of WC-CoCr coatings, than Cr_3C_2-NiCr coatings, contributes in significantly low volume loss rate.

Hong et al. in 2020 [85] in 2020 also investigated the flow velocity relationship with cavitation erosion behaviour of Cr_3C_2-NiCr (CN) and WC-Cr_3C_2-Ni(WCN) ceramic-metal coatings using 3.5% NaCl as test liquid. The possible wear mechanisms at different flow velocities along with microstructures, mechanical properties and electrochemical behaviours have also been investigated. The WCN coatings perform better than CN coatings in terms of hardness (H), modulus of elasticity (E), ratio of hardness to modulus of elasticity (H/E), H^3/E^2 and possess less porosity. This leads to significant increase in cavitation erosion resistance and less volume loss rate in NaCl medium at each value of velocity flow. The formation of oxide film and

pinholes, craters, pits, and micro cracks are reported as the possible wear mechanisms for CN and WCN coatings in NaCl medium.

Ding et al. in 2018 [86] used HVOF to prepare the conventional, multimodal and nanostructured WC-12Co coatings on AISI 304. The coatings were prepared with different WC particle size to analyse the effect of variation in particle size on cavitation erosion resistance. The developed coatings of thickness 420±20 μm were characterized for microstructure, phase analysis, porosity, microhardness and fracture toughness. The developed coatings were tested for cavitation erosion using vibratory cavitation testing method. The phase analysis through XRD study indicates the serious decarburization occurrence in nanostructured coating. The unmelted particles of WC in conventional coatings were observed. All the three coatings showed higher fracture toughness and denser microstructure. The nanostructured coatings possessed least porosity (0.63± 0.11%), followed by multimodal (1.76±0.27) and conventional coatings (1.18±0.21). The nanostructured coatings exhibit excellent CER in comparison with other developed coatings. The denser microstructure and strong cohesive strength are reported as the key factors for improvement in CER.

Basumatary et al. in 2017 [87] conducted experiments to examine cavitation erosion-corrosion wear behaviour of nickel aluminium bronze with oxide films. These films were formed: i) in air for 1 week ii) in immersion of 3.5% NaCl solution for 3 months. The experiments in three different test conditions, i) in distilled water for pure cavitation ii) using OCP (open circuit potentials) for pure in-situ electrochemical corrosion and iii) keeping at OCP in 3.5% NaCl solution for synergic effect of cavitation erosion and corrosion, were conducted. The performance of air-formed film under synergic effect was significantly more (almost 20 times) than the water-formed film. The water-formed films experienced pre-existing acid attack and corrosion, which results into higher mass loss. However, water-formed film, due to thick oxide layer (1-1.2 μm) formed in NaCl solution, shows higher corrosion wear resistance than air-formed film.

Quio et al. in 2017 [88] investigated the effect of oxygen flow, kerosene flow and spray distance on cavitation erosion resistance of Fe-based amorphous/nanocrystalline coatings. For investigation of effect of selected parameters Taguchi method was used. The coatings were prepared by HVOF technique on AISI 321 steel substrate. The authors concluded that the kerosene flow is most influential factor followed by spray distance and oxygen flow. The cavitation erosion resistance of Fe-based coatings, that were deposited at optimized spray parameters (oxygen flow rate 963 L/min, kerosene flow rate 28 L/hour and spray distance 330 mm), is increased significantly in distilled water. Also, the increase in hardness and decrease

in porosity leads to increase in the cavitation erosion resistance. However, the hardness had more influence on the cavitation erosion resistance than the porosity. The edges of pores and interfaces between half/un-melted particles offered favourable sites for crack initiation, which results into the delamination of coating.

Lavigne et al. in 2017 [89] investigated the effect of HVOF deposition conditions and powder ball milling of CaviTec (Fe based alloy) coatings on cavitation erosion resistance performance. The coatings deposited at four different conditions: i) unmilled low velocity (UM LV) ii) unmilled high velocity (UM HV) iii) ball milled for 6 hours at low velocity (M6 LV) iv) ball milled for 6 hours at high velocity (M6 HV), were also compared, in terms of CER, with popular cavitation resistant coatings like WC-CoCr and Stellite-6. The raw powder was prepared by water atomization technique. The cavitation erosion resistance of all the coatings, in terms of mass loss, was evaluated using indirect vibratory cavitation testing method with exposure time 480 min, stand-off distance 0.5 mm, amplitude 50 μm and frequency 20 kHz. It has been reported that the cavitation erosion resistance of M6 HV is comparable with Stellite-6 and WC-CoCr due to the high velocity and ball milling, which results into strong bonding between splats and less porosity. The defects such as pores and oxides located in splat boundary regions offers the initiation sites for cavitation erosion in deposited coatings. The comparison of mass loss, as a function of time, of all the studied samples is shown in Figure 2.2.

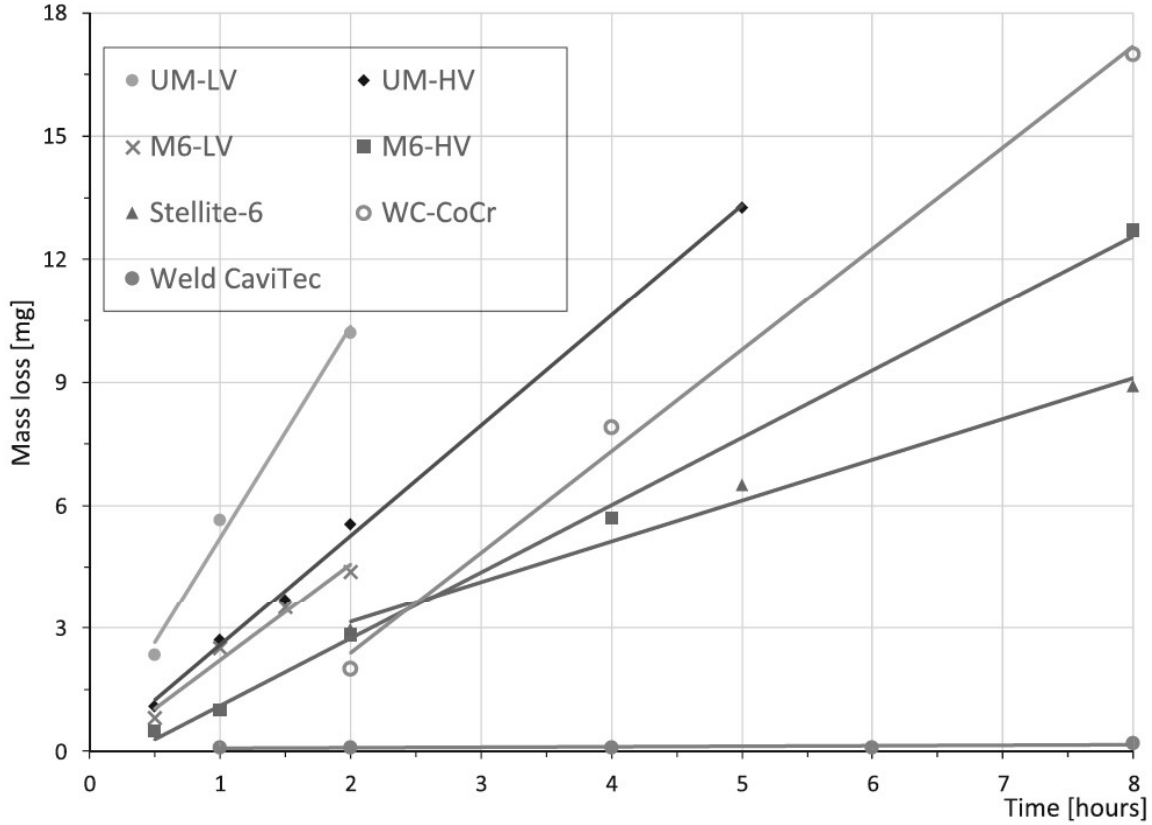

Figure 2.2: Graph of mass loss versus exposure time of all the studied samples [89]

Peng et al in 2017 [90] investigated the behaviour of pits initiation of Fe- based and stainless steel-reinforced amorphous composite coatings. The various electrochemical approaches such as electrochemical noise, polarization and scanning kelvin probe were used to investigate pitting behaviour. The experiments were carried out in 3.5 wt. % NaCl solution. The pitting mechanism is investigated by comparing the microstructure of the composite coating. The immersion and electrochemical tests confirm the deterioration in corrosion resistance of composite coatings. Also, the in-situ observations indicate the interfaces between amorphous matrix and stainless steel as pits initiation sites. The SS particles tend to oxidation during thermal spraying processes, which results into formation of nanosized Fe_3O_4 particles at interface of SS phase/matrix. These nanosized Fe_3O_4 particles contribute for high electrochemical activity of composite coatings. Therefore, after immersion for 15 days, the corrosion weight loss of composite coatings was approximately 3 times higher in comparison with monolithic amorphous coatings.

Kumar et al in 2016 [91] investigated the relationship between the variation in velocity of parameters such as spray particle and the cavitation erosion resistance of 86WC-10Co4Cr coatings deposited on SS 410 grade steel by using HVAF and HVOF technique. The spray particle velocity for HVOF was kept constant (680 m/s), while for HVAF three values of

velocity (865, 960, 1010 m/s) were used. The deposited coatings of 410 µm were characterized for microhardness, porosity, phase analysis, fracture toughness and cavitation erosion resistance. The indirect vibratory cavitation testing method was used to evaluate the cavitation erosion. The coatings deposited by HVAF technique performs better than HVOF, in terms of hardness, porosity and cavitation erosion. In particular, the HVAF coating deposited at highest spray particle velocity (1010 m/s) exhibits highest microhardness (1473±40 HV), least porosity (0.52±0.13%) and CER 3 times higher than HVOF coatings. The possible failure of HVOF coatings in the form of delamination is mainly caused by the microcracks of matrix that propagates along WC grain boundaries and pull the WC particles from matrix. While, the CoCr matrix phase formed in HVAF coatings provides higher crack resistance. The hardness and porosity are also reported as significant factor in improvement of CER.

Hong et al. in 2016 [92] fabricated the FeCrSiBMn amorphous/nanocrystalline and conventional WC-10Co-4Cr coatings through thermal spraying technique (HVOF) to investigate the synergistic effect of cavitation erosion and corrosion. The cavitation erosion-corrosion experiments were conducted through magnetostrictive-driven cavitation facility in 3.5% NaCl solution. The authors concluded that the microcracks and pores act as prefabricated cavitation erosion pits and corrosion starts from these sites, which results into high volume loss rate. However, the damage of WC-10Co-4Cr coatings in comparison with FeCrSiBMn amorphous/nanocrystalline is more due to corrosion component. The authors also concluded that the effect of significant damage of both the coatings is mainly caused by pure cavitation erosion.

Hong et al. in 2015 [93] prepared the WC-10Co-4Cr coatings using thermal spraying technique to investigate the behaviour and mechanism of cavitation erosion. The experiments were conducted using vibratory cavitation testing method using 3.5% NaCl as test liquid. The microstructure and porosity of deposited coatings were evaluated. The deposited coating of 200 µm thickness was found dense and with uniform and compact interface with substrate. The average porosity of coated region was reported 1%, however, some regions were observed with high porosity. Similar to numerous previous studies, the microcracks and pores are found responsible for initiation of cracks, which propagates and joined together to form crater. The possible wear mechanisms for the failure of coatings are concluded as i) brittle detachment of hard phases ii) erosion of binder phases and iii) formation of pitting corrosion. However, the prepared coatings perform 1.27 times better than substrate.

2.2.2 Enhancement of cavitation erosion resistance using laser as a heating source

The electromagnetic energy (like laser) is widely used for surface modification to enhance CER. The different laser processing methods such as cladding, laser sintering, laser surface melting and laser surface alloying, have been successfully used to increase the CER. The laser cladding provides better control over dilution and finer microstructure.

Zhang et al. in 2021 [94] used laser cladding and supersonic laser deposition technique to develop the clads of Stellite-6 on 17-4 PH stainless steel substrate. Different characterization techniques such as XRD, EBSD, SEM, OM, Vicker's hardness and nano-indentation were used to characterize the developed clads. The comparative CER performance of developed clads was investigated by vibratory cavitation apparatus using 3.5% NaCl as test liquid. The results show that clads developed by supersonic laser deposition technique performs 3.5 times better than laser cladding in same experimental conditions. The reasons attributed to the higher CER were the grain refinement, higher hardness and low dilution rate. However, the clads developed by supersonic laser deposition technique possess higher porosity than laser processed clads; and also, the pores act as initiation sites for cavitation erosion wear; the combined effect of low dilution rate, high hardness and grain refinement results in lower value of cumulative mass loss.

Bao et al. in 2021 [18]made an attempt to improve the cavitation erosion resistance of Q235 steel by deposited the coatings of the high entropy alloy $FeCoCrNiB_{0.2}$+ xWC (where x is 0%,10% and 20% by wt.) by using laser cladding. The effect of addition of tungsten carbide (WC) on microhardness and cavitation erosion was investigated. The Vicker's microhardness tester and vibratory cavitation apparatus was used to check microhardness and cavitation erosion wear, respectively. Both distilled water and 3.5% NaCl solution were used as test liquid to check the cavitation erosion resistance of developed clads. The highest microhardness and least cumulative mass loss was exhibited by the clads with highest concentration of WC (20% by wt.). The reason attributed to higher mass loss in the clads with lower concentration was the presence of chloride ions, which associate with cavitation erosion; and combined effect of corrosion-cavitation erosion accelerates the damage. By the addition of WC up to 20% by wt., the depth of pits reduced significantly and helped to weaken the effect of cavitation damage.

Yin et al. in 2020 [22] used electromagnetic energy (laser) to deposit claddings of high entropy alloys (AlCoCrxCuFe) on AISI 304 substrate. The percentage of Cr was varied (0.5,1,1.5 and 2) to study the effect of variation on phase transformation, micro-mechanical properties, microhardness and cavitation erosion resistance. The microstructure study of developed coatings of HEAs showed the duplex phase of BCC and FCC. The gradual increase in FCC

phase content with increase in Cr content was observed by the authors. The microstructure study showed the dendritic structure in BCC phase and interdendritic structure in FCC phase. It was observed that the increase in Cr content also increases the volume loss rate and the best cavitation erosion resistance was observed in AlCoCr0.5CuFe HEA. The results of volume loss rate against exposure time of all the samples are presented in Figure 2.3.

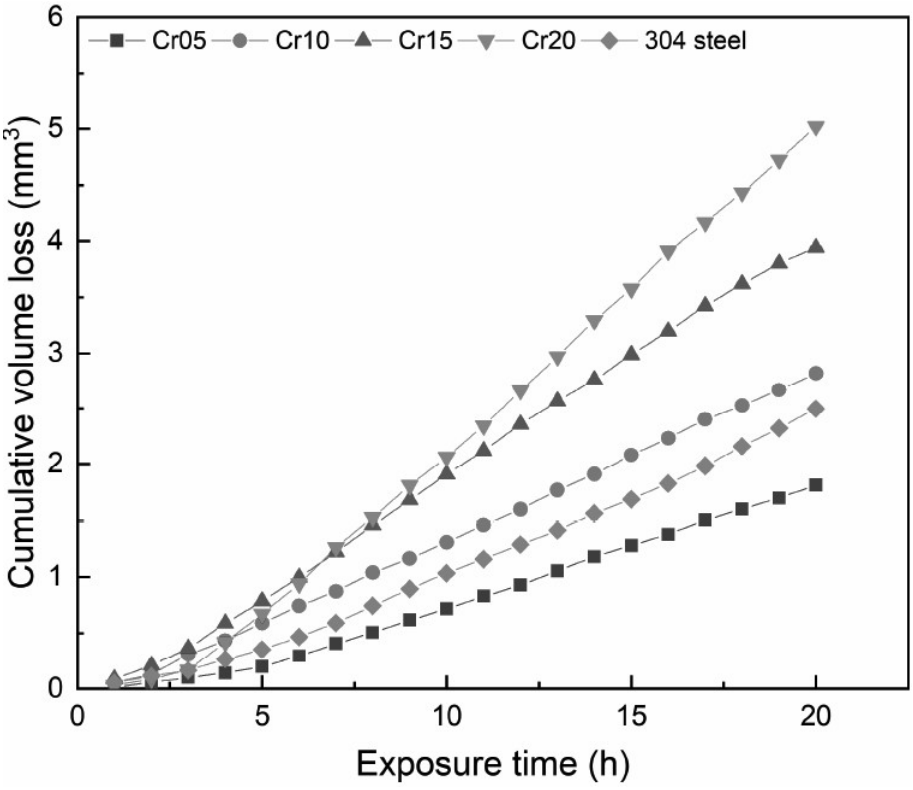

Figure 2.3: Cumulative volume loss versus exposure time graph of all the samples [22]

E et al. in 2019 [95] produced nickel-based and cobalt-based clads using TIG welding and laser cladding techniques. The produced clads were compared in terms of cavitation erosion (CER) and slurry erosion resistance (SER). The microstructure, phase constitution, elastoplasticity and hardness of all the developed clads were also analysed. The results exhibited that the CER of cobalt-based clads is higher (2.5 times) than nickel-based clads. On the other hand, the nickel-based clads perform extremely well (8.4 times) than cobalt-based clads in the terms of SER. The repeated impingement of micro jet flow results into the transformation in phase from the γ-Co to ε-Co of cobalt – based clads. This leads to dissipation of impact energy and higher CER than nickel-based clads. Contrary, in the slurry erosion the damage was governed by the cutting and ploughing action due to the impingement of sand particles at small impact angles. Therefore, without the phase transformation, the low hardness and elastoplasticity of cobalt-based clads be the cause of low SER of cobalt-based clads than nickel-based clads.

Hardes et al. in 2019 [96] investigated the cavitation erosion resistance of the selective laser melted SS-316L steel. It was observed that increase in hardness and yield strength of selective laser melted SS-316L steel results in significantly increase in incubation period. The increase in hardness was attributed to the finer grain size and increased dislocation density. XRD study after cavitation testing exhibited the development of compressive stresses in severe form. These also emerge after some time (a few seconds) of cavitation testing. However, due to these compressive stresses, restricts the immediate propagation of micro cracks. Also, the microstructure and damaged surface morphology highlighted the emergence of coarse grains, which leads to increase in surface roughness, increase in cavitation impact and local stress concentration.

Girelli et al. in 2018 [97] conducted the experiments to compare the cavitation erosion resistance of AlSi10Mg samples; manufactured by traditional casting process and Direct Metal Laser Sintering (DMLS) additive manufacturing process. The prepared samples were tested in different testing conditions in order to investigate the effect of T6 heat treatment and hot isostatic pressing (HIP) for DMLS; and in as-cast and T6 heat treatment conditions for traditional cast samples. The vibratory cavitation testing method (ASTM-G-32) was used for cavitation erosion testing. The samples produced by DMLS technique shows high CER and longer incubation period than traditionally cast samples. The ultra-fine microstructure of DMLS processed samples restricts the dislocation motion; and ultimately the significant less material loss value is reported. The heat treated samples showed less CER due to the coarsening of microstructure and increased porosity. However, the application of HIP results into reduction of detrimental effect of T6 heat treatment and lesser mass loss was recorded. The cumulative mass loss of all the samples after 1 hour and 8 hours is presented in Figure 2.4.

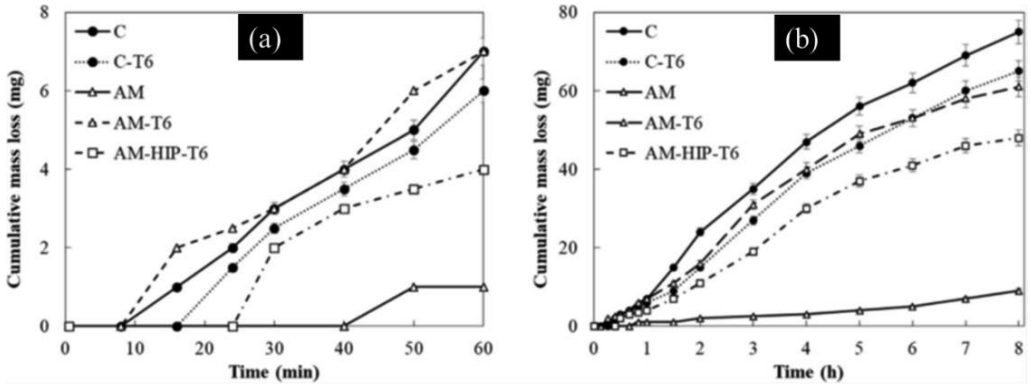

Figure 2.4: CML versus exposure time a) from 0 to 60 min b) up to 8 hours [97]

Wu et al.in 2017 [98] used the laser surface alloying method to deposit the coatings of high entropy alloys (FeCoCRAlNiTiX) on SS-304 substrate using laser surface alloying method.

The titanium was added and molar ratio was varied from 0 to 2 in order to investigate the effect of variation on cavitation erosion and corrosion resistance. The distilled water and 3.5% NaCl were selected as test liquid. The increase in Ti content influences the microhardness in the straight manner. The microhardness with highest Ti content alloy was found almost 3.6 times more than substrate. The presence of intermetallic leads to higher fracture and deformation resistance, which help to increase the cavitation erosion resistance of HEA than substrate in distilled water. On the other hand, the intermetallic act as cathodic phase, which reduces the microcell corrosion and results into poor corrosion resistance of HEA in 3.5% NaCl solution. Therefore, HEA coatings shows less CER than substrate in 3.5% NaCl solution. The mean depth of erosion, against the exposure time, results of all the samples are shown in Figure 2.5.

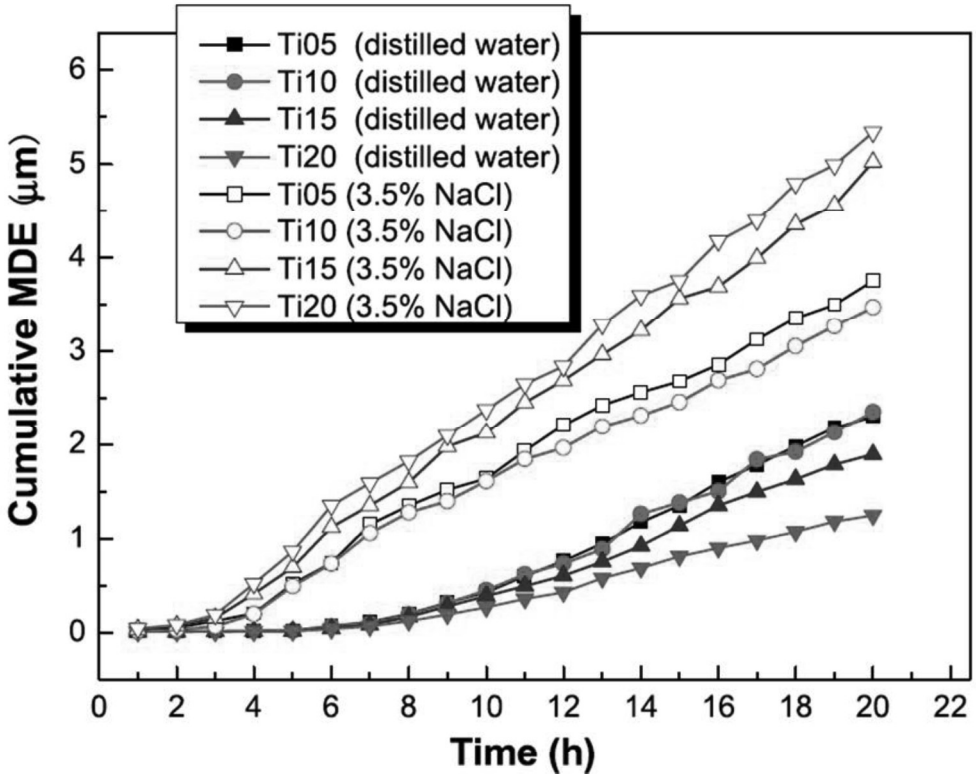

Figure 2.5: Cumulative mean depth of erosion versus exposure time graphical representation of all the samples [98]

Zhang et al. in 2016 [99]aimed to improve cavitation and corrosion resistance by developing NiCrSiB layer on Monel 400 using laser cladding technique. The developed clads were characterized for microstructure, chemical compositions, microhardness and phase constituents. A potentiodynamic polarization measurement and ultrasonic vibrator was used to evaluate the corrosion and cavitation erosion resistance, respectively. The results show that a hard layer with less defects such as air holes and cracks can be developed by varying the laser fluence. The developed clads (850 HV) exhibits almost 6.8 times more microhardness than the

Monel 400 substrate (125 HV). The developed clads perform better than substrate in both cavitation erosion and corrosion environment. The reason attributed for higher cavitation erosion resistance was combination of high hardness and toughness.

Singh et al. in 2014 [100] developed clads of stellite-6 on 13Cr - 4Ni steel using laser as heat source. The clads were developed at varied energy densities of laser i.e. 32, 37, 46 and 52 J/mm^2. The developed clads were tested for cavitation erosion and solid particle erosion. The developed clads, at varied laser energy densities, have been characterized for dilution, clad geometry, microhardness and microstructure. The highest microhardness (705 HV) of developed clad of thickness 1 mm was reported at 32 J/mm^2. The minimum dilution (4.48%) was reported at 32 J/mm^2. However, a sharp increase in dilution percentage with increase in energy density was also observed. Also, the CER and SPE of clads developed at 32 J/mm^2 was maximum. The damaged surface morphologies at different energy densities and untreated sample has been shown in Figure 2.6.

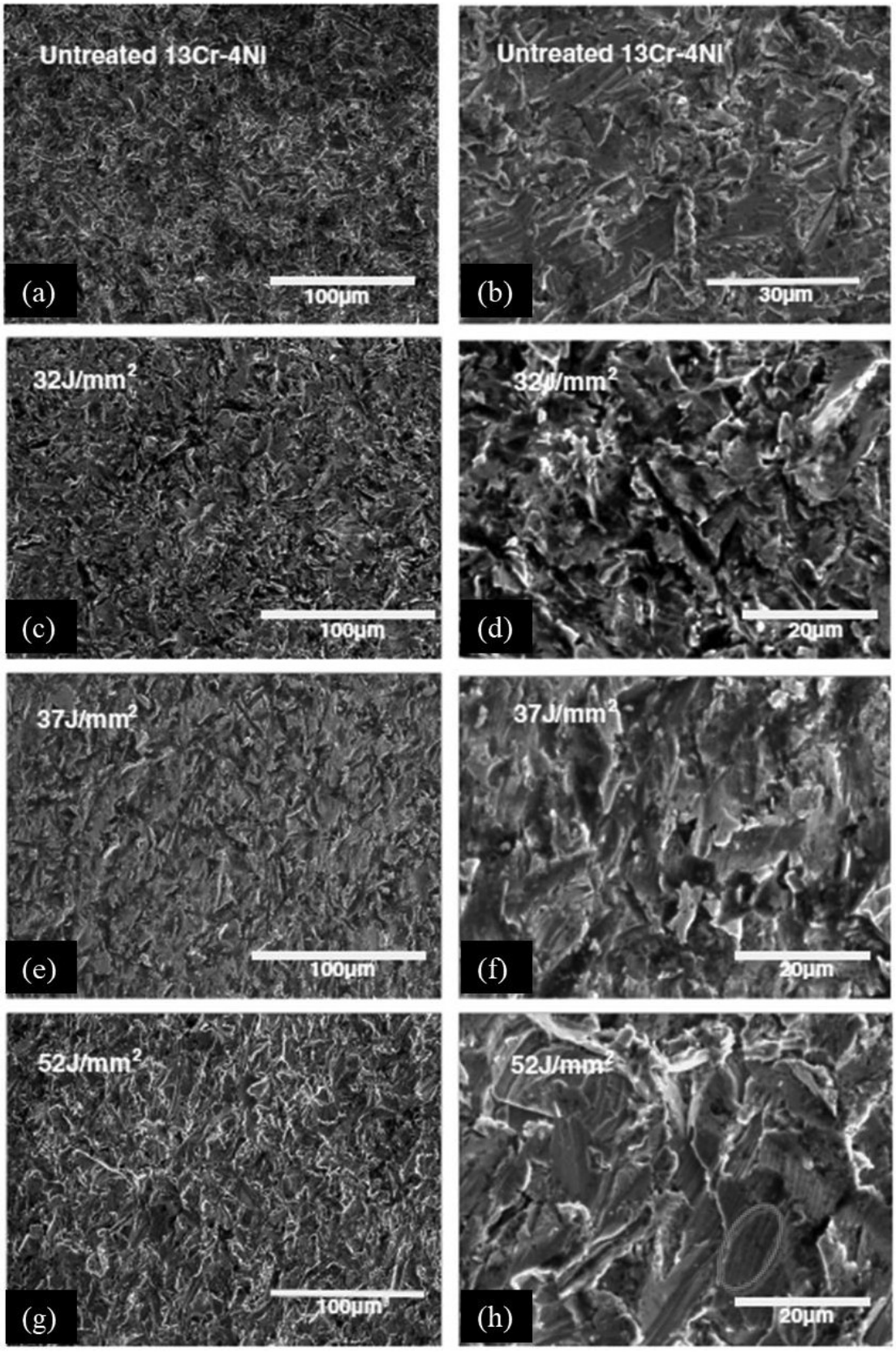

Figure 2.6: Damage surface morphologies at lower and higher magnification of a), b) untreated samples c), d) clad samples at 32 J/mm^2; e), f) clad samples at 37 J/mm^2; g), h) clad samples at 52 J/mm^2 [100]

Paul et al. in 2014 [101] investigated the wear behaviours of Laser processed Mecto41C (iron base alloy), stellite6 (Co-based alloy), and Colmonoy5 (nickel base alloy) claddings on stainless steel (SS 316L). The laser cladding was optimized using a 3.5 kW CO_2 laser-based system. The process parameters such as powder feed rate, scan speed, gas flow rate and laser power were found critical and experimentation was carried out to find the optimized parameters. The authors did not observe any significance difference in microhardness between single layer and double layer clads. However, the bonding and dilution of single layer clads were not satisfactory. The optimized process parameters (laser power- 1.6 kW, powder feed rate- 8 g/min, and scan speed- 0.6 m/min) were used for final experimentation. The cavitation erosion resistance of stellite-6, Metco-41C, and colmonoy-5 has been increased by 4.1, 3.7, and 1.6 times than substrate.

The literature survey shows that HVOF and laser processing techniques are well developed and used extensively to enhance CER, but, these techniques possess limitations (discussed in detail in section 1.5). Therefore, a novel material processing technology is required to overcome the existing limitations of currently used technologies.

2.3 Microwave Processing of Materials

The microwave energy can be effectively used as a heating source for processing of materials. This has the potential to overcome limitations of earlier used technologies. Earlier, most of the researchers focused on microwave processing of ceramics and cermet, because the absorption of microwave radiation by some ceramics, even at the ambient temperature, promotes diffusion rate at lower temperatures, which results in better mechanical and metallurgical properties [102], [103]. Also, it was a myth earlier that metals do not absorb microwaves. **Walkiewicz et al.** (1988) [104] and **Narasimhan et al.** (1995) [105] exposed the metals to microwaves at 2.45 GHz frequency in microwave oven, and reported the moderate heating from 120º to 768º C and 370º for Fe-alloys, respectively. Later, the researchers explored the opportunities in the field of microwave processing of metallic materials. However, the ceramics can't be replaced fully by metals and vice versa. The inherent properties of ceramics still attract the researchers and a lot of engineering applications need the combined properties of both metals and ceramics. Hence, the metal matrix composites can be a plausible solution to get the desired properties. The use of microwave energy to process metals and MMCs has been briefly discussed in this section.

2.3.1 Microwave sintering of metals/MMCs

Sintering process involves the compacting of loose powder and then heating it below the melting temperature to make a solid object. In past, the compact powder was sintered through resistance heating. In the recent years, the sintering of various materials has been successfully achieved using microwave as a heating source. The sintering of various materials was achieved in shorter processing time with better microstructures. The first successful sintering of metallic materials was reported by **Roy et al. in 1999** [66]. The authors successfully processed Fe + Cu (2%) + graphite (0.8%) metallic samples for 30 minutes at 1200º C in microwave field. **Cheng et al. in 1999** [106] used the microwave hybrid heating technique to successfully sintered the diamond-CuTi composites. The authors used SiC cavity with 2% starch and ZrO2 powder as microwave susceptor and insulation materials. The well bonded diamond particles with CuTi matrix with no traces of graphitization of diamond particles were reported by the authors. In recent studies, **Honnaiah et al. in 2017** [107] used microwave technology to process Al-SiCp metal matrix composites. The processed composites were studied for tribological characteristics (sliding wear) using pin on disc tribometer. The faster processing of composites and improved wear characteristics by addition of reinforcement were reported by the authors. **Ashwath et al. in 2018** [108] fabricated and characterized the AA2024 and AA2090 MMC's of SiC and Al_2O_3 as reinforcement in varying percentage (3,6,9) %. The processing through microwave route was reported beneficial to enhance the mechanical properties and refinement in microstructures. The authors reported that Al_2O_3 as compared to SiC had more effect on hardness, for the both composites, due to better bonding. **Himyan et al. in 2018** [109] used the microwave sintering technique to synthesize the Al matrix composites with addition of SiC nanoparticles (0.3, 0.6, and 0.9 vol.%) as reinforcement. The processed composites were investigated for the conductivity behaviour, physical, microstructure and mechanical properties. The compression strength and yield strength were also investigated. It has been reported that addition of reinforcement results better mechanical properties and the processed composites were found suitable for industrial and manufacture applications. **Rumman et al. in 2019** [110] sintered two distinguished types of WC-Co samples, with the help of microwave energy, at varying temperatures. The authors suggested that the energy transfer at atomic level significantly helps in improvement in quality of sintered product. The overall reduction in energy consumption and increment in toughness and hardness is also reported by the authors. **Prakash et al. in 2020** [111] successfully fabricated the porous Ti50Nb50−xHAx (x = 0, 10 and 20) composites using microwave sintering technique. The effect of input process parameters, such as weight percentage of hydroxyapatite, sintering temperature and

compacting pressure, was analysed on the compressive strength, structural porosity, and elastic modulus of sintered composite. The pores of 20-30 μm in size helps to enhance the bioactivity of material and also reduces the elastic modules of sintered product. The properties like highly porous structure, high compressive strength, low elastic modules along with enhanced corrosion resistance and bioactivity make the sintered product a suitable candidate for orthopaedic applications. **Kumar et al. in 2020** [112] optimized the range of microwave sintering parameters in order to achieve the better mechanical and physical properties of magnesium-based metal matrix composite (Mg3Zn1Ca15Nb). Also, the effect of independent parameters on physical/mechanical properties was investigated. It was reported that increase in heating rate helped to reduce micro cracks and agglomeration of heavier particles; which results into improvement of sintered density and ultimate compressive strength. The increase in sintering temperature significantly reduces the porosity. The holding time till 40 min results into formation of highly dense structure. **Kumar et al. in 2021** [113] successfully sintered the hybrid aluminium metal composite (h-AMMC) with varying percentage of MWCNT reinforcement using microwave hybrid heating technique. The sintered composites were tested for mechanical and tribological properties. The authors reported that the MWCNT played a significant role in the hardness improvement of the h-AMMCs. Wear and friction properties of h-composite found better than aluminium matrix and Al- SiC composite.

2.3.2 Microwave joining of metals/MMCs

The permanent joining of materials found wide applications in manufacturing and assembling industries. Welding, soldering and brazing are widely used conventional techniques for joining in industries. These techniques are associated with some limitations in regard to processing time, joint characteristics, environmental issues, easy processing and materials to be joined. To overcome above limitations, joining of materials using microwave energy is successfully achieved by many researchers in past. **Siores and Rego in 1995** [114], reported the successfully brazing of thin sheets of steel, ranging between 0.1 to 0.3 mm in thickness, using a magnetron of 2 kW. **Srinath et al in 2011** [70] reported the successful joining of bulk copper plate and bar of dimensions 15 mm × 12 mm × 4 mm and 12 mm × ø18 mm, respectively. Despite the fact that the copper is difficult to join by conventional methods due to its high heat conduction capacity, the complete melting of Cu powder layer of thickness 0.5 mm, placed between the two candidate materials, and metallurgical bonding with substrate material was successfully achieved in a domestic microwave oven of 900 W power and 2.45 GHz frequency. The observed porosity and hardness in the joint were 1.92% and 78±7 HV. The same authors

in the same year extended their research for other materials also and reported successful joining of bulk SS-316 in the domestic microwave oven[115]. The value of microhardness at interface was observed as 420±15 HV and average value of microhardness in joint was observed as 290±15 HV. The authors also conducted the experiments for successful joining of dissimilar metallic materials and reported the successful joining of bulk SS 316 and mild steel (MS) [116]. The findings of their work consists the well fused faying surfaces and metallurgical bonding with either side of substrate surface. The evidences of metallic carbides and cementite formation were found by the XRD study. The high hardness (133 HV) and less porosity (0.58 %) in the joint region was reported. **Bansal et al. in 2013** [117] successfully joined the MS plates through microwave hybrid heating route using Ni powder, in between the plates, as interface layer. The significant increase in microhardness (420 ± 30 HV) and complete melting of interface layer, which formed metallurgical bond between MS plates and interface powder particles, was reported. **Gupta et al. in 2015** [118] reported the successful joining of bulk cast iron. The presence of iron oxide phases in the joint region confirmed the intermixing of elements and supported the claim of metallurgical bond between the powder and substrate surface. **Gamit et al. in 2017** [119] studied the influence of interface powder particle size on the heating mechanism. It was reported that the heating of interface layer, for good fusion of candidate material with interface layer, can be improved by decrease in particle size. The increase in hardness of joint region (572 HV) than the base metal (397 HV) was observed. **Singh et al. in 2018** [120] successfully joined the Hastelloy through MHH route. The authors reported that the joint region was defect and crack free; and cellular grain growth in the joint region was observed. The unique nature of volumetric heating of MHH was reported as prime cause for finer microstructure. **Bansal et al. in 2019** [121] achieved butt joining of Alloy-718 in industrial microwave oven. The weldments joined by MHH technique reveals complete melting of powder particles and perfect diffusion bonding between parent materials. The heat treatment of fabricated weldments with conventional methods was carried out. The authors found the post heat treatment beneficial for increase in microhardness of fusion zone due to dissolution of the Laves phase. **Pal et al. in 2020** [122] used MHH technique to join SS-304 and SS-316 at optimized parameters. The authors also investigated the effect of input parameters such as type of material, processing time and grain size of filler material on the output parameters such as micro hardness and micro tensile strength. The grain size of filler material was found most influential parameter after type of material. The processing time was found least influential input parameter in this domain of study. The dense metallic microstructures in joint region were found helpful for improvement in microhardness and

micro tensile strength. **Samyal et al. in 2021** [123] successfully joined the lap joint specimens of SS202-SS202. The authors also modified the crucible setup, for better masking, to avoid arcing during heating process. The characteristics result show that joints produced at optimized parameters exhibit better bonding. The voids created by evaporated epoxy were filled by melted nickel powder with increase in exposure time. However, the amount of both the powders also played a decisive role in filling the cavities. The increase in exposure time failed to fill the voids when amount of epoxy was greater than nickel powder.

2.3.3 Microwave casting of metals/MMCs

The metal casting process is the primary and economical processes to produce useful components in industries. The conventional methods of casting are associated with certain limitations like unusual longer melting times, higher defects and higher energy consumptions. The researchers minimised the above-mentioned limitations, up to some extent, with use of non-conventional (laser melting) techniques, but, high set up costs of these non-conventional methods motivated the researchers to investigate novel low cost technologies that can deliver clean and green energy. **Singh et al. in 2016** [124] introduced a novel process on the development of metal ceramic castings using microwave hybrid heating technique. The same authors in the same year reported the successful development of composites castings of EWAC (Ni based metallic powder) and SiC powder as matrix and reinforcement, respectively, using microwave heating[125]. The developed castings exhibit the uniform dispersion of reinforcement with uniform equiaxed grain growth. The higher value of microhardness (920±28 HV) and lower value of porosity (1.7%) was reported. **Gouthama et al. in 2017** [126] melted bulk tin (60Sn40Pb) in conventional muffle furnace and microwave oven to compare the mechanical properties. It has been observed that microwave processed specimen perform better than muffle furnace processed specimen in terms of tensile strength (10 % higher) and microhardness (19.28% higher). **Lingappa et al. in 2017** [126] conducted experiments to study the parameters such as consumption of energy, time and material wastage by melting the non-ferrous metallic metals in microwave oven and conventional muffle electric furnace. The successful melting of aluminium, zinc, brass and tin using MHH was reported. It was reported that the microwave melting process consumed significantly less time and energy with much lesser material wastage. The volumetric heating nature of MHH helped to achieve lesser material wastage due to involvement of reduced thermal gradient. **Mishra et al. in 2018** [127] studied the role of formation of oxides during microwave heating. The effect of oxides formation in ambient temperature inside the mould cavity of three target materials aluminium,

copper and SS-316 was studied. It was reported that formed oxides influences the heating of exposed target materials. The reduction in heat transfer at low temperature is caused by formed oxides, whereas, at elevated temperature these formed oxides helped in absorption of microwaves. **Mishra et al. in 2018** [128] studied the effect of processing conditions on mold preheating, charge melting, and cast microstructure. The Al 7039 alloy was cast inside the three different applicators A1 (900 W), A2 (1400 W), and A3 (3000 W) and mold temperature was analysed. The experimental and simulation results showed comparable agreement (error within ±5%). It was observed that the cast structure highly depends upon solidification conditions. **Singh et al. in 2019** [129] successfully melted the nickel based (EWAC) and silicon carbide (SiC) reinforced metal matrix composite using microwave energy. The experiments were conducted using domestic microwave oven and MMC's with varying percentage of SiC were melted. The volumetric heating property of microwave energy helps in formation of fine equiaxed grains. The uniform dispersion of SiC particles inside EWAC matrix, formation of silicides and carbides and grain strengthening mechanism were found helpful in increase in microhardness. The fractured sample after tensile test was examined and it was observed that addition of SiC reinforcement shifts the fracture mode from ductile to mixed (brittle+ductile). **Singh et al. in 2020** [130] extended their previous work and explored the dry sliding wear behaviour of EWAC based and X%SiC reinforced MMCs processed through microwave energy. The mechanisms involved for degradation of material were also investigated. The authors reported that the formation of oxide based tribo-layers help in reduction in weight loss by avoiding the direct contact; and as a barrier between the surfaces. The weight loss mechanisms were significantly affected by variation in sliding velocities. The authors observed that after 1000 m sliding distance the rate of weight loss was stable as compared to higher weight loss rate at initial run. The increase in normal load also increases the rate of weight loss. **Gangwar et al. in 2020** [131] melted the AA-6063 using microwave hybrid heating technique and investigated the effect of three process parameters; i.e. solidification environment, microwave power and susceptor material on the hardness of cast AA-6063.The authors used Taguchi L9 orthogonal array for experimentation. The maximum hardness was reported at 900 W power; susceptor material was SiC and cast was placed outside the cavity for solidification.

2.3.4 Microwave processed metallic/MMCs claddings on metallic substrate

Since a long time, the metallic claddings on metallic substrate were not feasible due to the reflection of microwaves at room temperature by the metallic materials. The interaction of metallic materials with microwaves is highly depends upon a critical term "skin depth". The

skin depth, in simple terms, is depth upon which the microwaves can penetrate without losing their significant power. The skin depth is inversely propositional to the electrical conductivity of material. Therefore, the highly conductive metals are challenging to process through microwave at room temperature. To tackle this problem, **Gupta et al. in 2010** [132] filed an Indian patent for a new technique, microwave hybrid heating for development of claddings of metallic and non- metallic powders on metallic substrate using microwave as a heating source. The authors successfully developed the clads of EWAC (Ni-based powder) on steel substrate (SS 316) through MHH. The well metallurgical bonded clads of 1 mm thickness were observed as without any visible discontinuity and interfacial cracks. The presence of distinguished phases such as $Cr_{23}C_6$, $FeNi_3$ and NiSi was confirmed and the average microhardness in the clad region was observed as 304 ± 48 HV. Gupta et al. in 2011 [133] also developed the clads of Cu material on steel substrate (SS 316) using MHH route. The developed clad were homogenous, uniform and dense. The observed microhardness in the clad region was 270 ± 30 HV. **Zafar et al. in 2013** [134] reported the successful development of inconel 718 on steel substrate (SS 304) using MHH method. The clads were developed inside a domestic microwave applicator of 2.45 GHz frequency and 900 W power. The processing time was reported 720 s. The defects (pores, interfacial cracks) free clads with the formation of phases of chromium carbides and Ni_3Ti, in the clad region, were reported. **Gupta et al. in 2014** [135] reported the development of tungsten carbide (WC) based WC10Co2Ni cermet powder on SS-316 substrate through MHH route inside a domestic microwave applicator. The presence of uniformly distributed tungsten particles and carbides in the clad region is attributed to increase in microhardness of the clad region. **Kaushal et al. in 2016** [136] successfully developed the EWAC based and SiC (10% by wt.) reinforced clads on SS 420 substrate in domestic microwave oven. The authors reported that clads of ~1.25 mm thickness were developed in 720 s. The well metallurgical bonded and defects free developed clads exhibit average microhardness as 652±90 HV. **Singh et al. in 2018** [137] reported the successful development of EWAC+10% Al_2O_3 composite clads in microwave exposure time of 300 s on SS 304 substrate. The randomly dispersed hard facing particles(Al_2O_3) inside the tough nickel matrix were confirmed from microstructural analysis. The developed clads show 3.5 times more average hardness value than substrate. **Mago et al. in 2020** [138] reported the successful development of EWAC+40 Cr_3C_2 composite clad. The defect free clads exhibits excellent average microhardness (605±80 HV) along with high flexural strength (813.23±16.29 MPa) and fracture toughness (7.44±0.2 MP√m). The crack free and less porous clad region was attributed to high flexural strength and fracture toughness.

The Figure 2.7 shows, the use of the different types of hard reinforcements to produce composite clads. It shows that the development of microwave processed composite clads for different applications has a wide scope as per their requirements or need for working environment.

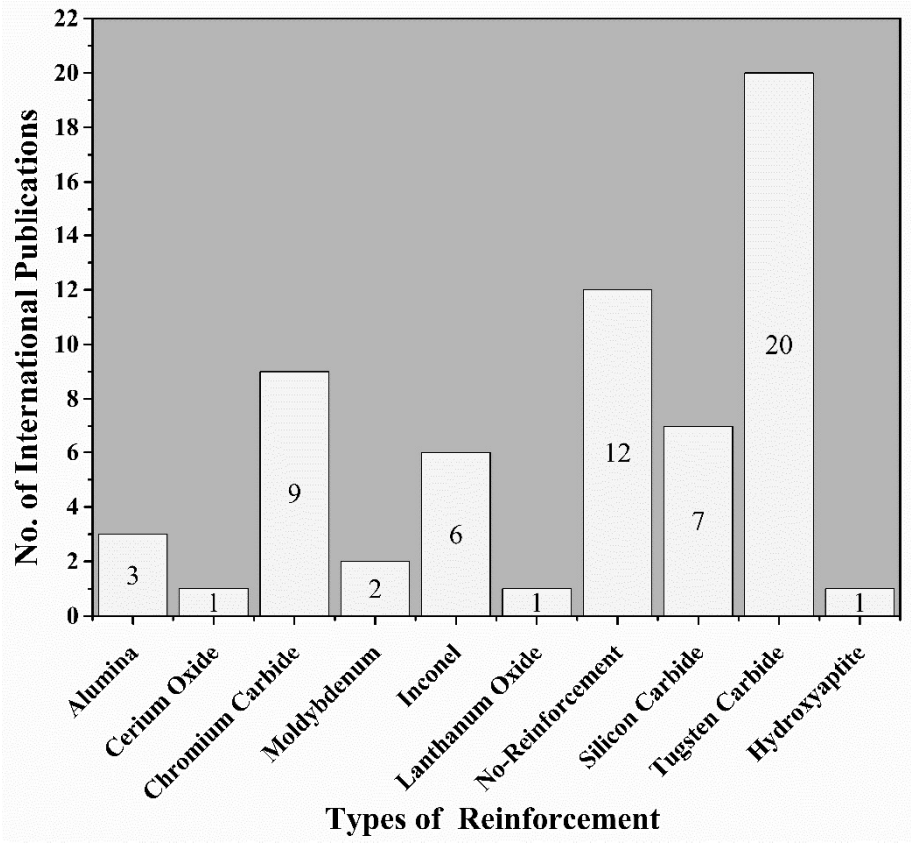

Figure 2.7: Bar chart showing the different type of reinforcement used to develop microwave processed clads

2.4 Tribological Performance Study of Microwave Processed Clads

The microwave processed clads have been tested for different tribological applications. **Gupta et al. in 2011** [139] developed WC10Co2Ni clads on SS 316L substrate. The developed clads of thickness approximate 2 mm exhibit significantly less porosity (0.89%) and high average microhardness (1064±99 HV). The developed clads were tested for sliding wear and it has been reported that resistance to sliding wear of clad surface had increased by 84 times. The summary of available literatures on the various tribological studies investigated by various researchers/academicians is further presented in the tabular form (Table 2.1) for better understanding.

Table 2.1: The available literature on different type of wear studies of microwave clads.

S.No.	Paper Title	Author & Year	Substrate Material	Coating Material	Observations & Conclusion	Type of Wear Study Carried Out
1	**Investigation on sliding wear performance of WC10Co2Ni cladding developed through microwave irradiation**	**Gupta et al. 2011** [139]	**SS-316L**	**WC10Co-2Ni**	Developed clads of thickness ~2 mm exhibits average microhardness 1064±99 HV and significantly less porosity (0.89%). Resistance to sliding wear of clad surface had increased by 84 times. The variation in sliding speed does not affect the wear.	**Sliding Wear**
2	**Dry erosion wear performance of Inconel 718 microwave clad**	**Zafar et al. 2014** [140]	**SS-304**	**Inconel 718**	Developed clads of thickness ~1 mm exhibit average microhardness 564±22 HV. The intermetallic phases (Ni_3Ti, Ni_3Al) in the tough nickel rich matrix improved the erosive wear performance of the Inconel 718 clads. The clads perform better at lower impact angle against erosive wear than higher impact angle.	**Erosive Wear**

3	**Abrasive Wear Behaviour of Inconel 718 Microwave Clad**	**Zafar et al. 2014** [141]	**SS-304**	**Inconel 718**	The abrasive wear behaviour of developed clads were analysed. It has been reported that the reduction of approximately 70% in average cumulative weight loss for Inconel 718 clads was observed.	**Abrasive Wear**
4	**Microstructure and Abrasive Wear Performance of Ni-Wc Composite Microwave Clad**	**Bansal et al. 2015** [142]	**Mild Steel**	**Ni-WC**	The clads of thickness 1 mm at 2.45 GHz frequency and power 1.1 KW were developed. The average microhardness (1028±90 HV) of the clad layer was observed. The developed clads show 70% higher wear resistance than the mild steel substrate. The XRD spectrum of the deposited clad indicated the presence of WC, W_2C, Ni_2W_4C, Fe_6W_6C, $FeNi_3$, NiSi, and Fe-Cr-Ni.	**Sliding Wear**

5	**Dry sliding wear performance of nanostructured WC – 12Co deposited through microwave cladding**	**Zafar et al. 2015** [143]	**SS-304**	**Nanostruct-ured WC–12Co**	The micrometric and nanometric clad powders of WC–12Co were used to develop clads using MHH technique. Clad Thickness – 1 mm. The observed value of microhardness of nanometric clad layer was more (1564±53 HV) than the micrometric clad layer1138±90 HV. The high volume fraction of nanocarbides were uniformly distributed in the clad region which results into ~54% high resistance to sliding wear.	**Sliding Wear**
6	**On Friction and Wear Behaviour of WC-12Co Microwave Clad On Friction and Wear Behaviour of WC-12Co Microwave Clad**	**Zafar et al. 2015** [144]	**AISI 304**	**WC-12Co**	The reduction of 67% and 56% in wear rate and friction coefficient, for WC-12Co microwave clad of thickness ~1 mm in comparison of AISI 304 substrate, was reported by the authors. The low friction coefficient in the case of WC-12Co clads can be attributed to the high hardness.	**Sliding Wear**

7	**Prediction of Tribological Behaviour of WC-12Co Nanostructured Microwave Clad through ANN**	**Zafar et al. 2016** [44]	**SS-304**	**Nano-structured WC–12Co**	The prediction of coefficient of friction and wear rate of microwave processed conventional-WC and nanostructured-WC clads were carried out using ANN model. Three input variable chosen for ANN model were nature of reinforcement, sliding distance and normal load. ANN model predicted the coefficient of friction and wear rate with good accuracy. The analysis of worn samples of CWC clad reveals deeper wear, whereas, for NWC microwave clad it was relatively smooth. This indicates the higher sliding wear resistance.	**Sliding Wear**
8	**Abrasive and erosive wear behaviour of nanometric WC – 12Co microwave clads**	**Zafar et al. 2016** [19]	**SS-304**	**Nano WC–12Co**	Microwave processed WC-12Co micrometric and nanometric powder clads were developed on SS-304 and tested for abrasive and erosive wear. The nanometric clads exhibit 1.37 times higher microhardness than micrometric clads. The nanometric clads also perform 1.6 and 3 times better in terms of abrasive and erosive wear behaviour, respectively.	**Erosive and Abrasive Wear**

9	**Microstructure and experimental design analysis of nickel-based clad developed through microwave energy**	**Hebbale et al. 2016** [145]	**SS-304**	**Nickel-Based Clads**	The microwave processed nickel based clads were developed and parameters were optimized by using Taguchi L9 orthogonal array. The crack free structure was developed in which significant less wear rate (0.03363 - 0.03570 g) was found. The slurry speed and impingement angle were reported as most influencing parameters in terms of mass loss.	**Slurry Erosion**
10	**Taguchi analysis on erosive wear behavior of cobalt based microwave cladding on stainless steel AISI-420**	**Hebbale et al. 2017** [146]	**AISI-420**	**Cobalt Based Alloy**	The factors that significantly affect the wear was gauged using Taguchi orthogonal array. ANOVA was used to determine the significant factors. It was observed that slurry speed influenced the most in causing mass loss and size of sand particles and impingement angle were after that for both substrate and clad surface. The different erosion mechanisms of worn surface were observed like fractures, ploughing and micro cutting, which indicates mixed mode of erosion.	**Sliding Wear**

11	**Fuzzy prediction of slurry erosive behaviour of cobalt-based clad developed through microwave energy**	**Srinath et al. 2017** [147]	**AISI-420**	**Cobalt Based Clad**	Taguchi L9 orthogonal array was used to optimize the factors that affect the wear. The effect of factors like slurry speed, particle size and impingement angle were studied and slurry speed was found most significant factor. The widely accepted fuzzy logic modal was adapted to predict the slurry erosive wear behaviour. The obtained results were compared experimental results and comparable error (13.80%) was reported.	**Erosive Wear**
12	**On Microstructure and Wear Behaviour of Microwave Processed Composite Clad**	**Kaushal et al. 2017** [148]	**SS-304**	**Ni + 20% WC8Co**	Developed clad of 1.2 mm thickness exhibit significant higher average microhardness (840±20 HV), and less porosity (1.2%). The significant increase in wear resistance (7 times) was reported. The presence of different phases such as $Cr_{23}C_{6,}$ NiSi, NiCr was confirmed from XRD study.	**Sliding Wear**
13	**On the surface modification of austenitic stainless steel using microwave processed Ni / Cr 3 C 2 composite cladding**	**Kaushal et al. 2017** [149]	**SS-304**	**Ni + 20%Cr_3C_2**	Developed clad of 0.6 mm thickness exhibit significant higher average microhardness (450±55 HV), and less porosity. The significant increase in wear resistance (3 times) was reported. The presence of different phases such as Cr_3C_2, $FeNi_3$, NiSi, Cr_3Ni_2 was confirmed. The reinforcement powder	**Sliding Wear**

					(Cr_3C_2) was uniformly dispersed into soft Ni matrix and form a cellular structure.	
14	**Sliding wear studies of microwave clad versus unclad surface of stainless steel 304**	**Akshata et al. 2018** [150]	**SS-304**	**WC-12Co**	In this study, input parameters such as sliding speed, sliding distance and normal load were selected and using Taguchi orthogonal array, wear studies were conducted. The clad surface performs significant well (0.001g) than unclad surface (0.043g) in terms of wear rate. The transfer of material between clad and counter surface was noticed at higher load (40N).	**Sliding Wear**
15	**On Development and Dry Sliding Wear Behaviour of Microwave Processed Ni / Al_2O_3 Composite Clad**	**Singh et al. 2018** [137]	**AISI 304**	**Ni + 10% Al_2O_3**	The domestic microwave oven was used to develop the alumina reinforced and Ni based clads. Developed clad of 0.6 mm thickness exhibit 3.5 times higher average microhardness (710±45 HV), than the substrate. The sliding wear studies were conducted on pin on disc type tribometer for developed clads. The excellent wear resistance (156 times) has been achieved. The failure analysis shows the craters and groove formation mechanism as responsible wear mechanism for clad material, whereas, plastic deformation was responsible for failure of substrate.	**Sliding Wear**

16	**Processing of Ni – WC – Cr_3C_2 -based metal matrix composite cladding on SS-316L substrate through microwave irradiation**	**Kaushal et al. 2018** [46]	**SS-316 L**	**Ni+ 10%WC8Co+10% Cr_3C_2**	Developed clad of 0.85 mm thickness exhibit 1.6 times higher average microhardness (503±34 HV), than the substrate. The significant increase in wear resistance was reported. The dilution of Fe from substrate results into presence of observed phases $FeNi_3$, Fe_6W_6C, Fe_7C_3, which confirms the metallurgical bonding between clad powders and substrate.	**Sliding Wear**
17	**Investigation of Dry Sliding Wear Behaviour of Ni-SiC Microwave Cladding**	**Kaushal et al. 2018** [136]	**SS-420**	**Ni + 10% SiC**	Developed clad of 1.25 mm thickness exhibit 3 times higher average microhardness (652±90 HV). The presence of different phases such as Fe_2Si, $CrSi_2$, $Cr_{23}C_6$, C_3Cr_7 was confirmed from XRD study. The wear resistance of clad surface had increased by 107 times.	**Sliding Wear**
18	**Microwave synthesized composite claddings with enhanced cavitation erosion resistance**	**Babu et al. 2019** [20]	**SS-316**	**Ni+10%SiC**	Cavitation erosion behaviour of composite claddings (nano, micro and bimodal reinforcement particles size distribution and weight fractions) synthesized using MHH and thermal spray coatings were investigated. Microwave NI-SiC coatings possessed superior degradation resistance. The absence of splat boundaries and high adhesion with substrate led to high cavitation erosion resistance	**Cavitation erosion wear**

					in microwave processed claddings. The microwave processed claddings were crack free and integral interface was free from defects.	

2.5 Literature Gap Analysis

The extensive literature survey has been carried out on the well-investigated/under investigation and matured/recently investigated methods for the development of coating/ claddings by using conventional sources of heating and microwave heating. The literature survey allowed the understanding of technologies and their mechanisms of processing with their limitations. The research work carried out on recently developing microwave processing of metallic materials used in multi-domain, like joining of bulk metals, casting of powders, claddings of hard facing metallic powders on metallic materials and sintering of powders are in investigation stages. The tribological characterizations of metallic claddings on metallic substrates are also explored. However, very less amount of investigation has been carried out on the development of Cavitation Erosion Resistant (CER) materials clads through the MHH concept.

The identified research gaps from the literature survey are as follows:

1. The literature reviews clearly depicted that very less amount of investigation has been carried out in the field of CER materials. However, researchers/academicians worked on in the field of other areas of tribology like sliding wear, erosive wear, abrasive wear and slurry erosion [19], [20], [143]–[151], [44], [46], [136], [137], [139]–[142] of metal, metal-ceramic powder by microwave cladding route.
2. Thermal spray and laser cladding are the customary techniques preferred for surface modification of the substrate which comes with many limitations. The major limitations of thermal spray are poor metallurgical bonding with the substrate, the presence of hard spots, high porosity, and chemical inhomogeneity in the coating. On the other hand, laser cladding has limitations such as thermal stresses, distortion, high porosity, residual stresses and solidification cracks. [41], [81], [152].
3. The limited study has been carried out on the effect of a stand-off-distance (SOD), the amplitude of on cumulative mass loss & incubation time during cavitation performance of the clads [81].

4. A limited amount of literature reveals parametric optimization of the MHH process and monitoring of online temperature variation during microwave processing has been reported [153].

2.6 Proposed Research Work

On the basis of research gaps identified through the available literature survey, the proposed research plan was developed and the various research objectives have been established, which are given below:

1. To optimize the processing conditions and analyse the variation in temperature during coupling of microwave radiation of 2.45 GHz during clads development.
2. To develop the metal-ceramic composite cavitation resistant clads through MHH on Austenitic Stainless steel (SS316) by using multimode domestic microwave oven.
3. Metallurgical and Tribological characterization of developed clads and Fractographic analysis of worn materials.
4. To study the effect of process parameters like amplitude of vibration, Stand-off distance on cumulative mass loss and incubation time during cavitation study of developed clads.

2.7 Proposed Plan of Work

Preplanning of work allows, prioritizing work systematically in logical manner and more work can be done in lesser time. Therefore, to accomplish work on time the methodology of the proposed plan of work is shown in Figure 2.8. The work is carried out in three stages:

Stage 1: Wise selection of substrate and clad powders to successfully achieve the desired properties.

Stage 2: Development of metal matrix composite clads at optimized parameters using microwave hybrid heating technique.

Stage 3: The developed clads are characterized for metallurgical, mechanical and tribological properties using SEM/EDS, X-ray diffraction (XRD), optical microscope (OM), Vicker's microhardness tester, ultimate tensile testing machine (UTM) and ultrasonic probe sonicator.
different phases during microwave processing. Relevant techniques will be used for the study of microstructures, which includes SEM, XRD, EDS, and optical micrographs.

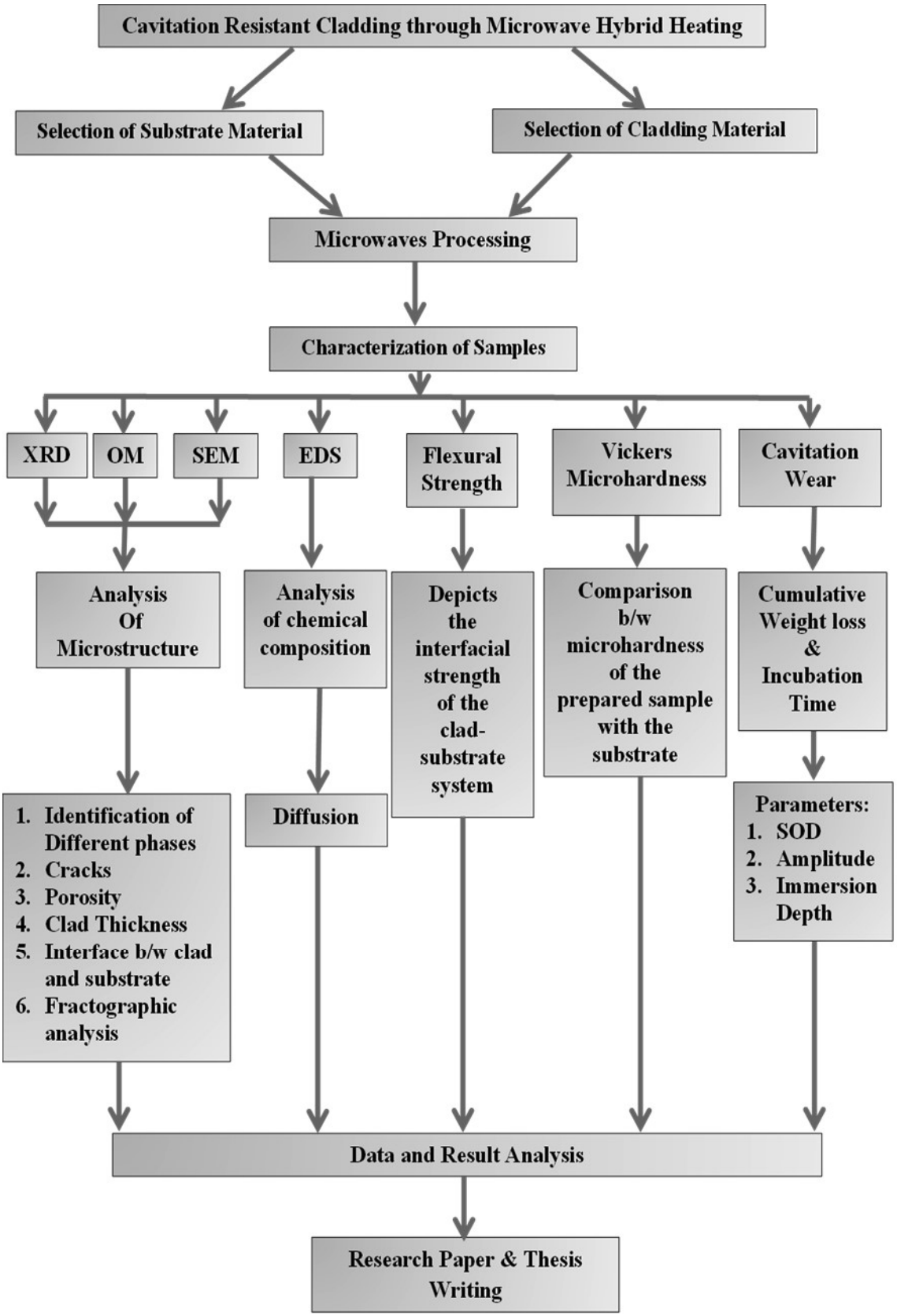

Figure 2.8: Proposed methodology of the research work

CHAPTER 3

MATERIAL SELECTION & THEIR CHARACTERIZATIONS

The wider varieties of the materials are already developed or in developing stage, which is as per the required functionality and needs by material scientist community. The selection of suitable materials from the materials library database is one of the challenging task to the user. The selection of suitable materials not only depends on their characteristics features or properties but also depends on processing such materials under given constraint and conditions. The aim of the present work is to develop cavitation erosion resistant claddings through microwave heating. The selection of substrate material, matrix material and reinforcement material is a perplexing task and should be done wisely as it lays the foundation of successful experimentation. The poor interaction of metallic materials with microwave irradiation at room temperature also makes this task challenging. Hence, in this chapter, the selection and characterization of materials (substrate, matrix material and reinforcement material) has been discussed in detail. The specifications and working principle of the apparatus and equipment used for mechanical, metallurgical and tribological characterization have also been discussed in details. The appropriate experimental design strategy applied to test the cavitation erosion wear at different test parameters has been discussed in detail

3.1 Material Selection

3.1.1 Selection of substrate material

The current work mainly focusses on the modification of surface of hydro-turbine materials to combat the poor cavitation erosion resistance (CER). The austenitic stainless steel (SS-316) is used as a substrate material for the development of CER cladding. This steel is selected due to its versatility in hydro industries [9], [79]. This is widely used in the power generation sector (hydraulic turbines) and chemical (pipes) industries owing to good corrosion resistance. The austenitic stainless steel having molybdenum ranges from 2.0% to 3.0%, provides good pitting and corrosion resistance. [80].

However, in severe working conditions, such as in gas and hydro- turbine plants, this grade of steel fails frequently, due to poor wear resistance characteristics, and be a cause of huge economic losses. The problem of poor wear resistance can be tackled by overlaying the surface with suitable hard and wear resistance material. Bhagat et. al. [154] observed in one of their findings that increase in microhardness results into logarithmic increase in cavitation

incubation time (Figure 3.1). However, high hardness associated with high toughness, in order to absorb the cavitation energy, is required to combat cavitation erosion, which is challenging to achieve with use of a single material. Hence, the use of metal matrix composite (MMC) could be a reasonable solution to this problem.

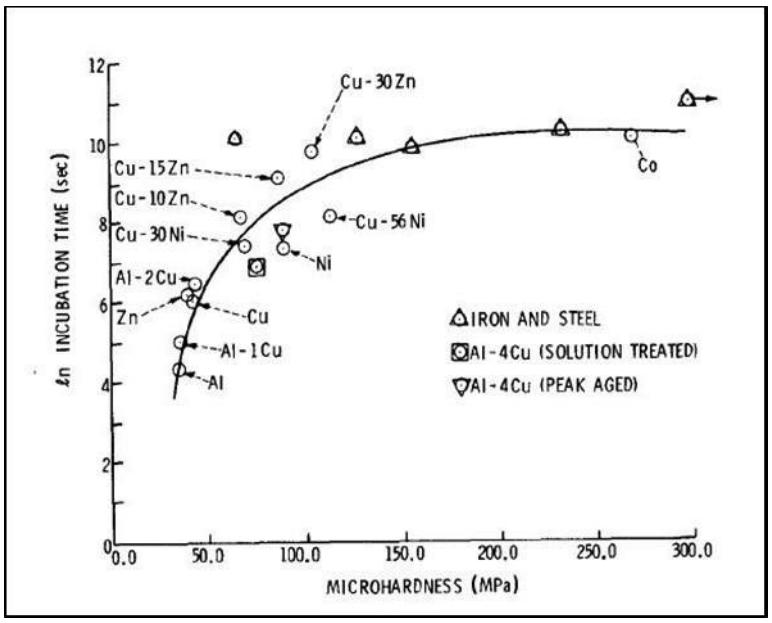

Figure 3.1: Relationship of microhardness on incubation time of different materials [154]

3.1.2 Selection of clad powders

The appropriate choice of matrix and reinforcement powder is crucial in order to achieve the combination of high hardness along with toughness. Some properties that should also be considered while selecting the matrix and reinforcement powders are:

i. Low stacking fault energy (low work hardenability)

ii. Less prone to transit from ductile to brittle phase (less strain-rate sensitivity)

iii. Good interfacial bonding to allow subsurface micro-buckling of hard reinforcement

iv. Relatively large diameter reinforcement which may undergo plastic deformation without fracturing

In line with the above requirements, the selection of matrix material and reinforcement material has been done.

3.1.3 Selection of matrix material

The Ferrum-based amorphous coatings are found most helpful as matrix material to enhance CER because of some inherent properties such as high hardness, comparatively low cost and glass forming ability[154]. But, Ferrum-based coatings are prone to corrode in cavitation environment [155]. However, both Co-based and Ni-based coatings prove their significance

against corrosion environment [156], but, Co-based materials have a carcinogenic effect on humans, if inhaled accidently [157]. These materials are also not economically viable. The Ni-based materials are well known for their high toughness, high corrosion and oxidation resistance, at elevated temperatures. The stacking fault energy is found to be equal for all of the three (Fe-based, Co-based and Ni-based) coating materials [158]. Despite of the fact that metals are difficult to process through microwave irradiation, Ni-based materials are also practical to process through novel microwave hybrid heating technique. In light of all these facts, Ni-based (EWAC-EN1004) is selected as matrix material for the current work.

3.1.4 Selection of reinforcement material

The prime function of reinforcement, when added into matrix material, is to obtain the better properties. The selection of reinforcement highly depends upon the specific properties that are required for particular application. The high hardness associated with high toughness is an essential property to significantly increase the tribological performance of functional surfaces of hydraulic components susceptible to cavitation erosion wear. The selection of reinforcement materials also highly depends upon the manufacturing process.

The ceramics are popular for extremely high hardness, poor thermal conductivity with high heat absorption capacity. The interstitial carbides such as chromium carbide (Cr_3C_2) and tungsten carbide (WC) show the highest thermal conductivity, when compared with all other type of carbides [159]. Therefore, these are suitable reinforcement materials for development of the metal matrix composite clads through microwave hybrid heating process. The excellent hardness of alumina (Al_2O_3) [137] also makes it suitable candidate to be selected as reinforcement. However, Al_2O_3 is transparent to microwaves and it is also a challenging task to process them. Therefore, being mindful of all these aspects, commercially available Cr_3C_2, WC and Al_2O_3 are selected as reinforcement material for the current work. The process makes considerable effect on the functionality of the processed material. The study of CER on the selected reinforcement materials used to develop clads by using microwave cladding technique also not yet explored.

3.2 Characterization Techniques

The microstructure, elemental composition, phase orientation, grain size and hardness influences the response and performance of any material. Therefore, the materials, to be processed, need to be characterized. Although, the materials can be characterized by several techniques, but, in the current work, the characterization was carried out by relevant techniques only. The materials in the current work were characterized for their metallurgical, mechanical

and tribological characteristics with the help of scanning electron microscope (SEM), energy dispersive x-ray spectroscopy (EDX), X-ray diffraction (XRD), Vicker's microhardness tester, inverted metallurgical microscope (OM) equipped with image analysis software, universal testing machine (UTM), and vibratory cavitation erosion test apparatus (probe sonicator). The relevant specifications and characteristics of the apparatus, used for characterization, are presented in Appendix (Figures A1-A8).

3.2.1 Microstructural characterization

3.2.1.1 Scanning electron microscopy

The SEM equipped with EDS (shown in Appendix-A, Figure A-1) has been used for microstructure investigation and elemental distribution in raw powders and developed clads. SEM is a type of electron microscope that uses a focused beam of electrons to scan the surface of a sample to produce images. The electrons interact with the atoms in the sample, producing a variety of signals that contain information about the sample's surface topography and composition. An image is created by scanning the electron beam in a raster scan pattern and combining the position of the beam with the intensity of the detected signal. The EDS-equipped SEM is useful for determining the chemical composition of the sample. In the current study, backscatter electron (BSE) detector at 20 kV voltage is used to characterize the top surface and transverse section of prepared clad. However, secondary electron imaging (SEI) detector at 20 kV voltage is used to characterize the obtained powders or materials and clad specimen after cavitation testing.

3.2.1.2 Optical microscopy

The optical or light microscopy is a type of microscope that uses visible light and a lens system to magnify images of small objects. In the current study, the porosity analysis of developed clads has been carried out by optical microscope equipped with image analyser software (shown in Appendix-A, Figure A-2).

3.2.1.3 X-ray diffraction

XRD is a non-destructive, rapid analytical technique that is primarily used for phase identification of crystalline materials and can provide information on unit cell dimensions. It is the most basic and cost-effective technique. A cathode ray tube generates X-rays, which are then filtered to produce monochromatic radiation, and directed these toward the sample. The diffracted rays are produced when incident rays interact with the sample, satisfying the condition of Bragg's Law ($n\lambda=2d\sin\theta$). This law describes the relationship between the wavelength of electromagnetic radiation and the diffraction angle and lattice spacing in a

crystalline sample. An XRD pattern is generated by detection, processing, and counting of these diffracted rays. The X-pert high score is used to identify peaks by matching the obtained data with reference patterns stored in the latest ICDD database. A view of facility is presented in Figure A-3 in the Appendix-A.

3.2.2 Mechanical characterization

3.2.2.1 Micro-hardness measurement

The simultaneous increase in hardness and toughness can reduce failure, possibly due to wear, by enhancing the wear resistance. The microhardness of developed clads was measured by Vicker's microhardness tester (shown in Appendix-A, Figure A-4). Three indentations were taken laterally across each layer to minimize the error in hardness results; and the average value of microhardness was considered.

3.2.2.2 Flexural strength test or 3-point bend test

The flexural strength of the specimen significantly affects the structural, mechanical and wear performance of the coatings/claddings on metallic substrates. The standard 3-point bend test (ASTM C1161-13) was used for calculating flexural strength (FS) of developed clads. The UTM was used for performing the test at room temperature. Prior to testing, the test samples were polished to eliminate any formed oxide layer. The clad surface was subjected to tensile loading, when point load was applied to SS-316 substrate, as shown in Figure 3.2.

The crosshead displacement speed and span between inner and outer dwell pins were kept as 1 mm^{-1} and 30 mm respectively. The relation 3.1 was used to calculate flexural strength. A view of facility is shown in Figure A-5 in the Appendix-A.

$$F_S = \frac{3P_{UT}L}{2wt^2} \tag{3.1}$$

Where FS, P_{UT}, L, w, t is flexure strength, ultimate load, span length, the width of specimen and thickness of specimen respectively.

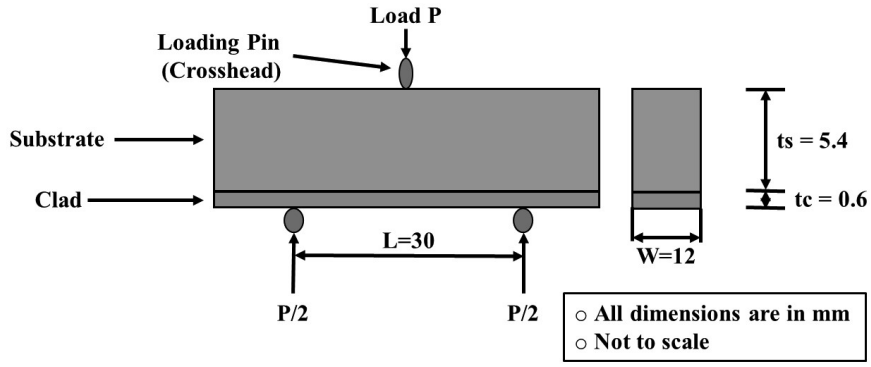

Figure 3.2: Schematic of 3-point bend test

3.2.3 Tribological characterization

3.2.3.1 Vibratory cavitation erosion testing

In the current research work, the indirect method (modified ASTM-G32-16) was used for cavitation erosion testing of the substrate and developed clads. In this method, the specimen is positioned opposite to the horn tip. The stream of generated bubbles is pushed towards the specimen surface. The explosion of these bubbles generates impact force on the specimen surface, which results in stress generation and removal of material [160]. The cavitation erosion testing was carried out on square specimens of size 15 ×15×6 mm^3 (thickness after cladding ~7 mm). Before testing, the specimens were polished with the emery paper, and the surface roughness according to ASTM-G32-16 (in between 0.2 µm to 0.8 µm) was successfully achieved. The probe sonicator-vibratory ultrasonic apparatus was used for indirect acoustic cavitation erosion testing for polished specimens (shown in Appendix-A, Figure A-6). The distilled water was used as the test liquid and the temperature of this test liquid was maintained constant at 25 ±5°C by circulating the cold water through a temperature cooling jacket throughout the experimentation. Each specimen was tested for 9 h (540 min).

3.2.4 Experimental design to study the effect of cavitation test parameter on cumulative weight loss

The appropriate design of experiments (DOE) helps to extract the maximum information from the minimal experiments and gives the right conclusion for the research goal. Basically, the design of experiments method is used for minimizing the number of experiments [161]–[163]. Three independent parameters were chosen for the present work for the cavitation erosion testing; all three parameters (amplitude- AMP, immersion depth- IMD, and stand-off distance-SOD) were varied at three levels. The levels of the input parameters (AMP and IMD) have been selected according to ASTM-G32-16. It has been mentioned in the standards that AMP and IMD should be in the range of 50±5µm and 100±10 mm, respectively. The different levels

of AMP, in order to check the effect of variation in test parameters on cavitation erosion behaviour, were selected according to apparatus feasibility, while levels for IMD were selected after initial trials. It had been observed by the author that for the narrow range (100±10 mm), there was negligible change in damage to the surface (weight loss) of samples. Therefore, a comparatively wide range (100±20 mm) had been selected. While, from literature review, it had been observed that maximum wear occurs at 0.5 mm SOD [164]. To check the combined effect of variation in these cavitation test parameters on cavitation erosion wear behaviour, the most feasible test level values had been selected.

Taguchi method has been widely used in engineering problems to optimize performance characteristics by means of selecting process parameters and their levels. This method is a combined form of mathematical and statistical tools operated for the process improvement and development of products. This method can provide optimal combinations of parameters with minimum variability. Taguchi's DOE technique proposed the design matrix of experimental trial runs based on the orthogonal array depending upon on the number of parameters and their levels. The parameters and their respective variation levels for the cavitation study are shown in Table 3.1. The complete experimental plan was generated using Minitab 17.0; and is shown in Table 3.2. The effect of the parameters of the cavitation test on the weight loss was studied. For each specimen, the cavitation test was performed for 9 h, and the weight loss due to cavitation erosion in the specimens was determined using a weighing

Table 3.1: Parameters and their levels for cavitation erosion testing

Parameters	**Units**	**Levels**		
		1	**2**	**3**
Stand-off Distance	**mm**	0.5	1	1.5
Amplitude	**µm**	40	50	60
Immersion Depth	**mm**	80	100	120

Table 3.2: Experimental plan for cavitation erosion testing (Taguchi L9 array)

Experimentation Parameter No.	**Stand-off Distance (mm)**	**Amplitude (µm)**	**Immersion depth (mm)**
1	0.5	40	80
2	0.5	50	100
3	0.5	60	120
4	1	40	100
5	1	50	120
6	1	60	80
7	1.5	40	120
8	1.5	50	80
9	1.5	60	120

machine of least count 0.1 mg. However, in order to determine the material failure mechanism during cavitation erosion, fractographic analysis of the eroded surface of the substrate and all developed clads was carried out by using SEM.

3.2.5 Clad characterization

The samples for characterizations of developed clads at optimized processing parameters have been prepared and tested by using following equipment:

3.2.5.1 Low speed diamond cutter

The developed clad specimens for characterization were cut along the cross-section with low-speed diamond cutter (shown in Appendix-A, Figure A-7). This type of cutter has diamond wafering blade which is well known to cut very hard materials. The scratches on the cut specimen surface should be minimum in order to use these specimen, after polishing, for SEM and optical microscopy (OM). The high quality cut with minimal damage can be achieved by using low-speed diamond cutter.

3.2.5.2 Polishing procedure

The sectioned specimen was first ground using emery papers of grade 100,150, 220, 320, 600, and 800. After that, the specimen surface was polished using fine grade emery papers starting from 1000 and then proceeds in series (1500, 2000, and 2500) up to 3000. At last, the specimen was polished using a diamond paste of 1 μm size and soft velvet cloth on disk polisher (shown in Appendix-A, Figure A-8) to achieve a mirror-like surface and remove scratches. The diamond polishing paste was held on a velvet cloth with a diamond-lapping compound, which was sprayed on the velvet cloth.

3.3 Characterization of the Materials

The austenitic stainless steel (SS-316) was characterised in its as-received condition to determine its purity and mechanical properties. Figure 3.3 depicts SEM micrographs of substrate (a-b). The spectrometer (Make: WAS, Model: Foundry Master) and microhardness tester was utilized to evaluate the chemical composition and Vickers microhardness of the substrate material. The results are presented in Table 3.3 and 3.5. The parameters for Vicker's microhardness test was selected as 300 g normal load and 20 s dwell time. Also, some other important physical and mechanical properties of substrate are tabulated in Table 3.5.

Table 3.3: Chemical composition of bulk SS-316 specimen

Elements	**P**	**C**	**Si**	**S**	**Mn**	**Mo**	**Ni**	**Cr**	**Fe**
Weight (%)	0.042	0.023	0.282	0.069	1.21	1.99	9.82	17.1	Balance

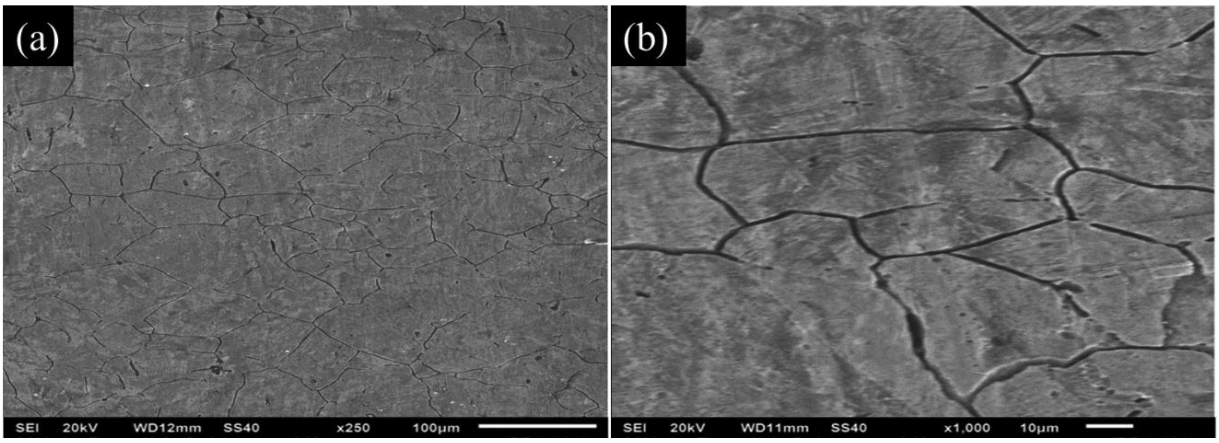

Figure 3.3: SEM micrographs of austenitic stainless steel (SS 316) at a) lower magnification b) higher magnification

3.3.1 Characterization of the EWAC powder

The commercially available EWAC1004 EN powder was purchased from EWAC alloy Pvt. Ltd. (Mumbai, India). The purchased powder was characterized to determine its purity. The typical spherical morphology of EWAC with average particle size of 40±10 µm is illustrated in Figure 3.4 (a).

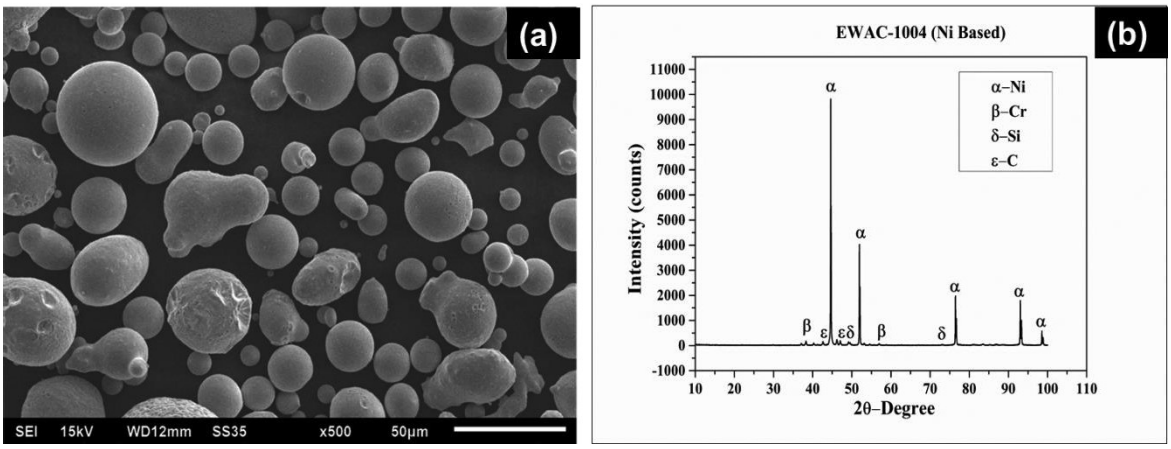

Figure 3.4: a) SEM micrograph of EWAC powder b) XRD pattern of EWAC powder

The XRD patterns of EWAC powder is illustrated in Figure 3.4 (b). Ni was present as a major constituent element and Cr, Si, and C are present as minor constituent elements in EWAC powder. The chemical composition of raw EWAC powder was measured using electron probe micro-analyser device having 15 kV accelerating voltage and 1 µm of beam diameter and the assessed values are presented in Table 3.4. The few other significant physical and mechanical properties of raw EWAC powder are tabulated in Table 3.5.

Table 3.4: Chemical composition of EWAC powder

Elements	Si	Cr	Ni
Weight (%)	3.89	2.06	Balance

Table 3.5: Mechanical & physical properties of SS-316 and raw powders [43], [137], [159], [165]–[168]

Properties	Materials				
	SS-316	EWAC Powder	Cr_3C_2 Powder	WC Powder	Al_2O_3 Powder
Vickers Hardness (HV)	190	75 [43]	1630 [159]	1500-1800 [159]	~1650 [137]
Melting Point (°C)	1375-1400 [166]	1455 [167]	1810 [159]	2870 [159]	2072 [159]
Destiny (g/cm^3)	7.98 [166]	8.91 [166]	6.74 [159]	15.6 [159]	3.95 [137]
Fracture Toughness (Mpa√m)	112 [82]	100 [43]	5.1 [167]	10-14 [167]	2.69 [167]
Elastic Modulus (GPa)	190 [82]	150 [43]	334 [167]	630-650 [167]	386 [167]

3.3.2 Characterization of the chromium carbide (Cr_3C_2) based powder

The commercially available chromium carbide based (Cr_3C_2) ceramic powder was purchased from Ms. Shankar Pvt. Ltd. (New Delhi, India). The typical morphology of reinforcement powder is sharp. This sharp edge morphology of Cr_3C_2 powder with average particle size of 50±10 µm is illustrated in Figure 3.5 (a). The XRD patterns of Cr_3C_2 powder is illustrated in Figure 3.5 (b). The existence of only Cr_3C_2 phase in Cr_3C_2 powder is established. The chemical composition of raw Cr_3C_2 powder is assessed and values are presented in Table 3.6. Some other significant physical and mechanical properties of raw Cr_3C_2 powder are tabulated in Table 3.5.

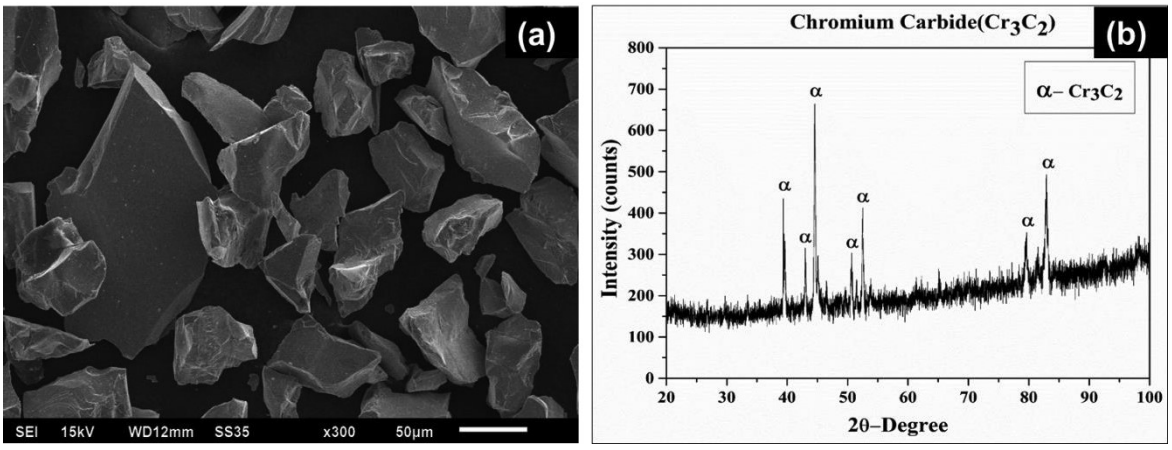

Figure 3.5: a) SEM micrograph of Cr_3C_2 powder b) XRD pattern of Cr_3C_2 powder

Table 3.6: Chemical composition of Cr_3C_2 powder

Elements	C	Cr
Weight (%)	31.9	68.1

3.3.3 Characterization of the tungsten carbide (WC) based powder

The commercially available tungsten carbide based (WC10Co2Ni) ceramic powder was purchased from Ms. Shankar Pvt. Ltd. (New Delhi, India). The typical pyramidal shape morphology of the WC powder with average particle size of 50±10 µm is illustrated in Figure 3.6 (a). The XRD patterns of WC powder is illustrated in Figure 3.6 (b). The presence of W and C as principal constituent and Ni and Co as minor constituent elements in the WC powder was confirmed.

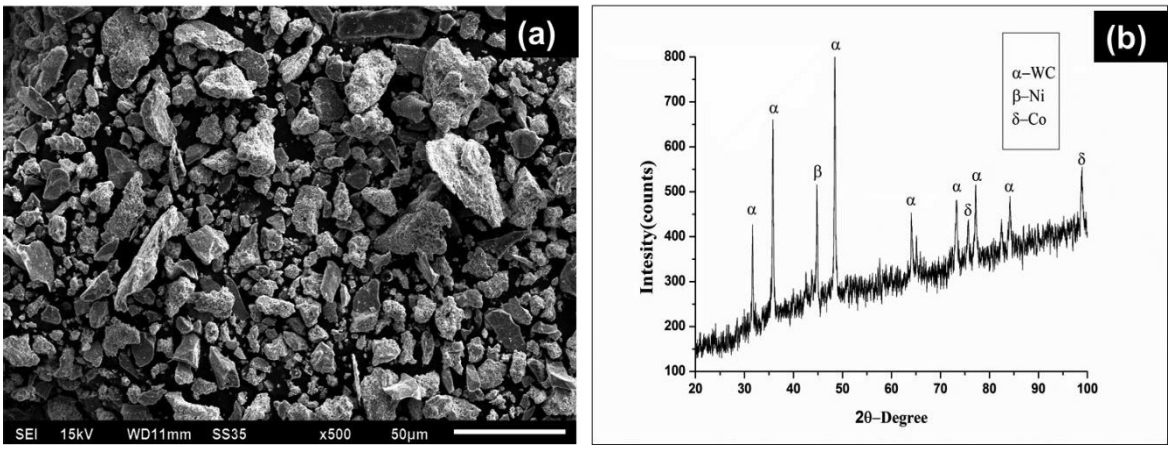

Figure 3.6: a) SEM micrograph of WC-based powder b) XRD pattern of WC-based powder

The chemical composition of raw WC-based powder is assessed and values are presented in Table 3.7. Few other significant physical and mechanical properties of raw WC-based powder are tabulated in Table 3.5.

Table 3.7: Chemical composition of WC-based powder

Elements	C	Co	Ni	W
Weight (%)	5	10	2	Balance

3.3.4 Characterization of the aluminium oxide (Al_2O_3) based powder

The commercially available Aluminium Oxide (Al_2O_3) based ceramic powder was purchased from Ms. Shankar Pvt. Ltd. (New Delhi, India). The Al_2O_3 powder exhibits sharp edge morphology like typical hard and brittle material, with average particle size of 30±10 µm (Figure 3.7 (a)). The XRD patterns of Al_2O_3 powder is illustrated in Figure 3.7 (b). The presence of mainly Al_2O_3 phase was confirmed from XRD patterns. The chemical composition

of raw Al_2O_3 powder is assessed and values are presented in Table 3.8. Few other significant physical and mechanical properties of raw Al_2O_3 powder are tabulated in Table 3.5.

Table 3.8: Chemical composition of Al_2O_3 powder

Elements	**Fe**	**Al**	**Si**	**O**
Weight (%)	5.64	35.2	10.91	Balance

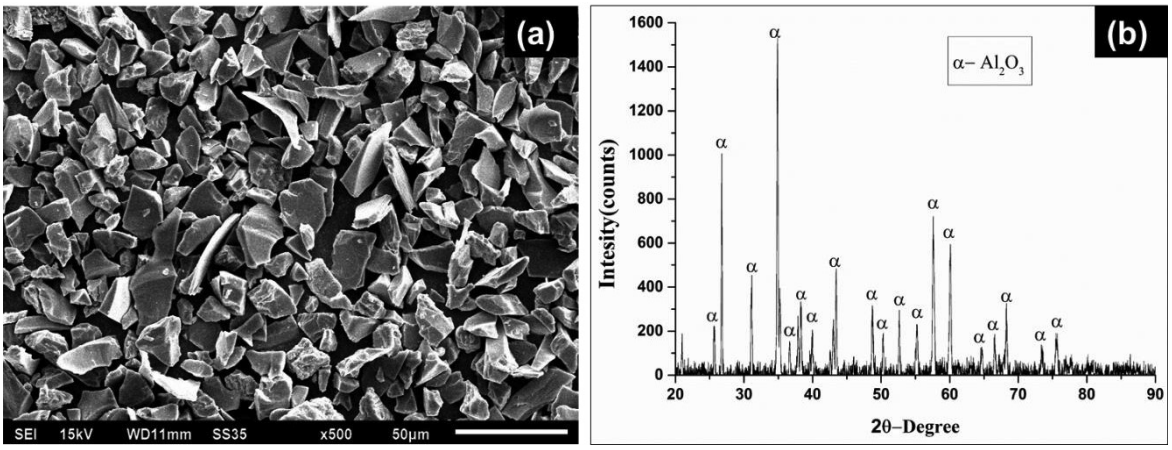

Figure 3.7: a) SEM micrograph of Al_2O_3 powder b) XRD pattern of Al_2O_3 powder

CHAPTER 4
EXPERIMENTAL DETAILS

The way to heat up the material for rising their temperature to melting state is one of the criteria for successful clads development with controlled dilution level. The conventional way for heating any materials, is started from their surface to the core of the material and hence the temperature gradient exists in the heated substances. The possibility of such phenomenon can be minimized by choosing any source of energy for heating materials, which can facilitate the heating at the molecular level. This can be achieved by using microwave radiations as a heating source. This results in uniform and rapid heating as compare to other conventional methods. The microwave radiations is not friendly with all class of materials and this limitation, restrict the users for use such energy as a heating source, despite of unique heating characteristic with these radiations. The challenge to process metallic material using microwave as a heating source can be tackled by using novel microwave hybrid heating (MHH) technique. A well planned approach is needed to successfully achieve the objective of clad development through this novel technique. The theoretically and scientifically knowledge of the process is essential. In the current chapter, the development of composite clads using MHH technique has been discussed in detail. Prior, the primary preparation before clad development is also discussed in detail, which is the prior requisite for successful bonding of clads with minimal defects at clad-substrate boundary interface. Multiple trials have been carried out to carefully optimize the process parameters.

4.1 Primary Preparation

The primary preparation is condemnatory for development of defect free and sound clads. The following section explains the preparation prior to the clad development through MHH.

4.1.1 Crushing/grinding of Charcoal

The MHH is based on the use of suitable susceptor material for helping the interaction of microwave radiations for opaque materials like metals. The susceptor material absorbs microwave radiations at ambient temperature and hence rises in their temperature. Further, the heat developed in this material will get transferred, through conventional mode of heat transfer, to substrate and preplaced powdered clad materials, in case of cladding. The powdered charcoal material is good absorber of microwave radiations[59], it is cheap and also easily available. Therefore, in the present study fine grain hard cock of high grade has been used. The received

hard cock was bulk in size. These large size lumps of charcoal were not appropriate for MHH, and need to be crushed into fine grain particles. The charcoal in as received condition was first crushed manually with the help of pestle and wedge rammer in mortar. Afterwards, it has been crushed to ultra-fine particles with the help of mechanical grinder. The state of charcoal prior and after crushing has been shown in Figure 4.1

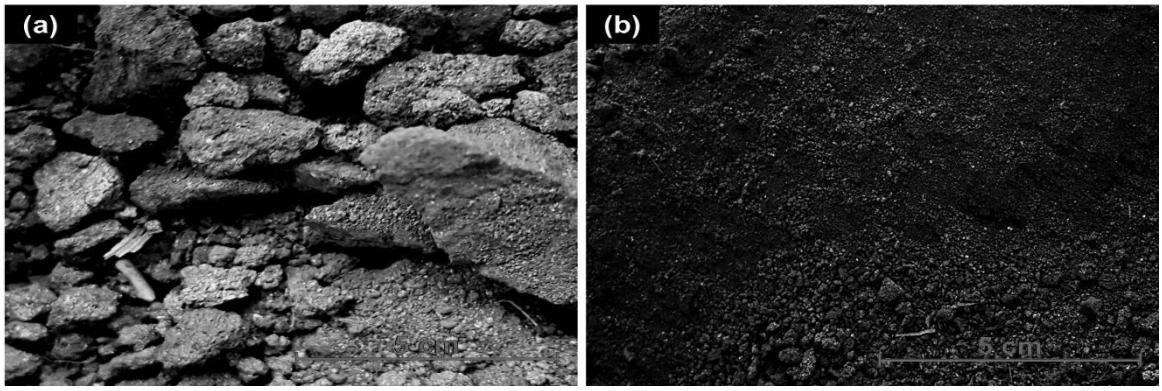

Figure 4.1: The state of charcoal (a) before crushing (b) after crushing

4.1.2 Specimen preparation

The austenitic stainless steel (SS-316) was purchased from the local supplier in the form of billet of cross section 50×6 mm^2. The specimen of different sizes for metallurgical characterization, vibratory cavitation erosion testing and flexural strength testing, were machined with the help of high speed hand abrasive cutter. The specimen size used for different purpose is presented in Table 4.1.

Table 4.1: Specimen size for metallurgical, tribological and flexural studies

Purpose	Size (mm^3)	ASTM No.
Metallurgical characterization	10×10×6	--
Vibratory cavitation testing	15×15×6	G-32-16
Flexural strength testing	40×12×6	C-1161-13

Afterwards, the cut specimens were ground to remove the burrs and other contaminations onto the surface. The top surface of machined specimen was ground with 200 and 600-grade emery paper to ensure the removal of any oxide layer. The artificial surface texture during grinding was developed which helps to form better metallurgical bonding with clad layer. Further, the top surface of specimens was cleaned with acetone to remove any dirt particles.

4.1.3 Powder mixing and preheating

The proper mixing of clad powders is essential to get the homogenous properties of developed clad. Therefore, the matrix material powder and reinforcement material powder were mixed in

a mechanical mixer blender for 2 hours at 80 rpm. The chances of defects formations, like, porosity and hydrogen embrittlement increases by the presence of moisture in the clad powder material [169]. Therefore, the properly mixed clad powders were preheated at 180º C in the domestic microwave oven by using the convention mode of heating. This eliminates the possibility of presence of any undesired moisture contents in the mixed powders.

4.2 Clad Development Process through MHH

Prior to the clad development, the different weight ratios of selected reinforcement materials (Cr_3C_2, WC10Co2Ni and Al_2O_3) have been decided. The details of decided weight ratios have been presented in Table 4.2. The weight percentage ratio of Al_2O_3 is selected different from Cr_3C_2 and WC in order to maintain uniformity due to different powder particle size.

Table 4.2: Weight ratios of reinforcement materials

Reinforcement material	Weight ratio (%)
Cr_3C_2	**10,20,30**
WC10Co2Ni	**10,20,30**
Al_2O_3	**5,10,15**

In general, the metallic materials do not interact with microwaves of low frequency (2.45 GHz) at room temperature due to the lower skin depth. The microwaves do not get absorbed by such poor skin depth materials owing to which materials will not reach at the elevated temperature, which requires for metallurgical bonding of preplaced materials with substrate. Hence, MHH technique has been used in the present work for the development of partial dilution of preplaced materials with substrate and vice versa. To facilitate microwave interaction with such materials, charcoal powder as a susceptor has been used and it is distributed uniformly above and around the metallic materials. To protect the contamination of the clad powder with susceptor material, 99.7 % pure alumina sheet of 1 mm thickness, which is having a skin depth of ~0.12 m [59], [165] and that is transparent to the microwave radiation, has been used as the separator. Figure 4.2 shows the schematic and actual cladding process by MHH. The experimentation has been carried out in atmospheric conditions.

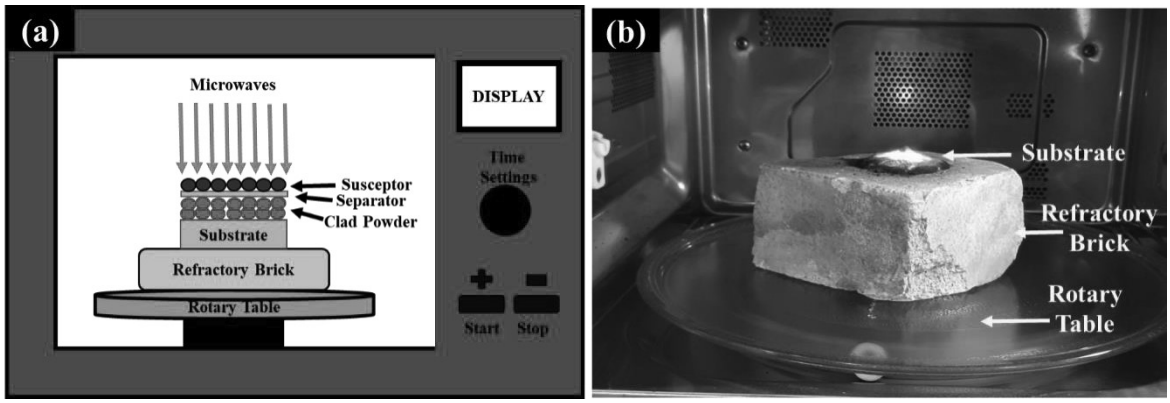

Figure 4.2: The microwave cladding process (a) schematic diagram (b) actual setup

4.2.1 Optimization of parameters

The initial trials have been carried out for the development of composite cladding of Ni-based (EWAC) as a matrix material and Cr_3C_2, WC10Co2Ni and Al_2O_3 are act as reinforced materials, with different weight percentage through MHH. The exposure power and time was optimized for the development of clads. The summary of experimental condition, materials and parameters selected during experiments has been presented in Table 4.3. The optimized exposure power and time required for EWAC-10Cr_3C_2, EWAC-10WC10Co2Ni and EWAC-5Al_2O_3 composite clads are as shown in Table 4.4-4.6, respectively.

Table 4.3: Microwave cladding conditions and used process parameters

Parameters	**Description**
Applicator	Multimode microwave oven (Model: Charcoal, Make: LG)
Frequency	2.45 GHz
Susceptor	fine grain charcoal Powder
Separator	Alumina Substrate (1 mm)
Powder Preheating Temperature	180ºC
Ambient Temperature	20ºC

Table 4.4: Microwave processing parameters and their effect on EWAC-10Cr_3C_2 clad

Processing Time (s)	**Microwave Power (W)**		
	540	**720**	**900**
60	Evaporation of moisture from charcoal	Partial heating of charcoal	Charcoal was red hot, heating of powder started
120	Partial heating of charcoal	Charcoal was red hot	Both powder and substrate was red hot
180	Charcoal was red hot	Heating of powder started	Sintering of particles started

240	Heating of powder started	Both powder and substrate was red hot	No melting of clad powder
300	Both powder and substrate was red hot	Sintering of particles started	Melting of clad powder started
360	Sintering of particles started	No melting of clad powder	Presence of unmelted particles
430	No melting of clad powder	Melting of clad powder started	Formation of cladding layer with good bonding
480	Partial melting of the powder particles and poor bonding with substrate and no evidence of substrate melting	Unmelted particles present and poor bonding	Deformation of substrate

Table 4.5: Microwave processing parameters and their effect on EWAC-10WC10Co2Ni clad

Processing Time (s)	**Microwave Power (W)**		
	540	**720**	**900**
60	Evaporation of moisture from charcoal	Partial heating of charcoal	Charcoal was red hot, heating of powder started
120	Partial heating of charcoal	Charcoal was red hot	Both powder and substrate was red hot
180	Charcoal was red hot	Heating of powder started	Sintering of particles started
240	Heating of powder started	Both powder and substrate was red hot	No melting of clad powder
300	Both powder and substrate was red hot	Sintering of particles started	Melting of clad powder started
360	Sintering of particles started	No melting of clad powder	Presence of unmelted particles
420	No melting of clad powder	Melting of clad powder started	Formation of cladding layer but poor bonding
450	Partial melting of clad powder	Formation of cladding layer but poor bonding	Formation of cladding layer with good bonding
480	Melting of the powder particles but poor bonding with substrate and no evidence of substrate melting	Formation of cladding layer	Complete deformation of substrate

Table 4.6: Microwave processing parameters and their effect on EWAC-5Al_2O_3 clad

Processing Time (s)	Microwave Power (W)		
	540	**720**	**900**
60	Evaporation of moisture from charcoal	Partial heating of charcoal	Charcoal was red hot, heating of powder started
120	Partial heating of charcoal	Charcoal was red hot	Both powder and substrate was red hot
180	Charcoal was red hot	Heating of powder started	Sintering of particles started
240	Heating of powder started	Both powder and substrate was red hot	No melting of clad powder
300	Both powder and substrate was red hot	Sintering of particles started	Still no melting of clad powder
360	Sintering of particles started	No melting of clad powder	Clad powder start melting
420	No melting of clad powder	Still no melting of clad powder	Presence of unmelted particles
480	Still no melting of clad powder	Melting of clad powder started	Formation of cladding layer but not well bonded
540	Partial melting of the powder particles and poor bonding with substrate and no evidence of substrate melting	Formation of cladding layer but not well bonded	Formation of cladding layer with good bonding
600	Clad layer formed	Partial deformation of substrate	Complete deformation of substrate

Similarly, the optimization of exposure time and power for other composition has been carried out. It has been observed during entire exhaustive experimentations, that the required minimum exposure microwave power 900 W to melt the powder material system and partial amount of substrate material to causes the dilution for development of metallurgical bonded clads of these powder systems. The microwave exposure time was varying with respect to different compositions of clads. The optimized processing time for all the compositions, at different specimen size, is presented in Table 4.7. Three experiments for each composition have been carried out. The processing time was varied for 10, 12 and 15 s for specimen prepared for metallurgical, tribological and flexural studies. No significant change was visualized at these variations. The average values have been considered.

Table 4.7: Optimized processing time for all compositions composite clad

Composition	Optimized Processing Time (s)		
	Sample Size (mm^3)		
	10×10×6	**15×15×6**	**40×12×6**
EWAC-10Cr_3C_2	430±10	750±15	1300±20
EWAC-20Cr_3C_2	420±10	720±15	1260±20
EWAC-30Cr_3C_2	390±10	700±15	1200±20
EWAC-10WC10Co2Ni	450±10	780±15	1360±20
EWAC-20WC10Co2Ni	430±10	760±15	1340±20
EWAC-30WC10Co2Ni	410±10	750±15	1300±20
EWAC-5Al_2O_3	530±10	720±15	1380±20
EWAC-10Al_2O_3	560±10	750±15	1410±20
EWAC-15Al_2O_3	590±10	790±15	1445±20

The addition of Cr_3C_2 and WC10Co2Ni powders facilitate the microwave absorption due to higher skin depth and therefore the processing time goes on decreasing by the increase in the weight percentage of these reinforcements into the matrix material. However, the melting temperature of WC10Co2Ni is more than Cr_3C_2, which results into higher processing time for all the specimen sizes. On the other hand, the Al_2O_3 is transparent to microwaves and does not facilitate the microwave absorption. Therefore, the processing time is higher in this case for all the specimen sizes.

The behaviour of the susceptor material during microwave interaction at optimized processing time and power has been analysed during experimental trial run at different intervals of time. The interaction of microwave radiation with charcoal powder is very complex in nature. Initially, trial runs have been carried out at an interval of 1 min of microwave exposure and the temperature of charcoal powder has been noted at the end of experiments by using Infrared thermometer. The respective experimental observation of EWAC-10Cr_3C_2 composite clad has been presented in Table 4.8. The monitoring of in-situ clad temperature during processing is not viable in present experimental set-up due to the fact that clad powder is fully covered with susceptor material. Hence, the effect of susceptor temperature on preplaced clad powder is linked for developing understanding of microwave interaction of powders and rise in their temperature during experimentations. The interpretations of observations at the end of each experiment have been made on the basis of susceptor temperature recorded and the

condition of material system. In initial run of experiments, it has been observed that the moisture present in charcoal powder evaporates after 15 s of microwave exposure and rise in the charcoal temperature was 105.1°C (Figure 4.3). The dynamics of microwave interaction with charcoal powder was extreme after 30 s and rise in their temperature was 235.7°C. The rate of coupling with charcoal powder was, to a great extent up to 120 s and it helps to turn the temperature at 751.8°C. It has been observed that at this temperature preplaced powder particles and substrate becomes red hot, it is owing to the conduction of heat from the charcoal powder towards the preplaced powder and substrate. After 240 s exposure of microwave radiation, the charcoal powder was converted into ash and hence no more contribution from them to further rise in temperature of preplaced particles. Hence, no more conductive heat transfers from charcoal ash/powder took place during experimentation after 240 s of microwave exposure. The state of matter at the end of experiments confirms the rise in the temperature of preplaced powder by direct coupling of microwave radiation with them.

After, 460 s of microwave exposure the clad and substrate diluted significantly and the purpose of clads has been lost. Further, the successful metallurgical bonded clads have been developed, when preplaced powder exposes of microwave radiation for 430 s.

Table 4.8: Temperature record of susceptor powder and observations during experimental trials of EWAC-10Cr_3C_2 composite clad

Test Run	**Exposure time (s)**	**Observations & Readings**	
		Observations	**Charcoal Avg. Temp. (°C)**
	15	Evaporation of moisture contents present in charcoal	105.1
	30	Heating of substrate but powder remains unaffected.	235.7
1	60	Charcoal started transferring heat to the substrate and the substrate starts heating. Heating of powder started and charcoal became red hot.	478.9
2	120	Both powder and substrate became red hot.	751.8
3	180	Sintering of particles started	873.2
4	240	Charcoal completely turned in ash, bonding with powder particles developing.	868.1
5	300	Melting of clad powder started.	837.4
6	360	Partially unmelted clad	812.2
7	430	Formation of cladding layer	740.1
8	460	Complete melting of Substrate	714.4

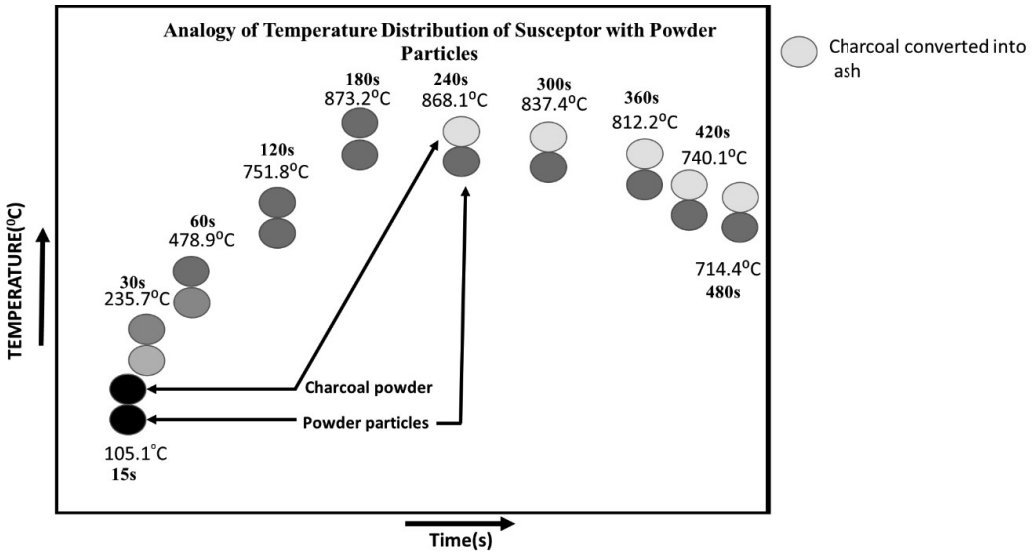

Figure 4.3: Analogy of temperature distribution of susceptor with powder particles

Table 4.9: Temperature record of susceptor powder during experimental trials of all composite clad

Processing Time (s)	Clad Powder Composition								
	EWAC + $10Cr_3C_2$	**EWAC + $20Cr_3C_2$**	**EWAC + $30Cr_3C_2$**	**EWAC + 10WC-based**	**EWAC + 20WC-based**	**EWAC + 30WC-based**	**EWAC + $5Al_2O_3$**	**EWAC + $10Al_2O_3$**	**EWAC + $15Al_2O_3$**
15	105.1	101.2	102.7	110.5	104.2	100.5	107.6	106.5	102.1
30	235.7	262.4	250.5	280.1	275.1	257.9	282.1	240.8	249.7
60	478.9	460.7	443.7	400.2	483.4	475.1	430.4	450.8	478.1
120	751.8	700.2	721.1	756.7	745.8	731.8	761.2	748.7	710.2
180	873.2	845.2	837.3	800.4	880.1	850.9	872.4	869.7	884.2
240	868.1	841.2	819.7	797.4	850.7	857.1	843.1	829.4	845.2
300	837.4	812.4	796.4	787.4	820	800.4	840.1	790.1	818.2
360	812.2	790.5	779.7	780.1	785.2	780.1	814.6	782.4	798.8
420	740.1	720.1	727.3	715.4	721.4	730.4	741.1	735.4	700.5
480	714.4	700.1	721.1	698.7	724.4	708.7	731.2	735.4	725.6

CHAPTER 5
METALLURGICAL AND MECHANICAL CHARACTERIZATION OF MICROWAVE CLADS

In the current work, Ni-based (EWAC) based composite clads with varying weight percentage of different reinforcement materials have been developed by using microwave radiations as a heating source. Microwave processing was carried out in domestic microwave oven of frequency 2.45 GHz. The associated unique characteristics of volumetric and hence uniform heating in microwave processing may yields fine microstructure, significantly lesser amount of porosity, and improved mechanical and tribological properties. In the current work, the developed clads have been characterized by using various sophisticated techniques/equipment. The details of the results of the various characterizations are presented in the current chapter.

5.1 Metallurgical and Mechanical Characterisation of the Clads

The metallurgical aspects of developed clads are characterized by using SEM/EDS, OM and XRD. These techniques/tools are giving understanding for microstructure like grain size and grain growth, phase, crystal structure, cracks and porosity. While, the developed clads are mechanically characterized for microhardness and flexural strength by using Vicker's microhardness tester and UTM. The details of characterization results are presented in the succeeding sections.

5.1.1 Microstructural characterization of EWAC-Cr_3C_2 developed clads

The tribological behaviour and quality of clad highly depends upon microstructure of clad. The sound clads must have good metallurgical bonding of clad material with substrate and defects like porosity and cracks (solidification and interfacial) should be minimum in amount. To identify the grain structure, phases present and morphology of grains, microstructure study plays a significant role. In microwave heating, the complete volume of preplaced powder is heated simultaneously. This leads to rapid heating of exposed surface of material at elevated temperature with significantly less thermal gradient. The sectioned view of EWAC-xCr_3C_2 (x=10, 20 and 30) % shows a distinguished pattern, which are as shown in Figures (5.1-5.3) respectively.

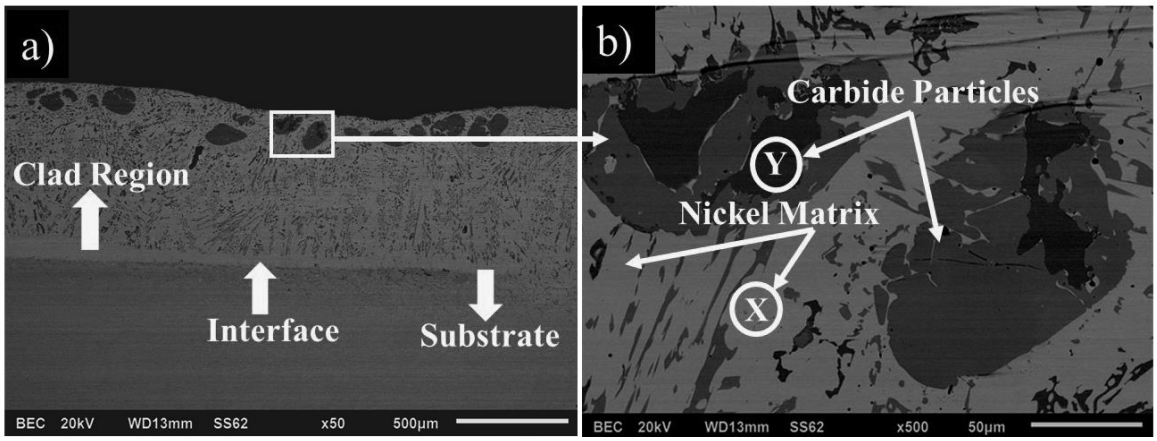

Figure 5.1: Typical BSE images of developed EWAC-10Cr_3C_2 clad a) showing distinguished clad region, substrate & interface b) enlarged view of clad region

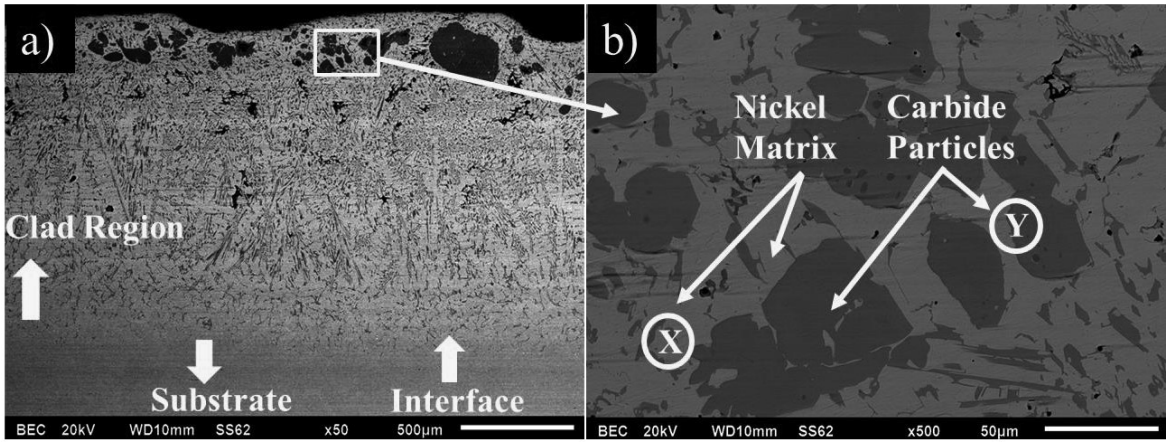

Figure 5.2: Typical BSE images of developed EWAC-20Cr_3C_2 clad a) clad region, substrate & interface b) enlarged view of clad region

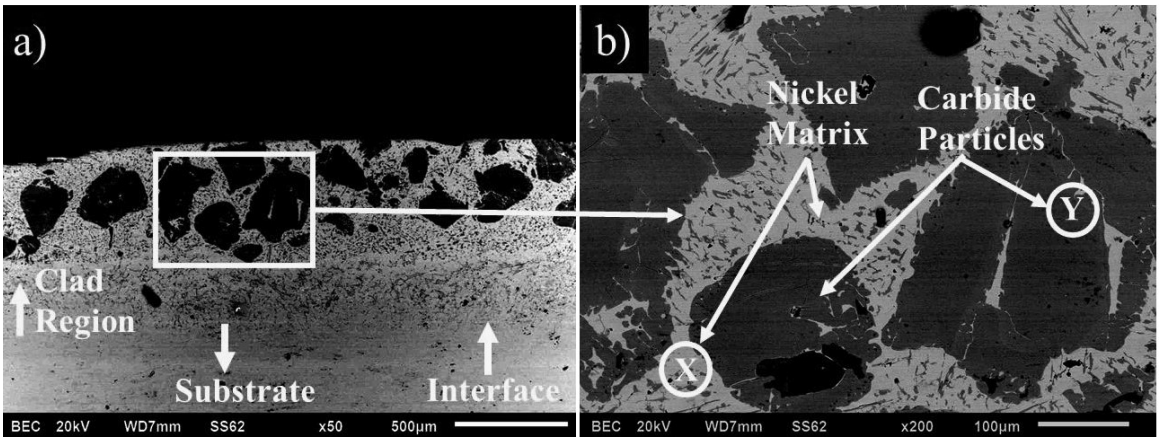

Figure 5.3: Typical BSE images of developed EWAC-30Cr_3C_2 clad a) clad region, substrate & interface b) enlarged view of clad region

The clads of approximately 720 µm, 750 µm and 600 µm are developed during microwave heating, which can be clearly seen from Figures (5.1-5.3 (a)), respectively. The microstructure

of composite clad compositions shows the lamellar bands like pattern. The elemental compositions at different locations (X and Y) of composite clads has been carried out by EDS analysis. The obtained results of these composite clads (EWAC+xCr_3C_2 (x=10, 20 and 30) %) are as shown in Figure (5.4-5.6) respectively. These lamellar bands are randomly oriented in different directions and these bands are composing of Cr-Fe-C rich phase and are distributed in the Ni-Fe-Cr rich matrix for all composition composite clads. The formation of these phases confirms, that clads are metallurgical bonded with substrate. The segregated dendrite formation is also observed in the BSE image of composite clads. In general, rapid and non-uniform cooling leads to dendrite formation. Like heating, cooling is not uniform, because the developed MMC clads have the differences in thermal conductivity of matrix base (EWAC) (90 W/ (m.K)) and reinforcement (Cr_3C_2) material (190 W/ (m.K)). This causes the heat dissipation at different rate (by EWAC and Cr_3C_2 particles) and leads to non-uniform cooling, which results into the dendrite formation possibly.

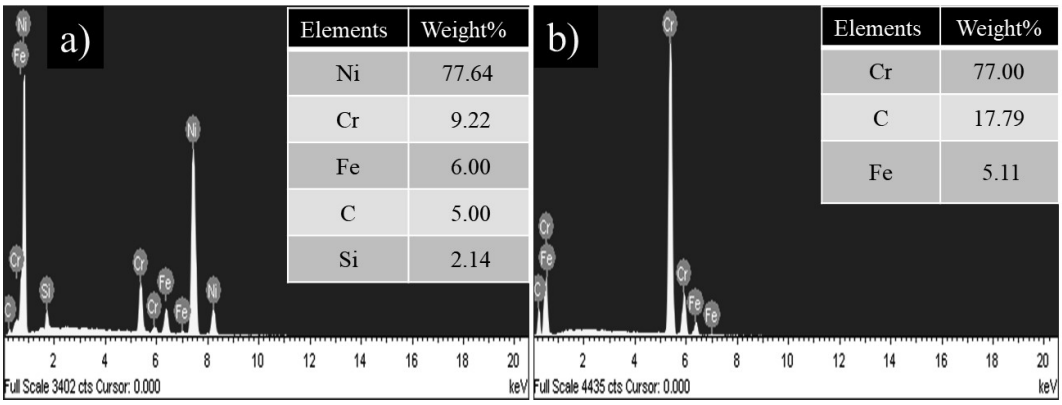

Figure 5.4: EDS analysis of developed EWAC-10Cr_3C_2 clad at a) phase X b) phase Y

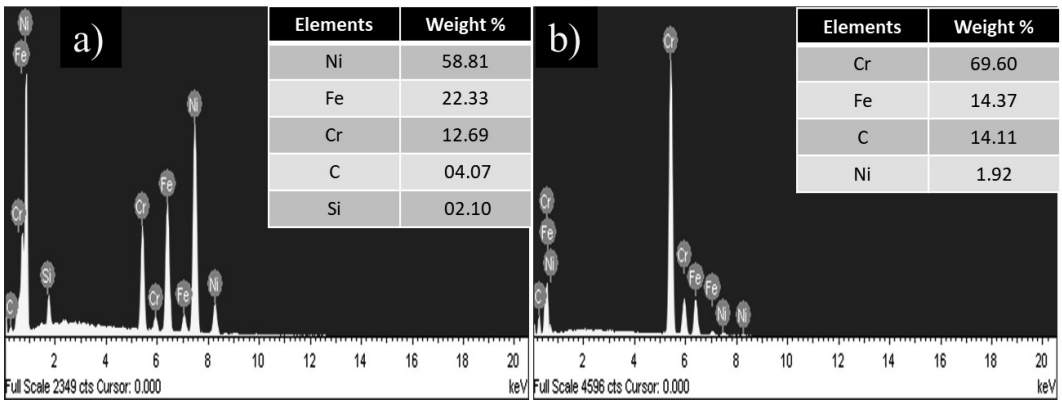

Figure 5.5: EDS analysis of developed EWAC-20Cr_3C_2 clad at a) phase X b) phase Y

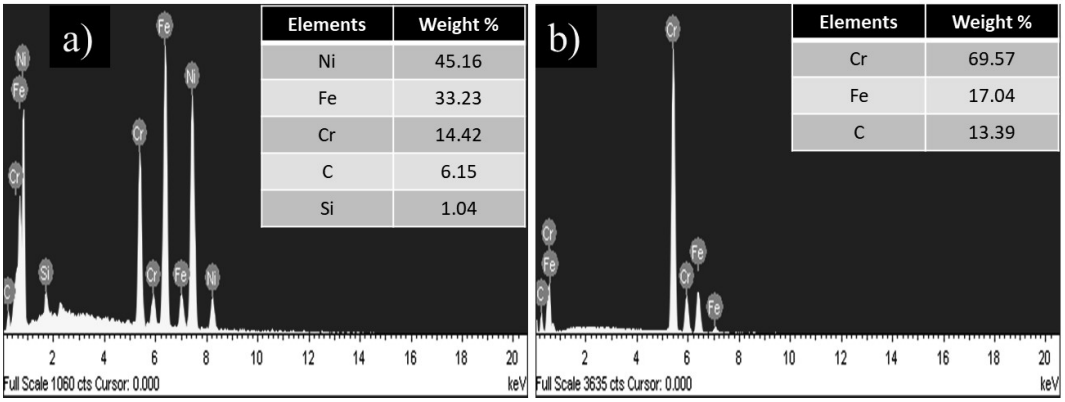

Figure 5.6: EDS analysis of developed EWAC-30Cr_3C_2 clad at a) phase X b) phase Y

The overall strength of developed composite clad can be achieved by the uniform dispersion of these reinforcement particles (black phase) inside the soft Ni matrix (white phase). Therefore, the elemental area mapping of the developed clad was carried out to investigate the dispersion of elements. The results of elemental area mapping of the clad region are presented in Figure (5.7-5.9).

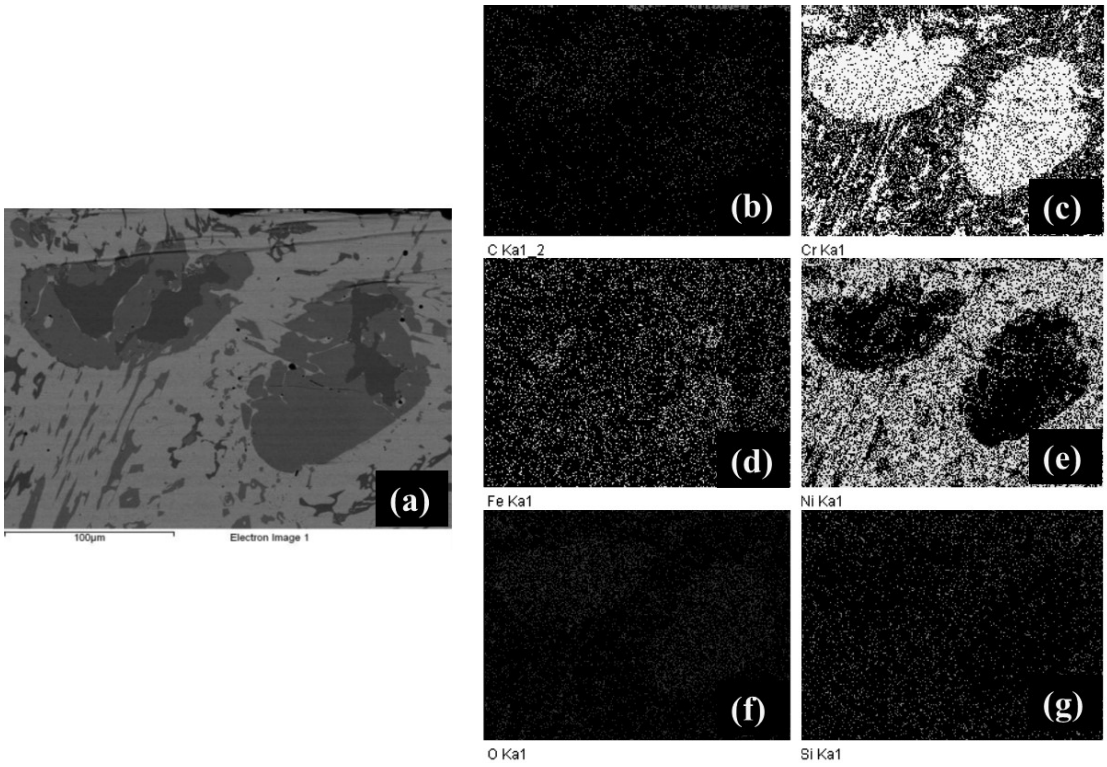

Figure 5.7: EDS mapping of developed EWAC-10Cr_3C_2 composite clad (a) area mapped location (b) C (c) Cr (d) Fe (e) Ni (f) O (g) Si

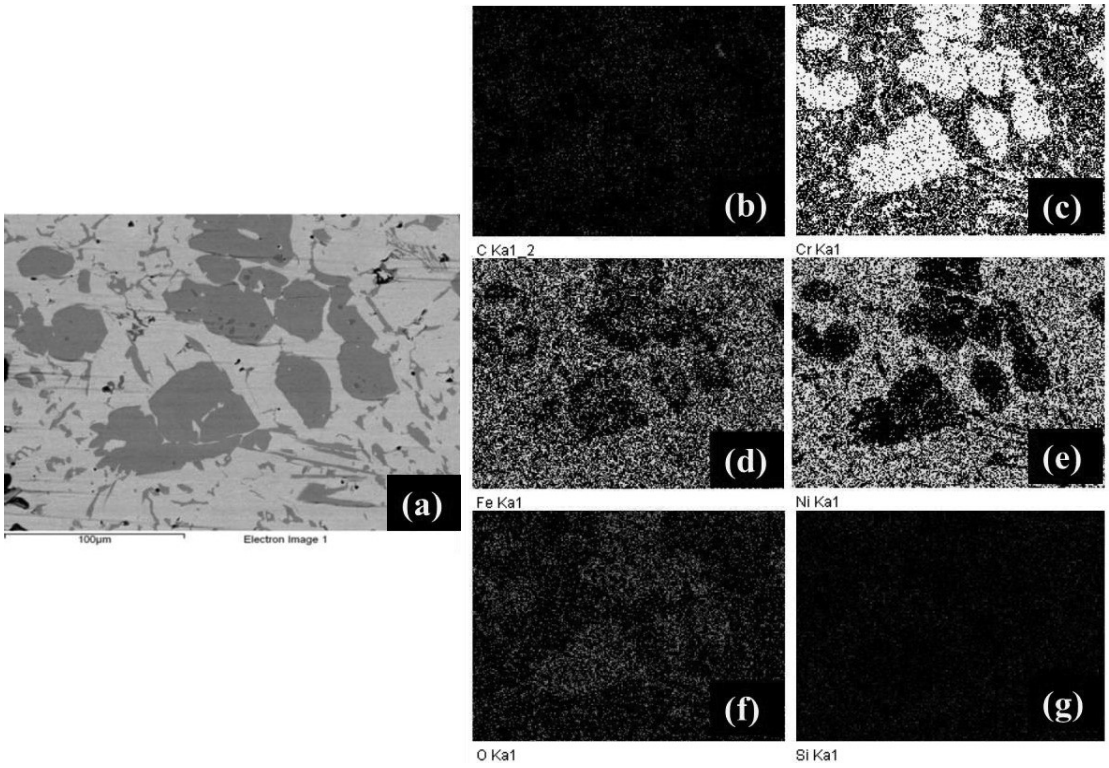

Figure 5.8: EDS mapping of developed EWAC-20Cr_3C_2 composite clad (a) area mapped location (b) C (c) Cr (d) Fe (e) Ni (f) O (g) Si

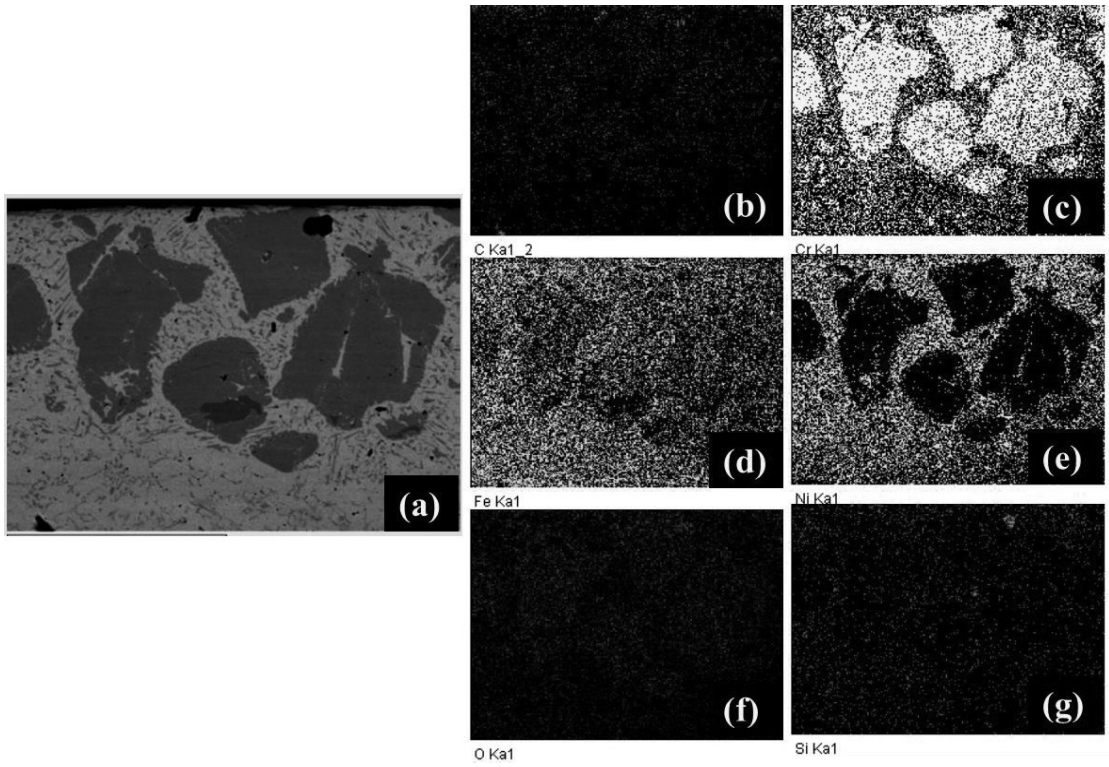

Figure 5.9: EDS mapping of developed EWAC-30Cr_3C_2 composite clad (a) area mapped location (b) C (c) Cr (d) Fe (e) Ni (f) O (g) Si

The results of mapping confirm the presence of Cr and C significantly in the grey region (Y) and presence of Ni, Si, Fe and O significantly in white region (X). This reveals that the white region (X) belongs to Ni-base while the grey region (Y) belongs to chromium and carbon enrich. The presence of Fe in clad region supports the claim of dilution of substrate into clads and hence confirms metallurgical bonds of clads with substrate. The possible reason behind the presence of O in the results of elemental mapping could be due to, the processing of samples in atmospheric environment conditions. The non-uniform microwave absorption nature of the matrix and reinforced powder may give the thermal imbalance during microwave heating. This thermal imbalance in powder system may form a localized melt pool in the clad region. This localized melt pool current is enough to agglomerate the carbide particles and hence, uniformly dispersed into soft and tough Ni-Fe rich metal matrix. Some other author has also reported the same result.[17], [149], [166].

5.1.2 Phase analysis of EWAC-Cr_3C_2 developed clads

The XRD is an analytical system, which is widely used for detection of phases present in the material system and also helps to get information regarding dimensions of unit cell. The references of known compounds have been used to match the obtained data with the diffraction peak positions and intensity values with the help of software (X'pert high score). The typical XRD spectrum of developed EWAC-xCr_3C_2 composite clads is presented in Figure 5.10.

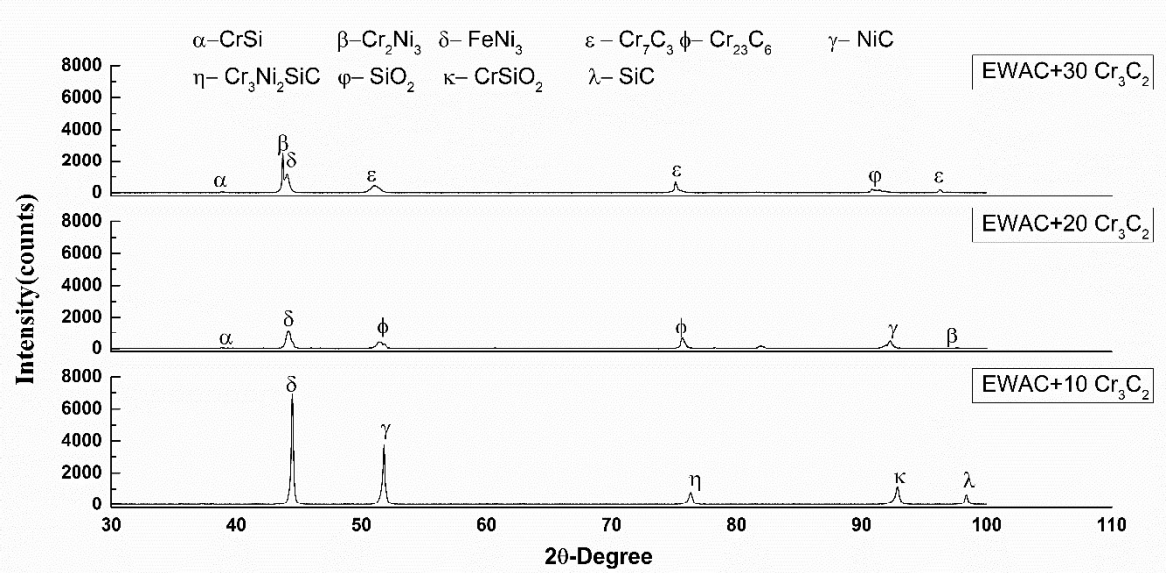

Figure 5.10: A typical XRD pattern of developed EWAC-xCr_3C_2 composite clad

The presence of phases Cr_2Ni_3, $Cr_{23}C_6$, Cr_7C_3, CrSi, $CrSi_2$, SiO_2, NiC, SiC, Cr_3Ni_2SiC and $FeNi_3$ in the developed clads is confirmed from XRD spectrum. The chromium and iron elements were present in the raw powder. The formation of Cr_2Ni_3 and $FeNi_3$ phases claims the reaction of chromium and iron elements with nickel element, respectively. These phases are

formed due to the dilution of iron and chromium element from the substrate region, which ensures the metallurgical bonding of clads with substrate. The Cr_3C_2 powders may get decomposes into Cr and C elements due to the involvement of high temperature during the microwave processing with least thermal gradient. This free carbon further reacts with the elements present (Si and Ni) into the raw clad powder and may forms SiC and NiC phases. Other than these phases some minor peaks of Cr_7C_3, $Cr_{23}C_6$, CrSi, $CrSi_2$ and $SiO_2$are also observed. The formation of these phases shows the reaction between decomposed raw powders during microwave heating and reacts with diluted elements coming from substrate to clads region and causes to form hard phases. Some complex carbide Cr_3Ni_2SiC has also been formed during microwave irradiation.

The normalized intensity ratio (NIR) method was used to assess the developed EWAC-xCr_3C_2 composite clads on a quantitative basis. However, the exact proportion of present phases in the developed clad region is not given by the NIR method. The results are presented in Table 5.1-5.3. Equation 5.1 was used to calculate the NIR of corresponding peaks. Earlier, other authors also use this equation [46], [170].

$$NIR_1 = \frac{I_1 - I_{back}}{I_1 + I_2 + I_3 + \cdots \ldots I_N + -NI_{back}} \quad (5.1)$$

Where I_1, I_2, I_N represents different corresponding peak values, and I_{back} represents background intensity.

Table 5.1: Normalized intensity ratio values of EWAC-10Cr_3C_2 composite clad

S. No.	Phase	I_1	I_2	I_3	I_4	I_5	I_{back}	NIR (%)
1	**$FeNi_3$**	6936.71	-	-	-	-	25	**53.63**
2	**NiC**	-	3751.95	-	-	-	25	**28.92**
3	**Cr_3Ni_2SiC**	-	-	769.54	-	-	25	**5.77**
4	**$CrSi_2$**	-	-	-	987.25	-	25	**7.47**
5	**SiC**	-	-	-	-	568.37	25	**4.21**

Table 5.2: Normalized intensity ratio values of EWAC-20Cr_3C_2 composite clad

S.No.	Phase	I_1	I_2	I_3	I_4	I_5	I_6	I_{back}	NIR(%)
1	**CrSi**	360.75	-	-	-	-	-	15	**11.96**
2	**$FeNi_3$**	-	1135.38	-	-	-	-	15	**38.74**
3	**$Cr_{23}C_6$**	-	-	397.58	-	-	-	15	**13.23**
4	**$Cr_{23}C_6$**	-	-	-	608.08	-	-	15	**20.51**
5	**$CrSi_2$**	-	-	-	-	453.48	-	15	**15.16**
6	**Cr_2Ni_3**	-	-	-	-	-	26.69	15	**0.40**

Table 5.3: Normalized intensity ratio values of EWAC-30Cr_3C_2 composite clad

S. No.	Phase	I_1	I_2	I_3	I_4	I_5	I_6	I_7	I_{back}	NIR (%)
1	**CrSi**	42.9	-	-	-	-	-	-	25	**0.36**
2	**Cr_2Ni_3**	-	2520.16	-	-	-	-	-	25	**50.75**
3	**$FeNi_3$**	-	-	1106.51	-	-	-	-	25	**22.00**
4	**Cr_7C_3**	-	-	-	433.62	-	-	-	25	**8.31**
5	**Cr_7C_3**	-	-	-	-	646.93	-	-	25	**12.65**
6	**SiO_2**	-	-	-	-	-	164.57	-	25	**2.84**
7	**Cr_7C_3**	-	-	-	-	-	-	176.51	25	**3.08**

The results of NIR of particular phases for different weight compositions of reinforced particle reveals that the phases of different natures (harder carbide phases and softer metal matrix phases) are present in different percentages in clads.

5.1.3 Microhardness study of EWAC-Cr_3C_2 developed clad

Bhagat et al. [154] reported that increases in hardness generally, increases in incubation time. However, till date, no direct effect of hardness, on incubation time, is reported by authors. The failure possibility of material due to wear can be reduced by increasing the hardness and toughness of materials simultaneously and hence, this results into enhancing the wear resistance. However, it is very much critical for any material system to increase both properties

simultaneously. Hence, composite clads have been developed to address these issues. The microhardness indentations were taken across the lateral section of developed composite clads (Figures 5.11-5.13). The indents are made at a distance of 60 μm, for EWAC-10Cr_3C_2 and EWAC-20Cr_3C_2, and 50 μm for EWAC-30Cr_3C_2 respectively (owing to variation in clad thickness), starting from top of clad in direction of substrate and same distance is maintained towards right and left of each indent also. For better understanding an average of 12 set of indents is evaluated.

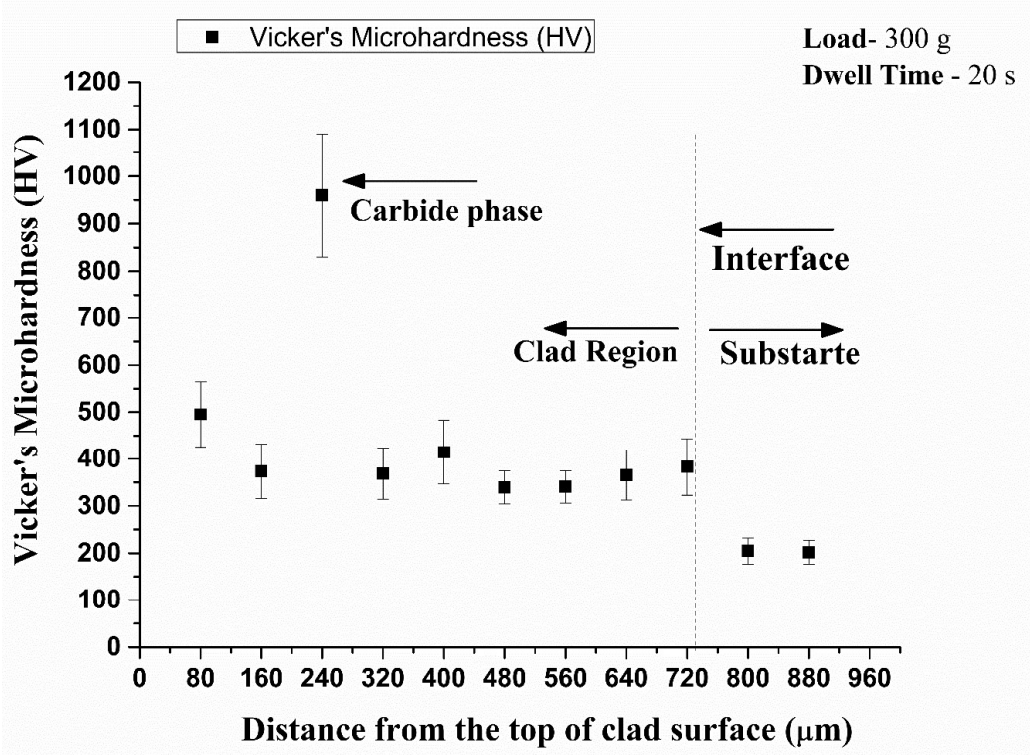

Figure 5.11: Microhardness profile of the developed EWAC-10Cr_3C_2 composite clad

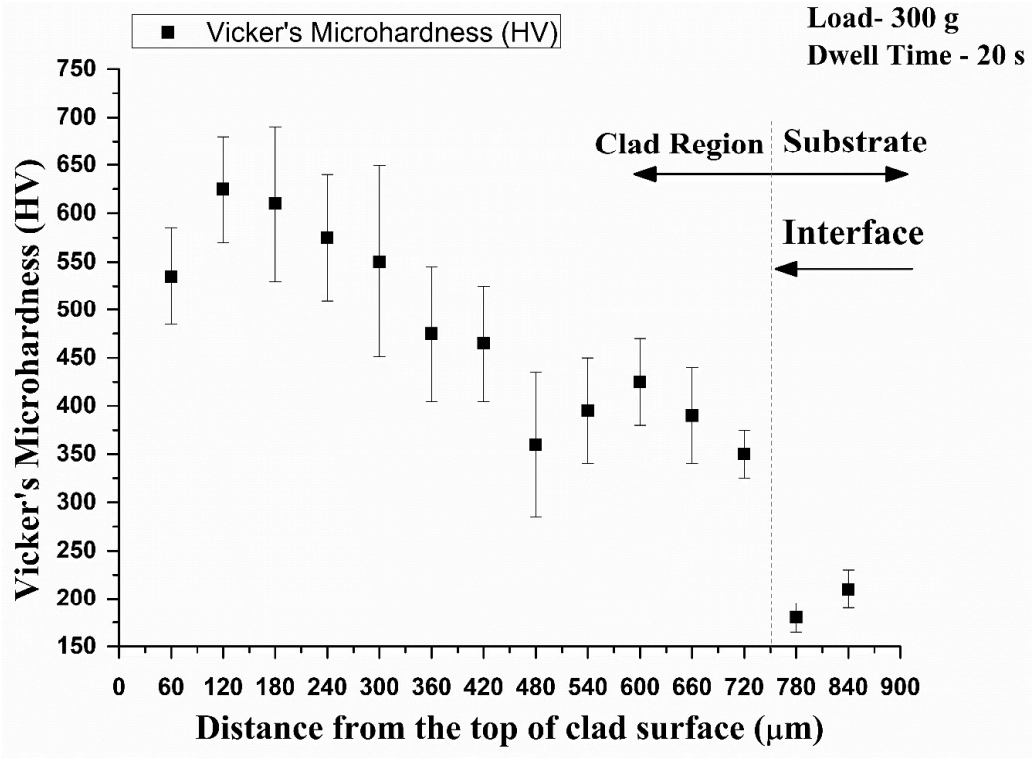

Figure 5.12: Microhardness profile of the developed EWAC-20Cr_3C_2 composite clad

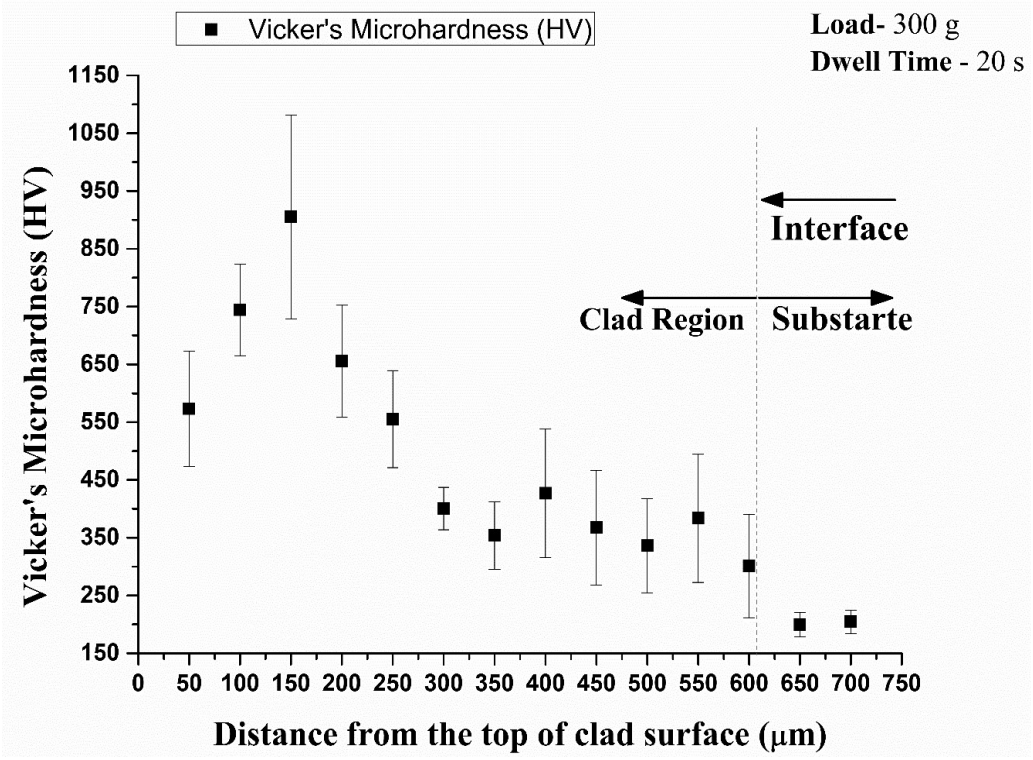

Figure 5.13: Microhardness profile of the developed EWAC-30Cr_3C_2 composite clad

The higher microhardness of clad region is due to the presence of hard carbide phases. The achieved average microhardness value for EWAC-10Cr_3C_2, EWAC-20Cr_3C_2 and EWAC-30Cr_3C_2 composite clads is 430±65 HV, 470±60 HV and 580±99 HV respectively, which is 2.47, 2.65 and 3.39 times larger than the substrate material microhardness (180±20 HV). The

large amount of standard deviation in the readings is observed, which might be due to the indentations are made on hard carbide phases and soft Ni matrix as well. The non-uniformity in microhardness in clad region attributed to the presence of multi phases of different natures formed during cladding and which is confirmed during XRD study. The indentation made on carbide particle region shows much higher values. The decreased value of hardness at interface zone of clad –substrate could be due to the fact that metallic dissolution increases at the interface. The synergy of high toughness and hardness makes the developed clads suitable for anti-cavitation wear applications.

5.1.4 Porosity assessment of EWAC-Cr_3C_2 developed clad

The porosity analysis of the clad region is essential as porosity is a significant factor that has great influence on functional characteristics of cladding. The mechanical properties like ductility and fatigue strength have been affected by porosity which further reduces the cavitation erosion resistance[171]. The cracks and pores are preferential locations for cavitation erosion wear [172], [173], hence, less porous and defect free clads are an essential requirement in cavitation erosion wear applications. Therefore, porosity must be assessed in the clad region. The porosity analysis of EWAC-x$Cr_3C_2$is shown in Figure 5.14-5.16.

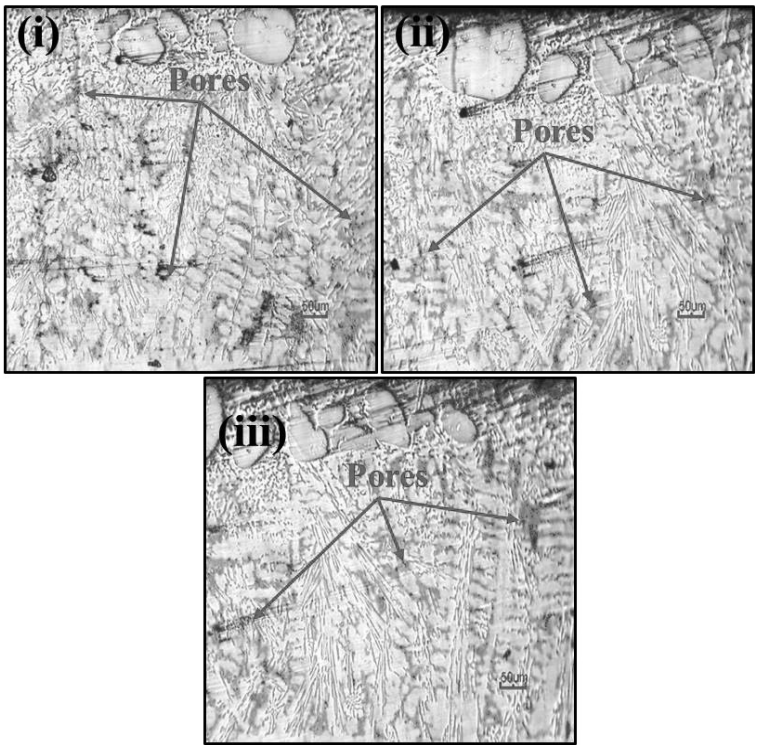

Figure 5.14: Optical micrographs of EWAC-10Cr_3C_2 composite clad showing porosity (a) region 1 (b) region 2 (c) region 3

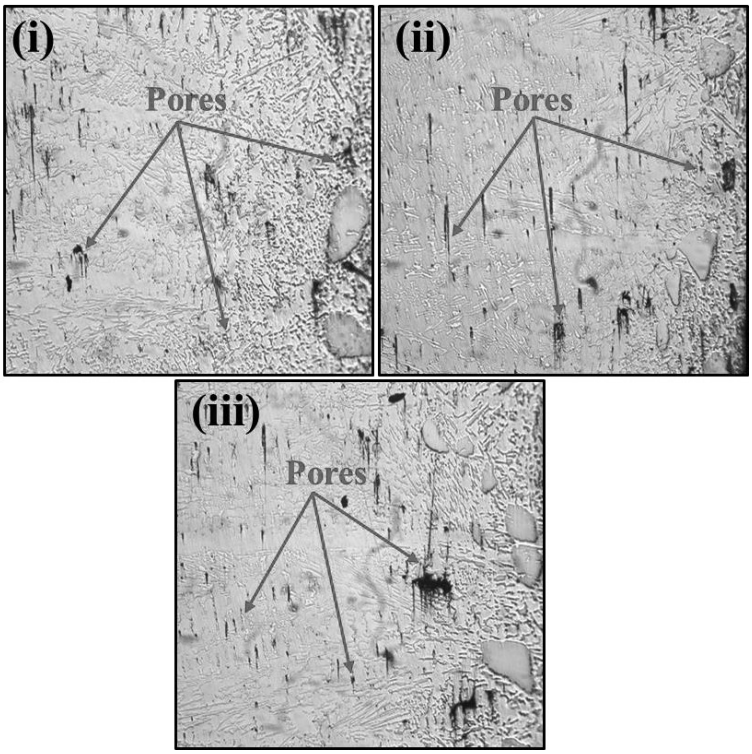

Figure 5.15: Optical micrographs of EWAC-20Cr_3C_2 composite clad showing porosity (a) region 1 (b) region 2 (c) region 3

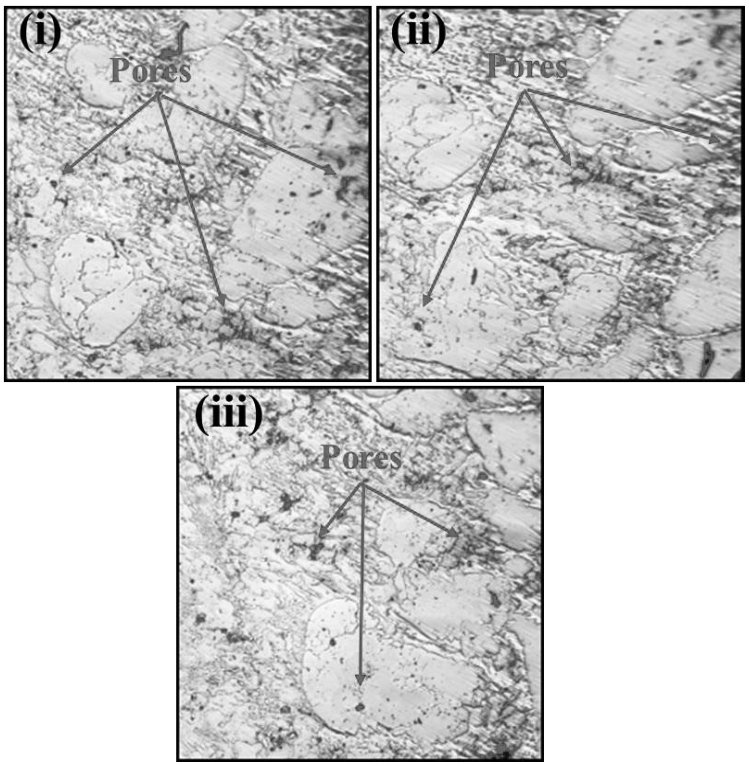

Figure 5.16: Optical micrographs of EWAC-30Cr_3C_2 composite clad showing porosity (a) region 1 (b) region 2 (c) region 3

The porosity is indicated by small red spots shown in clad region and results are presented in Table 5.4. The clad region is partitioned into three different sub regions and for better understanding, average value of porosity is reported.

Table 5.4: The results of porosity measurement of EWAC-xCr_3C_2 composite clad

Percentage porosity					
Composition		**Region**			**Mean**
		(i)	**(ii)**	**(iii)**	
EWAC-10Cr_3C_2	**Total pores**	8145	4816	5450	6137
	Pores %	1.35	1.19	1.21	**1.25**
EWAC-20Cr_3C_2	**Total pores**	4245	3061	3118	3475
	Pores %	1.40	0.80	1.10	**1.10**
EWAC-30Cr_3C_2	**Total pores**	469	366	714	516
	Pores %	1.00	0.66	1.28	**0.98**

The significantly less values of porosity are achieved as compare to other matured processes used for cladding [174], [175]. The presence of lower levels of porosity occurring in the so developed clads are due to the presence of reducing atmosphere during processing. This reducing atmosphere is due to the presence of charcoal used to improve the dynamics of microwave interaction with the poor microwave absorbing materials. This atmosphere prevents the further entrapment of the gases into clads during processing.

5.1.5 Flexural strength studies of EWAC-Cr_3C_2 developed clad

Flexure strength is one of the most significant utility indicators of many engineering components. The flexural strength of microwave processed developed clads has been assessed by a standard 3-point bend test. The observations after examine the flexural behaviour on developed EWAC-xCr_3C_2composite clads showed three-stage (Figures 5.17-5.20) load-displacement nature before failure.

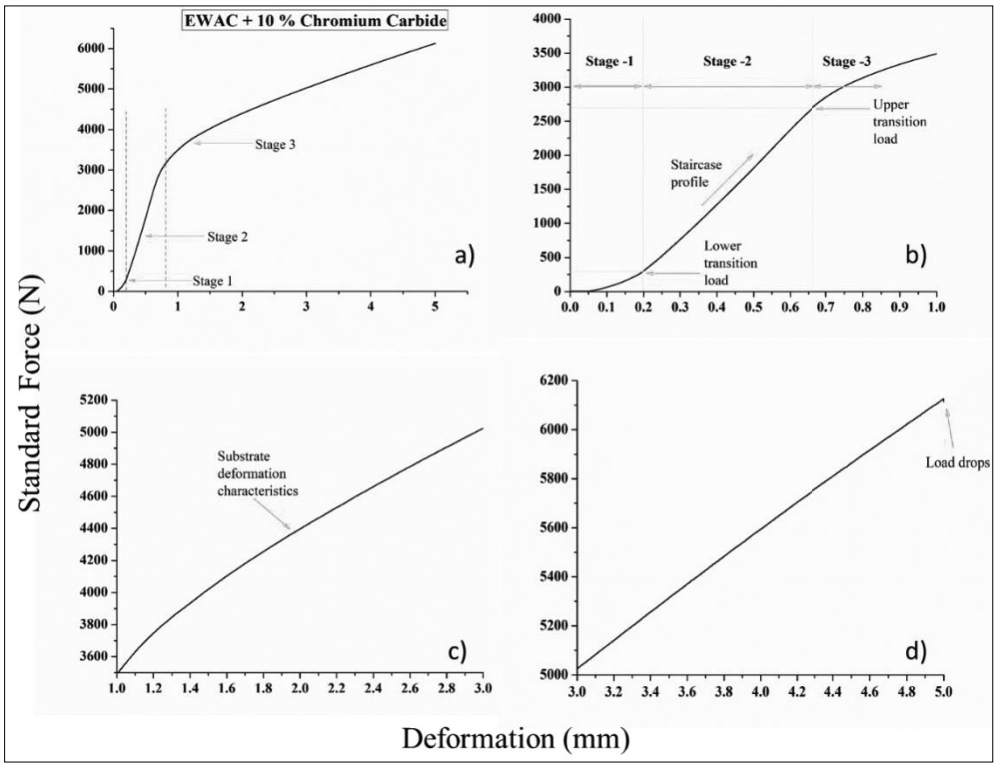

Figure 5.17: a) Load-displacement characteristics of developed EWAC-10Cr_3C_2 clad through microwave heating during standard 3-point bend test; magnifying views of load-displacement characteristics b) up to 1 mm c) between 1 mm to 3 mm d) ahead of 3 mm

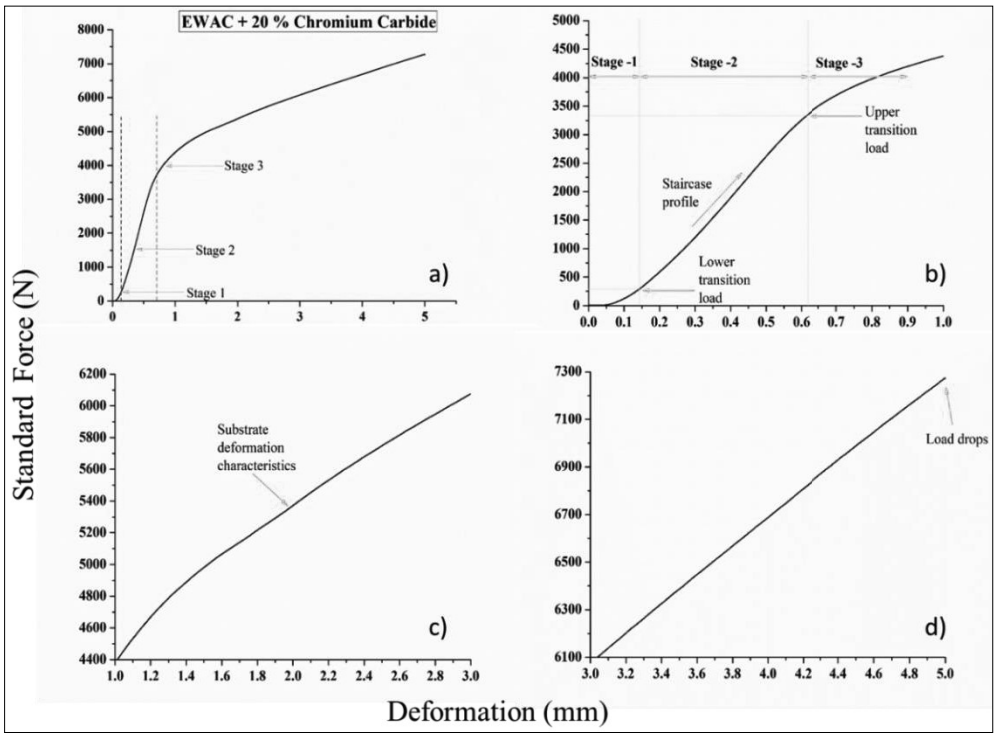

Figure 5.18: a) Load-displacement characteristics of developed EWAC-20Cr_3C_2 clad through microwave heating during standard 3-point bend test; magnifying views of load-displacement characteristics b) up to 1 mm c) between 1 mm to 3 mm d) ahead of 3 mm

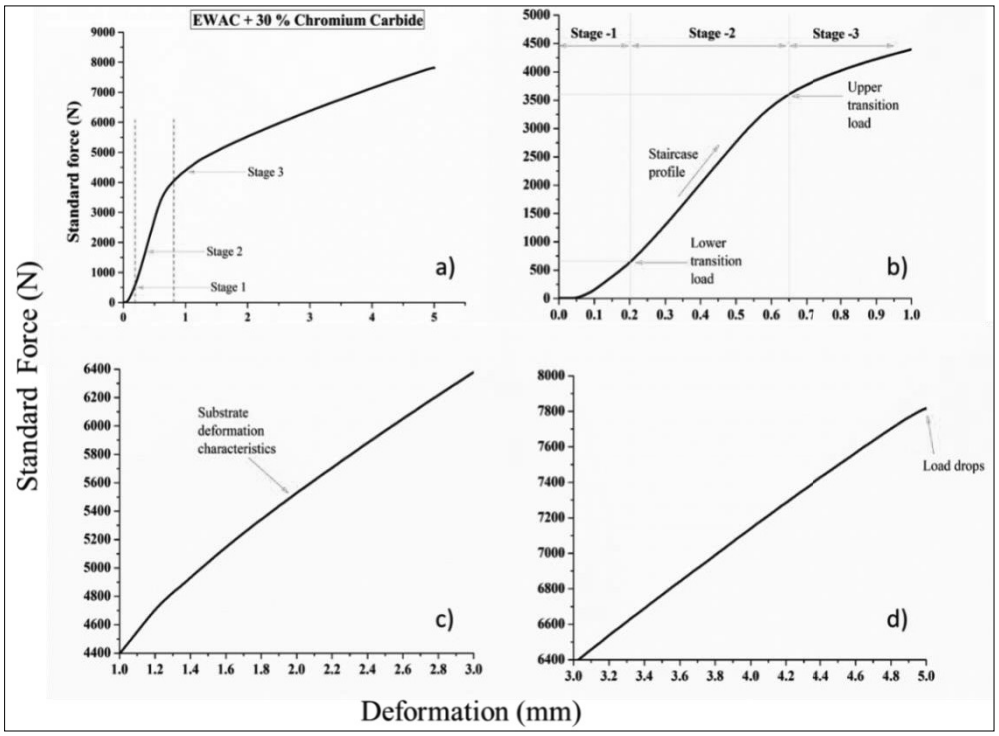

Figure 5.19: a) Load-displacement characteristics of developed EWAC-30Cr_3C_2 clad through microwave heating during standard 3-point bend test; magnifying views of load-displacement characteristics b) up to 1 mm c) between 1 mm to 3 mm d) ahead of 3 mm

The stage I, shows the linear displacement of developed clad up to lower transition load. The matrix phase of developed clads behaves elastically in this stage. Further, the developed clads experienced plastic deformation ahead of lower transition load. As the load increases, more amount of micro cracks formation started at top surface of clad layer. This growth and propagation of micro cracks in the hard carbide phase remain up to upper transition load (stage II). The stress may get release during the propagation of micro cracks. Further increase in load, the micro cracks started to propagate in multi direction and finally it reaches to interface of clad substrate. At this stage of load transmission, the developed clad may get fails owing to the debonding of clads from substrate.

The developed clads have been analysed using a parameter (deformation index (DI)), by which behaviour of coatings/clads can be assessed under flexure loading. Three samples of each composition have been tested and average values have been considered. The equation 5.2 [166] used for calculation of deformation index (DI) is

$$DI = \frac{\Delta\delta}{\Delta P} (\text{mm N}^{-1}) \tag{5.2}$$

Where ΔP = ±10% change in load at 50% rupture load P(N)

and $\Delta\delta$ = Corresponding change in flexural deformation (mm)

The resistance to the deformation of developed clads has been indicated by DI. The different observations of flexure testing are tabulated in Table 5.5.

Table 5.5: Observations of developed EWAC- xCr_3C_2 composite clads during flexural testing

Composition	S. No.	LTL (N)	UTL (N)	δ at UTL (mm)	FS (MPa)	Maximum load (N)	Maximum δ (mm)	Deformation index [$\times 10^{-4}$] (mm N^{-1})
EWAC + $10Cr_3C_2$	1	291	2696	0.66	638	6125	5.1	3.41
	2	324	2720	0.67	644	6210	5.3	3.40
	3	315	2710	0.67	641	6160	5.1	3.49
	Mean	**310**	**2709**	**0.67**	**642±5**	**6165**	**5.17**	**3.43**
EWAC + $20Cr_3C_2$	1	298	3562	0.67	758	7274	5.3	2.40
	2	331	3587	0.67	761	7305	5.4	2.39
	3	350	3601	0.68	750	7199	5.2	2.38
	Mean	**326**	**3583**	**0.67**	**756±6**	**7259**	**5.3**	**2.39**
EWAC + $30Cr_3C_2$	1	640	3593	0.60	825	7920	5.4	2.28
	2	653	3710	0.68	802	7700	5.5	2.42
	3	648	3638	0.65	815	7824	5.4	2.19
	Mean	**647**	**3647**	**0.64**	**814±11**	**7815**	**5.43**	**2.30**

LTL- lower transition load, UTL-upper transition load, δ- deformation, FS- flexural strength

It has been observed from Table 5.5 that there is an increase in the LTL of EWAC based and Cr_3C_2 reinforced composite clads with increase in weight percentage of reinforcement. The possible reason behind this is the increase in average microhardness of clad region (discussed in section 5.1.3). This results into requirement of more loads for starting the deformation in the clad region. Similar trend has also been observed for UTL, but the observed percentage change in the values of UTL is more, when the weight percentage of reinforcement has been increased from 10% to 20% in comparison from 20% to 30%. This may be due to the comparatively more agglomeration of carbide particles (observed in microstructure of clad region in section 5.1.1) in toughen matrix of Ni-Fe when the weight percentage has been increased from 20% to 30%. The interfacial bonding strength of agglomerated carbide particles with matrix material is low, therefore the deformation in the clad region has been observed at lower load. Hence, less percentage change in the values of UTL has been observed. However, the lower values of DI at all weight percentage show that the developed clads perform well under flexural loading. The higher flexural strength and lower DI values are due to the non-severity of the cracks.

The mode of fracture during flexural testing of composite clads has been assessed by fractographic analysis of 3-point bend tested clad samples. The tested sample images, as shown in Figure 5.20-5.22, show the transversal cracks development at the end of the test.

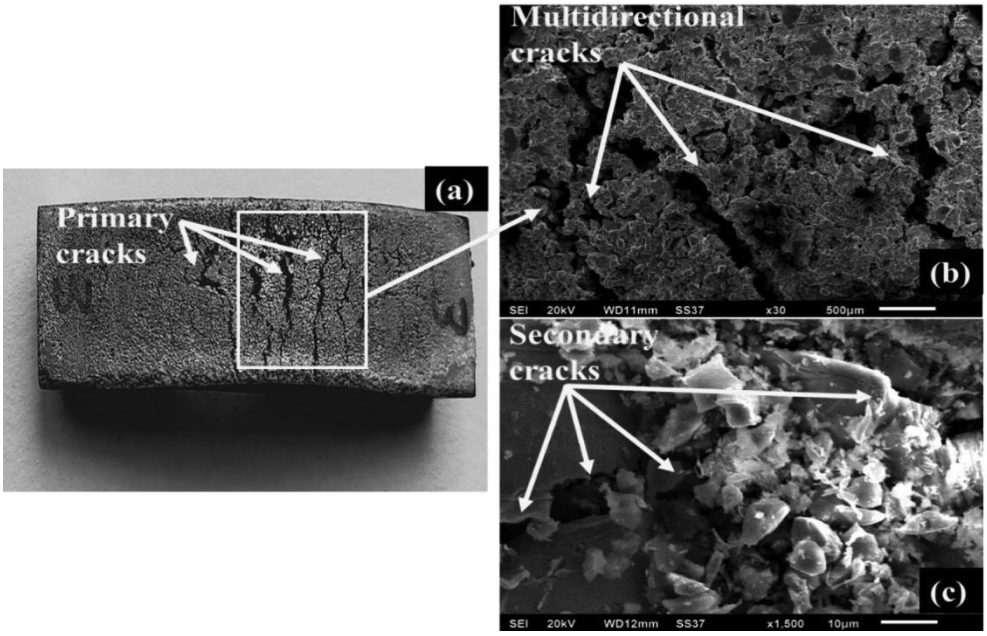

Figure 5.20: Fractured EWAC-10Cr_3C_2 clad specimen after 3-point bend test (a) Photograph of the top surface; SEM micrograph showing (b) primary cracks (c) secondary cracks

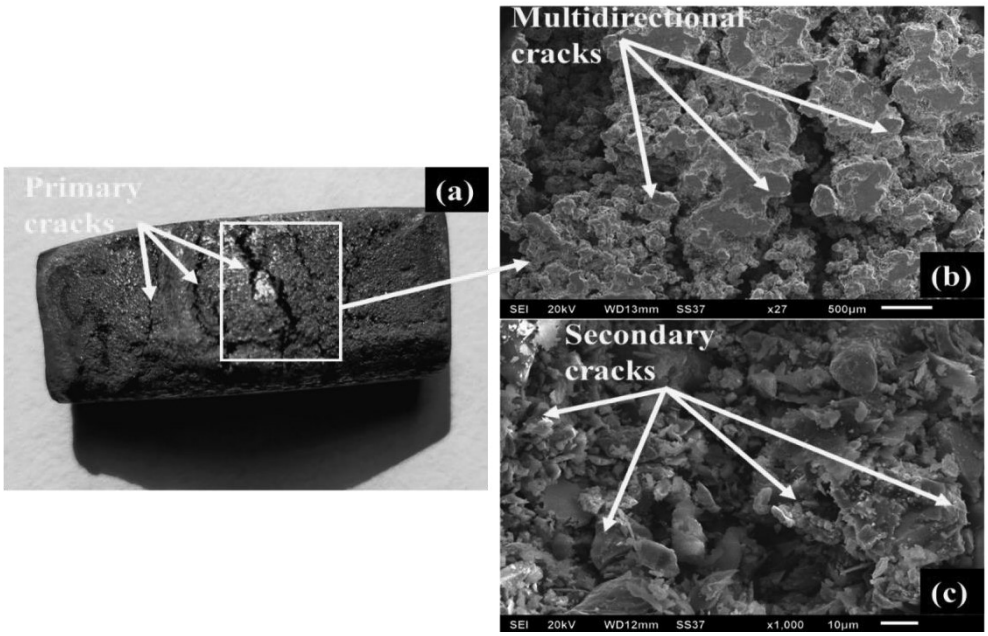

Figure 5.21: Fractured EWAC-20Cr_3C_2 clad specimen after 3-point bend test (a) Photograph of the top surface; SEM micrograph showing (b) primary cracks (c) secondary cracks

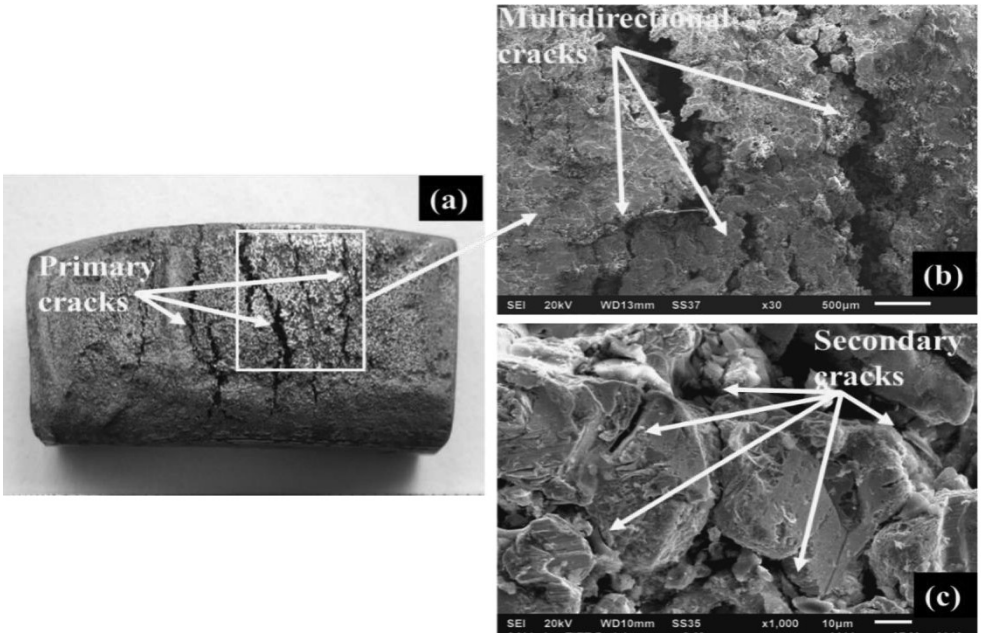

Figure 5.22: Fractured EWAC-30Cr_3C_2 clad specimen after 3-point bend test (a) Photograph of the top surface; SEM micrograph showing (b) primary cracks (c) secondary cracks

The SEM images of tested samples show multidirectional cracks (primary and secondary cracks) within the matrix and hard carbide reinforced phases. The presence of multidirectional cracks in the so developed clads is featured to the existence of multi-phase material system in EWAC-Cr_3C_2 based clads. The existence of hard carbide phases as shown in XRD spectrum (section 5.1.2) in the soft Ni-Fe matrix gives rise to the higher toughness in the developed clads. The features of mixed mode of fracture like primary and secondary cracks have been seen by closer inspection of fractured surfaces. The cracks are formed due to the mergence of nucleated micro cracks in developed clads and further increasing of loading widened the cracks and results into observed parallel cracks as well.

5.1.6 Microstructural characterization of EWAC-WC10Co2Ni developed clads

The sectioned views of EWAC-10WC10Co2Ni, EWAC-20WC10Co2Ni and EWAC-30WC10Co2Ni are shown in Figure 5.23-5.25, respectively. The metallurgical bonded clads of thickness 520 µm, 680 µm and 820 µm are developed. The developed clads are observed as without any visible defects and solidification/interfacial cracks (Figures 5.23-5.25(a)).

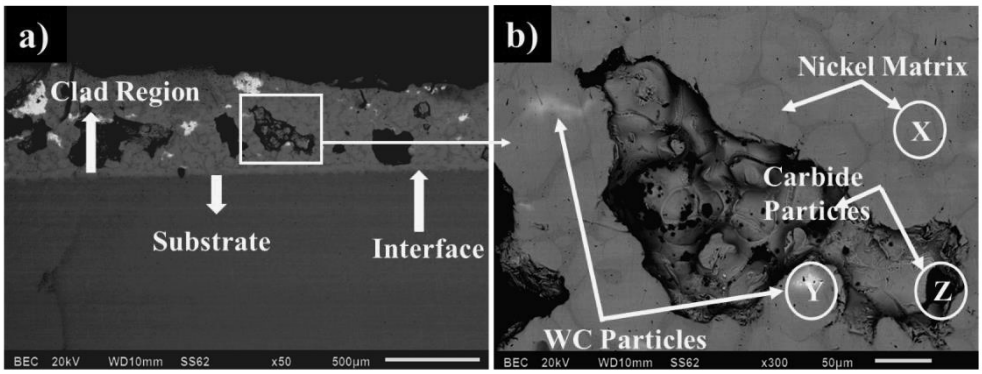

Figure 5.23: Typical BSE images of developed EWAC-10WC10Co2Ni clad a) clad region, substrate & interface b) enlarged view of clad region

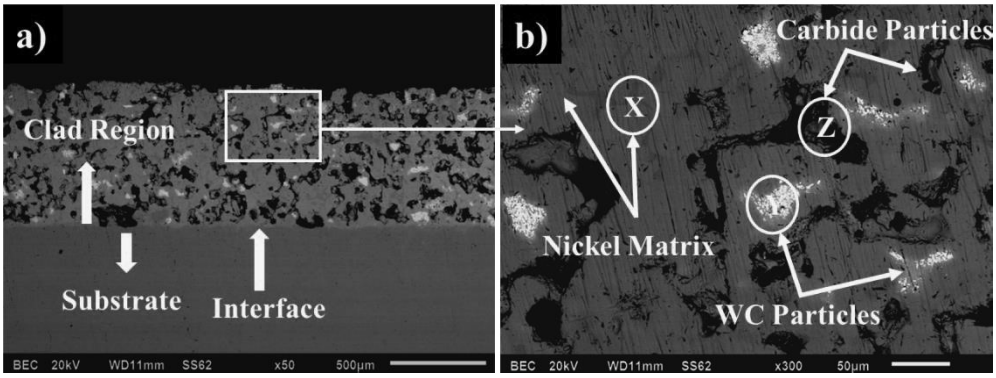

Figure 5.24: Typical BSE images of developed EWAC-20WC10Co2Ni clad a) clad region, substrate & interface b) enlarged view of clad region

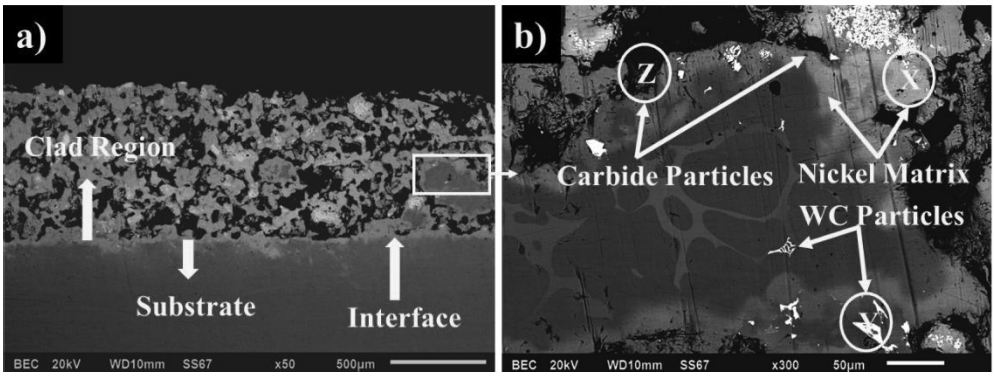

Figure 5.25: Typical BSE images of developed EWAC-30WC10Co2Ni clad a) clad region, substrate & interface b) enlarged view of clad region

The cellular like structure of the clad surface can be seen in an enlarged view (Figure 5.23 (b)). The unique property of volumetric heating of microwave processing leads to cellular growth in developed clad. The direction of heat flow controls the direction of cell growth, as the cell growth tendency always is towards the highest thermal gradient [166]. Further, there is not much difference between the thermal conductivity of the matrix base (90W/m K) and reinforcement (84W/m k) [176], which leads to uniform cooling of the clad surface and results

in the non-transition of cellular to the dendritic structure. The formation of a skeleton-like structure (Figure 5.25(b)) results from the typical slow cooling rate of the melt pool[19], [144]. EDS study of all the clads, at marked locations X, Y, and Z, is carried out (Figures 5.23-5.25(b)). The results are presented in Figures 5.26-5.28, respectively.

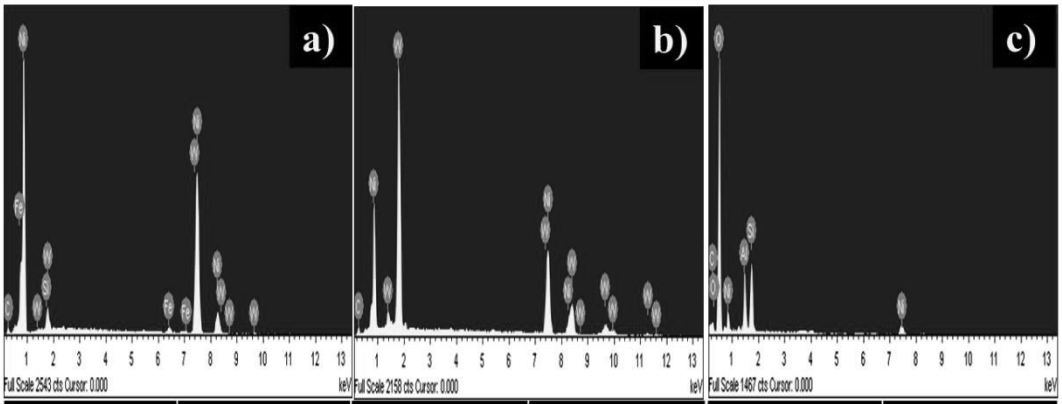

Elements	Weight %
Ni	82.02
Fe	7.61
W	4.78
Others	5.59

Elements	Weight %
W	60.83
Ni	33.13
C	6.04

Elements	Weight %
O	52.29
Ni	24.59
Fe	7.88
Others	15.24

Figure 5.26: EDS analysis of developed EWAC-10WC10Co2Ni clad at a) phase X b) phase Y c) phase Z

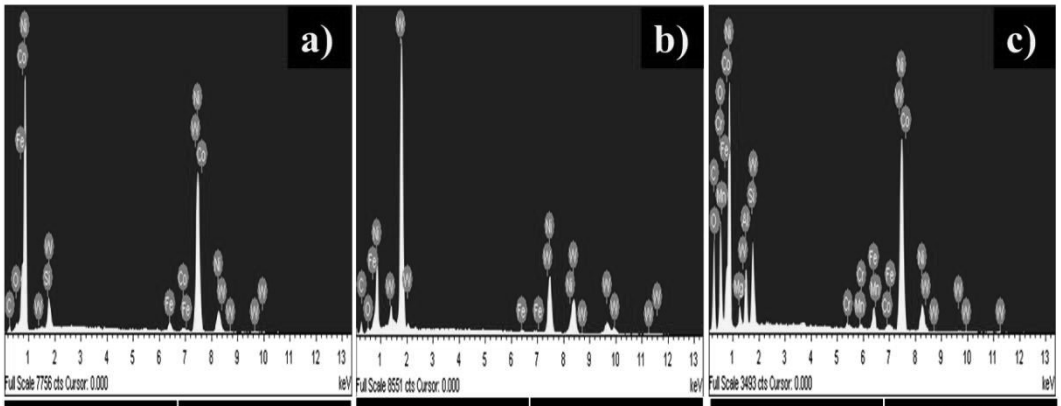

Elements	Weight %
Ni	79.96
W	7.06
Fe	6.15
Others	6.83

Elements	Weight %
W	68.40
Ni	18.23
C	7.58
Others	5.79

Elements	Weight %
Ni	39.87
C	28.97
O	16.75
Others	14.41

Figure 5.27: EDS analysis of developed EWAC-20WC10Co2Ni clad at a) phase X b) phase Y c) phase Z

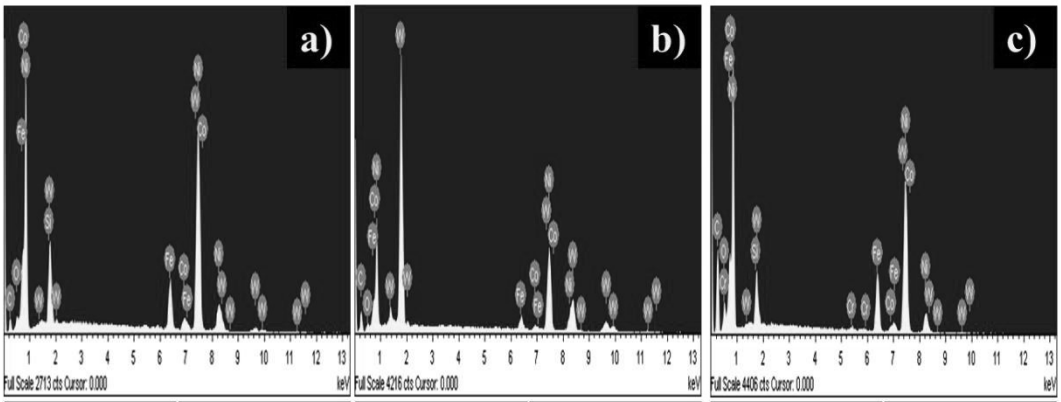

Elements	Weight %	Elements	Weight %	Elements	Weight %
Ni	61.93	W	52.67	Ni	42.36
W	15.47	Ni	29.13	C	33.32
Fe	8.75	C	11.87	Fe	10.02
Others	13.85	Others	6.33	Others	15.30

Figure 5.28: EDS analysis of developed EWAC-30WC10Co2Ni clad at a) phase X b) phase Y c) phase Z

The EDS study confirms that the grey region (point X) consists mainly Fe-Ni phase, which exhibits that Fe is diluted into the clad region, which strengthen the claim of metallurgical bonded clad powder with substrate. The white region (point Y) and the black region (point Z) consist of W rich phase along with Ni and C element, while in the Z region of 10% chromium carbide reinforcement clads shows the oxides of nickel phase. However as increase in chromium carbide reinforcement to 20% and 30%, the “Z” region as marked is manly composed of Ni-C and Oxygen element phase.

The elemental area mapping of the clad region has been carried out and presented in Figure 5.29-5.31.

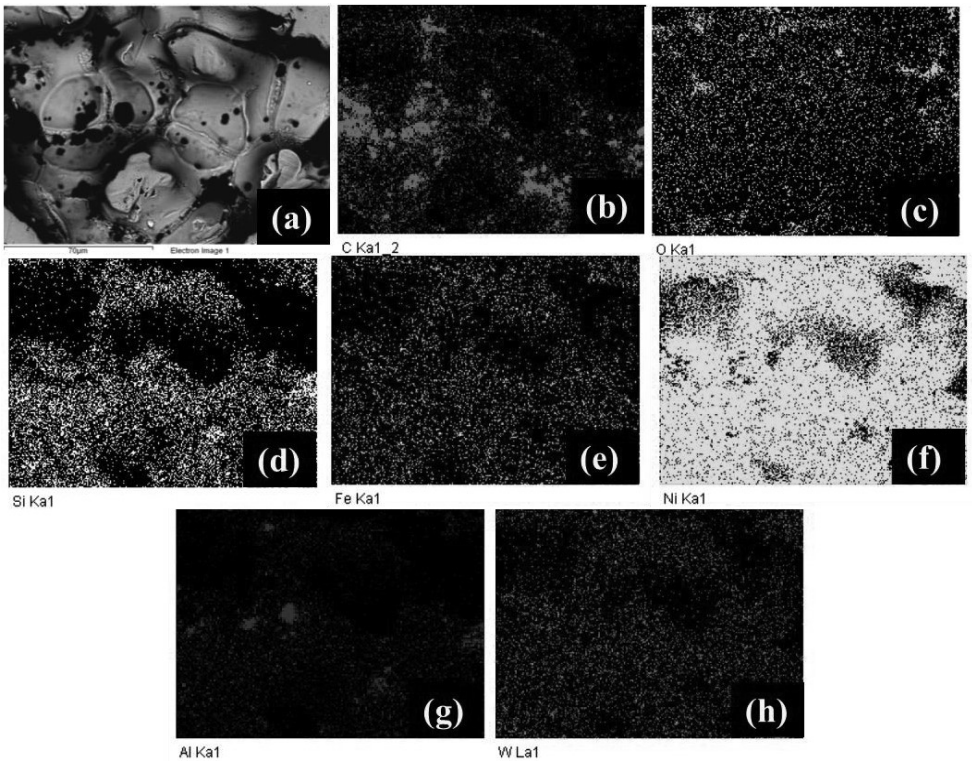

Figure 5.29: EDS mapping of developed EWAC-10WC10Co2Ni composite clad (a) area mapped location (b) C (c) O (d) Si (e) Fe (f) Ni (g) Al (h) W

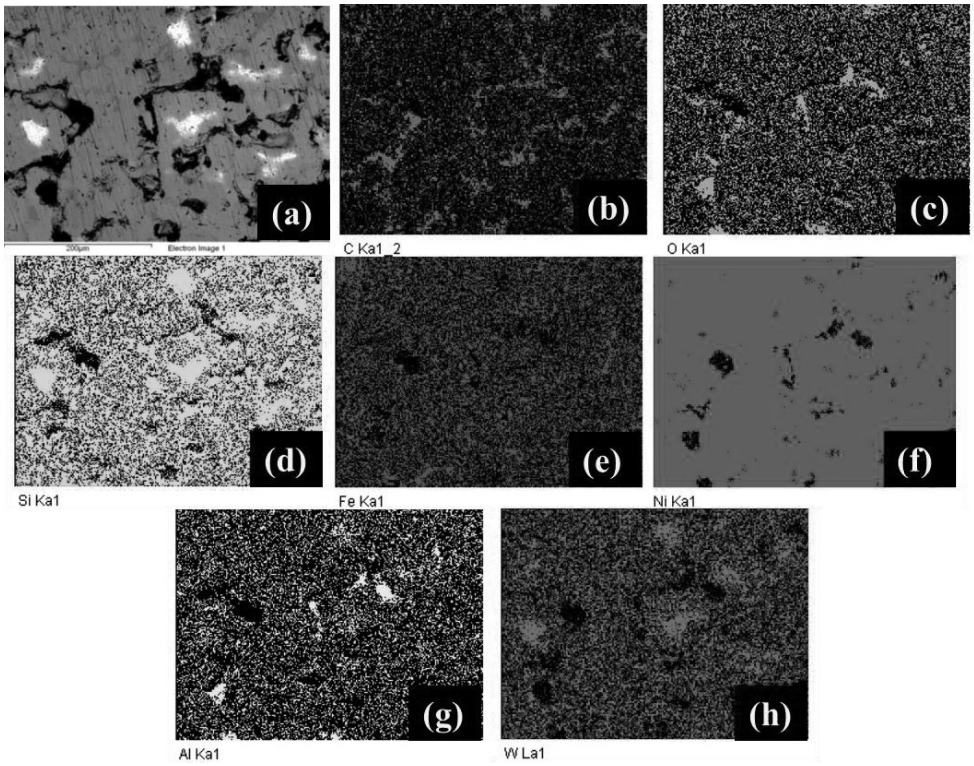

Figure 5.30: EDS mapping of developed EWAC-20WC10Co2Ni composite clad (a) area mapped location (b) C (c) O (d) Si (e) Fe (f) Ni (g) Al (h) W

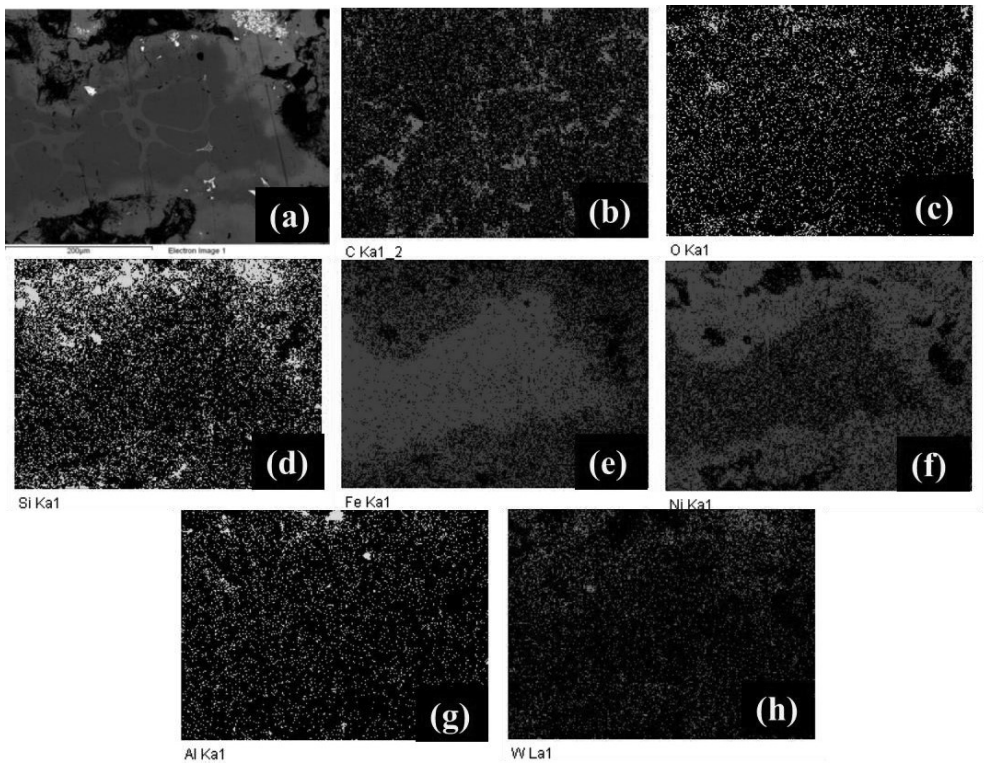

Figure 5.31: EDS mapping of developed EWAC-30WC10Co2Ni composite clad (a) area mapped location (b) C (c) O (d) Si (e) Fe (f) Ni (g) Al (h) W

The results of mapping confirm the presence of Ni-Fe matrix in grey region (X) and black region (Z) whereas, the presence of W and C significantly in the white region (Y). The agglomeration of reinforcement particles is the result of the non-uniform microwave absorption nature of the clad region due to the different physical properties of matrix and reinforcement powder, which results in thermal imbalance (discussed in section 5.1.1). The random dispersion of hard carbide phases into a comparatively soft Fe-Ni rich matrix also helps in achieving the combination of high hardness and toughness, which is an essential requirement to increase the CER of the developed clad.

5.1.7 Phase analysis of EWAC- WC10Co2Ni developed clads

The XRD spectra of developed composite clad of EWAC-xWC10Co2Ni (x=10,20,30) % is shown in Figure 5.32. The presence of different phases such as $NiCo_2O_4$, Ni_2W_4C, Ni_2Si, $NiAl_2O_4$, W_2C, Ni_3Si, Cr_3C_2, FeNi is observed from the obtained XRD spectra. The phases such as Ni_2W4_C, W_2C, Ni_3Si, and Cr_3C_2 are observed (high intensity peaks) as major phases. Nickel and chromium were present as major elements in EWAC powder. The microwave heating produces very high temperature and results into decomposition of W_2C into W and C. Further, the reaction of this decomposed tungsten (W) and carbon (C) with elements present in EWAC powder results into formation of Ni_2W_4C and Cr_3C_2. Cr and Si diluted into molten

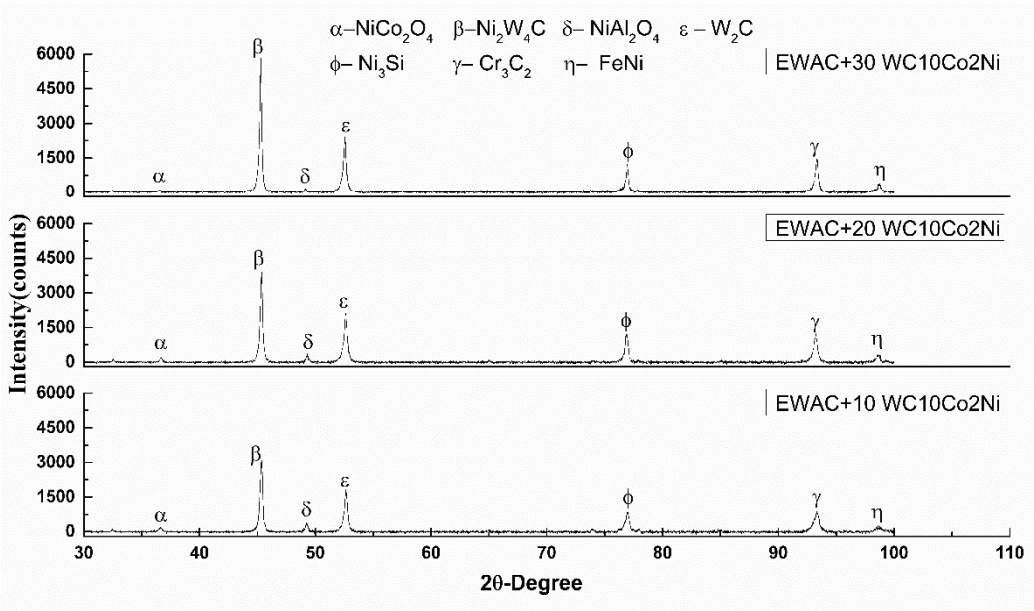

Figure 5.32: A typical XRD pattern of developed EWAC-xWC10Co2Ni composite clad

pool, when the matrix material melts. But, the C has low solubility in Ni liquid solution; hence, results into formation of Ni_3Si at high temperature owing to the reaction of Ni with Si. Few less intensity peaks of $NiCo_2O_4$, Ni_2Si, $NiAl_2O_4$, and FeNi were also present. The formation of $NiCo_2O_4$ is the result of reaction between decomposed Co with Ni and O present in reinforcement powder, matrix powder and atmosphere, respectively. The very high temperature produced during microwave irradiation results into formation of $NiAl_2O_4$ phase, because alumina sheet, which was directly in contact with the molten layer, reacts with Ni. The formation of phase FeNi evidenced that Fe diluted from substrate to clad region.

The results of NIR values are presented in Table 5.6-5.8.

Table 5.6: Normalized intensity ratio values of EWAC-10WC10Co2Ni composite clad

S. No.	Phase	I_1	I_2	I_3	I_4	I_5	I_6	I_7	I_{back}	NIR (%)
1	**$NiCo_2O_4$**	60.97	-	-	-	-	-	-	45	**0.16**
2	**Ni_2W_4C**	-	5823.33	-	-	-	-	-	45	**58.27**
3	**$NiAl_2O_4$**	-	-	90.81	-	-	-	-	45	**0.46**
4	**W_2C**	-	-	-	2023.42	-	-	-	45	**19.95**
5	**Ni_3Si**	-	-	-	-	896.13	-	-	45	**8.58**
6	**Cr_3C_2**	-	-	-	-	-	1090.65	-	45	**10.55**
7	**FeNi**	-	-	-	-	-	-	245.34	45	**2.02**

Table 5.7: Normalized intensity ratio values of EWAC-20WC10Co2Ni composite clad

S. No.	Phase	I_1	I_2	I_3	I_4	I_5	I_6	I_7	I_{back}	NIR (%)
1	**$NiCo_2O_4$**	169.05	-	-	-	-	-	-	41	**1.47**
2	**Ni_2W_4C**	-	3854.76	-	-	-	-	-	41	**43.80**
3	**$NiAl_2O_4$**	-	-	290.49	-	-	-	-	41	**2.87**
4	**W_2C**	-	-	-	2063.21	-	-	-	41	**23.22**
5	**Ni_3Si**	-	-	-	-	1163.1	-	-	41	**12.89**
6	**Cr_3C_2**	-	-	-	-	-	1163.1	-	41	**12.89**
7	**FeNi**	-	-	-	-	-	-	290.53	41	**2.87**

Table 5.8: Normalized intensity ratio values of EWAC-30WC10Co2Ni composite clad

S. No.	Phase	I_1	I_2	I_3	I_4	I_5	I_6	I_7	I_{back}	NIR (%)
1	**$NiCo_2O_4$**	174.15	-	-	-	-	-	-	33	**2.18**
2	**Ni_2W_4C**	-	2534.42	-	-	-	-	-	33	**38.65**
3	**$NiAl_2O_4$**	-	-	324.26	-	-	-	-	33	**4.50**
4	**W_2C**	-	-	-	1743.1	-	-	-	33	**26.43**
5	**Ni_3Si**	-	-	-	-	815.31	-	-	33	**0.93**
6	**Cr_3C_2**	-	-	-	-	-	759.95	-	33	**12.09**
7	**FeNi**	-	-	-	-	-	-	158.64	33	**1.02**

The contribution of phase Ni_2W_4C is highest in the developed EWAC-10-30WC10Co2Ni clads. This phase contributes 58.27 %, 43.80% and 38.65% in the developed EWAC-10-30 WC10Co2Ni clads, respectively. Phase W_2C has identified as second major phase which contributes 19.95%, 23.22% and 26.43% in the developed EWAC-10-30WC10Co2Ni clads, respectively.

5.1.8 Microhardness study of EWAC- xWC10Co2Ni developed clad

Hardness is an essential property of microwave processed clad, which significantly influences the wear characteristics. The hard carbides present in the matrix region might result in the higher hardness of the clad region. This fact is verified by taking the microhardness indentations across the lateral section of developed composite clads. The indents for EWAC-10WC10Co2Ni, EWAC-20WC10Co2Ni and EWAC-30WC10Co2Ni, are made at a distance of 40 µm, 60 µm, and 70 µm, respectively, according to variation in thickness of developed clad (Figures 5.33-5.35). The indents are made starting from top of clad and proceeding in direction of the substrate surface. The indents, at a distance of 60 µm, at the either sides of each indent are also made. An average of 12 sets of indents is evaluated for better understanding.

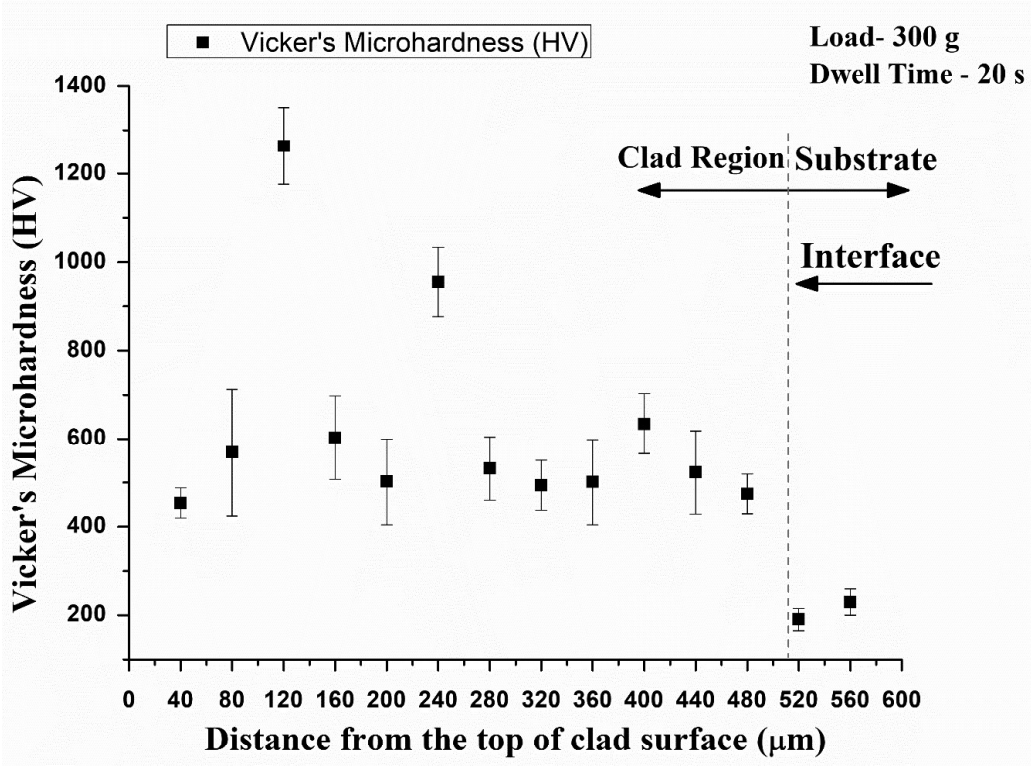

Figure 5.33: Microhardness profile of the developed EWAC-10WC10Co2Ni composite clad

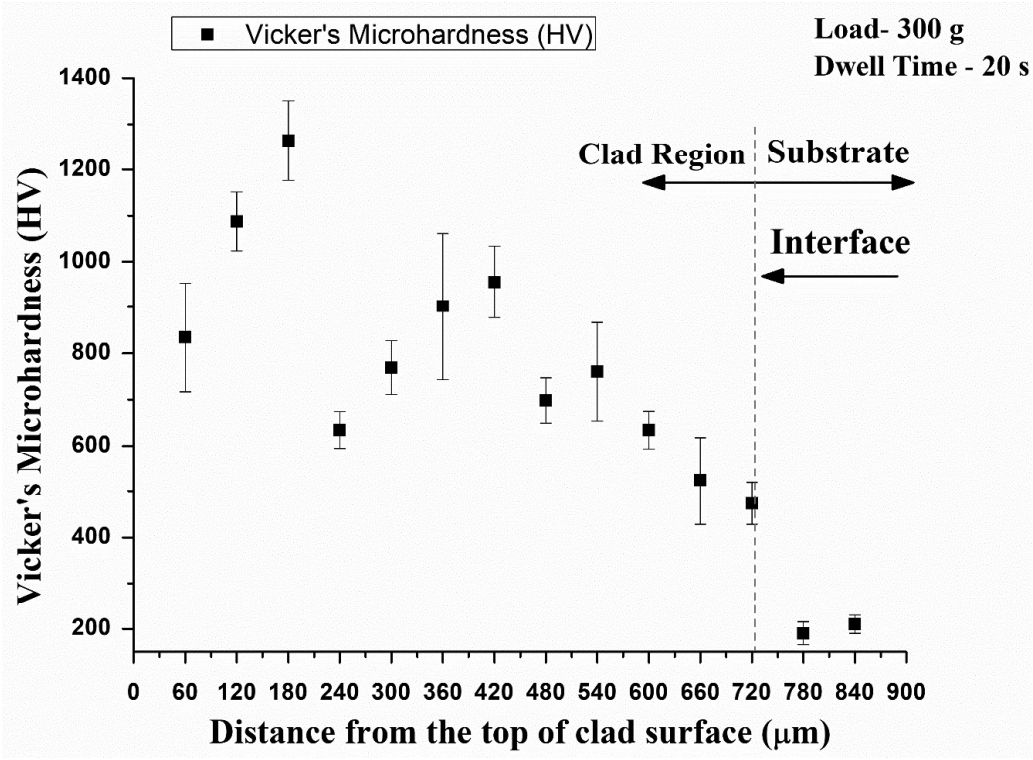

Figure 5.34: Microhardness profile of the developed EWAC-20WC10Co2Ni composite clad

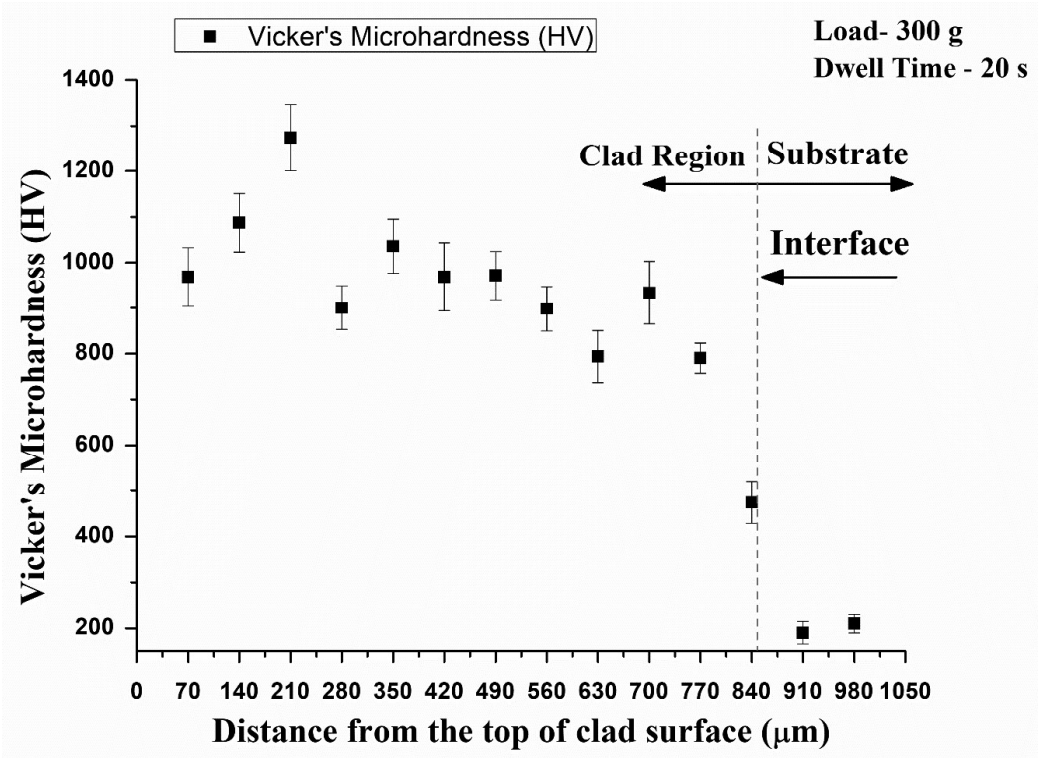

Figure 5.35: Microhardness profile of the developed EWAC-30WC10Co2Ni composite clad

The observed average microhardness values of EWAC-10WC10Co2Ni, EWAC-20 WC10Co2Ni and EWAC-30WC10Co2Ni are 625±81 HV, 795±78 HV, and 925± 57 HV,

which are almost 3.53, 4.36 and 4.91 times higher than substrate microhardness value. The variation in hardness in the clad region shows that indents on the soft matrix and hard phases are made. The least average microhardness was observed in EWAC-10WC10Co2Ni. This is because very few carbide phases were present in the clad region, and indents are mostly fallen at comparatively soft Nickel matrix. Similarly, the volume fraction of carbide particles was more in EWAC-30WC10Co2Ni. Therefore, the formation of carbide phases is more, which results into fall of most indents on hard carbide phases and results into higher hardness. In EWAC-20WC10Co2Ni, the formation of carbide phases was less than EWAC-30WC10Co2Ni and more than EWAC-10WC10Co2Ni, therefore, the indents fell on soft nickel matrix as well as on carbide phases. Due to less plastic deformation at carbide phases, the observed hardness value was more and high plastic deformation at soft matrix results into less hardness value. Therefore, higher hardness value was observed in higher concentration of reinforcement. The clad microhardness analysis verifies the combination of high hardness associated with high toughness.

5.1.9 Porosity assessment of EWAC- xWC10Co2Ni developed clad

The porosity of developed EWAC-xWC10Co2Ni composite clads is assessed. The porosity in the three different regions of each clad is assessed and the average porosity is considered (Table 5.9).

Table 5.9: The results of porosity measurement of EWAC- xWC10Co2Ni composite clad

Percentage porosity					
Composition		**Region**			**Mean**
		(i)	**(ii)**	**(iii)**	
EWAC-10WC10Co2Ni	**Total pores**	1502	3485	1443	2143
	Pores %	0.85	1.08	0.79	**0.90**
EWAC-20WC10Co2Ni	**Total pores**	14117	11968	11860	12648
	Pores %	1.38	1.36	1.04	**1.20**
EWAC-30WC10Co2Ni	**Total pores**	20774	21695	18948	20472
	Pores %	1.50	1.3	1.37	**1.39**

The average values of porosity for EWAC-10WC10Co2Ni, EWAC-20WC10Co2Ni and EWAC-30WC10Co2Ni are found as 0.90%, 1.20% and 1.39%, respectively. The reason for low porosity in microwave processed clad is presence of less thermal gradient and lower solidification rate associated during microwave processing. The volumetric nature of heating and hybrid mode of heating is helps to achieve such conditions and hence yields low level of porosity in developed composite clads.

5.1.10 Flexural strength studies of EWAC-xWC10Co2Ni developed clad

The observations after examine the flexural behaviour on developed EWAC-xWC10Co2Ni composite clads showed three-stage (Figures 5.36-5.38) load-displacement nature before failure.

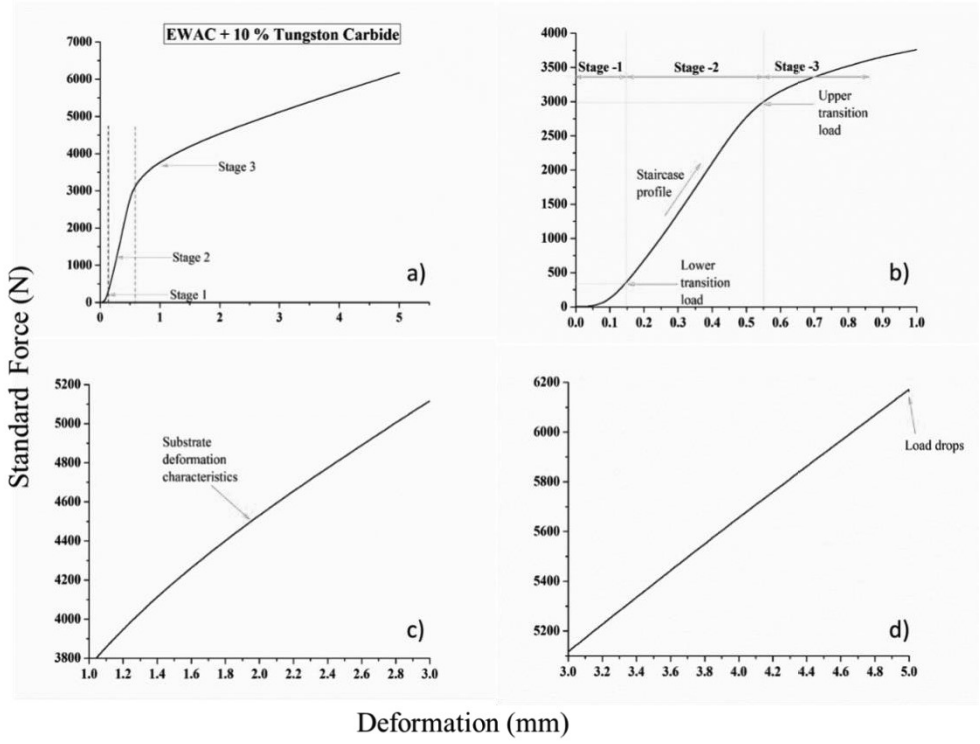

Figure 5.36: a) Load-displacement characteristics of developed EWAC-10WC10Co2Ni clad through microwave heating during standard 3-point bend test; magnifying views of load-displacement characteristics b) up to 1 mm c) between 1 mm to 3 mm d) ahead of 3 mm

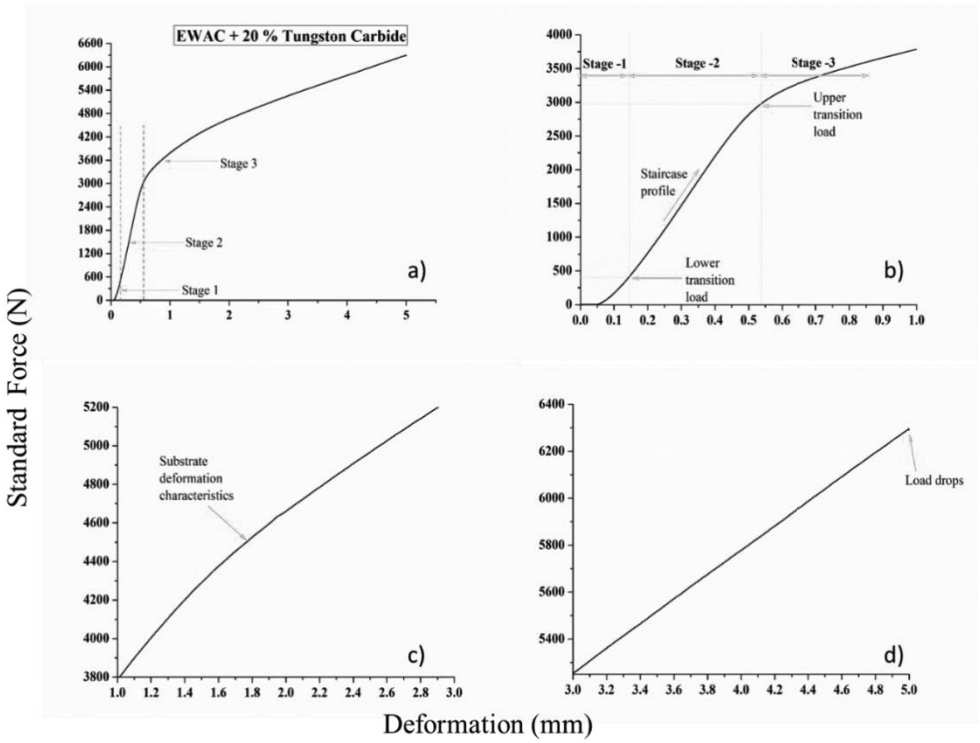

Figure 5.37: a) Load-displacement characteristics of developed EWAC-20WC10Co2Ni clad through microwave heating during standard 3-point bend test; magnifying views of load-displacement characteristics b) up to 1 mm c) between 1 mm to 3 mm d) ahead of 3 mm

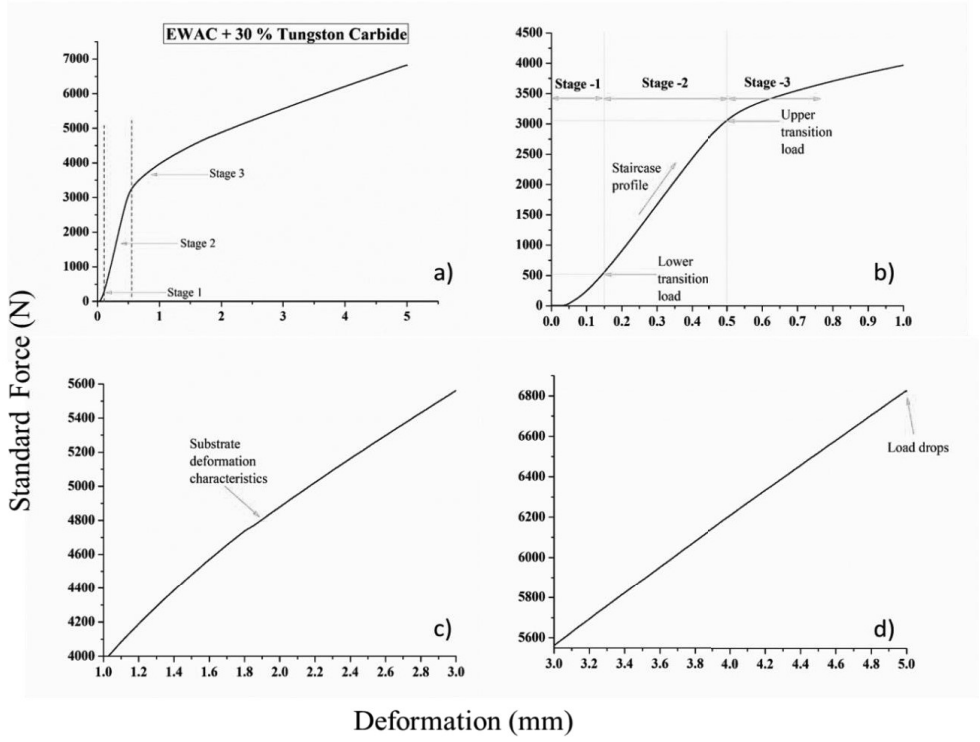

Figure 5.38: a) Load-displacement characteristics of developed EWAC-30WC10Co2Ni clad through microwave heating during standard 3-point bend test; magnifying views of load-displacement characteristics b) up to 1 mm c) between 1 mm to 3 mm d) ahead of 3 mm

The stage I, shows the linear displacement of developed clad up to lower transition load (303, 410 and 547 for EWAC-10WC10Co2Ni, EWAC-20WC10Co2Ni, EWAC-30WC10Co2Ni, respectively). The elastic behaviour of matrix phase of developed clads is observed in this stage. The developed clads experienced plastic deformation ahead of lower transition load. With further increase in load, the formation of micro cracks start increasing at top surface of clad layer. This continues up to upper transition load (stage II) (3100, 2972 and 3055 for EWAC-10WC10Co2Ni, EWAC-20WC10Co2Ni, EWAC-30WC10Co2Ni, respectively). The stress may get release during the propagation of micro cracks. Further increase in load, the micro cracks started to propagate in all directions and it reaches to interface of clad substrate. At this stage of load transmission, the developed clad fails owing to the detachment of clad layer from substrate region.

Table 5.10: Observations of developed EWAC- xWC10Co2Ni clads during flexural testing

Composition	S. No.	LTL (N)	UTL (N)	δ at UTL (mm)	FS (MPa)	Maximum load (N)	Maximum δ (mm)	Deformation index [$\times 10^{-4}$] (mm N^{-1})
EWAC + 10WC10Co2Ni	1	303	3100	0.58	643	6171	5.4	2.33
	2	289	2979	0.55	635	6098	5.2	2.37
	3	298	3002	0.55	638	6122	5.1	2.36
	Mean	**297**	**3027**	**0.56**	**639±4**	**6130**	**5.23**	**2.35**
EWAC + 20WC10Co2Ni	**1**	410	2972	0.54	656	6296	5.4	2.26
	2	425	3015	0.54	661	6345	5.5	2.23
	3	455	3095	0.55	658	6315	5.4	2.23
	Mean	**430**	**3028**	**0.54**	**658±3**	**6319**	**5.43**	**2.24**
EWAC + 30WC10Co2Ni	**1**	547	3055	0.50	711	6826	5.0	2.05
	2	590	3190	0.51	738	7087	5.2	2.01
	3	625	3261	0.55	725	6956	5.3	1.99
	Mean	**587**	**3169**	**0.52**	**725±14**	**6956**	**5.17**	**2.02**

LTL- lower transition load, UTL-upper transition load, δ- deformation, FS- flexural strength

It has been observed from Table 5.10 that LTL has gradually increased with increase in the weight percentage of WC10Co2Ni reinforcement in the EWAC based composite clads like Cr_3C_2 reinforced composite clads. The reason attributed behind this is the gradual increase in the average microhardness of clad region (discussed in section 5.1.8). However, for UTL, the interfacial bonding strength of carbide particles with matrix material also play a significant role. The wettability of tungsten carbide particles with Ni is low due to large contact angles [177]. The value of average microhardness in the EWAC-10WC10Co2Ni composite clads was low (625±81 HV), therefore, the interfacial bonding strength plays a dominating role. Similar trend has been observed for EWAC-20WC10Co2Ni. However, for EWAC-30WC10Co2Ni a significant increase in UTL was observed, which is due to the corresponding significant increase in the average microhardness of clad region (925± 57 HV). Therefore, in this case, the

microhardness possibly dominates the interfacial bonding strength. The low values of DI confirm that the cracks formation was not severe. Three samples of each composition have been tested and average values have been considered.

The 3-point bend tested clad samples SEM images are shown in Figure 5.39-5.41. It was observed that the primary micro cracks occurred in the developed composite clads are due to initial loading. The continuous increase in load results into widened these micro cracks and ultimately fails of clad layer. However, even at such high applied load, good metallurgical bonding of clad layer helps to prevents the peeling of the clad layer from substrate.

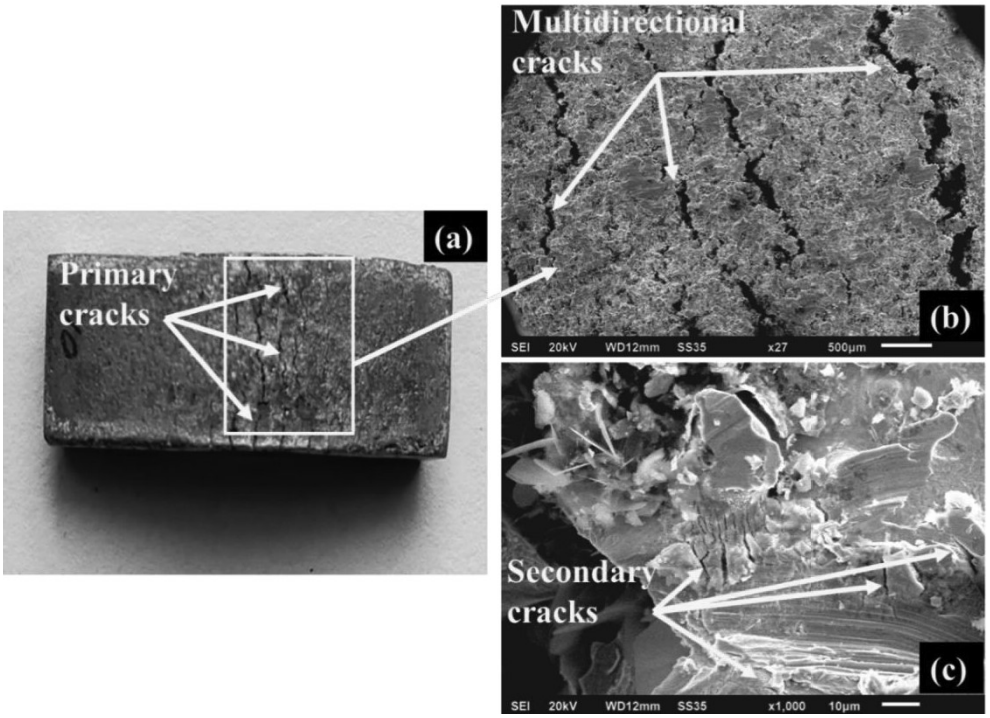

Figure 5.39: Fractured EWAC-10WC10Co2Ni clad specimen after 3-point bend test
(a) Photograph of the top surface; SEM micrograph showing (b) primary cracks (c) secondary cracks

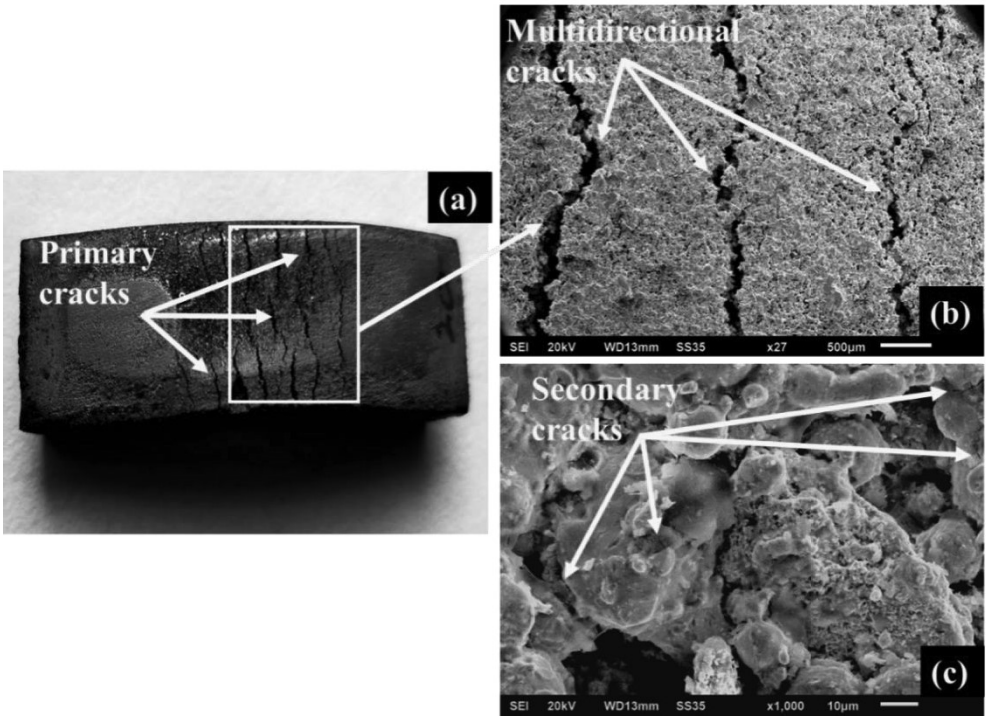

Figure 5.40: Fractured EWAC-20WC10Co2Ni clad specimen after 3-point bend test

(a) Photograph of the top surface; SEM micrograph showing (b) primary cracks (c) secondary cracks

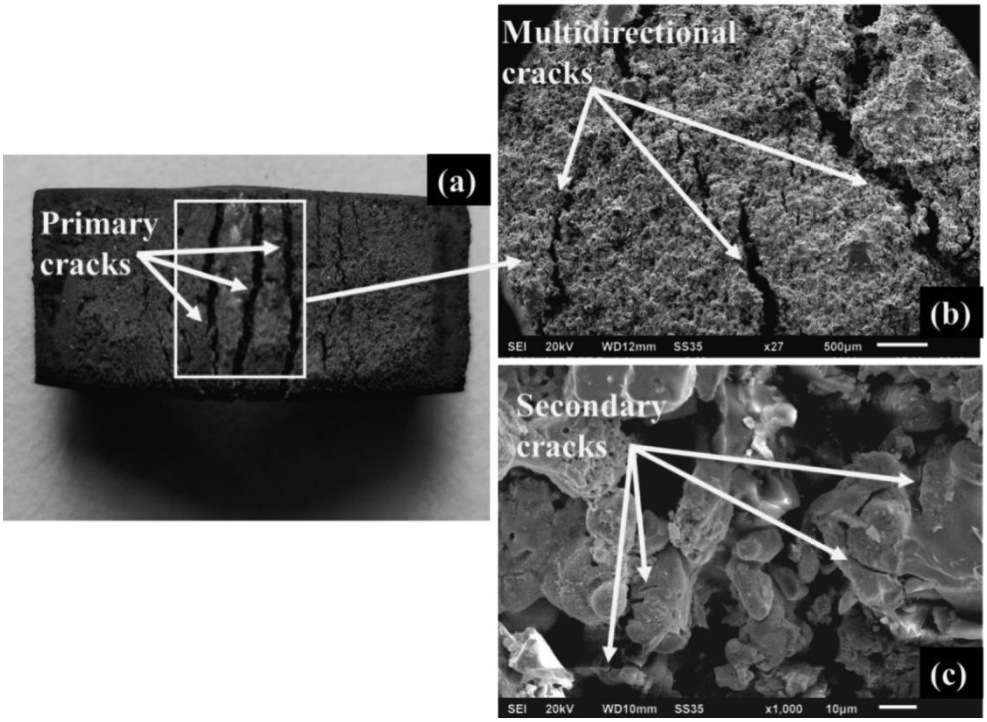

Figure 5.41: Fractured EWAC-30WC10Co2Ni clad specimen after 3-point bend test

(a) Photograph of the top surface; SEM micrograph showing (b) primary cracks (c) secondary cracks

5.1.11 Microstructural characterization of developed EWAC-xAl_2O_3composite clads

The BSE images of the cross-section of microwave synthesized EWAC-5Al_2O_3, EWAC-10Al_2O_3 and EWAC-15Al_2O_3composite clads are shown in Figure 5.43-5.45. The clads of almost uniform thickness ~540 µm,970µm and1090 µm were successfully deposited, which can be clearly seen from Figure 5.42-5.44 (a).

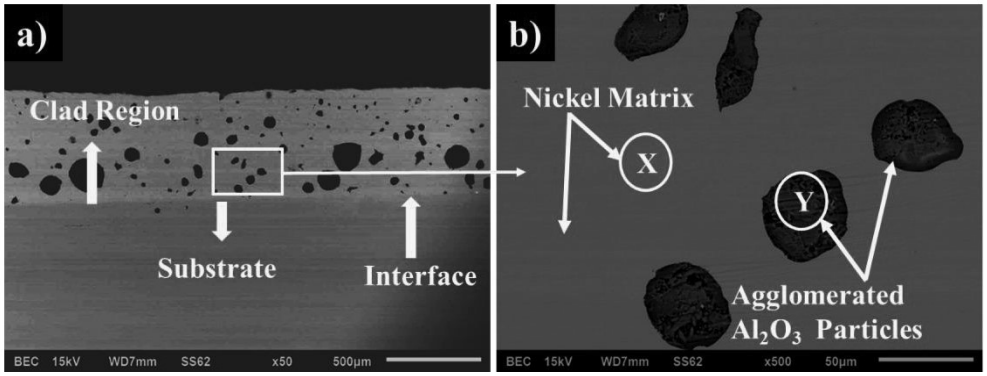

Figure 5.42: Typical BSE images of developed EWAC-5Al_2O_3 clad a) clad region, substrate & interface b) enlarged view of clad region

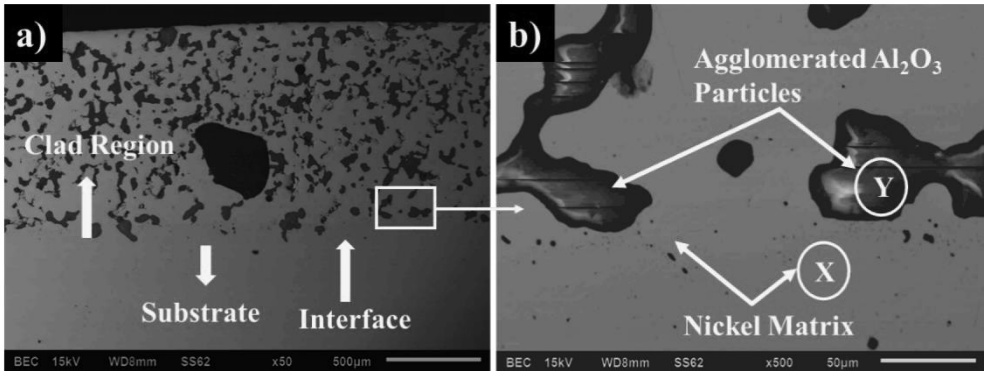

Figure 5.43: Typical BSE images of developed EWAC-10Al_2O_3 clad a) clad region, substrate & interface b) enlarged view of clad region

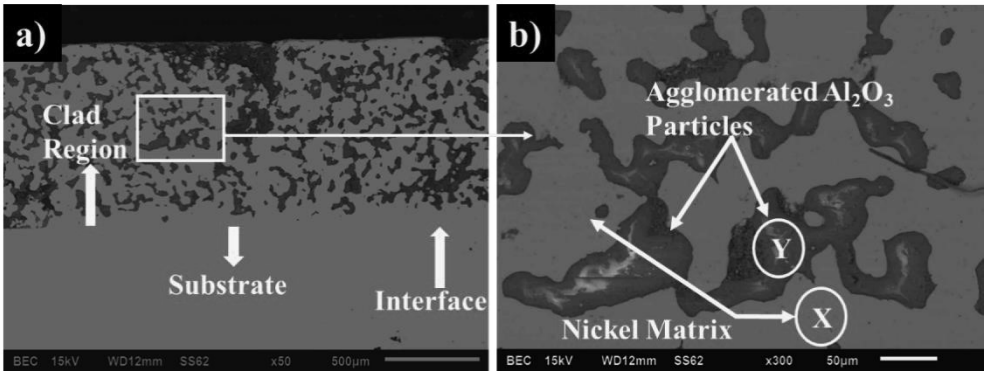

Figure 5.44: Typical BSE images of developed EWAC-15Al_2O_3 clad a) clad region, substrate & interface b) enlarged view of clad region

The clear wavy interface is free from visible discontinuities, and the clad region is free of solidification and interfacial cracks, which are generally present in other cladding/coating processes. The absence of dendrite formation of cells in the clad region is due to the uniform thermal gradient, restricting the cell transition into dendrites [178]. The EDS analysis was carried out to verify the elemental composition of the white and black phases. For this purpose, the white phase location marked as X and the black phase location marked as Y (Figure 5.42-5.44 (b)) were analyzed. The EDS spectra of both locations are shown in Figure 5.45-5.47.

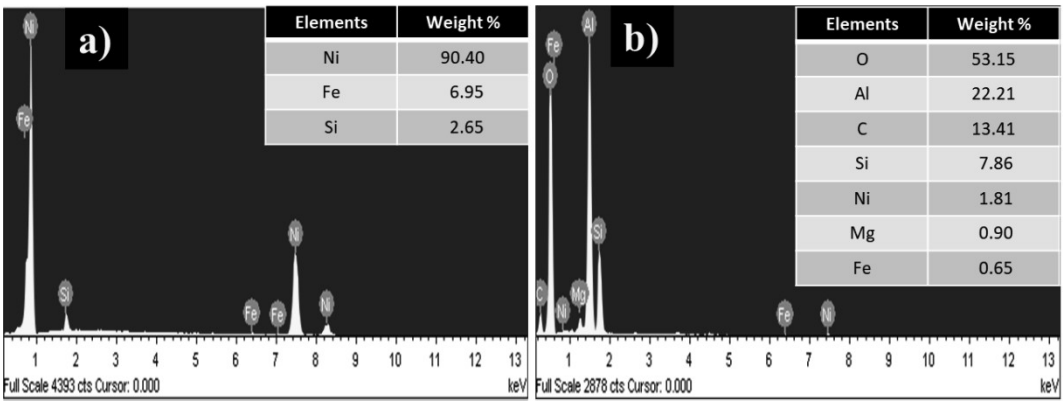

Figure 5.45: EDS analysis of developed EWAC-5Al_2O_3 clad at a) phase X b) phase Y

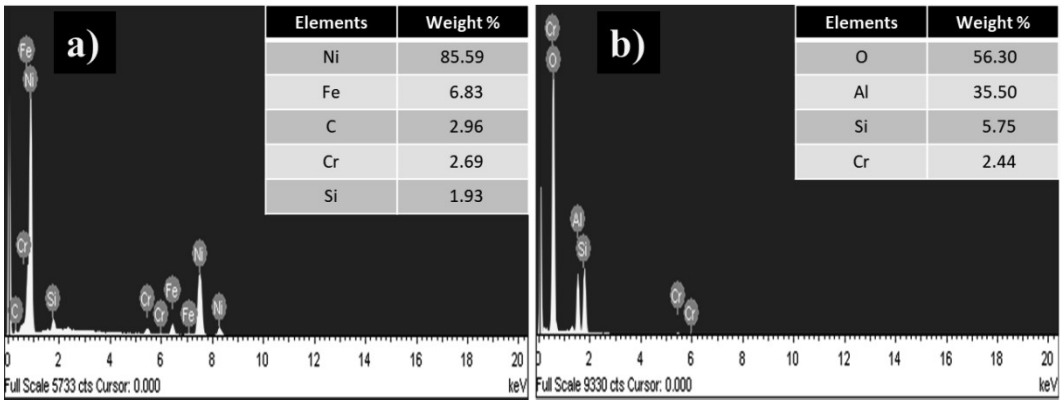

Figure 5.46: EDS analysis of developed EWAC-10Al_2O_3 clad at a) phase X b) phase Y

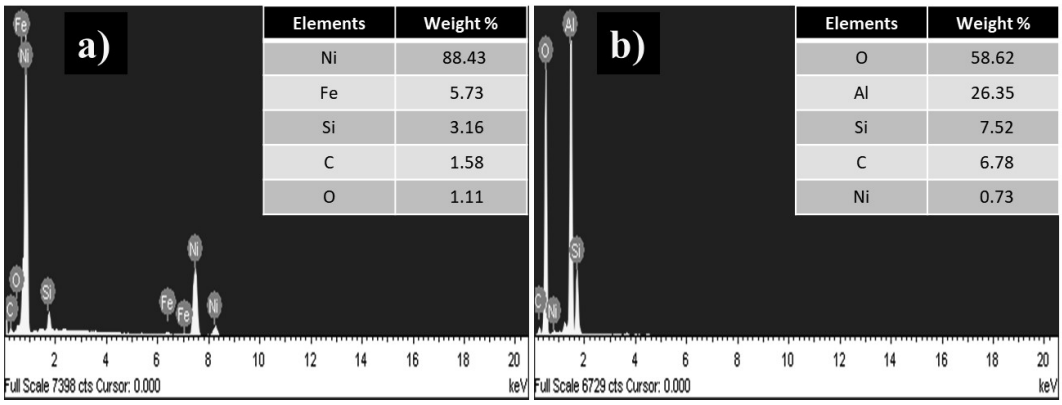

Figure 5.47: EDS analysis of developed EWAC-15Al_2O_3 clad at a) phase X b) phase Y

The enlarged view of the particular selected region (Figure 5.43-5.45(b)) shows randomly dispersed and partially agglomerated Al_2O_3(black phase) reinforced particles in Ni-based matrix (white phase), as a dispersed pattern, throughout the cladding. The setup of convective current during microwave heating is responsible for the agglomeration of Al_2O_3 particles in the clad region. The overall strength of developed composite clad can be achieved by the uniform dispersion of these reinforcement particles (black phase) inside the soft Ni matrix (white phase) [166]. Therefore, the elemental area mapping of the developed clad was carried out to investigate the dispersion. The location and results of the EDS area mapping are presented in Figure 5.48-5.50. The mapping results reveal that the Al and O are uniformly dispersed throughout the matrix. Simultaneously, the darker spots (Al and O presence in bulk) corresponding to black phases, again confirmed that these are agglomerated Al_2O_3 particles. Further, it is also exhibited that all the other minor elements (C, Si, Cr, and Fe) are well dispersed in the Ni-based matrix.

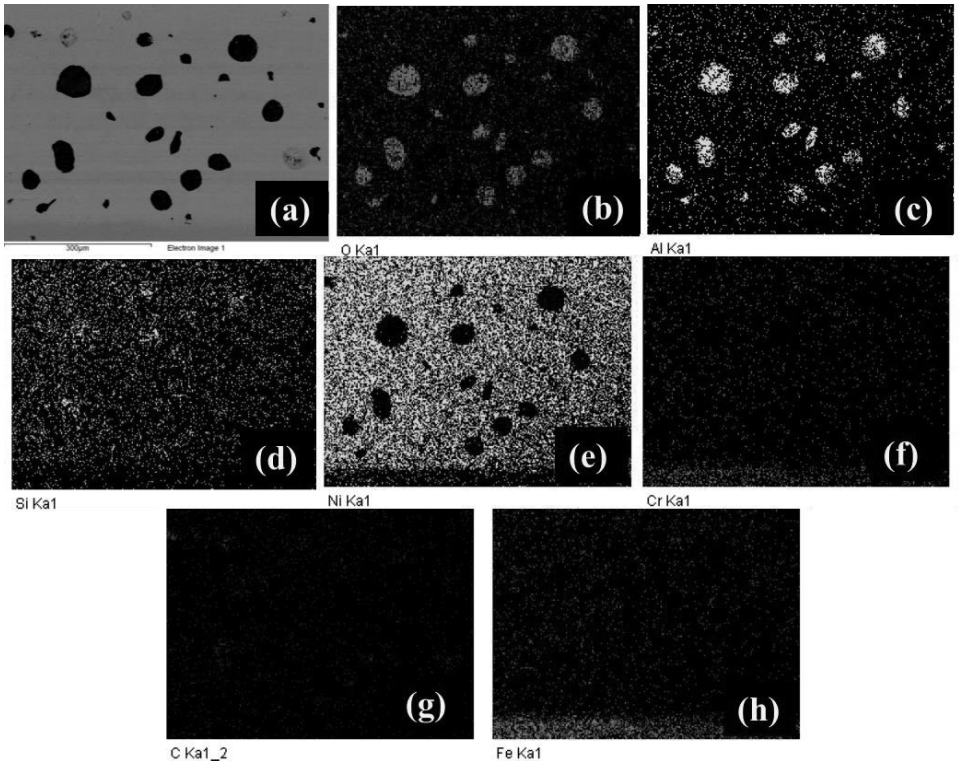

Figure 5.48: EDS mapping of developed EWAC-5Al_2O_3 composite clad (a) area mapped location (b) O (c) Al (d) Si (e) Ni (f) Cr (g) C (h) Fe

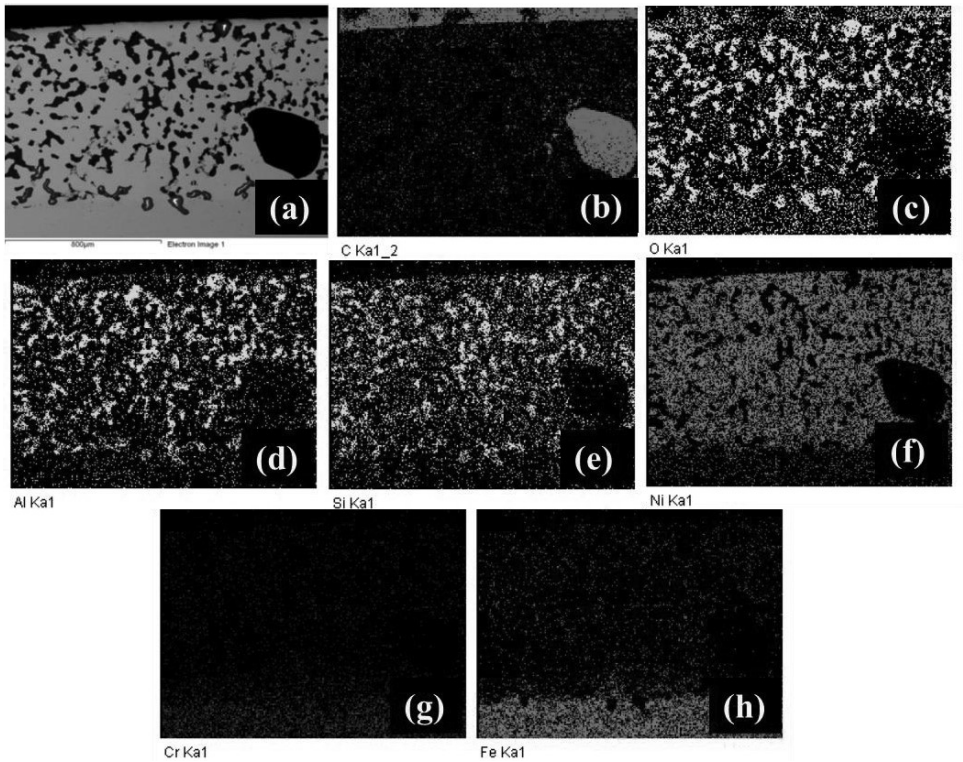

Figure 5.49: EDS mapping of developed EWAC-10Al_2O_3 composite clad (a) area mapped location (b) C (c) O (d) Al (e) Si (f) Ni (g) Cr (h) Fe

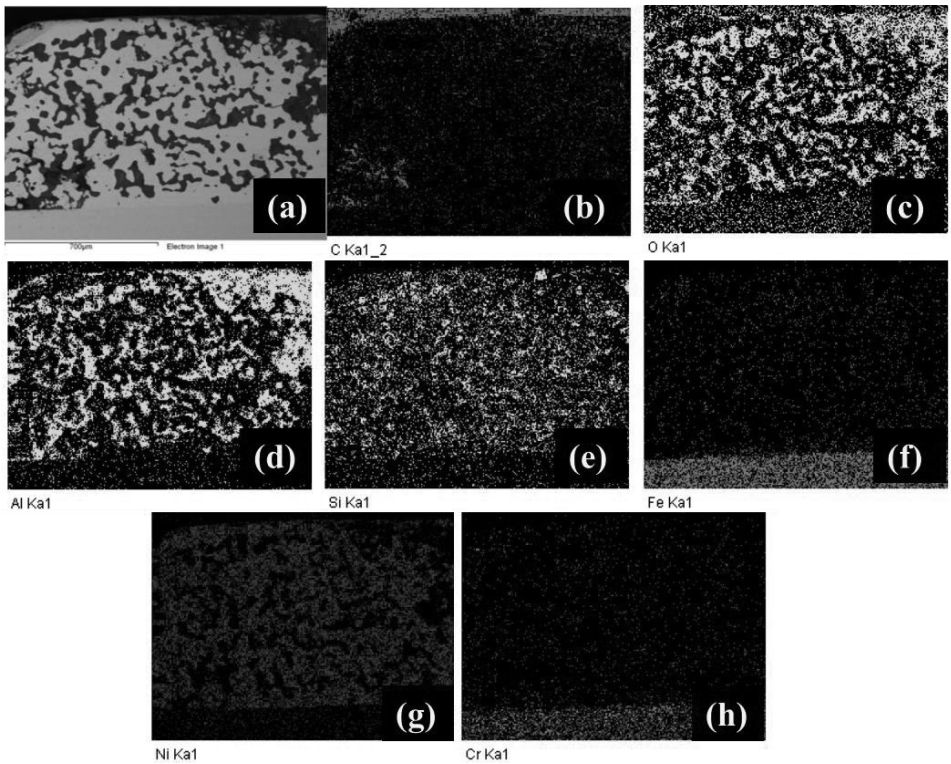

Figure 5.50: EDS mapping of developed EWAC-15Al_2O_3 composite clad (a) area mapped location (b) C (c) O (d) Al (e) Si (f) Fe (g) Ni (h) Cr

5.1.12 Phase analysis of EWAC-xAl$_2$O$_3$ developed clads

The XRD pattern of the microwave synthesized EWAC-xAl$_2$O$_3$(x= 5,10,15) % composite clads is shown in Figure 5.51.

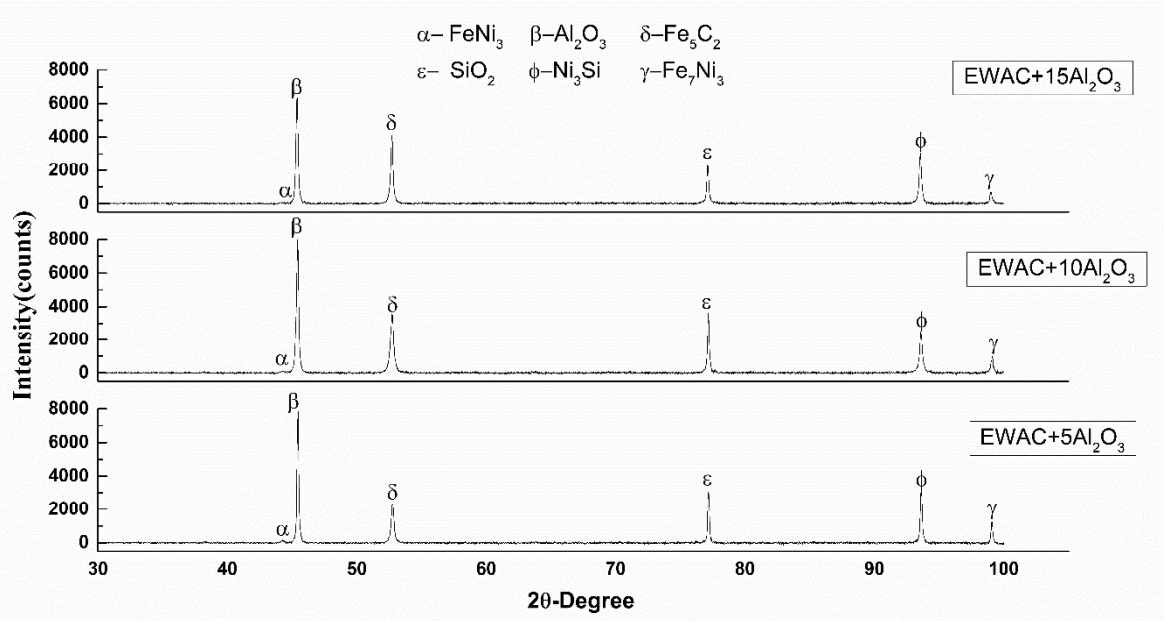

Figure 5.51: A typical XRD pattern of developed EWAC-xAl$_2$O$_3$composite clads

The analyzed XRD results confirm that the microwave synthesized EWAC-xAl$_2$O$_3$ composite clads are composed of the following phases: Intermetallics (Ni$_3$Si, FeNi$_3$, and Fe$_7$Ni$_3$), Carbides (Fe$_5$C$_2$) and Oxides (Al$_2$O$_3$ and SiO$_2$). Ni and Si both were constituents of raw clad powder, and the increase in affinity of Ni and Si at high-temperature during intense microwave heating results in the formation of the Ni$_3$Si phase [137]. However, the formation of phases like FeNi$_3$, Fe$_7$Ni$_3$ and Fe$_5$C$_2$ reveals that the Fe from the substrate has reacted with the Ni and C of clad powder. Moreover, the formation of FeNi$_3$, Fe$_7$Ni$_3$and Fe$_5$C$_2$ phase in developed composite clads validate the claim of Fe dilution into the clad region. Since Fe was not present initially in the significant percentage in Ni-based clad powder, it also supports the claim of metallurgical bonding. Al$_2$O$_3$ material particles are transparent to microwave till 600ºC [179], i.e., the Al$_2$O$_3$particles have remained dispersed in the soft Ni-based matrix in their original form after the microwave heating. Also, the O present in the atmosphere might have reacted with the Si, present in both the clad powders, and resulted in the formation of the SiO$_2$ phase. In contrast, the formation of the SiO$_2$ layer is advantageous to some extent because it further increases the oxidation resistance [159]. Further, the XRD quantitative evaluation results of the developed EWAC-xAl$_2$O$_3$composite clads in terms of NIR values are presented in Table 5.11-5.13.

Table 5.11: Normalized intensity ratio values of EWAC-5Al_2O_3 composite clad

S.No.	Phase	I_1	I_2	I_3	I_4	I_5	I_6	I_{back}	NIR(%)
1	**$FeNi_3$**	119.55	-	-	-	-	-	45.5	**0.44**
2	**Al_2O_3**	-	7694.99	-	-	-	-	45.5	**45.40**
3	**Fe_5C_2**	-	-	2312.1	-	-	-	45.5	**13.45**
4	**SiO_2**	-	-	-	2723.49	-	-	45.5	**15.89**
5	**Ni_3Si**	-	-	-	-	3036.9	-	45.5	**17.75**
6	**Fe_7Ni_3**	-	-	-	-	-	1234.76	45.5	**7.06**

Table 5.12: Normalized intensity ratio values of EWAC-10Al_2O_3 composite clad

S.No.	Phase	I_1	I_2	I_3	I_4	I_5	I_6	I_{back}	NIR(%)
1	**$FeNi_3$**	98.53	-	-	-	-	-	40	**0.32**
2	**Al_2O_3**	-	8030.34	-	-	-	-	40	**43.53**
3	**Fe_5C_2**	-	-	3549.89	-	-	-	40	**19.12**
4	**SiO_2**	-	-	-	3569.39	-	-	40	**19.23**
5	**Ni_3Si**	-	-	-	-	2374.56	-	40	**12.72**
6	**Fe_7Ni_3**	-	-	-	-	-	973.07	40	**5.08**

Table 5.13: Normalized intensity ratio values of EWAC-15Al_2O_3 composite clad

S.No.	Phase	I_1	I_2	I_3	I_4	I_5	I_6	I_{back}	NIR(%)
1	**$FeNi_3$**	78	-	-	-	-	-	50	**0.18**
2	**Al_2O_3**	-	6225.22	-	-	-	-	50	**39.19**
3	**Fe_5C_2**	-	-	3898.55	-	-	-	50	**24.42**
4	**SiO_2**	-	-	-	2285.43	-	-	50	**14.19**
5	**Ni_3Si**	-	-	-	-	2941.65	-	50	**18.35**
6	**Fe_7Ni_3**	-	-	-	-	-	630.22	50	**3.68**

The contribution of phase Al_2O_3 is highest in the developed EWAC-5-15Al_2O_3 clads. This phase contributes 45.40 %, 43.53% and 39.19% in the developed EWAC-5-15Al_2O_3 clads, respectively.

5.1.13 Microhardness study of EWAC-xAl_2O_3 developed clad

The microhardness and other mechanical properties are entirely associated with the microstructure of the material. Microstructure depends on the clad powder composition, size, experimental conditions like heating rate, cooling rate and heating profile [16], [20], [180]–[182]. The composite clads developed using microwave irradiation and Al_2O_3 reinforcements, in different weight percentage, are expected to enhance the clad region's microhardness. Therefore, to authenticate this fact, the microhardness of the clad region was evaluated. The microhardness profiles of the EWAC-xAl_2O_3composite clads are shown in Figures 5.52-5.54.

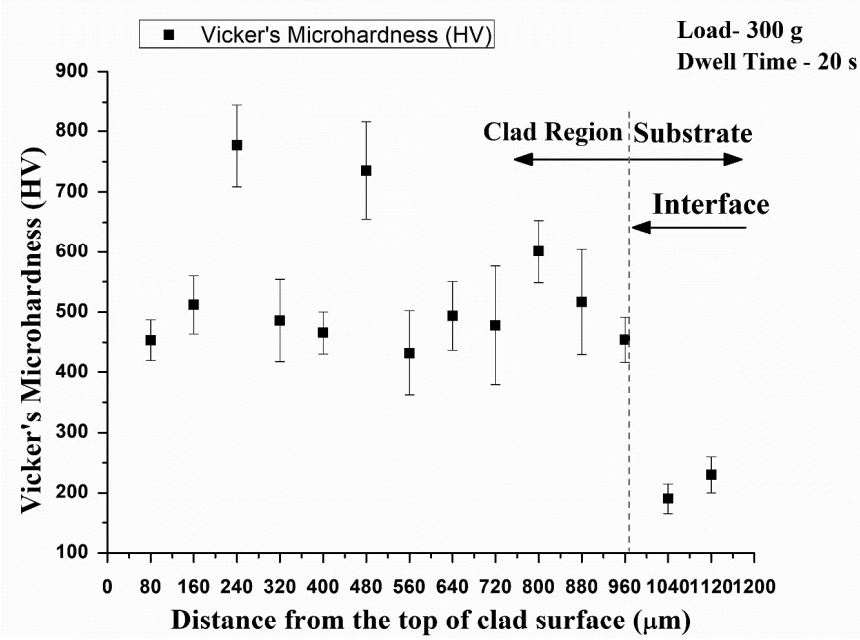

Figure 5.52: Microhardness profile of the developed EWAC-5Al_2O_3 composite clad

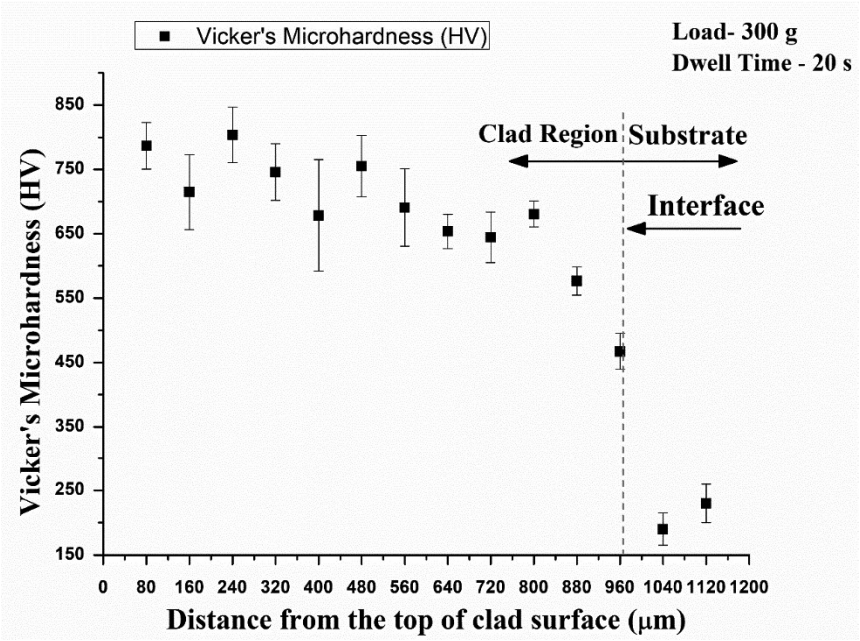

Figure 5.53: Microhardness profile of the developed EWAC-10Al_2O_3 composite clad

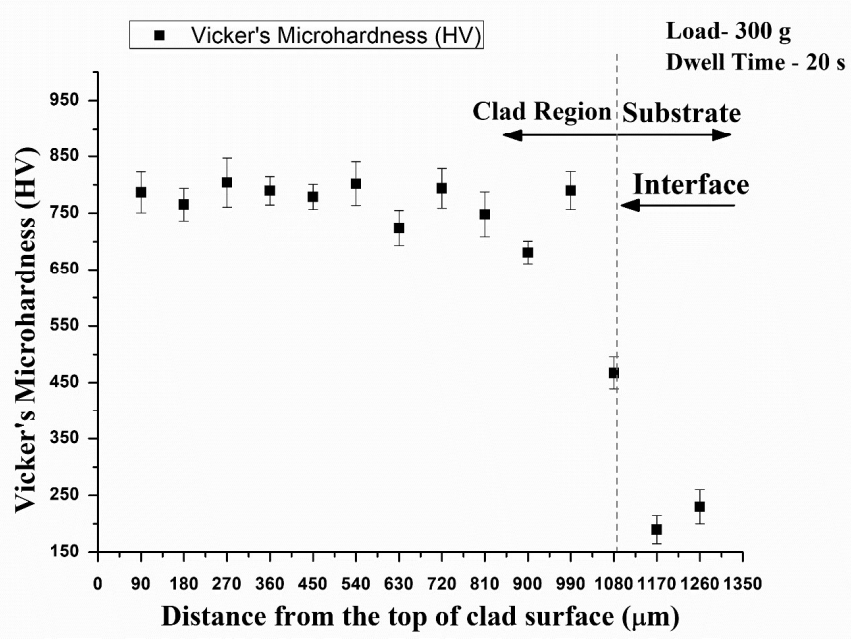

Figure 5.54: Microhardness profile of the developed EWAC-15Al_2O_3 composite clad

The clad region's average microhardness came out 533.68±61 HV, 683.29±42 HV and 744.12±32 HV, for EWAC-5Al_2O_3, EWAC-10Al_2O_3 and EWAC-15Al_2O_3 respectively, which is roughly 3.42, 3.62 and 3.88 more than the substrate. The non-uniformity in the microhardness profile is due to indentation made on hard phases (Al_2O_3 and Fe_5C_2), shows a steep increase in microhardness compared to indentation made on the soft matrix phase. The maximum microhardness value is observed when indentation was made on the Al_2O_3 phase(~850 HV). The inherent hardness of alumina particles restricts plastic deformation and results in maximum hardness. However, soft Ni- matrix cannot restrict plastic deformation significantly and results in less microhardness value.

5.1.14 Porosity assessment of EWAC-xAl_2O_3 developed clad

Porosity dramatically affects the mechanical properties of developed composite clad and influences clad behaviour when subjected to cavitation erosion environment. The porosity measurement of the developed EWAC-xAl_2O_3composite clads was carried out. The porosity analysis results are presented in Table 5.14. The average porosity of microwave synthesized EWAC-xAl_2O_3 composite clads was measured as 1.20%, 1.30%, and 1.33% which is appreciably less than other cladding/coating processes. Only the volumetric heating characteristics of microwave heating could be responsible for developing cladding having significantly less porosity [64].

Table 5.14: The results of porosity measurement of EWAC-xAl_2O_3composite clad

Percentage porosity					
Composition		**Region**			**Mean**
		(i)	**(ii)**	**(iii)**	
EWAC-5Al_2O_3	**Total pores**	3215	2499	2925	2880
	Pores %	1.24	1.18	1.20	**1.20**
EWAC-10Al_2O_3	**Total pores**	9717	8471	7054	8414
	Pores %	1.25	1.41	1.26	**1.30**
EWAC-15Al_2O_3	**Total pores**	8000	9037	8772	8603
	Pores %	1.21	1.45	1.35	**1.33**

5.1.15 Flexural strength studies of EWAC-xAl_2O_3 developed clad

The observations after examine the flexural behaviour on developed EWAC-x$Al_2O_3$are shown in Figure 5.55-5.57.

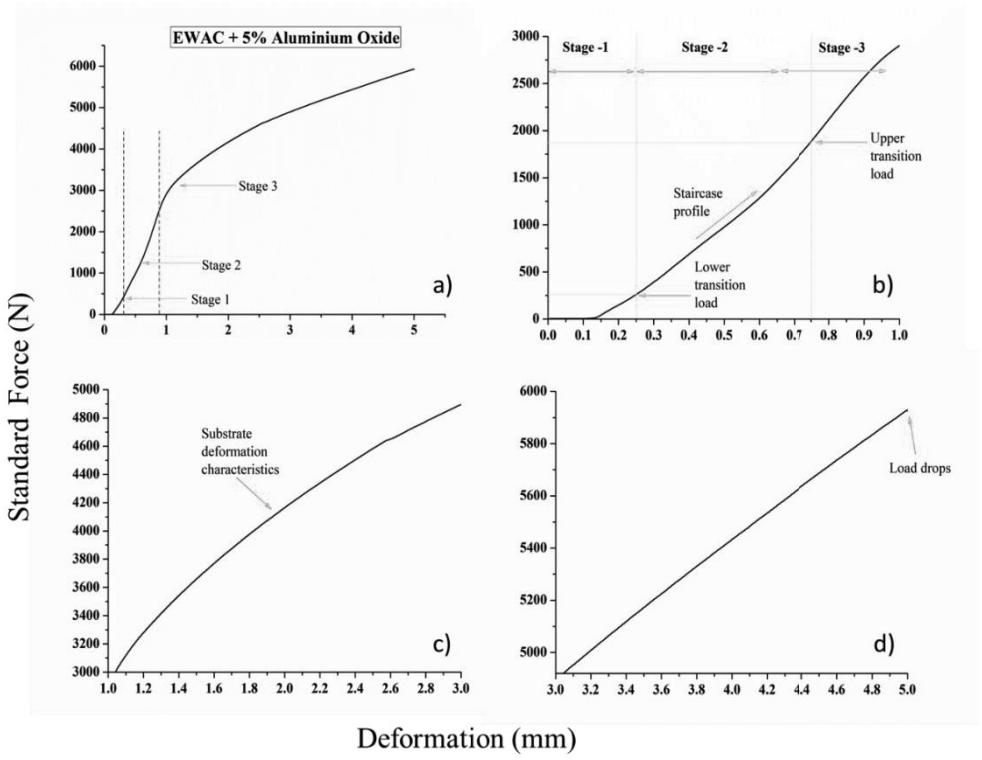

Figure 5.55: a) Load-displacement characteristics of developed EWAC-5Al_2O_3 clad through microwave heating during standard 3-point bend test; magnifying views of load-displacement characteristics b) up to 1 mm c) between 1 mm to 3 mm d) ahead of 3 mm

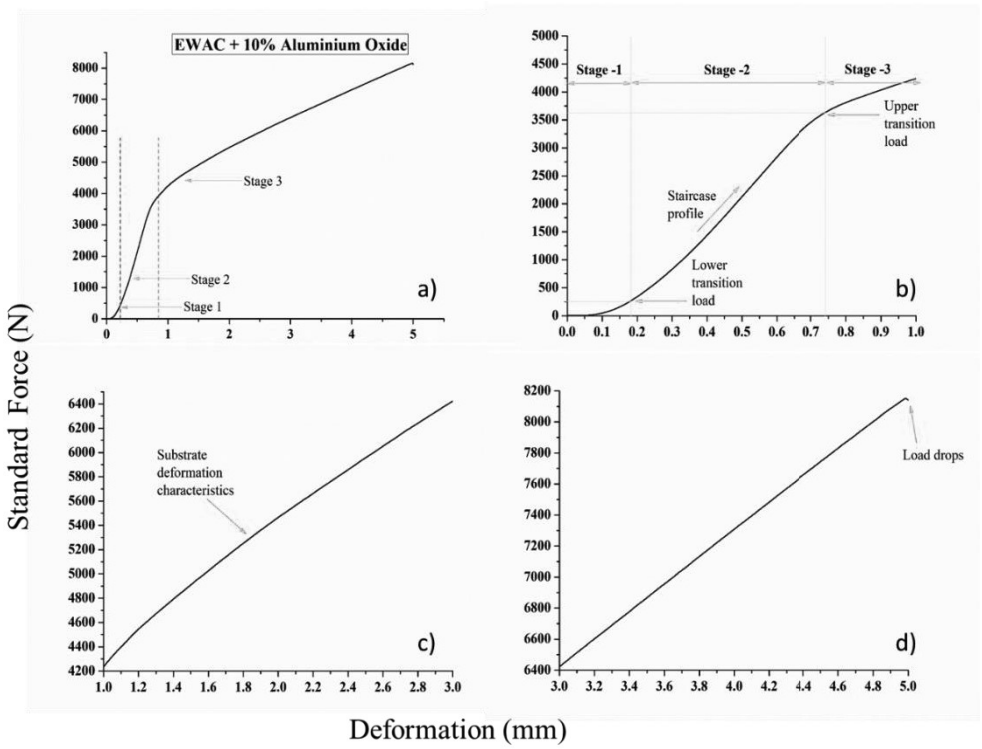

Figure 5.56: a) Load-displacement characteristics of developed EWAC-10Al_2O_3 clad through microwave heating during standard 3-point bend test; magnifying views of load-displacement characteristics b) up to 1 mm c) between 1 mm to 3 mm d) ahead of 3 mm

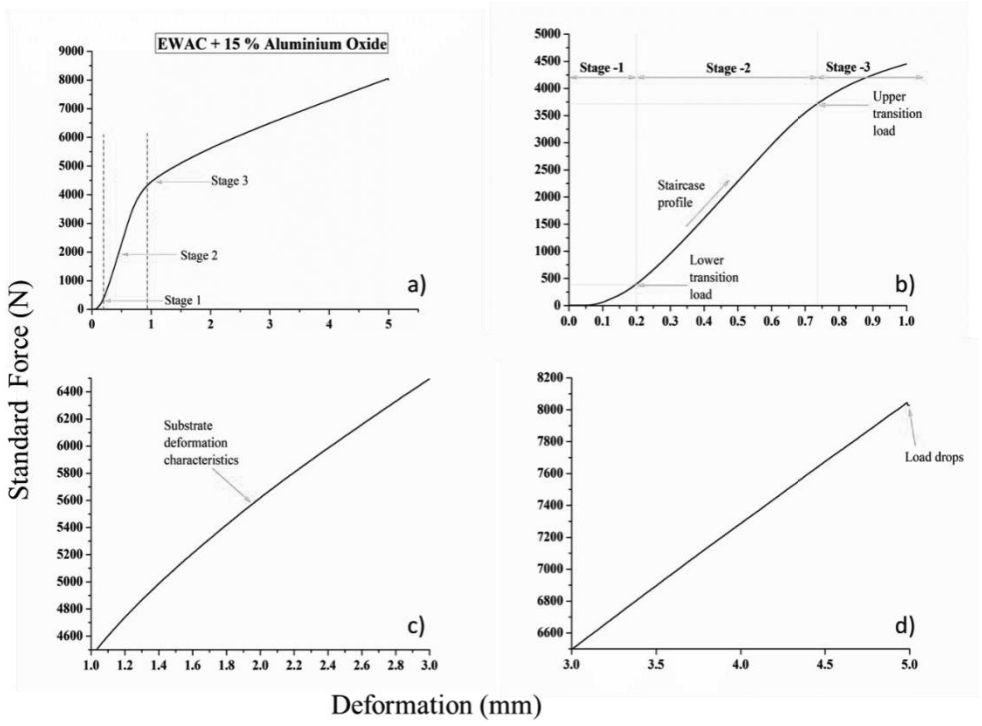

Figure 5.57: a) Load-displacement characteristics of developed EWAC-15Al_2O_3 clad through microwave heating during standard 3-point bend test; magnifying views of load-displacement characteristics b) up to 1 mm c) between 1 mm to 3 mm d) ahead of 3 mm

During stage-1, the ductile Ni-based matrix underwent elastic deformation due to the applied load, as the load increase beyond the lower transition load and Ni-based matrix start elongating due to tensile stresses, which is stage-2. Later in this stage, the applied load is shifted to the Al_2O_3 reinforcement phase. Therefore, the staircase profile is observed (Figures 5.55-5.57 (b)), which indicates that a tremendous amount of load is borne by developed clads with less deformation. During stage-2, the clads have experienced plastic deformation, and the increase in load results in the formation of more micro-cracks on the top surface of developed composite clad. These micro-cracks grow and propagate up to upper transition load (stage 2). The induced stresses may also get released during this stage due to the propagation of micro cracks. Further, in stage-3, an increase in load results in the propagation of micro-cracks in all directions, and finally, these cracks reached up to substrate-clad interface. The developed clads failed, and the load is transferred to the substrate. The substrate load vs deformation characteristics is shown in Figure 5.55-5.57 (c). The de-bonding of cladding and substrate causes failure and load start dropping, as illustrated in Figure 5.55-5.57 (d).

The higher flexural or peel-off strength of the developed composite clads is attributed to the metallurgical bonding of the clad to the substrate due to partial dilution. The observed flexural strength and DI values are tabulated in Table 5.15.

Table 5.15: Observations of developed EWAC-xAl_2O_3 clads during flexural testing

Composition	S. No.	LTL (N)	UTL (N)	δ at UTL (mm)	FS (MPa)	Maximum load (N)	Maximum δ (mm)	Deformation index [$\times10^{-4}$] (mm N^{-1})
EWAC + 5Al_2O_3	1	262	1870	0.74	618	5929	5.0	5.78
	2	270	1900	0.68	626	6010	5.2	5.75
	3	288	1950	0.65	630	6050	5.4	5.70
	Mean	**273**	**1907**	**0.69**	**625±6**	**5996**	**5.20**	**5.74**
EWAC + 10Al_2O_3	1	412	3923	0.85	849	8152	5.5	2.70
	2	515	4080	0.92	855	8210	5.4	2.66
	3	399	3879	0.83	841	8071	5.6	2.71
	Mean	**442**	**3961**	**0.87**	**848±7**	**8144**	**5.50**	**2.69**
EWAC + 15Al_2O_3	1	361	4323	0.93	838	8044	5.1	2.48
	2	478	4502	1.03	854	8198	5.4	2.44
	3	528	4657	1.14	870	8350	5.6	2.42
	Mean	**456**	**4494**	**1.04**	**854±16**	**8197**	**5.37**	**2.44**

LTL- lower transition load, UTL-upper transition load, δ- deformation, FS- flexural strength

The Table 5.15 shows that in the EWAC based and Al_2O_3 reinforced composite clads the similar trend has been observed as Cr_3C_2 and WC10Co2Ni reinforced composite clads for LTL. For UTL, the same trend has been observed as Cr_3C_2 reinforced composite clads. However, the agglomeration in EWAC based and Al_2O_3 reinforced composite clads is comparatively lower because Al_2O_3 is transparent to microwave irradiation. Also, the density of Al_2O_3 is least (3.97

g/m^3) [183] among all the studied reinforcements. Therefore, the interfacial region is the highest in EWAC-15Al_2O_3 composite clads, which results into higher resistance to crack growth and propagation. This is the possible reason that the highest flexural strength value is observed in EWAC-15Al_2O_3 composite clads.

The top surfaces of the fractured test specimens are shown in Figure 5.58-5.60. The SEM images show that, the loading on the surface creates multidirectional macro cracks in the clad. The cracks spread as the secondary cracks (Figure 5.58-5.60(c)) to the interface as the load progresses. The EWAC-xAl_2O_3 composite clads have greater ductility due to the presence of Ni in the matrix. However, the Al_2O_3 particles, due to their brittle nature, act as a crack formation point between the reinforcement and the matrix phase.

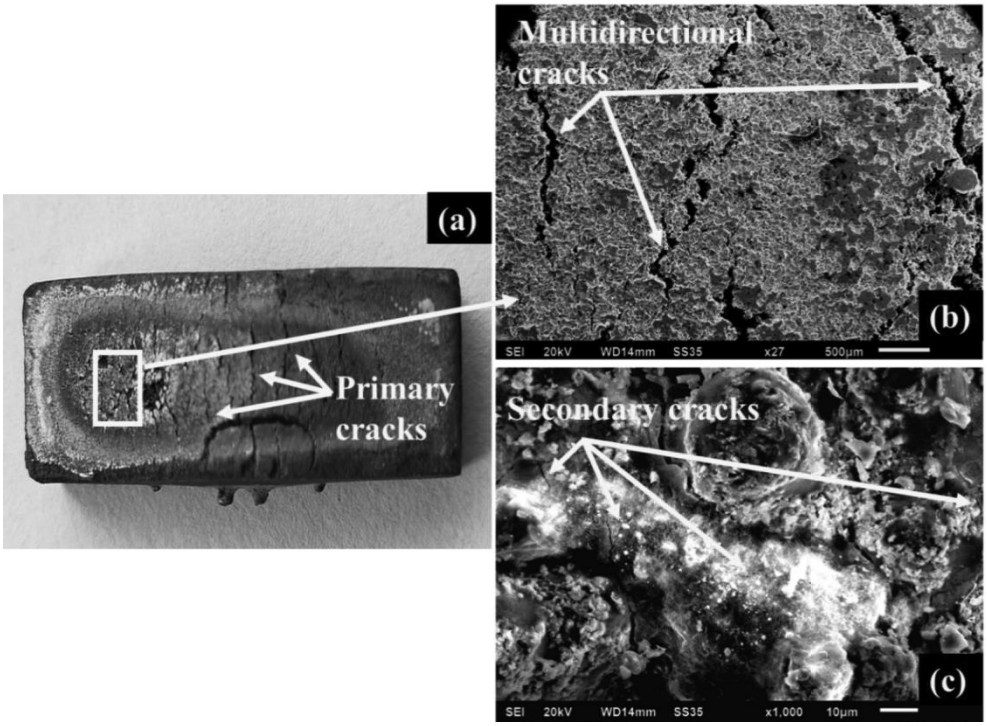

Figure 5.58: Fractured EWAC-5Al_2O_3 clad specimen after 3-point bend test (a) Photograph of the top surface; SEM micrograph showing (b) primary cracks (c) secondary cracks

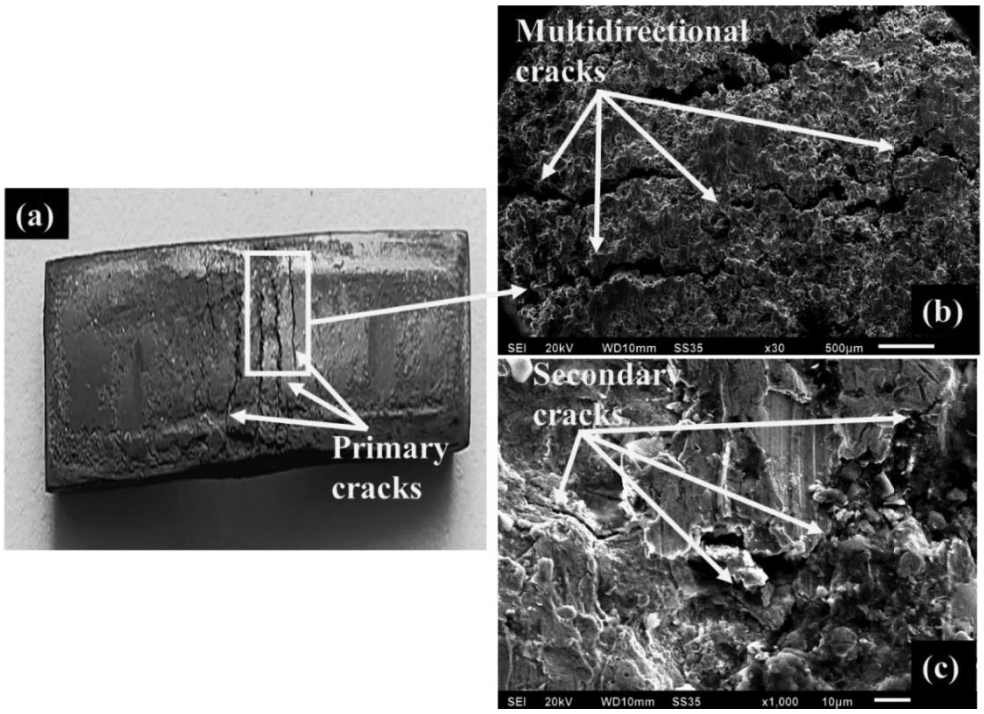

Figure 5.59: Fractured EWAC-10Al_2O_3 clad specimen after 3-point bend test (a) Photograph of the top surface; SEM micrograph showing (b) primary cracks (c) secondary cracks

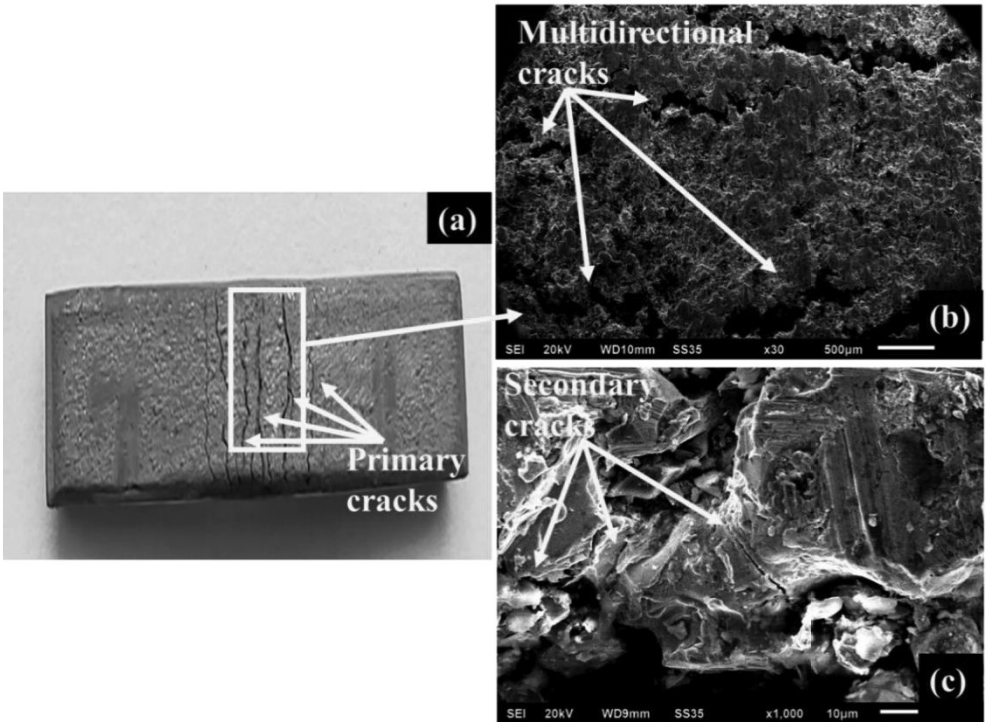

Figure 5.60: Fractured EWAC-15Al_2O_3 clad specimen after 3-point bend test (a) Photograph of the top surface; SEM micrograph showing (b) primary cracks (c) secondary cracks

CHAPTER 6
TRIBOLOGICAL PERFORMANCE OF THE CLADS

Wear in engineering components is a serious problem that degrades the functionality of engineering components. The common causes of wear are cavitation (interaction with fluid), adhesion, abrasion, corrosion, surface fatigue, fretting, and erosion. The components of hydro turbines are more prone to cavitation and get replaced frequently, which leads to huge revenue loss and lowers the hydro plant efficiency. Austenitic stainless steel is widely used in the power generation sector (hydraulic turbines). The stainless steel used in engineering applications experiences extreme metallic wear, therefore, it is not suggested in extreme wear conditions.

The different metal matrix composites are widely used to combat cavitation erosion wear in power generation sector. In the current work, the Nickel based (EWAC) and; chromium carbide, tungsten carbide and alumina reinforced, in different weight percentage, MMCs are developed on SS-316 substrate through novel MHH technique. The developed clads are tested, to check their tribological performance, using vibratory cavitation testing apparatus. The current chapter presents the results of tribological characterizations of developed clads in detail. In start, the results of cavitation erosion parametric study of SS-316, EWAC-xCr_3C_2 (x=10,20,30) % composite clads, EWAC-xWC10Co2Ni (x=10,20,30) % composite clads and EWAC-xAl_2O_3 (x=5,10,15) % composite clads are presented in terms of weight loss. Later, the effect of parameters stand-off distance, amplitude and immersion depth on cavitation erosion behaviour of developed clads has been discussed in detail. In last, the fractographic analysis of the worn surfaces to know the possible wear mechanism using SEM has been reported.

6.1 Results of Parametric Study of Cavitation Erosion Behaviour of SS-316 and Developed Clads

The Taguchi L9 orthogonal array is used for cavitation erosion wear testing of the stainless steel-316 substrate and developed EWAC-xCr_3C_2, EWAC-xWC10Co2Ni & EWAC-xAl_2O_3 composite clads. The obtained experimental results in terms of cumulative mass loss or cumulative weight loss (CWL) were further converted in other terms like cumulative volume loss (CVL), cavitation erosion rate (CER); mean depth of erosion (MDE); means erosion rate (MER) and incubation time (IBT) in order to effectively compare the results of various

compositions. The relations used for calculation of the above-mentioned terms according to ASTM G32-16 Standards are:

i. **Volume loss or CVL (mm^3)** = $\frac{\Delta W}{\rho} \times 1000,$ Where, ΔW is weight loss in mg and ρ is density in g/cm^3.

ii. **CER (mg/h)** = $\frac{\Delta W}{\Delta t}$, Where, ΔW is weight loss in mg and Δt is time interval in hours.

iii. **MDE (µm)** = $\frac{\Delta W}{10 \times \rho \times A}$, and **MER (µm/h)** = $\frac{\Delta W}{10 \times \rho \times A \times \Delta t}$, Where, ΔW is weight loss in mg, ρ is the density of the material in g/cm^3, A is the area of eroded specimen in cm^2 (In current study it is taken equal to area of the ultrasonic horn, Diameter of horn = 1.5 cm and area = πr^2 = 1.77 cm^2 or 176.7 mm^2).

iv. **IBT (Minutes/Hours) =** The incubation period is the first stage of cavitation erosion, during which cavitation erosion is zero or negligible in comparison to later stages. Materials subjected to cavitation testing have a higher resistance to impingement jets during the incubation period. Because the material initially has a lower cavitation erosion rate, therefore, the period up to which only 10% of maximum recorded weight loss has occurred, is considered as the incubation period in this study.

6.1.1 Results of parametric study of cavitation erosion behaviour of SS-316 (substrate)

The cavitation erosion testing has been carried out, according to Taguchi L9 orthogonal array (with optimization goal- larger is better). The Taguchi L9 orthogonal array has four columns, where three columns are assigned to each parameter or control factor (SOD-standoff distance, AMP-Amplitude and IMD-immersion depth) and the fourth column is assigned to the error. The experimental results of cavitation testing of substrate are tabulated in Table 6.1.

Table 6.1: Cavitation erosion study results for substrate

Run Order	SOD (mm)	AMP (µm)	IMD (mm)	CWL (mg)	CVL (mm^3)	CER (mg/h)	MDE (µm)	MDER (µm/h)	IBT (min)
1	0.5	40	80	34.9	4.4	3.88	15.8	1.75	126.7
2	0.5	50	100	36.8	4.6	4.09	16.6	1.85	122.81
3	0.5	60	120	40.9	5.1	4.54	18.5	2.05	91.20
4	1	40	100	25.6	3.2	2.84	11.6	1.28	134.89
5	1	50	120	26.9	3.4	2.99	12.1	1.35	126.49
6	1	60	80	40.1	5.0	4.46	18.1	2.01	95.22
7	1.5	40	120	10.2	1.3	1.13	4.6	0.51	288.20
8	1.5	50	80	25	3.1	2.78	11.3	1.25	133.18
9	1.5	60	100	27.5	3.4	3.06	12.4	1.38	130.49

It is clear from the Table 6.1 that the highest weight loss in substrate has occurred at test parameter 3, when SOD was least (0.5 mm) and amplitude and IMD was highest (60 µm and 120 mm). At this test parameter, the highest mean erosion rate of 2.05 µm/h and least incubation period of 91.20 min was recorded. The plot of cumulative weight loss as a function of cavitation erosion test time for all substrate specimens is shown in Figure 6.1.

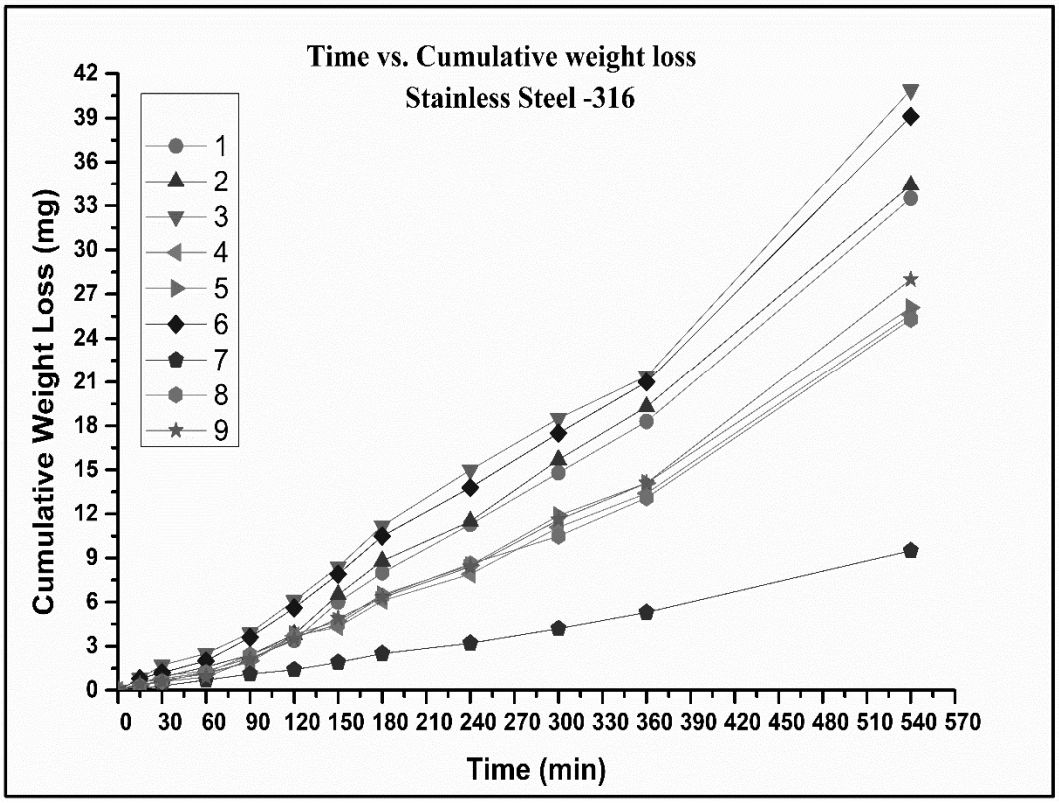

Figure 6.1: Line plot showing weight loss as the function of time for cavitation erosion wear of substrate at different parameters

The less weight loss, due to cavitation erosion wear, was observed in the initial phase; but at later stages (increase in testing time) the weight loss increases. The steady or constant erosion rate has been observed in the initial phase. After 120 min of cavitation erosion testing; the sudden increase in the weight loss can be seen. This indicates the higher erosion rate at later stages during cavitation phenomena.

6.1.2 Results of statistical analysis of cavitation erosion behaviour of substrate

The most commonly used response variable by researchers in cavitation studies is the cumulative weight loss. Therefore, it was selected further; as the response variable for statistical analysis and mathematical modelling. The main effect plot for means of process parameters is shown in Figure 6.2.

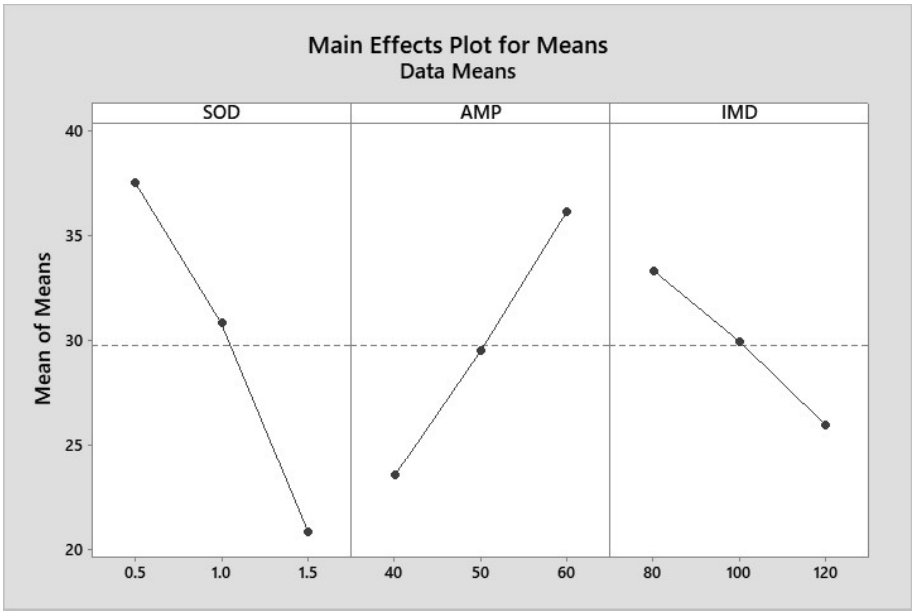

Figure 6.2: Main effect plots for cumulative weight loss of substrate

It is monitored from the plots that the closeness and inclination of parameter line decides the significance of factor. The more inclined parameter line to horizontal axis represents the more significance of control factor. It is easy to understand from the plots that SOD is most influencing and significant control factor for the weight loss of substrate surface followed by AMP, and IMD is least influencing and significant control factor in this domain of study. It can be seen clearly from the Figure 6.2, that the weight loss has been decreased when separation distance and immersion depth is increased and amplitude is decreased.

Further, to study the statistical significance and percentage contribution of the test parameters toward cavitation erosion, analysis of variance (ANOVA) was carried out; the confidence interval was taken as 95%. Table 6.2 presents the ANOVA results for response characteristics (cumulative weight loss).

Table 6.2: ANOVA results for cumulative weight loss of substrate- Taguchi L9 array analysis

Source	DF	Seq SS	Adj SS	Adj MS	F	P	Percentage Contribution
SOD (mm)	2	420.447	420.447	210.223	130.3	0.008	**56.60**
AMP (µm)	2	238.32	238.32	119.16	73.86	0.013	**32.08**
IMD (mm)	2	80.847	80.847	40.423	25.06	0.038	**10.88**
Residual Error	2	3.227	3.227	1.613			**0.43**
Total	8	742.84					

It is clear from the ANOVA table that the role of all three-test parameters (SOD, IMD, AMP) is statistically significant (p-value less than 0.05 is considered as a significant parameter). Table 6.2 shows that the weight loss of SS-316 is most influenced by SOD (56.60 %), followed by

AMP (32.08%) and IMD (10.88%). The cavitation-testing phenomenon, due to the involvement of the simultaneous action of many factors, such as SOD, AMP, IMD, test liquid temperature, target material properties, and machine error, becomes challenging to understand. Although, an attempt was made to reduce the influence of some of the factors, such as maintained the test liquid temperature constant at 25 ±5°C. Moreover, the specimens were tested at 20 kHz for 9 h so that the possibility of the influence of machine error can be reduced to the lowest due to a large number of testing cycles (32,400 s × 20,000 = 6.48 × 10^9 cycles). Therefore, the percentage contribution of error in the present study is 0.43% only.

The response table for the weight loss values of substrate is presented in Table 6.3. The response table helps to monitor the effect of control factors with the help of delta statistics.

Table 6.3: Response table for cumulative weight loss in substrate

Level	SOD (mm)	AMP (µm)	IMD (mm)
1	37.53	23.57	33.33
2	30.87	29.57	29.97
3	20.9	36.17	26
Delta	**16.63**	**12.6**	**7.33**
Rank	**1**	**2**	**3**

The delta statistics is determined by the difference between highest and lowest average value of the individual factor and based on these values the rank of delta statistics is assigned. Higher the value of delta, higher is the rank and vice versa. This delta statistic helps to collect more data. The weight loss of surface is most influenced by the factor having the highest delta value. From the Table 6.3. it is again clear that SOD is the most influential factor followed by AMP and IMD. Furthermore, the cumulative weight loss has been mathematically modelled. Minitab 17.0 was used to create the linear fit regression equation. The ANOVA table of regression analysis obtained is shown in Table 6.4.

Table 6.4: ANOVA results for cumulative weight loss of substrate- Regression analysis

Source	DF	Adj SS	Adj MS	F	P	Percentage Contribution
SOD (mm)	1	415.002	415.002	229.75	0	**55.87**
AMP (µm)	1	238.14	238.14	131.84	0	**32.06**
IMD (mm)	1	80.667	80.667	44.66	0.001	**10.86**
Residual Error	5	9.032	1.806			**1.22**
Total	8	742.84				

Each of the three parameters has a significant impact on weight loss. According to the last column of the Table 6.4, the percentage contributions of SOD (55.87%) and AMP (32.06%)

are relatively higher than IMD (10.86%). Also, due to many uncontrollable factors, error contribution of 1.22% is observed.

The cumulative weight loss in substrate at various cavitation test parameters can be calculated using regression equation 6.1.

$$\boldsymbol{CWL(mg) = 33.23 - 16.63\,SOD + 0.6300\,AMP - 0.1833\,IMD} \qquad 6.1$$

The model summary of the regression equation is tabulated in Table 6.5.

Table 6.5: Regression model summary for cumulative weight loss of substrate

Model Summary			
S	**R-Sq**	**R-Sq(Adj)**	**R-Sq(Pred)**
1.344	98.78%	98.05%	96.38%

The R^2 (R-squared) value indicates the goodness of fit; or how well the regression model fits the observed data. In general, a higher R^2 indicates a better model fit. The R^2 value of 98.78% of current model shows that 98.78% data points are close to the developed linear equation. The relation between the regression model prediction for the new responses is indicated by the R^2 (predicted). The R^2 (predicted) value of 96.38% of current model shows that this model can successfully predict results for new responses with accuracy of 96.38%.

The optimization of the test parameter is required to get the desired output. It is clear from Table 6.3 that the optimum test parameters at which weight loss is maximum are 0.5 mm SOD, 60 µm AMP and 80 mm IMD. Therefore, the prediction model at 95% confidence level for weight loss at these parameters has been generated. The prediction model summary at optimal test parameters is tabulated in Table 6.6.

Table 6.6: Predicted values for cumulative weight loss of substrate

Prediction Model Summary			
Variable Input (SOD-0.5 mm, AMP-60 µm, IMD-80 mm)			
Fit	**SE Fit**	**95% CI**	**95% PI**
48.05	1.05065	(45.3492, 50.7508)	(43.6648, 52.4352)

It shows that values of the weight loss at optimal test parameters must lie between 43.6648 to 52.4352 mg. These values are useful to compare the results with the confirmatory or validatory experiments.

6.1.3 Results of parametric study of cavitation erosion behaviour of EWAC-xCr_3C_2 (where x= 10,20,30) % composite clad

Likewise, the developed EWAC-xCr_3C_2 composite clads have been tested for cavitation erosion wear behaviour. According to L9 Taguchi orthogonal array, 9 specimens of each composition (total 27 for EWAC-xCr_3C_2) have been tested. The experimental results of cavitation testing of EWAC-10Cr_3C_2, EWAC-20Cr_3C_2 and EWAC-30Cr_3C_2 are tabulated in Table 6.7-6.9, respectively.

Table 6.7: Cavitation erosion study results for EWAC-10Cr_3C_2

Run Order	SOD (mm)	AMP (µm)	IMD (mm)	CWL (mg)	CVL (mm^3)	CER (mg/h)	MDE (µm)	MDER (µm/h)	IBT (min)
1	0.5	40	80	13	1.5	1.44	6.4	0.71	90.15
2	0.5	50	100	13.8	1.6	1.53	6.8	0.75	87.95
3	0.5	60	120	15.3	1.8	1.70	7.5	0.84	78.81
4	1	40	100	9	1.0	1.00	4.4	0.49	127.82
5	1	50	120	9.4	1.1	1.04	4.6	0.51	118.86
6	1	60	80	14	1.6	1.56	6.9	0.77	81.37
7	1.5	40	120	3.1	0.4	0.34	1.5	0.17	>540
8	1.5	50	80	7.6	0.9	0.84	3.7	0.42	161.83
9	1.5	60	100	10	1.1	1.11	4.9	0.55	119.77

Table 6.8: Cavitation erosion study results for EWAC-20Cr_3C_2

Run Order	SOD (mm)	AMP (µm)	IMD (mm)	CWL (mg)	CVL (mm^3)	CER (mg/h)	MDE (µm)	MDER (µm/h)	IBT (min)
1	0.5	40	80	6.7	0.8	0.74	3.2	0.36	164.21
2	0.5	50	100	7.2	0.8	0.80	3.5	0.38	146.47
3	0.5	60	120	8.1	1.0	0.90	3.9	0.43	119.77
4	1	40	100	4.9	0.6	0.54	2.4	0.26	289.48
5	1	50	120	5.3	0.6	0.59	2.5	0.28	173.35
6	1	60	80	7.9	0.9	0.88	3.8	0.42	113.37
7	1.5	40	120	2.1	0.2	0.23	1.0	0.11	>540
8	1.5	50	80	5	0.6	0.56	2.4	0.27	239.74
9	1.5	60	100	5.9	0.7	0.66	2.8	0.32	157.44

Table 6.9: Cavitation erosion study results for EWAC-30Cr_3C_2

Run Order	SOD (mm)	AMP (µm)	IMD (mm)	CWL (mg)	CVL (mm^3)	CER (mg/h)	MDE (µm)	MDER (µm/h)	IBT (min)
1	0.5	40	80	6.1	0.7	0.68	2.9	0.32	166.10
2	0.5	50	100	6.4	0.8	0.71	3.0	0.33	148.92
3	0.5	60	120	7.1	0.9	0.79	3.3	0.37	130.01
4	1	40	100	4.5	0.5	0.50	2.1	0.23	291.93

5	1	50	120	4.8	0.6	0.53	2.3	0.25	274.85
6	1	60	80	7	0.8	0.78	3.3	0.37	155.43
7	1.5	40	120	1.8	0.2	0.20	0.8	0.09	>540
8	1.5	50	80	4.3	0.5	0.48	2.0	0.22	336.11
9	1.5	60	100	4.8	0.6	0.53	2.3	0.25	301.73

It can be observed from the experimental results that maximum weight loss of 15.3 mg, 8.1 mg and 7.1 mg for EWAC-10Cr_3C_2, EWAC-20Cr_3C_2 and EWAC-30Cr_3C_2, respectively, has recorded at parametric set-3. At this test parameter, the mean erosion rate for developed EWAC-10Cr_3C_2, EWAC-20Cr_3C_2 and EWAC-30Cr_3C_2 is recorded as 0.84 µm/h, 0.43 µm/h and 0.37 µm/h, respectively. The plots of cumulative weight loss as a function of cavitation erosion test time for all EWAC-xCr_3C_2 composite clads are shown in Figure 6.3-6.5.

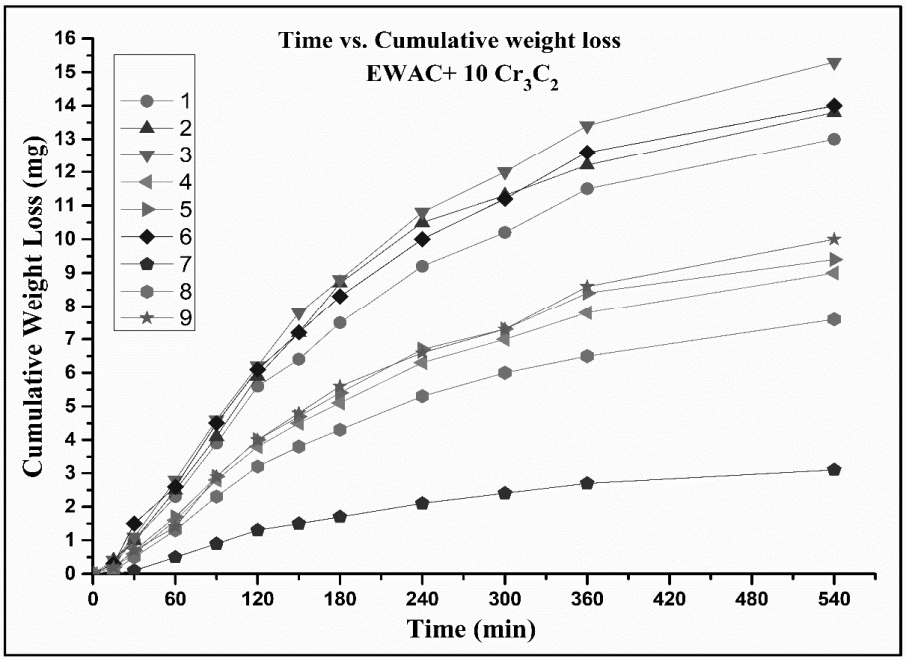

Figure 6.3: Line plot showing weight loss as the function of time for cavitation erosion wear of EWAC-10Cr_3C_2 specimens at different parameters

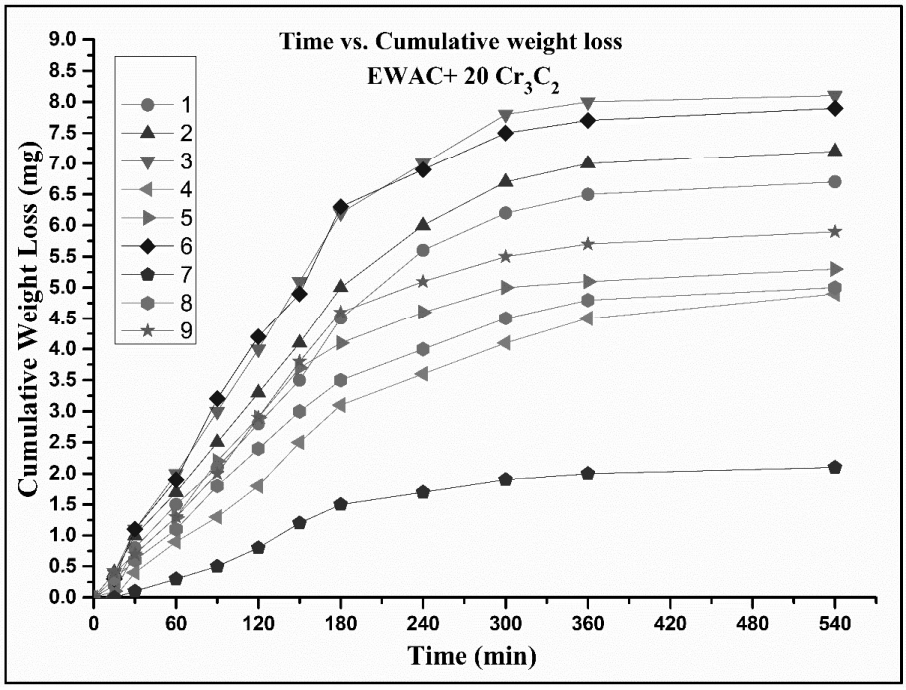

Figure 6.4: Line plot showing weight loss as the function of time for cavitation erosion wear of EWAC-20Cr_3C_2 specimens at different parameters

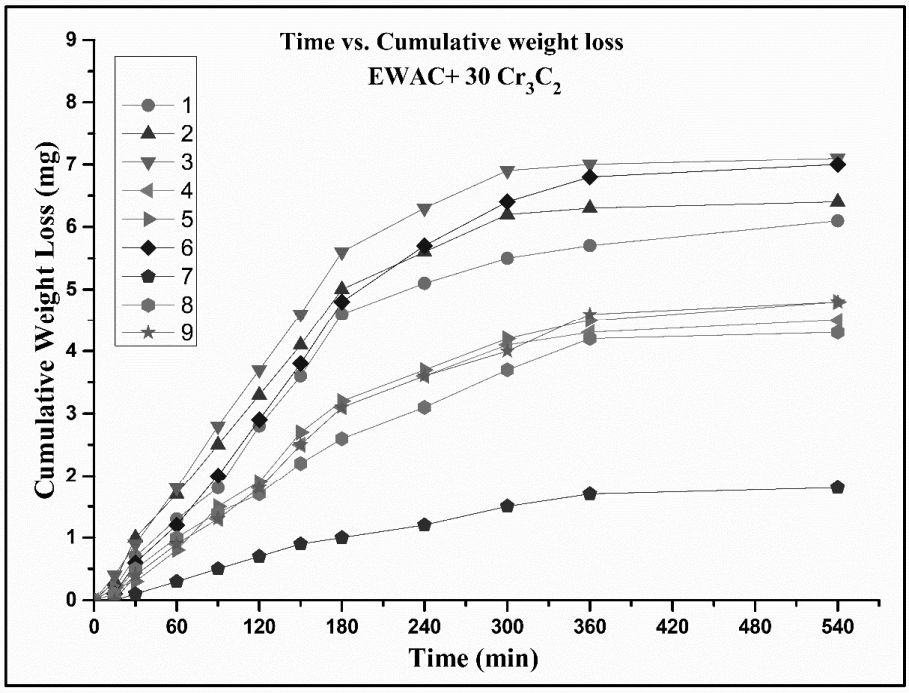

Figure 6.5: Line plot showing weight loss as the function of time for cavitation erosion wear of EWAC-30Cr_3C_2 specimens at different parameters

This is observed from Figures 6.3-6.5 that at the early stage of cavitation erosion testing the weight loss of EWAC base composite clads was more than the substrate (Figure 6.2). The substrate material shows better CER at earlier stages of testing, because the substrate surface has less initiation sites for cavitation erosion wear than the clad surface.

After initial phase, the trend reverses. The possible reason behind this is the removal of any unbounded or unmelted particles at earlier stage and the role of clad starts at this time. This is also proved by the further testing, where the weight loss of developed composite clad surface decreases significantly. On the other hand, it increases rapidly for substrate. The porosity analysis exhibits that the porosity of EWAC base clads was significantly less, which helps in reduction of cavitation erosion wear. The sites around pores become weak due to stress concentration and offer less resistance to cavitation erosion wear. This is interesting to note (Tables 6.7-6.9) that, developing EWAC-10Cr_3C_2 clad on substrate surface increases CER and increase in weight percentage of hard reinforcement (from 10% to 20%) results into sudden increase in CER. But, further addition of hard reinforcement (30%) did not contribute significantly in enhancement of CER. This is because that the toughness is also an essential property for CER and adding hard reinforcement into soft matrix decreases its toughness. Although, presence of hard carbide phases restricts the crack growth and results into lesser weight loss in all developed EWAC-xCr_3C_2 clad specimens. The weight loss in the developed EWAC base composite clads is lesser as compared to substrate at all experimental conditions. However, at some experimental conditions, even after 9 h of cavitation erosion testing, the recorded weight loss was not significant. The developed EWAC-xCr_3C_2 composite clads experience 2.67, 5.04 and 5.76 times lesser weight loss for EWAC-10Cr_3C_2, EWAC-20Cr_3C_2 and EWAC-30Cr_3C_2, respectively, as compared to substrate at same experimental conditions.

6.1.4 Results of statistical analysis of cavitation erosion behaviour of EWAC-xCr_3C_2 composite clads

Figures 6.6-6.8 show the graphical effect of all three test parameters. It can be observed that with the increase in SOD the weight loss decreases suddenly, whereas, with the increase in AMP the abrupt increase in the weight loss was observed. However, main effect plot shows that the minimal decrease in weight loss has been observed with the increase of IMD.

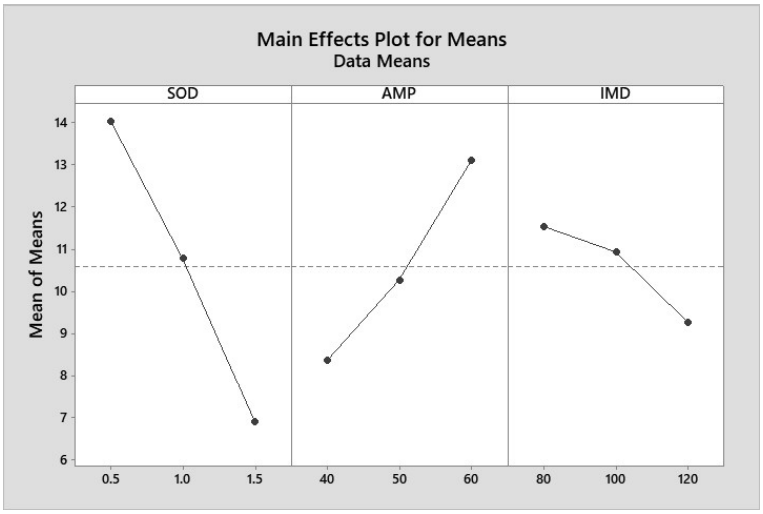

Figure 6.6: Main effect plots for cumulative weight loss of EWAC-10Cr_3C_2

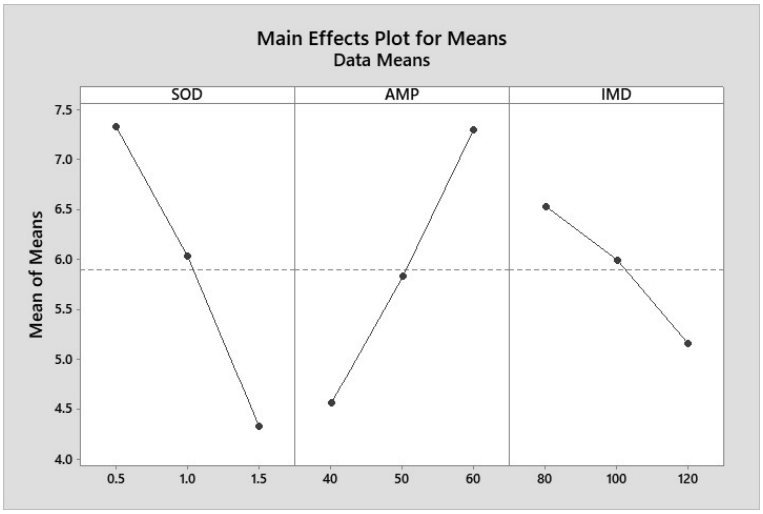

Figure 6.7: Main effect plots for cumulative weight loss of EWAC-20Cr_3C_2

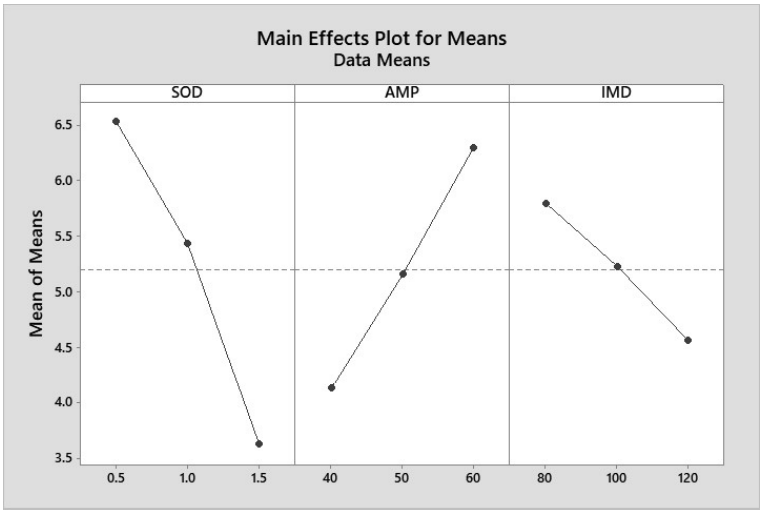

Figure 6.8: Main effect plots for cumulative weight loss of EWAC-30Cr_3C_2

To study the statistical significance and percentage contribution of the test parameters towards cavitation erosion, analysis of variance (ANOVA) was carried out; the confidence interval was taken as 95%. Table 6.10 present the ANOVA results for response characteristics (weight loss) of EWAC-xCr_3C_2 composite clads.

Table 6.10: ANOVA results for cumulative weight loss of EWAC-xCr_3C_2 - Taguchi L9 array analysis

	Source	DF	Seq SS	Adj SS	Adj MS	F	P	Percentage Contribution
EWAC + 10Cr_3C_2	**SOD (mm)**	2	76.549	76.5489	38.2744	196.84	0.005	**64.19**
	AMP (µm)	2	34.042	34.0422	17.0211	87.54	0.011	**28.55**
	IMD (mm)	2	8.276	8.2756	4.1378	21.28	0.045	**6.94**
	Residual Error	2	0.389	0.3889	0.1944			**0.33**
	Total	8	119.256					
EWAC + 20Cr_3C_2	**SOD (mm)**	2	13.58	13.58	6.79	107.21	0.009	**48.88**
	AMP (µm)	2	11.2267	11.2267	5.61333	88.63	0.011	**40.41**
	IMD (mm)	2	2.8467	2.8467	1.42333	22.47	0.043	**10.25**
	Residual Error	2	0.1267	0.1267	0.06333			**0.46**
	Total	8	27.78					
EWAC + 30Cr_3C_2	**SOD (mm)**	2	12.86	12.86	6.43	148.38	0.007	**57.72**
	AMP (µm)	2	7.0467	7.0467	3.52333	81.31	0.012	**31.63**
	IMD (mm)	2	2.2867	2.2867	1.14333	26.38	0.037	**10.26**
	Residual Error	2	0.0867	0.0867	0.04333			**0.39**
	Total	8	22.28					

From the ANOVA table, it has been observed that all of three test parameters are statistically and physically significant, as the p-value of all three test parameters is less than 0.05. Also, like substrate, the value of percentage influence of SOD on response is more as compare to AMP and IMD.

Further, delta statistics has been used to examine the results (Table 6.11). The procedure of the delta analysis has already been discussed in section 6.1.2. The higher delta value of SOD

confirms that the SOD has more effect on weight loss during cavitation erosion testing of developed composite clads, followed by AMP and IMD.

Table 6.11: Response table for cumulative weight loss in EWAC-xCr_3C_2

	Level	SOD (mm)	AMP (µm)	IMD (mm)
EWAC + 10Cr_3C_2	1	14.033	8.367	11.533
	2	10.8	10.267	10.933
	3	6.9	13.1	9.267
	Delta	**7.133**	**4.733**	**2.267**
	Rank	**1**	**2**	**3**
EWAC + 20Cr_3C_2	1	7.333	4.567	6.533
	2	6.033	5.833	6
	3	4.333	7.3	5.167
	Delta	**3**	**2.733**	**1.367**
	Rank	**1**	**2**	**3**
EWAC + 30Cr_3C_2	1	6.533	4.133	5.8
	2	5.433	5.167	5.233
	3	3.633	6.3	4.567
	Delta	**2.9**	**2.167**	**1.233**
	Rank	**1**	**2**	**3**

To set up the relation between weight loss and test parameters, the mathematical modelling of the cumulative weight loss has been done; the linear regression equations have been developed by regression analysis at 95% confidence level. The obtained ANOVA results of regression analysis are presented in Table 6.12.

Table 6.12: ANOVA results for cumulative weight loss of EWAC- xCr_3C_2-Regression analysis

	Source	DF	Adj SS	Adj MS	F	P	Percentage Contribution
EWAC + 10Cr_3C_2	**SOD (mm)**	1	76.327	76.3267	236.22	0	**64.00**
	AMP (µm)	1	33.607	33.6067	104.01	0	**28.18**
	IMD (mm)	1	7.707	7.7067	23.85	0.005	**6.46**
	Residual Error	5	1.616	0.3231			**1.36**
	Total	8	119.256				
EWAC + 20Cr_3C_2	**SOD (mm)**	1	13.5	13.5	248.47	0	**48.60**
	AMP (µm)	1	11.2067	11.2067	206.26	0	**40.34**
	IMD (mm)	1	2.8017	2.8017	51.56	0.001	**10.09**
	Residual Error	5	0.2717	0.0543			**0.98**
	Total	8	27.78				
EWAC + 30Cr_3C_2	**SOD (mm)**	1	12.615	12.615	184.61	0	**56.62**
	AMP (µm)	1	7.0417	7.0417	103.05	0	**31.61**
	IMD (mm)	1	2.2817	2.2817	33.39	0.002	**10.24**
	Residual Error	5	0.3417	0.0683			**1.53**
	Total	8	22.28				

According to the analysis, the most important parameter with respect to weight loss during cavitation erosion testing is SOD, followed by AMP and IMD.

Using the least square method in Minitab 17.0, the following Equations (6.2-6.4) were developed for cumulative weight loss as a response variable. The summary of the prepared mathematical model is tabulated in Table 6.13. The developed model has R^2 (predicted) value more than 95% for all compositions. This indicates that the developed model can predict more than 95 % accurate results in future.

EWAC-10Cr_3C_2

$$\boldsymbol{CWL(mg) = 11.54 - 7.133\,SOD + 0.2367\,AMP - 0.0567\,IMD} \quad (6.2)$$

EWAC-20Cr_3C_2

$$\boldsymbol{CWL(mg) = 5.483 - 3.000\,SOD + 0.13667\,AMP - 0.03417\,IMD} \quad (6.3)$$

EWAC-30Cr_3C_2

$$\boldsymbol{CWL(mg) = 5.767 - 2.900\,SOD + 0.1083\,AMP - 0.03083\,IMD} \quad (6.4)$$

Table 6.13: Regression model summary for cumulative weight loss of EWAC-xCr_3C_2 composite clads

Model Summary				
Composition	**S**	**R-Sq**	**R-Sq(Adj)**	**R-Sq(Pred)**
EWAC-10Cr_3C_2	0.568429	98.65%	97.83%	95.92%
EWAC-20Cr_3C_2	0.233095	99.02%	98.44%	96.93%
EWAC-30Cr_3C_2	0.261406	98.47%	97.55%	95.50%

The predication modelling details are summarized in Table 6.14.

Table 6.14: Predicted values for cumulative weight loss of EWAC-xCr_3C_2 composite clads

Prediction Model Summary				
Variable Input (SOD-0.5 mm, AMP-60 µm, IMD-80 mm)				
Composition	**Fit**	**SE Fit**	**95% CI**	**95% PI**
EWAC-10Cr_3C_2	17.6444	0.444361	(16.5022,18.7867)	(15.7898,19.4991)
EWAC-20Cr_3C_2	9.45	0.182219	(8.98159, 9.91841)	(8.68945, 10.2105)
EWAC-30Cr_3C_2	8.35	0.204351	(7.82470, 8.87530)	(7.49708, 9.20292)

As per prediction calculations at the optimized experimental condition (SOD 0.5 mm, AMP 60 µm and IMD 80 mm), the last column of the Table 6.14 shows the values of weight loss for different compositions. To validate the prediction results, confirmatory experiments were performed, and the results of the confirmatory experiments are presented in section 6.4.

6.1.5 Results of parametric study of cavitation erosion behaviour of EWAC-xWC10Co2Ni (where x= 10,20,30) % composite clad

Similarly, the experimental cavitation erosion testing was conducted, according to Taguchi L9 design plan, for EWAC-xWC10Co2Ni composite clad to assess the effect of cavitation erosion and indirect method parameters SOD, AMP, and IMD on the CWL. Table 6.15-6.17 illustrates the experimental results of the CWL, CVL, CER, MDE, MDER and IBT. It has been observed that the maximum weight loss has occurred at test parameters set-3, which is 6.2 mg, 4.2 mg and 3.2 mg for EWAC-10WC10Co2Ni, EWAC-20WC10Co2Ni and EWAC-30WC10Co2Ni, respectively. The mean erosion rate at these particular experimental conditions is 0.37 µm/h, 0.27 µm/h and 0.22 µm/h for EWAC-10WC10Co2Ni, EWAC-20WC10Co2Ni and EWAC-30WC10Co2Ni, respectively.

Table 6.15: Cavitation erosion study results for EWAC-10WC10Co2Ni

Run Order	SOD (mm)	AMP (µm)	IMD (mm)	CWL (mg)	CVL (mm^3)	CER (mg/h)	MDE (µm)	MDER (µm/h)	IBT (min)
1	0.5	40	80	5.1	0.5	0.57	2.8	0.31	212.85
2	0.5	50	100	5.5	0.6	0.61	3.0	0.33	187.98
3	0.5	60	120	6.2	0.6	0.69	3.4	0.37	156.16
4	1	40	100	3.5	0.4	0.39	1.9	0.21	>540
5	1	50	120	4.1	0.4	0.46	2.2	0.25	374.42
6	1	60	80	5.9	0.6	0.66	3.2	0.36	169.51
7	1.5	40	120	1.5	0.2	0.17	0.8	0.09	>540
8	1.5	50	80	3.6	0.4	0.40	2.0	0.22	>540
9	1.5	60	100	4.2	0.4	0.47	2.3	0.25	328.97

Table 6.16: Cavitation erosion study results for EWAC-20WC10Co2Ni

Run Order	SOD (mm)	AMP (µm)	IMD (mm)	CWL (mg)	CVL (mm^3)	CER (mg/h)	MDE (µm)	MDER (µm/h)	IBT (min)
1	0.5	40	80	3.5	0.3	0.39	2.0	0.23	>540
2	0.5	50	100	3.6	0.3	0.40	2.1	0.23	>540
3	0.5	60	120	4.2	0.4	0.47	2.4	0.27	360.98
4	1	40	100	2.6	0.3	0.29	1.5	0.17	>540
5	1	50	120	2.8	0.3	0.31	1.6	0.18	>540
6	1	60	80	4	0.4	0.44	2.3	0.26	539.98
7	1.5	40	120	1.4	0.1	0.16	0.8	0.09	>540
8	1.5	50	80	2.6	0.3	0.29	1.5	0.17	>540
9	1.5	60	100	2.8	0.3	0.31	1.6	0.18	>540

Table 6.17: Cavitation erosion study results for EWAC-30WC10Co2Ni

Run Order	SOD (mm)	AMP (µm)	IMD (mm)	CWL (mg)	CVL (mm^3)	CER (mg/h)	MDE (µm)	MDER (µm/h)	IBT (min)
1	0.5	40	80	2.7	0.2	0.30	1.7	0.19	>540
2	0.5	50	100	2.8	0.3	0.31	1.7	0.19	>540
3	0.5	60	120	3.2	0.3	0.36	2.0	0.22	>540
4	1	40	100	2.1	0.2	0.23	1.3	0.14	>540
5	1	50	120	2.2	0.2	0.24	1.4	0.15	>540
6	1	60	80	3.1	0.3	0.34	1.9	0.21	>540
7	1.5	40	120	1.1	0.1	0.12	0.7	0.08	>540
8	1.5	50	80	1.8	0.2	0.20	1.1	0.12	>540
9	1.5	60	100	2	0.2	0.22	1.2	0.14	>540

The weight loss of EWAC-xWC10Co2Ni composite clads as a function of time is shown in Figures 6.9-6.11.

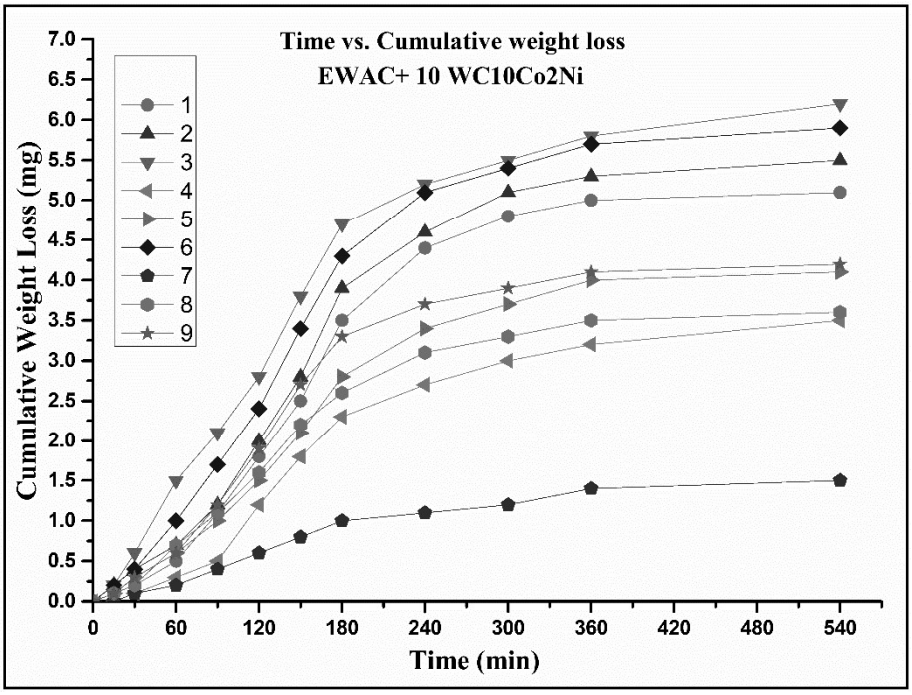

Figure 6.9: Line plot showing weight loss as the function of time for cavitation erosion wear of EWAC-10WC10Co2Ni specimens at different parameters

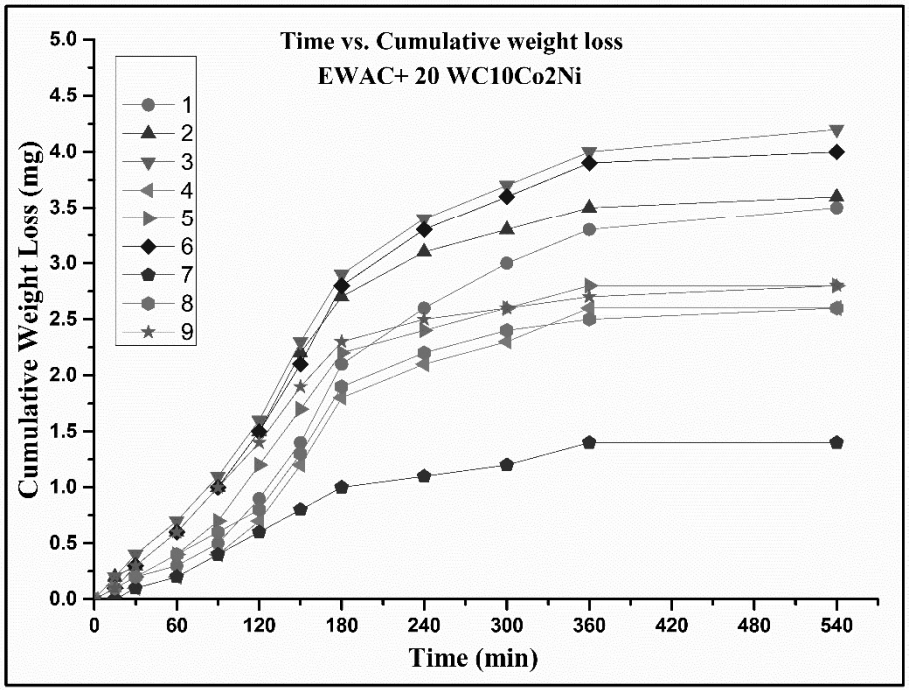

Figure 6.10: Line plot showing weight loss as the function of time for cavitation erosion wear of EWAC-20WC10Co2Ni specimens at different parameters

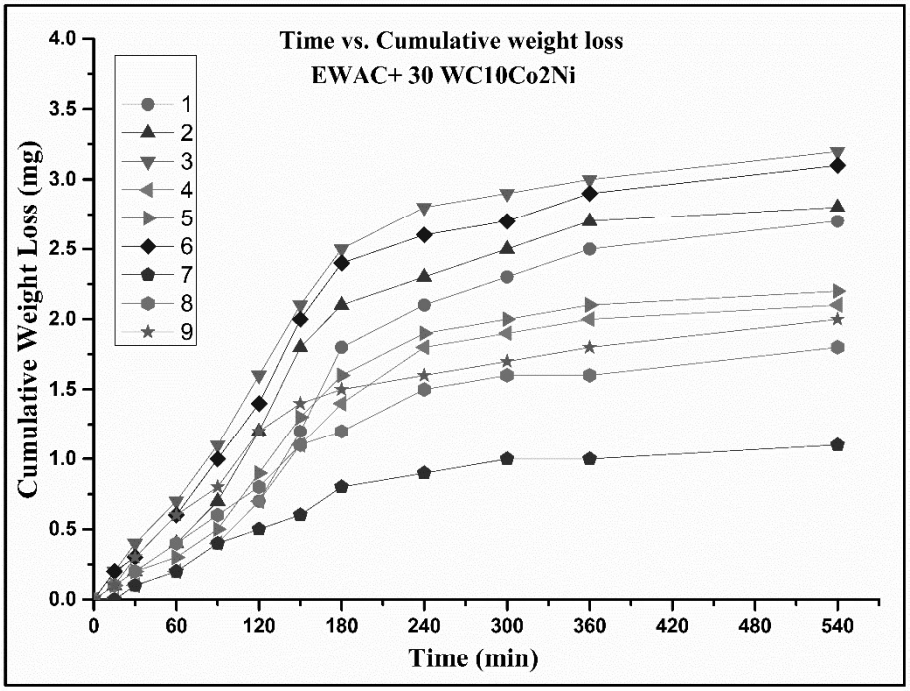

Figure 6.11: Line plot showing weight loss as the function of time for cavitation erosion wear of EWAC-30WC10Co2Ni specimens at different parameters

It is observed that EWAC based and xWC10Co2Ni reinforced composite clads perform better than SS 316 substrate surface at all set of experiments. The weight loss due to cavitation erosion wear is continuously decreased by increasing the concentration of reinforcement into matrix. The least weight loss is observed in highest concentration (EWAC-30WC10Co2Ni). In

EWAC-30WC10Co2Ni composite clad surface, the incubation period has not noticed even after 540 min of testing for all set of experimentation parameters (Table 6.17). However, the percentage change in weight loss goes on decreasing by increasing weight percentage of reinforcement into matrix (Table 6.18).

Table 6.18: Percentage change in cumulative weight loss of developed EWAC- xWC10Co2Ni clads

Materials	Weight loss (mg)	%age change in weight loss
SS 316	40.9	-
EWAC-10WC10Co2Ni	6.2	84.84
EWAC-20 WC10Co2Ni	4.2	89.73
EWAC-30 WC10Co2Ni	3.2	92.17

The addition of WC10Co2Ni up to 10% into EWAC matrix results in a significant reduction in weight loss due to increased hardness and toughness. The reinforcement particles coupled directly with microwave irradiation might also advance the atomic diffusion rate from substrate. This tends to reduce the stacking fault energy[157] and helps to increase cavitation erosion resistance of MMC. However, a very less percentage change in weight loss is observed when the concentration of reinforcement increases (up to 20% and 30%), despite of significant increase in hardness. This might be due to increased porosity with an increase in weight percentage of reinforcement[184]. The stress concentration around the pore sites reduces the strength, and pores become preferential sites for cavitation erosion wear. The cavitation erosion wear can be combat with a combination of hardness and toughness, and an increase in hardness adversely affect the toughness; therefore, the clads with the highest concentration (30%) experience marginal weight loss than the lower concentration (20%), despite of much higher hardness.

6.1.6 Results of statistical analysis of cavitation erosion behaviour of EWAC-xWC10Co2Ni composite clads

The graphical effects of all three test parameters are shown in Figures 6.12-6.14. It can be seen that increasing SOD and IMD reduces weight loss significantly, whereas increasing AMP causes an abrupt increase in weight loss.

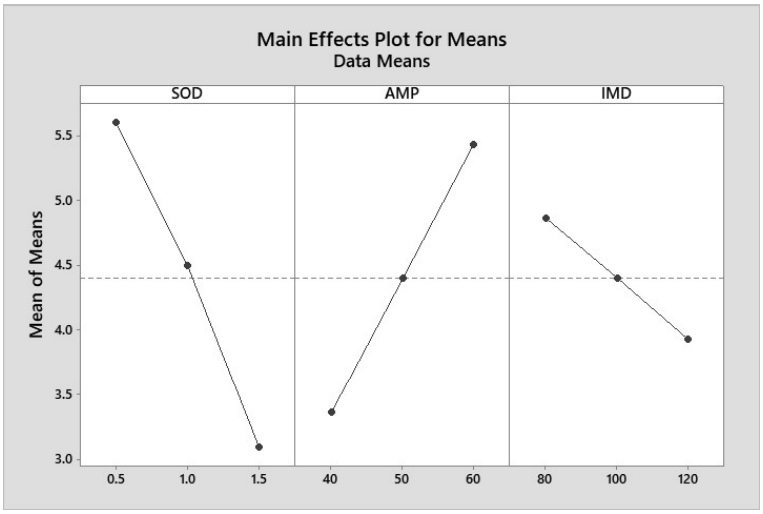

Figure 6.12: Main effect plots for cumulative weight loss of EWAC-10WC10Co2Ni

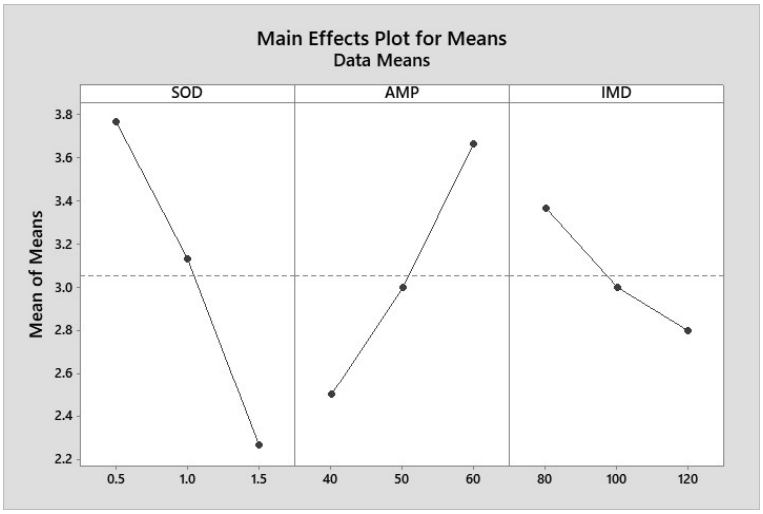

Figure 6.13: Main effect plots for cumulative weight loss of EWAC-20WC10Co2Ni

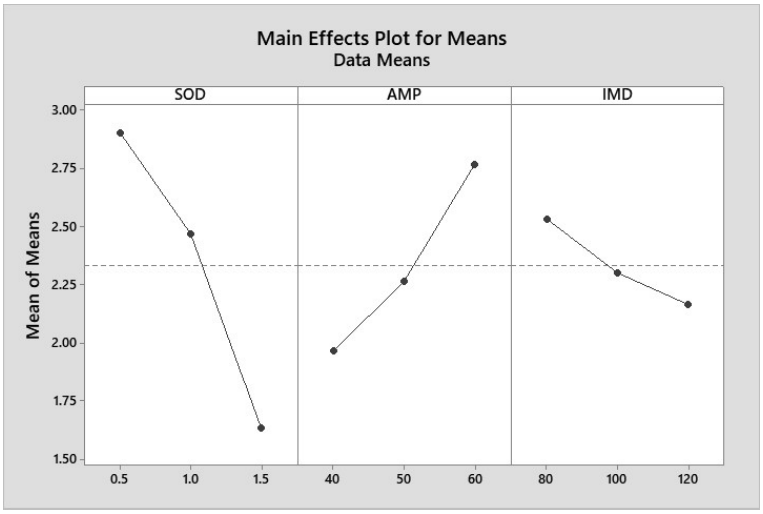

Figure 6.14: Main effect plots for cumulative weight loss of EWAC-30WC10Co2Ni

The obtained ANOVA results (Table 6.19) for CWL showed that SOD has maximum contribution in weight loss; followed by AMP and IMD of all the developed EWAC-xWc10Co2Ni composite clads.

Table 6.19: ANOVA results for cumulative weight loss of EWAC-xWC10Co2Ni -Taguchi L9 array analysis

	Source	DF	Seq SS	Adj SS	Adj MS	F	P	Percentage Contribution
EWAC + 10WC-based	**SOD (mm)**	2	9.42	9.42	4.71	201.86	0.005	**54.83**
	AMP (µm)	2	6.4067	6.40667	3.20333	137.29	0.007	**37.29**
	IMD (mm)	2	1.3067	1.30667	0.65333	28	0.034	**7.61**
	Residual Error	2	0.0467	0.04667	0.02333			**0.27**
	Total	8	17.18					
EWAC + 20WC-based	**SOD (mm)**	2	3.40222	3.40222	1.70111	117.77	0.008	**56.87**
	AMP (µm)	2	2.05556	2.05556	1.02778	71.15	0.014	**34.36**
	IMD (mm)	2	0.49556	0.49556	0.24778	17.15	0.049	**8.28**
	Residual Error	2	0.02889	0.02889	0.01444			**0.49**
	Total	8	5.98222					
EWAC + 30WC-based	**SOD (mm)**	2	2.48667	2.48667	1.24333	373	0.003	**67.57**
	AMP (µm)	2	0.98	0.98	0.49	147	0.007	**26.63**
	IMD (mm)	2	0.20667	0.20667	0.10333	31	0.031	**5.62**
	Residual Error	2	0.00667	0.00667	0.00333			**0.18**
	Total	8	3.68					

Table 6.20 shows response table for the weight loss values of EWAC-xWc10Co2Ni composite clads surface. It helps to monitor the effect of control factors with the help of delta statistics. This delta statistic helps to collect more data. The weight loss of surface is most influenced by the factor having the highest delta value. It is clear that, like substrate and EWAC-xCr_3C_2 composite clads, SOD is the most influential factor followed by AMP and IMD.

Table 6.20: Response table for cumulative weight loss in EWAC-xWC10Co2Ni composite clads

	Level	SOD (mm)	AMP (µm)	IMD (mm)
EWAC + 10WC10Co2Ni	1	5.6	3.367	4.867
	2	4.5	4.4	4.4
	3	3.1	5.433	3.933
	Delta	**2.5**	**2.067**	**0.933**
	Rank	**1**	**2**	**3**
EWAC + 20WC10Co2Ni	1	3.767	2.5	3.367
	2	3.133	3	3
	3	2.267	3.667	2.8
	Delta	**1.5**	**1.167**	**0.567**
	Rank	**1**	**2**	**3**
EWAC + 30WC10Co2Ni	1	2.9	1.967	2.533
	2	2.467	2.267	2.3
	3	1.633	2.767	2.167
	Delta	**1.267**	**0.8**	**0.367**
	Rank	**1**	**2**	**3**

To establish the relationship between weight loss and test parameters, mathematical modelling of CWL was performed; linear regression was developed using regression analysis at a 95% confidence level. Table 6.21 present the ANOVA results of the regression analysis.

Table 6.21: ANOVA results for cumulative weight loss of EWAC-xWC10Co2Ni - Regression analysis

	Source	DF	Adj SS	Adj MS	F	P	Percentage Contribution
EWAC + 10WC10Co2Ni	**SOD (mm)**	1	9.375	9.375	511.36	0	**54.57**
	AMP (µm)	1	6.4067	6.40667	349.45	0	**37.29**
	IMD (mm)	1	1.3067	1.30667	71.27	0	**7.61**
	Residual Error	5	0.0917	0.01833			**0.53**
	Total	8	17.18				
EWAC + 20WC10Co2Ni	**SOD (mm)**	1	3.375	3.375	201.16	0	**56.42**
	AMP (µm)	1	2.04167	2.04167	121.69	0	**34.13**
	IMD (mm)	1	0.48167	0.48167	28.71	0.003	**8.05**
	Residual Error	5	0.08389	0.01678			**1.40**
	Total	8	5.98222				
EWAC + 30WC10Co2Ni	**SOD (mm)**	1	2.4067	2.40667	107.76	0	**65.40**
	AMP (µm)	1	0.96	0.96	42.99	0.001	**26.09**
	IMD (mm)	1	0.2017	0.20167	9.03	0.03	**5.48**
	Residual Error	5	0.1117	0.02233			**3.03**
	Total	8	3.68				

SOD is the most influencing parameter in terms of weight loss during cavitation erosion testing, according to the analysis, followed by AMP and IMD. The following equations (6.5-6.7) were developed using same method as discussed in section 6.1.4, for CWL as a response variable.

EWAC-10WC10Co2Ni

$$\boldsymbol{CWL(mg) = 4.067 - 2.500\,SOD + 0.10333\,AMP - 0.02333\,IMD} \quad 6.5$$

EWAC-20WC10Co2Ni

$$\boldsymbol{CWL(mg) = 3.056 - 1.500\,SOD + 0.05833\,AMP - 0.01417\,IMD} \quad 6.6$$

EWAC-30WC10Co2Ni

$$\boldsymbol{CWL(mg) = 2.517 - 1.267\,SOD + 0.04000\,AMP - 0.00917\,IMD} \quad 6.7$$

Table 6.22 contains a summary of the prepared mathematical model. The significant R^2 (predicted) values (greater than 90 %) show that the developed model is capable to predict result in future with good accuracy (more than 90 %).

Table 6.22: Regression model summary for cumulative weight loss of EWAC-xWC10Co2Ni

Model Summary				
Composition	**S**	**R-Sq**	**R-Sq (Adj)**	**R-Sq (Pred)**
EWAC-10WC10Co2Ni	0.135401	99.47%	99.15%	98.34%
EWAC-20WC10Co2Ni	0.129529	98.60%	97.76%	96.18%
EWAC-30WC10Co2Ni	0.149443	96.97%	95.14%	91.98%

Table 6.23 summarises the details of the prediction modelling. At optimized experimental conditions, the prediction of weight loss values, for validation through confirmatory experiments, can be seen from the last column of table.

Table 6.23: Predicted values for cumulative weight loss of EWAC-xWC10Co2Ni composite clads

Prediction Model Summary				
Variable Input (SOD-0.5 mm, AMP-60 µm, IMD-80 mm)				
Composition	**Fit**	**SE Fit**	**95% CI**	**95% PI**
EWAC-10WC10Co2Ni	7.15	0.105848	(6.87791, 7.42209)	(6.70821, 7.59179)
EWAC-20WC10Co2Ni	4.67222	0.101258	(4.41193, 4.93251)	(4.24959, 5.09485)
EWAC-30WC10Co2Ni	3.55	0.116825	(3.24969, 3.85031)	(3.06239, 4.03761)

6.1.7 Results of parametric study of cavitation erosion behaviour of EWAC-xAl_2O_3 (where x= 5,10,15) % composite clad

The cavitation erosion testing to investigate the effect of cavitation erosion parameters for EWAC-xAl_2O_3 composite clads was conducted in the same manner mentioned above. Tables 6.24-6.26 illustrate the experimental results of the CWL. Other terms such as CVL, CER, MDE, MDER and IBT have also been calculated.

Table 6.24: Cavitation erosion study results for EWAC-5Al_2O_3

Run Order	SOD (mm)	AMP (µm)	IMD (mm)	CWL (mg)	CVL (mm^3)	CER (mg/h)	MDE (µm)	MDER (µm/h)	IBT (min)
1	0.5	40	80	8.4	1.0	0.93	4.1	0.46	152.94
2	0.5	50	100	8.9	1.0	0.99	4.4	0.49	144.48
3	0.5	60	120	9.9	1.1	1.10	4.9	0.54	120.02
4	1	40	100	6.2	0.7	0.69	3.1	0.34	223.40
5	1	50	120	6.5	0.7	0.72	3.2	0.36	194.20
6	1	60	80	9.7	1.1	1.08	4.8	0.53	126.72
7	1.5	40	120	2.5	0.3	0.28	1.2	0.14	>540
8	1.5	50	80	6	0.7	0.67	3.0	0.33	210.29
9	1.5	60	100	6.6	0.8	0.73	3.2	0.36	179.75

Table 6.25: Cavitation erosion study results for EWAC-10Al_2O_3

Run Order	SOD (mm)	AMP (µm)	IMD (mm)	CWL (mg)	CVL (mm^3)	CER (mg/h)	MDE (µm)	MDER (µm/h)	IBT (min)
1	0.5	40	80	4.9	0.6	0.54	2.3	0.26	300.26
2	0.5	50	100	5	0.6	0.56	2.4	0.26	258.20
3	0.5	60	120	5.8	0.7	0.64	2.8	0.31	180.30
4	1	40	100	3.8	0.5	0.42	1.8	0.20	>540
5	1	50	120	4	0.5	0.44	1.9	0.21	539.64
6	1	60	80	5.6	0.7	0.62	2.7	0.30	198.22
7	1.5	40	120	2	0.2	0.22	1.0	0.11	>540
8	1.5	50	80	3.3	0.4	0.37	1.6	0.17	>540
9	1.5	60	100	3.6	0.4	0.40	1.7	0.19	>540

Table 6.26: Cavitation erosion study results for EWAC-15Al_2O_3

Run Order	SOD (mm)	AMP (µm)	IMD (mm)	CWL (mg)	CVL (mm^3)	CER (mg/h)	MDE (µm)	MDER (µm/h)	IBT (min)
1	0.5	40	80	4.2	0.5	0.47	1.9	0.22	487.34
2	0.5	50	100	4.5	0.5	0.50	2.1	0.23	410.17
3	0.5	60	120	5	0.6	0.56	2.3	0.26	260.76
4	1	40	100	3	0.4	0.33	1.4	0.15	>540
5	1	50	120	3.1	0.4	0.34	1.4	0.16	>540

6	1	60	80	4.5	0.5	0.50	2.1	0.23	388.96
7	1.5	40	120	1.3	0.2	0.14	0.6	0.07	>540
8	1.5	50	80	2.4	0.3	0.27	1.1	0.12	>540
9	1.5	60	100	3.2	0.4	0.36	1.5	0.17	>540

From the experimental results, it has been observed that, in this case also, the maximum weight loss has recorded at same test parameters set-3. The maximum recorded cumulative weight loss at this parameter was 9.9 mg, 5.8 mg and 5 mg for EWAC-5Al_2O_3, EWAC-10Al_2O_3 and EWAC-15Al_2O_3, respectively.

The cumulative weight loss of EWAC-xAl_2O_3 composite clads as a function of time is shown in Figures 6.15-6.17. The performance of Al_2O_3 reinforced and EWAC based composite clads at all set of parameters was better than substrate specimens. The increase in weight percentage of hard reinforcement into matrix results into continuous decrease of weight loss. However, the change in weight loss was not significant, when weight percentage of reinforcement was increased from 10% to 15%.

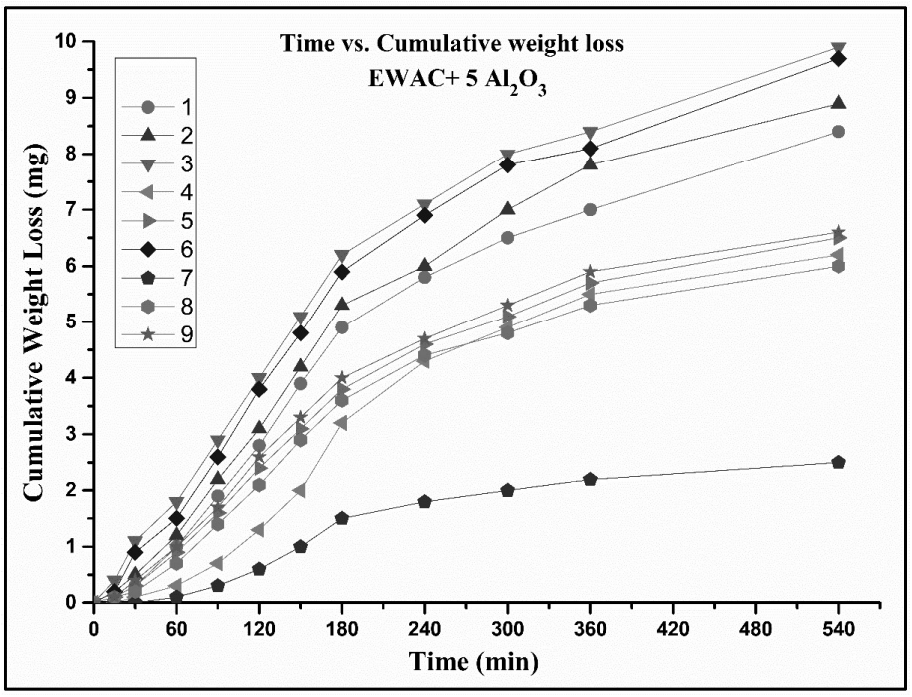

Figure 6.15: Line plot showing weight loss as the function of time for cavitation erosion wear of EWAC-5Al_2O_3 specimens at different parameters

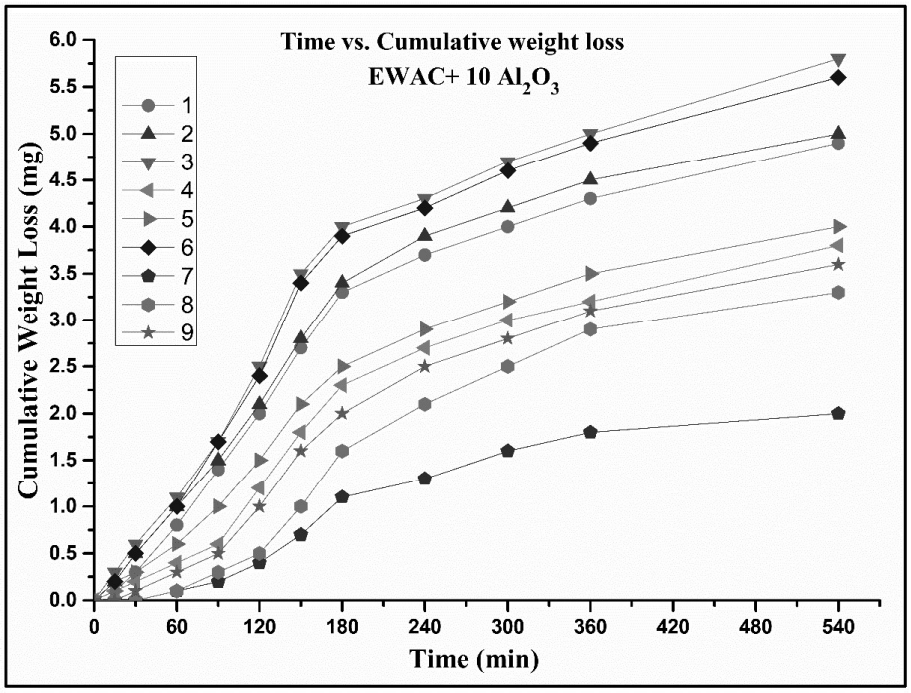

Figure 6.16: Line plot showing weight loss as the function of time for cavitation erosion wear of EWAC-10Al_2O_3 specimens at different parameters

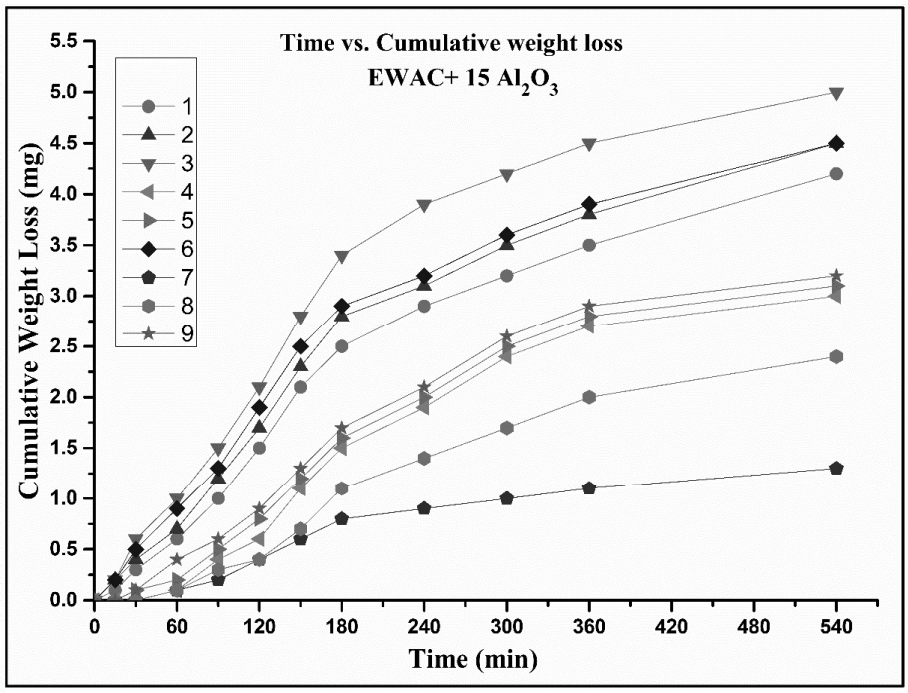

Figure 6.17: Line plot showing weight loss as the function of time for cavitation erosion wear of EWAC-15Al_2O_3 specimens at different parameters

This is observed from Figures 6.15-6.17 that the Al_2O_3 reinforced composite clads behave almost similar to Cr_3C_2 and WC10Co2Ni reinforced composite clads. The experimental parameter sets 1,2,3 and 6 were found more significant and experimental parameter set 7 was

found least significant for weight loss in all the Al_2O_3 reinforced composite clads. The significant less porosity, higher flexural strength and higher hardness helps the developed composite clads to resist cavitation erosion wear. The developed EWAC-xAl_2O_3 composite clads show 4.17, 7.05 and 8.18 times lesser weight loss for EWAC-5Al_2O_3, EWAC-10Al_2O_3 and EWAC-15Al_2O_3, respectively, as compared to substrate at same experimental conditions.

6.1.8 Results of statistical analysis of cavitation erosion behaviour of EWAC-xAl_2O_3 composite clads

The mean effect plots for means of all the three test parameters for EWAC-xAl_2O_3 composite clads, shown in figures 6.18-6.20, show that increase in SOD and IMD inversely affects the

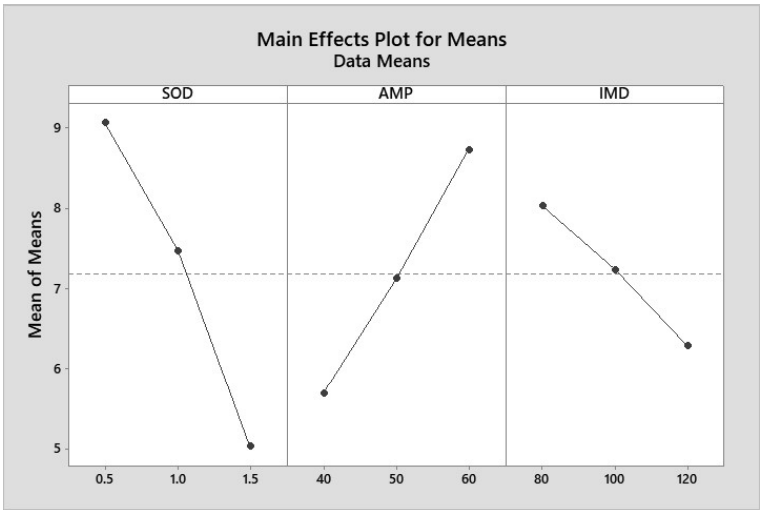

Figure 6.18: Main effect plots for cumulative weight loss of EWAC-5Al_2O_3

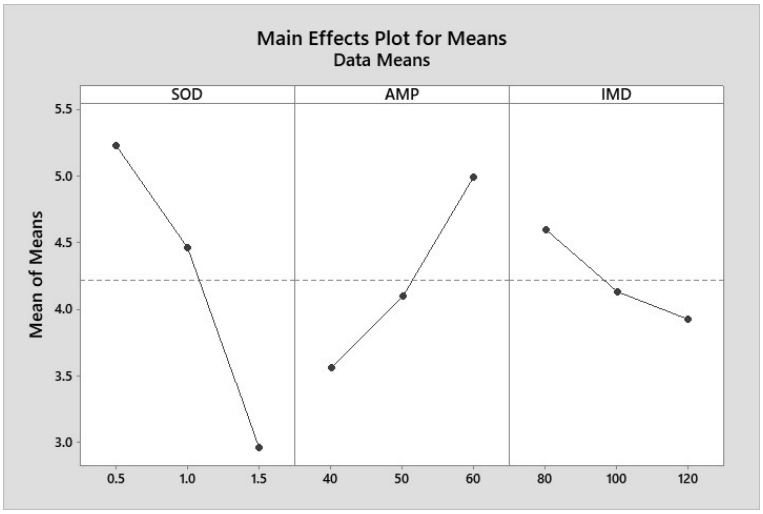

Figure 6.19: Main effect plots for cumulative weight loss of EWAC-10Al_2O_3

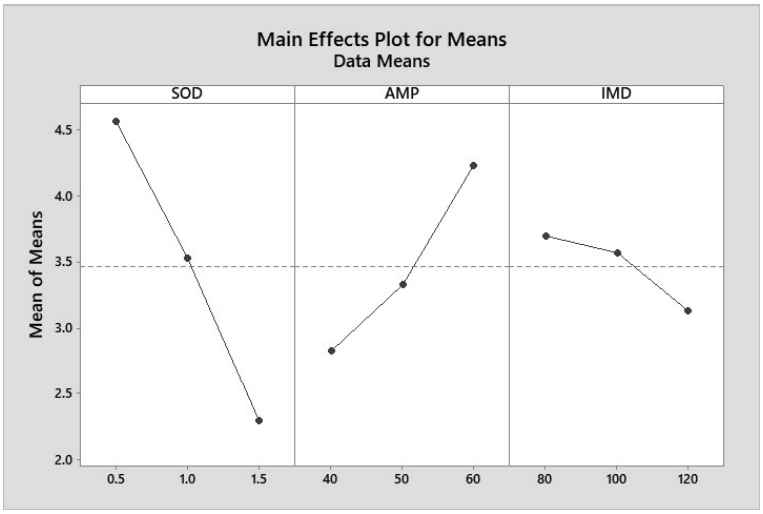

Figure 6.20: Main effect plots for cumulative weight loss of EWAC-15Al_2O_3

weight loss. Whereas, increase in AMP directly affects the weight loss and weight loss increases with increase in AMP for all the developed composite clads.

Table 6.27 indicates that SOD is most significant and IMD is least significant factor for Al_2O_3 reinforced composite clads, similar to substrate, Cr_3C_2 and WC10Co2Ni reinforced composite clads. The contribution of SOD in all the developed Al_2O_3 reinforced composite clads is more than 50%.

Table 6.27: ANOVA results for cumulative weight loss of EWAC-xAl_2O_3- Taguchi L9 array analysis

	Source	DF	Seq SS	Adj SS	Adj MS	F	P	Percentage Contribution
EWAC + 5Al_2O_3	**SOD (mm)**	2	24.7489	24.7489	12.3744	146.54	0.007	**57.22**
	AMP (µm)	2	13.8156	13.8156	6.9078	81.8	0.012	**31.94**
	IMD (mm)	2	4.5156	4.5156	2.2578	26.74	0.036	**10.45**
	Residual Error	2	0.1689	0.1689	0.0844			**0.39**
	Total	8	43.2489					
EWAC + 10Al_2O_3	**SOD (mm)**	2	7.9756	7.97556	3.98778	276.08	0.004	**67.27**
	AMP (µm)	2	3.1489	3.14889	1.57444	109	0.009	**26.56**
	IMD (mm)	2	0.7022	0.70222	0.35111	24.31	0.04	**5.92**
	Residual Error	2	0.0289	0.02889	0.01444			**0.25**
	Total	8	11.8556					

EWAC + 15Al$_2$O$_3$	**SOD (mm)**	2	7.7267	7.72667	3.86333	1159	0.001	**68.50**
	AMP (µm)	2	3.02	3.02	1.51	453	0.002	**26.77**
	IMD (mm)	2	0.5267	0.52667	0.26333	79	0.013	**4.67**
	Residual Error	2	0.0067	0.00667	0.00333			**0.06**
	Total	8	11.28					

The delta statistics values of Al_2O_3 reinforced composite clads are shown in Table 6.28. This shows that SOD is the most influential factor followed by AMP and IMD.

Table 6.28: Response table for cumulative weight loss in EWAC-xAl_2O_3 composite clads

	Level	**SOD (mm)**	**AMP (µm)**	**IMD (mm)**
EWAC + 5Al$_2$O$_3$	1	9.067	5.7	8.033
	2	7.467	7.133	7.233
	3	5.033	8.733	6.3
	Delta	**4.033**	**3.033**	**1.733**
	Rank	**1**	**2**	**3**
EWAC + 10Al$_2$O$_3$	1	5.233	3.567	4.6
	2	4.467	4.1	4.133
	3	2.967	5	3.933
	Delta	**2.267**	**1.433**	**0.667**
	Rank	**1**	**2**	**3**
EWAC + 15Al$_2$O$_3$	1	4.567	2.833	3.7
	2	3.533	3.333	3.567
	3	2.3	4.233	3.133
	Delta	**2.267**	**1.4**	**0.567**
	Rank	**1**	**2**	**3**

The mathematical modelling helps to relate the weight loss with test parameters. The results of linear regression at 95% confidence level are presented in Table 6.29. The analysis shows that, in this case also, SOD is the most influencing parameter in terms of weight loss during cavitation erosion testing followed by AMP and IMD.

Table 6.29: ANOVA results for cumulative weight loss of EWAC-xAl_2O_3- Regression analysis

	Source	**DF**	**Adj SS**	**Adj MS**	**F**	**P**	**Percentage Contribution**
EWAC + 5Al$_2$O$_3$	**SOD (mm)**	1	24.4017	24.4017	226.41	0	**56.42**
	AMP (µm)	1	13.8017	13.8017	128.06	0	**31.91**
	IMD (mm)	1	4.5067	4.5067	41.81	0.001	**10.42**
	Residual Error	5	0.5389	0.1078			**1.25**
	Total	8	43.2489				

EWAC + 10Al_2O_3	**SOD (mm)**	1	7.7067	7.70667	96.2	0	**65.00**
	AMP (µm)	1	3.0817	3.08167	38.47	0.002	**25.99**
	IMD (mm)	1	0.6667	0.66667	8.32	0.034	**5.62**
	Residual Error	5	0.4006	0.08011			**3.38**
	Total	8	11.8556				
EWAC + 15Al_2O_3	**SOD (mm)**	1	7.7067	7.70667	254.07	0	**68.32**
	AMP (µm)	1	2.94	2.94	96.92	0	**26.06**
	IMD (mm)	1	0.4817	0.48167	15.88	0.01	**4.27**
	Residual Error	5	0.1517	0.03033			**1.34**
	Total	8	11.28				

The regression equations (6.8-6.10) were developed for cumulative weight loss as a response variable. These equations are helpful for calculating CWL for EWAC-xAl_2O_3 composite clads at different test parameter values of SOD, AMP and IMD.

EWAC-5Al_2O_3

$$\boldsymbol{CWL(mg) = 7.972 - 4.033\,SOD + 0.1517\,AMP - 0.04333\,IMD} \quad (6.8)$$

EWAC-10Al_2O_3

$$\boldsymbol{CWL(mg) = 4.572 - 2.267\,SOD + 0.0717\,AMP - 0.01667\,IMD} \quad (6.9)$$

EWAC-15Al_2O_3

$$\boldsymbol{CWL(mg) = 3.650 - 2.267\,SOD + 0.07000\,AMP - 0.01417\,IMD} \quad (6.10)$$

Table 6.30 presents a summary of the prepared mathematical model. The significant R^2 (predicted) values (greater than 90%) shows the viability of developed model.

Table 6.30: Regression model summary for cumulative weight loss of EWAC-xAl_2O_3 composite clads

Model Summary				
Composition	**S**	**R-Sq**	**R-Sq(Adj)**	**R-Sq(Pred)**
EWAC-5Al_2O_3	0.328295	98.75%	98.01%	96.34%
EWAC-10Al_2O_3	0.283039	96.62%	94.59%	91.27%
EWAC-15Al_2O_3	0.174165	98.66%	97.85%	96.39%

Table 6.31 summarises the details of the prediction modelling. At optimized experimental conditions (SOD 0.5 mm, AMP 60 µm, and IMD 80 mm) the prediction of weight loss values can be seen from the last column of table.

Table 6.31: Predicted values for cumulative weight loss of EWAC-xAl_2O_3 composite clads

Prediction Model Summary				
Variable Input (SOD-0.5 mm, AMP-60 µm, IMD-80 mm)				
Composition	**Fit**	**SE Fit**	**95% CI**	**95% PI**
EWAC-5Al_2O_3	11.5889	0.25664	(10.9292, 12.2486)	(10.5177, 12.6601)
EWAC-10Al_2O_3	6.40556	0.221262	(5.83678, 6.97433)	(5.48205, 7.32906)
EWAC-15Al_2O_3	5.58333	0.136151	(5.23335, 5.93332)	(5.01506, 6.15160)

6.2 Effect of Test Parameters on Cavitation Erosion Behaviour of Materials

6.2.1 Effect of Stand-off Distance on cavitation erosion behaviour of materials

The distance between the specimen surface and the ultrasonic horn is called stand-off distance. The effect of varying SOD on cavitation erosion behaviour of developed clads and as received SS-316 was examined by measuring the weight loss of all the specimen surfaces. In the currently adopted cavitation erosion testing method, the stream of vapour bubbles was generated by the ultrasonic vibration of horn. Further, these generated vapour bubbles were pushed towards the specimen surface by the shock wave produced by the horn. However, due to pressure differences, the vapour bubbles start collapsing, and the collapse of these bubbles creates micro jets, and those micro jets apply impact force on the specimen surface, which results in stress generation and removal of material [185]. In the present study, the maximum weight loss is occurred at 0.5 mm SOD followed by 1 mm and 1.5 mm at all levels of AMP and IMD. This could be due to the fact that energy of produced shockwave by ultrasonic horn is insufficient to direct the whole stream of formed vapour bubbles towards target surface. The bubbles escape from bubble stream without targeting the surface of specimen. Moreover, liquid jet that formed by bubbles, which explode near horn, losses kinetic energy due to travel more distance, by increasing separation distance. Therefore, the surfaces of all specimens' damage only by explosion of that bubbles which are able to reach near the surface and explodes there; and/or that bubbles which explode near horn but have sufficient kinetic energy to damage the surface permanently even after travelling more distance. Consequently, the exposed surfaces of clads and substrate specimen experience less damage which leads to lesser weight loss of all the surfaces at increased separation distance. Cladded surfaces have shown better CER (lesser weight loss) than SS- 316 at all test conditions.

6.2.2 Effect of Amplitude on cavitation erosion behaviour of materials

Vibration amplitude is an important parameter that directly affects the quantity of vapour bubbles (empty cavities) generation and the collapse pressure intensity. At low AMP, the cavities' pressure intensity upon collapse is less, and also size growth of cavities is low owing to smaller negative vibrating cycles of the horn. On the other hand, larger negative vibrating cycles lead to a higher growth size of cavities. Further, these cavities agglomerate with neighbouring vapour cavities and produce higher pressure intensity after the collapse. Therefore, very few high energy bubbles collapse near the specimen surface at lower AMP and result in a lesser damaged surface. It has been observed that at lower AMP, the weight loss is less for all the materials at all levels of SOD. This observation also helps to characterize the

ultrasonic system for diverse applications. For cleaning applications like optics, biological cell disruption, and jewellery, low AMP and high SOD can be used, and high AMP and low SOD can be suitable for applications like surface erosion, decontamination, and treatment of metallic and non-metallic surfaces.

6.2.3 Effect of Immersion Depth on cavitation erosion behaviour of materials

The weight loss of all the surfaces is affected by variation in horn immersion depth into distilled water (test liquid). It is clear from experimental results that an increase in horn IMD into test liquid decreases the weight loss of all the surfaces. The increase in IMD increases static fluid pressure. In the formation and growth of the cavitation bubble, static fluid pressure plays an important role. When the static pressure is high, the acoustic AMP needs to be more to induce sufficient negative pressure, which facilitates the vapour bubble growth and vice versa [186]. Thus, in the current study, high weight loss is recorded at low horn IMD comparable to high horn IMD.

6.3 Fractographic Analysis of Worn Surfaces of Materials

The cavitation erosion wear studies of worn surface have been carried out to find out the wear mechanism of Ni-based and microwave processed composite clads surface and as received substrate surface. The results of the material failure mechanism after cavitation erosion testing for 9 h were studied under SEM and are presented in this section.

6.3.1 Fractographic analysis of worn surface of substrate specimens and developed composite clads

The surface topography of the substrate and developed composite clads, prior to cavitation erosion, is shown in Figure 6.21.

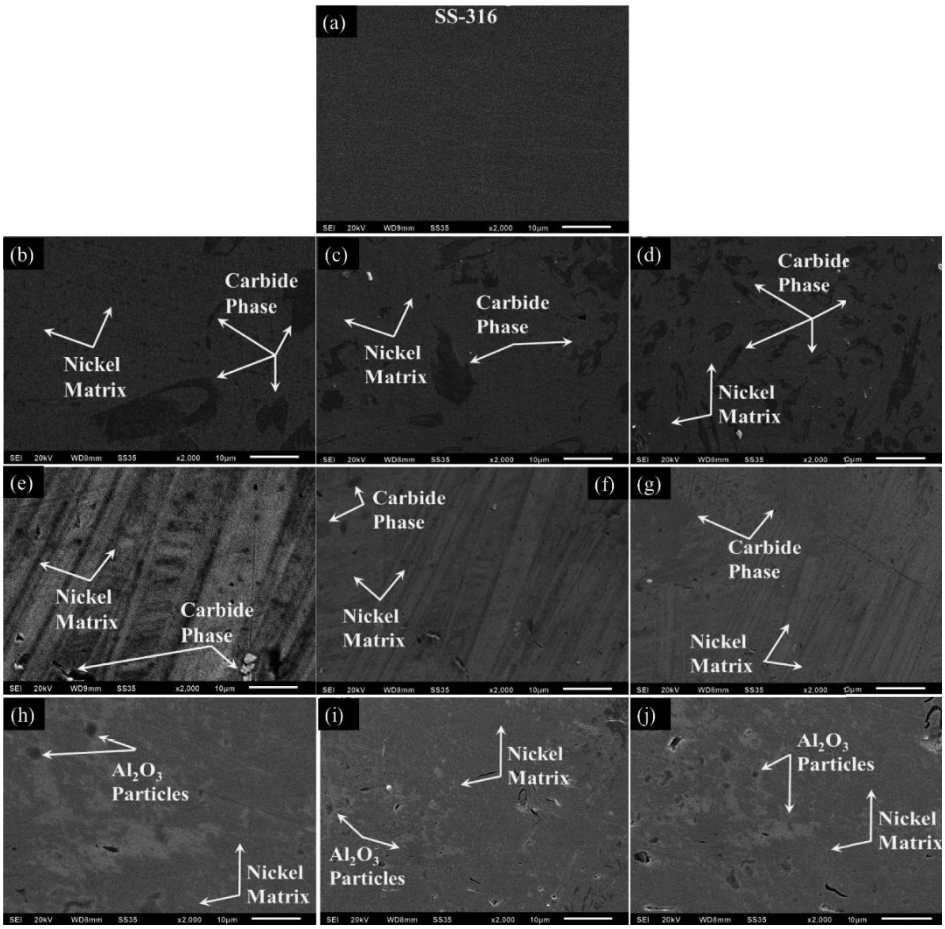

Figure 6.21: SEM micrographs showing the polished surface before cavitation erosion of a) substrate b) EWAC-10Cr_3C_2 c) EWAC-20Cr_3C_2 d) EWAC-30Cr_3C_2 e) EWAC-10WC10Co2Ni f) EWAC-20WC10Co2Ni g) EWAC-30WC10Co2Ni h) EWAC-5Al_2O_3i) EWAC-10Al_2O_3 j) EWAC-15Al_2O_3

It shows that the surface is well polished and free of scratches prior to cavitation erosion testing. On the other hand, the eroded surface of substrate and developed composite clads tested at experimental parametric sets 3 and 5, and 7, respectively is shown in Figures 6.22-6.24. The maximum, moderate and minimum weight loss has been occurred at parameter sets 3, 5 and 7, respectively. Therefore, the surface morphologies of specimens subjected to these parameters are examined to find a plausible erosion mechanism. From the SEM images, it was observed that the damage to the surface occurred in the form of known mechanisms such as pits, craters, plastic deformation, lip formation, and impingement marks, etc.

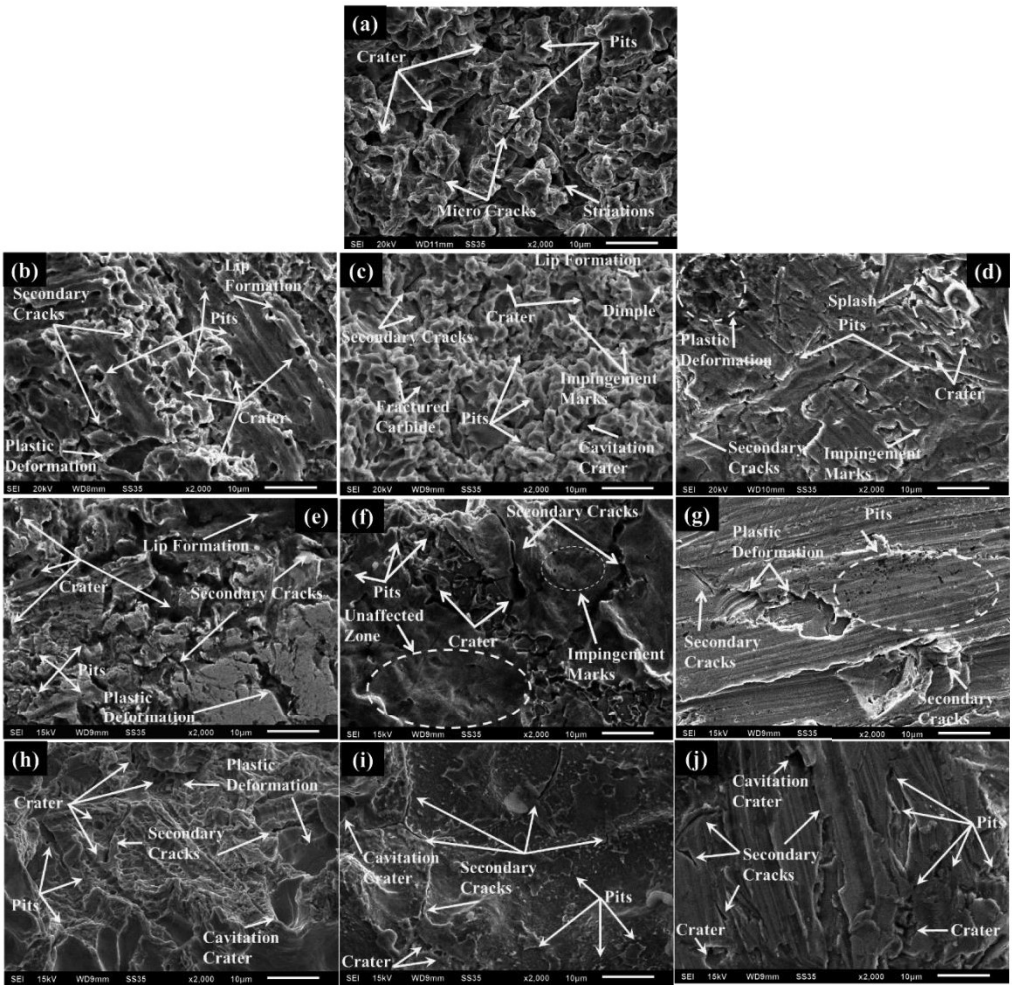

Figure 6.22: SEM micrographs showing the damaged surface morphology at experimental parameter no. 3 of a) substrate b) EWAC-10Cr_3C_2 c) EWAC-20Cr_3C_2 d) EWAC-30Cr_3C_2 e) EWAC-10WC10Co2Ni f) EWAC-20WC10Co2Ni g) EWAC-30WC10Co2Ni h) EWAC-5Al_2O_3 i) EWAC-10Al_2O_3 j) EWAC-15Al_2O_3

Figure 6.22 clearly shows that the collapse of vapor bubbles during 9-h cavitation erosion testing severely damages substrate and developed composite clads surface during experimental parameter 3. It is clear from SEM images that the surface got severely damage in the form of large numbers of pits, craters, striations, micro-cracks and lips formation, plastic deformation, and secondary cracks. The presence of the features mentioned above confirms that damage to the surface is caused by heavy impact loading, resulting from impingement jets formed during the collapse of vapor bubbles. The reason behind severe damage to the surfaces is the formation of vapor bubbles at this parameter that are in large quantity due to the high AMP, and at smaller SOD collapse of these vapor bubbles are near the specimen surface without escaping from the bubbles stream and losing their significant kinetic energy. The collapse of these vapor bubbles near the surface leads to high impact loading, causing plastic deformation. When the impact

energy exceeds the material's mechanical strength, the material finally gets fractured in the form of pits. As the testing continues, the impingement jets keep forming and attacking both the surface with their high impact energy and later, pits transformed into micro cracks and craters.

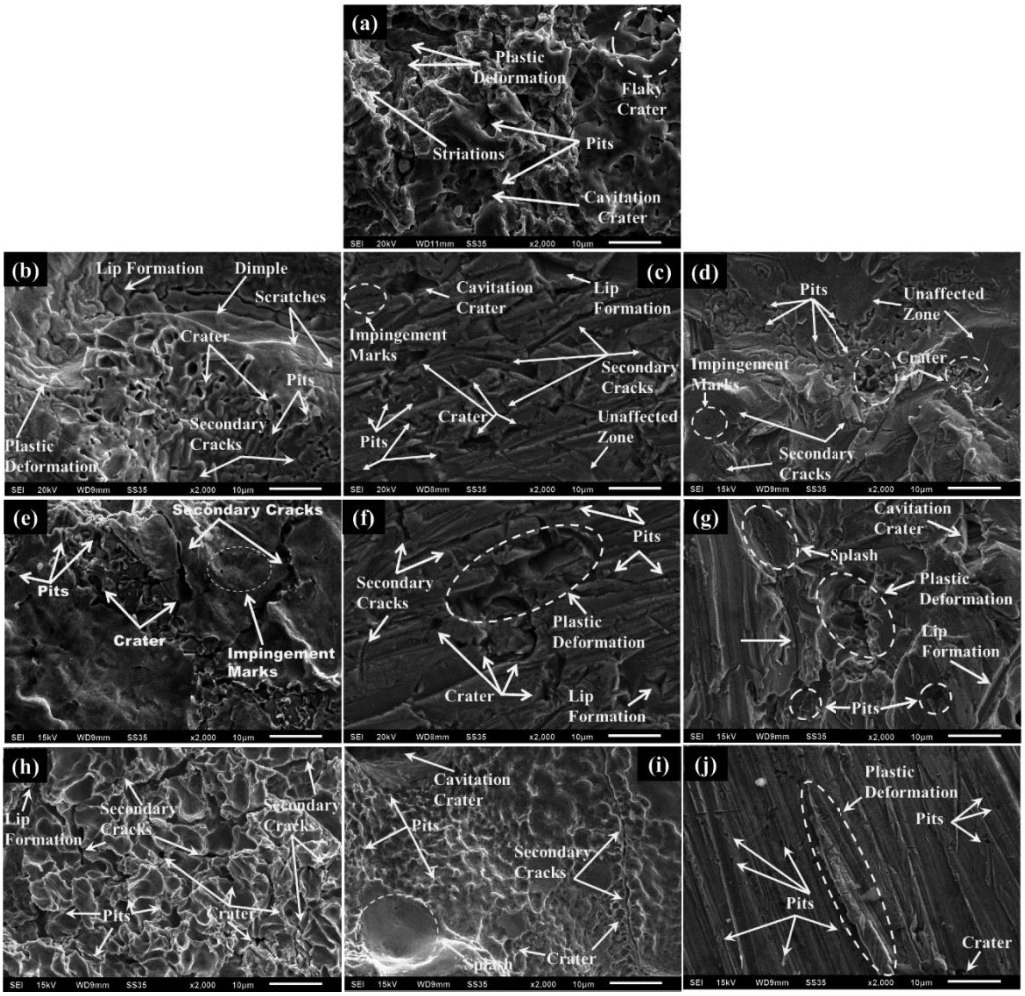

Figure 6.23: SEM micrographs showing the damaged surface morphology at experimental parameter no. 5 of a) substrate b) EWAC-10Cr_3C_2 c) EWAC-20Cr_3C_2 d) EWAC-30Cr_3C_2 e) EWAC-10WC10Co2Ni f) EWAC-20WC10Co2Ni g) EWAC-30WC10Co2Ni h) EWAC-5Al_2O_3 i) EWAC-10Al_2O_3 j) EWAC-15Al_2O_3

Figure 6.23 shows that during experimental parameter 5, the severity of the surface damage is lesser than experimental parameter 3. Since the amplitude was less at this parameter set, that leads to less formation of vapor bubbles. The separation distance between the horn and specimen was also higher than the former parameter, leading to loss of the bubbles from the bubble stream because while traveling from horn tip to specimen surface, bubbles lose their

kinetic energy imparted by shock waves. Therefore, comparatively less bubbles contributed in the cavitation erosion mechanism, which causes lesser weight loss of all the surface.

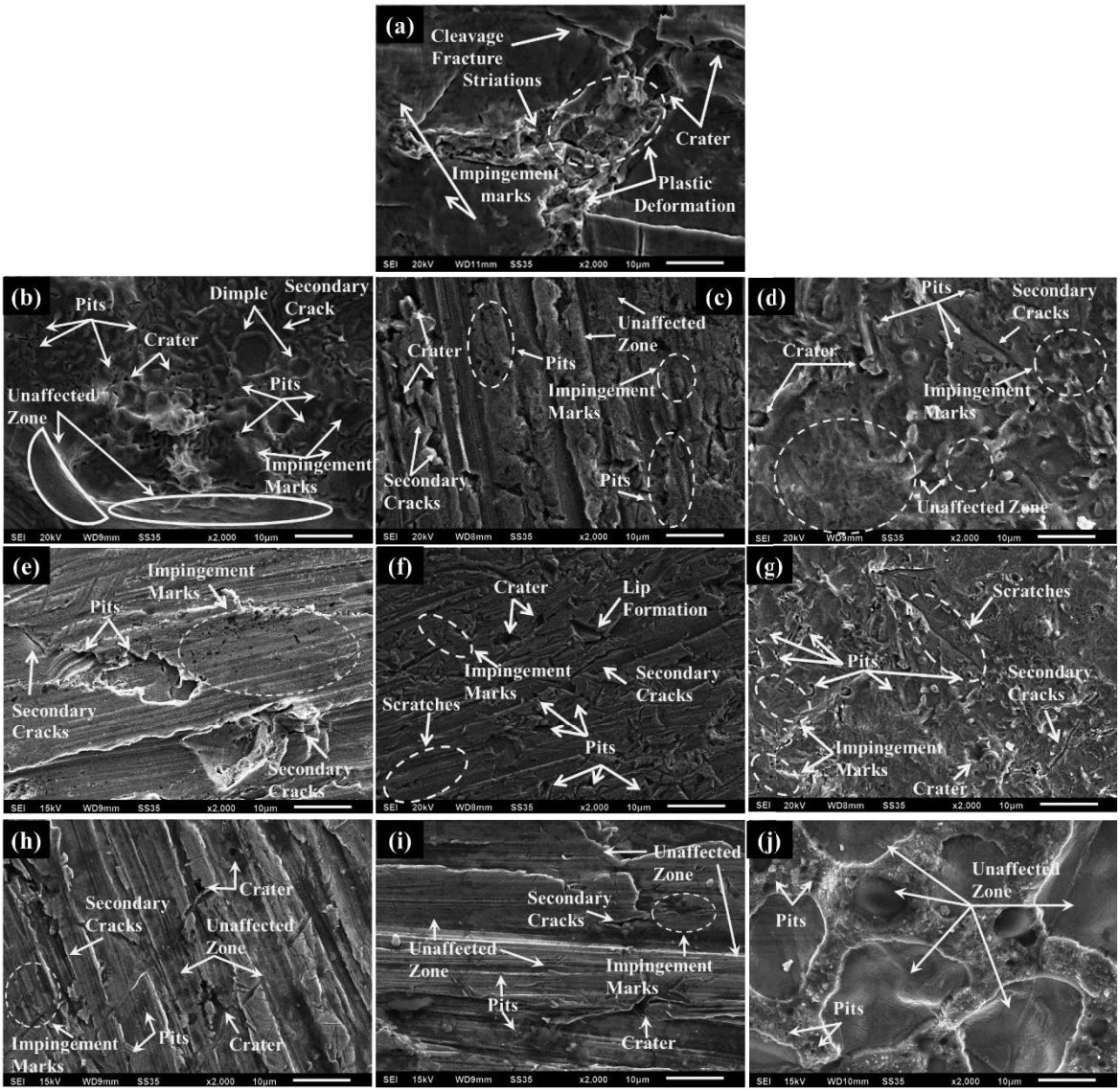

Figure 6.24: SEM micrographs showing the damaged surface morphology at experimental parameter no. 7 of a) substrate b) EWAC-10Cr_3C_2 c) EWAC-20Cr_3C_2 d) EWAC-30Cr_3C_2 e) EWAC-10WC10Co2Ni f) EWAC-20WC10Co2Ni g) EWAC-30WC10Co2Ni h) EWAC-5Al_2O_3 i) EWAC-10Al_2O_3 j) EWAC-15Al_2O_3

From figure 6.24 it is observed that, during experimental parameter 7, the specimen surface was mainly damaged in the form of the crater, plastically deformed lips, cleavage fracture, and impingement marks. Since at experimental parameter 7, significantly less value of the weight loss is recorded for all the surfaces. Also, it is noticeable from that a major portion of developed clad surfaces remain unaffected; only a few pits, scratches, and impingements marks are present. The pits did not accumulate, which prevents the formation of crater and causes lesser weight loss in the developed clad surface. From the SEM images shown in Figure 6.24, it can

be said that it is a much earlier stage of material for cavitation erosion. During experimental parameter 7, the formed bubbles are very less in quantity due to the least AMP, and many vapor bubbles escaped from the bubble stream without targeting the surface, as they have lost their kinetic energy imparted by the acoustic horn as the SOD is highest (in this domain of study). Therefore, the surfaces are not severely damaged. The presence of impingement marks also confirms that insufficient impingement jets impact energy fails to cause permanent damage. This is observed that the least damage has occurred at experimental parameter 7 in all cases. Moreover, these marks are showing some directional patterns, which are the consequences of releasing shock wave energy due to high SOD in a particular manner. However, some zones of less severe plastic deformation are also observed in surface topography.

6.4 Results of Confirmatory or Validatory Experiments

The confirmatory experiments have been performed at optimized cavitation test parameters (0.5 mm SOD, 60 μm AMP, and 80 mm IMD). Pure EWAC clads have also been developed and tested for cavitation erosion wear, for better understanding. Three experiments (E1, E2 and E3) of each sample have been performed to check the repeatability (Table 6.32). The average values have been considered. The other terms such as CVL, CER, MDE, MDER and IBT have also been tabulated. The results of comparison of cumulative weight loss and incubation time of substrate, pure EWAC and all developed composite clads tested at optimized parameters have been presented graphically in Figure 6.25 and Figure 6.26, respectively.

Table 6.32: Cavitation erosion study results of substrate and developed clad samples at optimized parameters

Run Order	Cumulative weight loss (mg)				CVL (mm^3)	CER (mg/h)	MDE (μm)	MDER (μm/h)	IBT (min)
	E1	E2	E3	Average					
Substrate	52.41	52.36	51.12	**51.9±0.73**	6.6	5.81	23.6	2.62	92.37
EWAC	27.76	26.7	28.08	**27.5±0.72**	3.1	3.06	13.9	1.54	72.93
EWAC + 10Cr_3C_2	19.48	18.38	17.6	**18.5±0.94**	2.1	2.05	9.1	1.01	84.55
EWAC + 20Cr_3C_2	10.1	9.56	9.75	**9.8±0.27**	1.2	1.09	4.7	0.52	130.25

EWAC + 30Cr_3C_2	7.59	8.29	8.62	**8.2±0.53**	1.0	0.91	3.8	0.43	151.03
EWAC + 10 WC-based	6.84	7.2	7.41	**7.2±0.29**	0.7	0.79	3.9	0.43	178.64
EWAC + 20 WC-based	4.4	4.7	4.95	**4.7±0.28**	0.5	0.52	2.7	0.30	>540
EWAC + 30 WC-based	3.6	3.5	3.95	**3.7±0.24**	0.3	0.41	2.3	0.25	>540
EWAC + 5 Al_2O_3	11.25	12.1	10.66	**11.3±0.72**	1.3	1.26	5.6	0.62	135.41
EWAC + 10Al_2O_3	6.2	6.7	7.2	**6.7±0.50**	0.8	0.74	3.2	0.35	279.70
EWAC + 15Al_2O_3	5.26	5.5	5.89	**5.6±0.32**	0.7	0.62	2.6	0.29	426.46

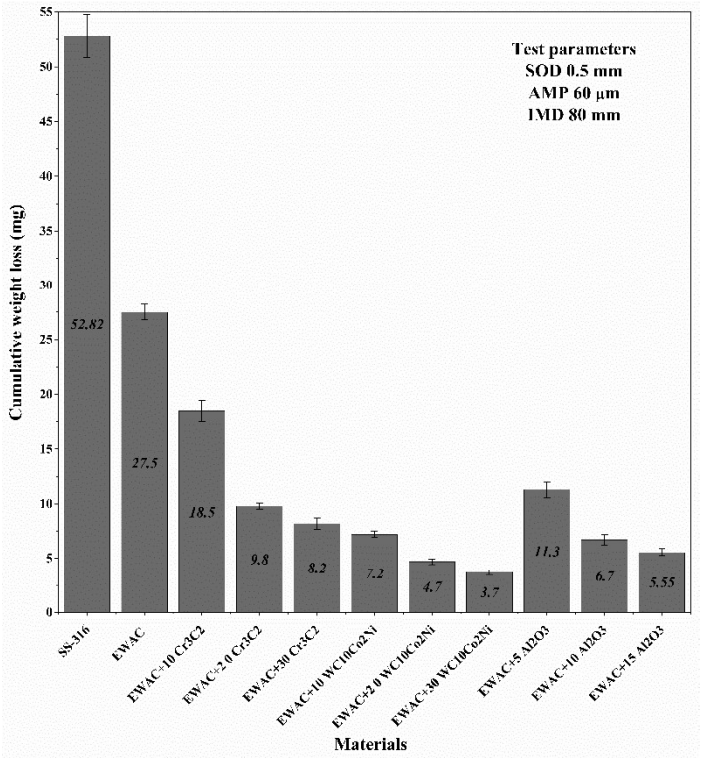

Figure 6.25: Comparison of cumulative weight loss of substrate and developed clad samples at optimized parameters

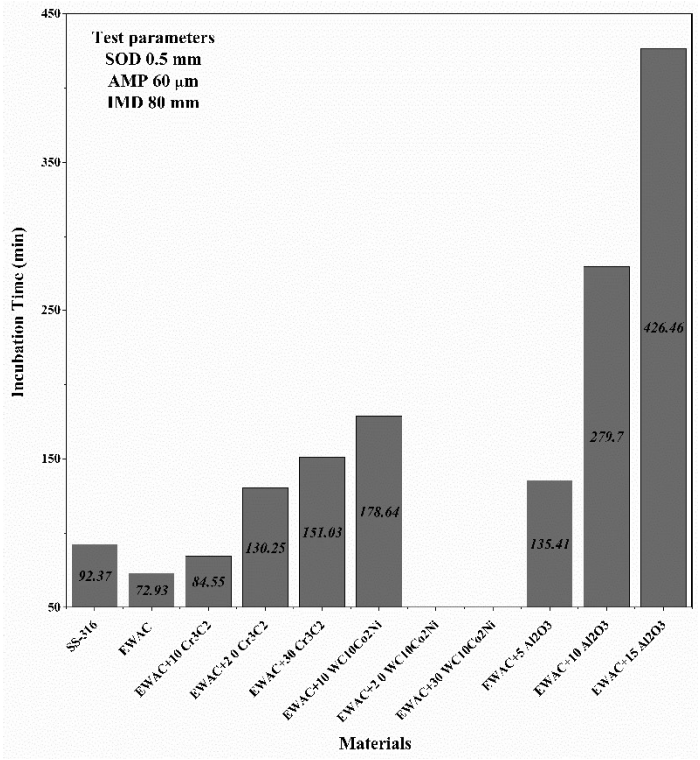

Figure 6.26: Comparison of incubation time of substrate and developed clad samples at optimized parameters

It has been observed that substrate experiences maximum weight loss. The result shows that the maximum weight loss of 52.82 mg has been observed in the substrate, which is within the range of the statistical predicted value of weight loss for the substrate at optimized parameters (Table 6.6). The weight loss of all developed composite clads is also in the statistically predicted range. However, the cumulative weight loss of pure EWAC clad after 540 min of testing is lessen than the substrate, but it has shortened incubation period than SS 316. This is because at initial stage the substrate resists cavitation erosion more efficiently than pure EWAC clad due to absence of any voids or pores. The reason behind the comparatively higher weight loss of pure EWAC clads than developed composite clads is attributed to the high stacking fault energy of the Ni element. This energy decreases the work hardenability during the cavitation phenomenon and results in a higher weight loss of pure EWAC clads. Further, addition of different reinforcements results in a significant reduction in weight loss due to increased hardness and fracture toughness. The reinforcement particles coupled directly with microwave irradiation might also advance the atomic diffusion rate from substrate. This tends to reduce the stacking fault energy [157] and helps to increase cavitation erosion resistance of MMC. The high hardness of MMC, owing to hard ceramic phases formed during microwave heating and results in overall high strength, resist the formation of pits and initiation of cracks

at earlier stages. At later stages, these hard ceramic phases hinder merging pits developed in the ductile matrix. The measured hardness of substrate was least in the present work, which fails to resist crack initiation and pits formation at earlier stages, and crack propagation and pits accumulation at later stages, which result in the highest weight loss. However, a very less percentage change in weight loss is observed when the concentration of reinforcement increases (up to 20% and 30% in case of Cr_3C_2 and WC10Co2Ni and up to 10% to 15% in case of Al_2O_3), despite of increased hardness in all the MMC's. This might be due to increased porosity, except the Cr_3C_2 reinforced clads, with an increase in weight percentage of reinforcement. The stress concentration around the pore sites reduces the strength, and pores become preferential sites for cavitation erosion wear. The cavitation erosion wear can be combat with a combination of hardness and toughness, and an increase in hardness adversely affect the toughness; therefore, the clads with the highest concentration (30% and 15%) experience marginal weight loss than the lower concentration (20% and 10%), despite of much higher hardness.

CHAPTER 7
CONCLUSIONS & OPPORTUNITIES FOR FUTURE WORK

The development of wear resistant clad surfaces by using microwave radiation as a heating source on metallic substrate is a challenging task. It is owing to the reflection of microwaves by metals at room temperature. An extensive literature review indicates that claddings of metal matrix composites on metallic substrate by using microwave radiations provide a plausible solution by improving mechanical and tribological properties of tailored surfaces. However, the metal matrix composite (MMC) clads developed by using microwave radiations are not much explored for application in cavitation erosion environment. Hence, by using material of Ni-based matrix while Cr_3C_2, WC10Co2Ni and Al_2O_3 are reinforced materials for development of MMC clads have been developed on austenitic stainless steel (SS-316) substrate. The clads are developed by using 2.45 GHz frequency and 900 W power in a domestic microwave oven at optimized processing parameters. The developed clads have been characterized for metallurgical, mechanical and tribological aspects. The ANOVA analysis was carried out to investigate the combined effect of variation in cavitation erosion process parameters (stand-off distance, amplitude and immersion depth); that are involved in indirect vibratory cavitation erosion method. The major conclusions drawn from the current study, followed by opportunities for the future work in this area are indicated in the following sections.

7.1 Conclusions

7.1.1 Development of metal-ceramic based composite clads at optimized parameters using microwave heating

The results showed that the use of microwave radiation of frequency 2.45 GHz at optimized parameters helps to efficiently develop the metal matrix composites clad. The major conclusions drawn from the current experimentation are as follow;

1. The processing time required to develop the composite clads is directly influenced by the microwave power level. An increase in power level significantly decreases the required processing time. The minimum exposure microwave power 900 W (maximum capacity of used domestic microwave oven) is required to melt the powder material system and partial amount of substrate material to cause the dilution for development of metallurgical bonded clads.

2. The processing time required for the metallurgical bonded clads vary from 390 s to 590 s, for metallurgical characterization specimens of MMC clads. The least processing time of 390 s for EWAC-30Cr_3C_2 and highest processing time of 590 s for EWAC-15Al_2O_3 was required. Similarly, for the same compositions, the processing time required for tribological characterization specimens was 700 s and 790 s; and for flexural studies specimens was 1200 s and 1445 s.

7.1.2 Metallurgical and mechanical characterization of the microwave processed clads

The developed microwave processed Ni-based MMC clads of Cr_3C_2, WC10Co2Ni and Al_2O_3 reinforced (in different weight percentage) were characterized by various metallurgical and mechanical characterization techniques. The major conclusions drawn from the results of different studies are as follows:

1. The microstructural investigation revealed that the EWAC-10Cr_3C_2, EWAC-20Cr_3C_2, and EWAC-30Cr_3C_2 composite clads of approximately 720 µm, 750 µm and 600 µm thickness, respectively, were developed on SS-316 substrate through microwave hybrid heating technique in 430±10 s, 420±10 s and 390±10 s.
2. The microstructural investigation revealed that a good metallurgical bonded composite clads of thickness 520 µm, 680 µm and 820 µm for EWAC-10WC10Co2Ni, EWAC-20 WC10Co2Ni, and EWAC-30WC10Co2Ni, respectively, were developed in 450±10 s, 430±10 s and 410±10 s.
3. The microstructural investigation revealed that the clads of almost uniform thickness ~540 µm, 970 µm and 1090 µm for EWAC-5Al_2O_3, EWAC-10Al_2O_3 and EWAC-15Al_2O_3 were successfully deposited in 530±10 s, 560±10 s and 590±10 s.
4. The volumetric or uniform heating nature of the microwaves helps to achieve composite clads, that are almost free from all types of cracks (interfacial and solidification cracks), which is clear from smooth interface.
5. The XRD analysis of the various microwave processed Ni-based and Cr_3C_2 reinforced composite clads reveals the formation of Cr_2Ni_3, $Cr_{23}C_6$, Cr_7C_3, CrSi, $CrSi_2$, SiO_2, NiC, SiC, Cr_3Ni_2SiC and $FeNi_3$ which is due to the intense microwaves heating. Further, NIR analysis results reveals that the $FeNi_3$ has highest contribution in EWAC-10Cr_3C_2 (53.63%) and EWAC-20Cr_3C_2 (38.74%) whereas, Cr_2Ni_3 (50.74%) is the main content that is present in the EWAC-30Cr_3C_2.
6. The XRD analysis of the Ni-based and WC10Co2Ni reinforced composite clads revealed the presence of different phases such as $NiCo_2O_4$, Ni_2W_4C, Ni_2Si, $NiAl_2O_4$, W_2C, Ni_3Si,

Cr_3C_2, and FeNi. The phase Ni_2W_4C (high intensity peaks) is observed as major phase. The NIR analysis results show that the phase Ni_2W_4C has contribution of 58.27%, 43.80% and 38.65 % in EWAC-10WC10Co2Ni, EWAC-20WC10Co2Ni and EWAC-30WC10Co2Ni, respectively.

7. The analyzed XRD results of Ni-based and Al_2O_3 reinforced composite clads confirm the following phases: Intermetallics (Ni_3Si, $FeNi_3$, and Fe_7Ni_3), Carbides (Fe_5C_2) and Oxides (Al_2O_3 and SiO_2). The Al_2O_3 is dispersed in its original form in the matrix and detected as major phase. The NIR results confirm Al_2O_3 has contribution of 45.40%, 43.53% and 39.19% in EWAC-5Al_2O_3, EWAC-10Al_2O_3 and EWAC-15Al_2O_3, respectively.
8. The mean value of porosity for Ni based composite clads (MMC) was observed in range of 0.9%-1.39%. These values are significantly less than other cladding/coating processes. The presence of lower porosity levels was due to the uniform heating nature of microwave irradiations.
9. The results of Vickers micro-hardness of microwave processed MMCs exhibit that EWAC-30WC10Co2Ni exhibits highest average microhardness (925±57 HV), among all developed MMCs, which is almost 4.91 times higher than SS-316. The higher micro-hardness values were exhibited due to the formation of various intermetallic and hard carbides during microwave heating.
10. The presence of high strength carbides and intermetallics in the microwave processed MMCs also resulted in higher flexural strength of these MMCs. The highest average value of flexural strength of EWAC-15Al_2O_3 is observed as 854±16 MPa. Flexural strength study of developed specimens using fractographic analysis revealed that even after the substrate cracked, the top layer of clad still remained attached to it.

7.1.3 Functional characterization of the microwave processed clads

To check the tribological performance (cavitation erosion resistance) of the substrate and developed microwave processed composite clads, the parametric study using Taguchi L9 orthogonal array was carried out. The key findings are discussed and it is as follows:

1. The weight loss of stainless steel substrate and all developed clad surface was profoundly affected by varying all the three parameters AMP, IMD, and SOD. The increase in SOD and IMD leads to a decrease in weight loss, while an increase in the weight loss by increasing AMP was observed.
2. The ANOVA analysis at 95% confidence level of all the three parameters of cavitation erosion testing reveals that the SOD is the most influential parameter with contribution in

the range of 68.50% - 48.88% while amplitude only contributes in the range of 40.41% - 26.56% in weight loss of substrate and developed clad surfaces. The immersion depth with the range of 10.44%- 4.67% contribution is the least influential parameter in this domain of the study.

3. The reason for the lower weight loss at higher SOD is that, as SOD increases, the shockwave velocity decreases, resulting in a smaller pressure pulse, lower acoustic pressure, and lower impact energy of the impingement jets. As a result, both the material damage and the weight loss reduced at higher SOD.
4. The larger weight loss was observed at the higher amplitude because higher amplitude generates larger negative cycles, causing the cavitation bubble to grow larger and collapse at higher pressure, causing severe damage to the material; hence, higher weight loss.
5. The lower weight loss was recorded at the higher horn immersion depth because at this state the static fluid pressure increases. Higher static fluid pressure leads, higher acoustic amplitude to induce sufficient negative pressure, which facilitates the vapor bubble growth and vice versa.
6. The parameter optimization was carried out using a delta statistics response table, with the optimization goal as higher is better. The 0.5 mm SOD, 60 µm amplitude, and 80 mm horn immersion depth are observed as optimal parameters.
7. The regression equations for weight loss in SS-316 and all developed MMCs were developed. Following that, a prediction analysis was also performed at a 95% confidence level. The predicted results of weight loss, at the optimized parameters, were further utilized to compare with the confirmatory experiments. The results of confirmatory experiments show that the developed mathematical models are justified because the results of weight loss fall within the predicted intervals.
8. All the developed clad surfaces performed very well against cavitation action as significantly less average cumulative weight loss was observed. The least cumulative weight loss (3.2 mg) was observed in EWAC-30WC10Co2Ni composite clad and it performed ~12.78 times better than the substrate at the same parametric conditions.
9. The fractographic analysis of the worn surfaces of SS-316 and developed composite clads specimens tested at parametric sets 3, 5, and 7. The SEM images revealed that the specimens tested at parametric set-3 had more severe damage than the other two sets.

7.1.4 Comparative study of the various materials and developed clads

The comparison between the substrate and all developed MMCs on the basis of incubation time and cavitation erosion resistance (at optimized test parameters SOD = 0.5 mm, AMP = 60 μm and IMD = 80 mm) was carried out. The major conclusions of the study are listed below:

1. The developed EWAC-30 WC10Co2Ni composite clad exhibits highest incubation period (> 9 hours) at optimized parameters also.
2. The EWAC-30WC10Co2Ni composite clad exhibits least cumulative weight loss (3.7 mg). The developed clad shows 14.27 times better CER than substrate. The reason attributed to the higher CER is the higher microhardness, good metallurgical bonding between clad and substrate, and almost cracks free & less porous surfaces of the microwave processed clads.

7.2 Opportunities for Future Work

Clads developed by using microwave radiations of frequency 2.45 GHz is recently explored and researchers have done the studies on the development and characterization of microwave processed clads of various substrate and powdered materials. However, still much scope is available in this growing technique to test the viability of the developed clads for different tribological environment. The various material systems which is well accepted by industries are not yet tested/processed through this technique. The following are some suggestive ideas drawn from the current work; and, can be studied in near future:

1. The Clads can be developed by using a single mode applicator, and the results can be further compared to those obtained by using clads developed by multimode applicator.
2. A possibility to use high power industrial microwave furnaces of high frequency can be used to develop clads for the complicated geometries and effect on the processing time can be observed.
3. Mathematical model can be developed to establish a relationship between microwave processing parameters such as processing time, microwave power level, preheating temperature, quantity of susceptor and size of substrate for the given material.
4. The vibratory cavitation erosion studies can be conducted on microwave processed functionally graded materials.
5. The cavitation erosion testing of microwave processed clads in the different corrosive environments can be conducted.

REFERENCES

[1] Iea.org., "Global energy & CO_2 status report: CO_2 emissions." (2019). [online] Available at: https://www.iea.org/geco/emissions/ [Accessed 1 Dec. 2021].

[2] M. Bilgili, A. Ozbek, B. Sahin, and A. Kahraman, "An overview of renewable electric power capacity and progress in new technologies in the world," *Renew. sustain. energy rev.*, vol. 49, pp. 323–334, Sep. 2015, doi: 10.1016/j.rser.2015.04.148.

[3] "Moving on up – India now world's 5th largest hydropower producer," International water power and dam construction, 2020. [online] Available at: https://www.waterpowermagazine.com/features/featuremoving-on-up-india-now-worlds-5th-largest-hydropower-producer-7949240/ [Accessed 1 Dec. 2021].

[4] "Executive summary power sector november 2021 Report, Central electricity authority, ministry of power, Govt. of India," 2021.

[5] "Physical progress (achievements), Ministry of new and renewable energy, Govt. of India," 2021.

[6] S. Li, "Tiny bubbles challenge giant turbines: Three Gorges puzzle," *Interface focus*, vol. 5, no. 5, p. 20150020, Oct. 2015, doi: 10.1098/rsfs.2015.0020.

[7] Repairengineering.com. (2019). Cavitation. [online] Available at: http://www.repairengineering.com/cavitation.html [Accessed 1 Dec. 2021].

[8] M. K. Padhy and R. P. Saini, "A review on silt erosion in hydro turbines," *Renew.Sustain. energyrev.*, vol.12, no.7, pp.1974-1987, Sep.2008, doi: 10.1016/j.rser.2007.01.025.

[9] D. Momčilović, Z. Odanović, R. Mitrović, I. Atanasovska, and T. Vuherer, "Failure analysis of hydraulic turbine shaft," *Eng. Fail. Anal.*, vol. 20, pp. 54–66, Mar. 2012, doi: 10.1016/j.engfailanal.2011.10.006.

[10] S. C. Li, S. H. Liu, and Y. L. Wu, "A new type of cavitation damage triggered by boundary-layer turbulent production," *Mod. Phys. Lett. B*, vol. 21, no. 20, pp. 1285–1296, Aug. 2007, doi: 10.1142/S0217984907013456.

[11] B. K. Sreedhar, S. K. Albert, and A. B. Pandit, "Cavitation damage: Theory and measurements – A review," *Wear*, vol. 372–373, no. February, pp. 177–196, Feb. 2017, doi: 10.1016/j.wear.2016.12.009.

[12] P. Kumar and R. P. Saini, "Study of cavitation in hydro turbines—A review," *Renew. sustain.energy rev.*,vol.14,no.1,pp. 374–383, Jan. 2010, doi: 10.1016/j.rser.2009.07.024.

[13] X. Escaler, E. Egusquiza, M. Farhat, F. Avellan, and M. Coussirat, "Detection of cavitation in hydraulic turbines," *Mech. Syst. Signal Process.*, vol. 20, no. 4, pp. 983–1007, May 2006, doi: 10.1016/j.ymssp.2004.08.006.

[14] A. K. Krella, D. E. Zakrzewska, and A. Marchewicz, "The resistance of S235JR steel to cavitation erosion," *Wear*, vol.452–453, p.203295, Jul.2020, doi: 10.1016/j.wear.2020.203295

[15] M. Neopane, H.P., Dahlhaug, O., Cervantes, "Sediment erosion in hydraulic turbines," *Glob. j. res. eng. mech. mech. eng.*, vol. 11, no. 6, p. Version 1.

[16] X. Ding, X.-D. Cheng, C.-Q. Yuan, J. Shi, and Z.-X. Ding, "Structure of micro-nano WC-10Co4Cr coating and cavitation erosion resistance in NaCl solution," *Chinese j.*

mech. eng., vol. 30, no. 5, pp. 1239–1247, Sep. 2017, doi: 10.1007/s10033-017-0162-9.

[17] F. T. Cheng, C. T. Kwok, and H. C. Man, "Laser surfacing of S31603 stainless steel with engineering ceramics for cavitation erosion resistance," *Surf. coatings technol.*, vol. 139, no. 1, pp. 14–24, May 2001, doi: 10.1016/S0257-8972(00)01103-8.

[18] Y. Bao *et al.*, "Effects of WC on the cavitation erosion resistance of FeCoCrNiB0.2 high entropy alloy coating prepared by laser cladding," *Mater. today commun.*, vol. 26, p. 102154, Mar. 2021, doi: 10.1016/j.mtcomm.2021.102154.

[19] S. Zafar and A. K. Sharma, "Abrasive and erosive wear behaviour of nanometric WC–12Co microwave clads," *Wear*, vol. 346–347, pp. 29–45, Jan. 2016, doi: 10.1016/j.wear.2015.11.003.

[20] A. Babu, H. S. Arora, H. Singh, and H. S. Grewal, "Microwave synthesized composite claddings with enhanced cavitation erosion resistance," *Wear*, vol. 422–423, pp. 242–251, Mar. 2019, doi: 10.1016/j.wear.2019.01.072.

[21] U. Dorji and R. Ghomashchi, "Hydro turbine failure mechanisms: An overview," *Eng. fail. anal.*, vol. 44, pp. 136–147, Sep. 2014, doi: 10.1016/j.engfailanal.2014.04.013.

[22] D. Yin, G. Liang, S. Fan, and S. Li, "Ultrasonic cavitation erosion behavior of AlCoCrxCuFe high entropy alloy coatings synthesized by laser cladding," *Materials (Basel).*, vol. 13, no. 18, 2020, doi: 10.3390/ma13184067.

[23] A. Kjolle, *Hydropower in Norway – mechanical equipment. Norway: Norwegian University of Science and Technology*. 2001.

[24] R. C. Reed, Z. Shen, J. M. Robinson, and T. Akbay, "Laser transformation hardening of steel: effects of beam mode, beam size, and composition," *Mater. sci. technol.*, vol. 15, no. 1, pp. 109–118, Jan. 1999, doi: 10.1179/026708399773003385.

[25] R. C. Reed, Z. Shen, T. Akbay, and J. M. Robinson, "Laser-pulse heat treatment: Application to reaustenitisation from ferrite/cementite mixtures," *Mater. sci. eng. A*, vol. 232, no. 1–2, pp. 140–149, Jul. 1997, doi: 10.1016/S0921-5093(97)00113-5.

[26] A. Holmberg, K., Mathews, *Coatings tribology*, 2nd ed. Elsevier B.V., 1994.

[27] D. Gupta and A. K. Sharma, "Microwave cladding: A new approach in surface engineering," *J. manuf. process.*, vol. 16, no. 2, pp. 176–182, Apr. 2014, doi: 10.1016/j.jmapro.2014.01.001.

[28] G. Bolelli *et al.*, "Tribology of HVOF- and HVAF-sprayed WC–10Co4Cr hardmetal coatings: A comparative assessment," *Surf. coatings technol.*, vol. 265, pp. 125–144, Mar. 2015, doi: 10.1016/j.surfcoat.2015.01.048.

[29] C. Duraipandi, A. Khan M, J. J. T. Winowlin, N. M. Ghazaly, and P. M. Mashinini, "Solid particle erosion studies of thermally deposited alumina-titania coatings on an aluminum alloy," *Int. j. miner. metall. mater.*, vol. 28, no. 7, pp. 1186–1193, Jul. 2021, doi: 10.1007/s12613-020-2099-8.

[30] S. Watanabe, T. Tajiri, N. Sakoda, and J. Amano, "Fatigue cracks in hvof thermally sprayed wc-co coatings," *J. therm. spray technol.*, vol. 7, no. 1, pp. 93–96, Mar. 1998, doi: 10.1361/105996398770351098.

[31] Kekes, D., Psyllaki, P., Vardavoulias, M., "Wear micro-mechanisms of composite WC-Co/Cr-NiCrFeBSiC coatings. Part I: Dry sliding," *Tribol. ind.*, vol. 36, pp. 361–374, 2014.

[32] K. Ushashri and M. Masanta, “Hard TiC coating on AISI304 steel by laser surface engineering using pulsed Nd:YAG Laser,” *Mater. manuf. process.*, vol. 30, no. 6, pp. 730–735, Jun. 2015, doi: 10.1080/10426914.2014.973593.

[33] N. Jeyaprakash, C.-H. Yang, and D. Raj Kumar, “Laser surface modification of materials,” in *practical applications of laser ablation*, IntechOpen, 2021.

[34] T. Tlale, P. Mashinini, and D. Mukhawana, “Investigation of mechanical properties of friction and laser welded Ti-6Al-4V rods,” in *2021 IEEE 12th International conference on mechanical and intelligent manufacturing technologies (ICMIMT)*, May 2021, pp. 158–164, doi: 10.1109/ICMIMT52186.2021.9476153.

[35] J. David Raja Selvam, I. Dinaharan, and P. M. Mashinini, “Microstructure and mechanical characterization of Nd:YAG laser beam welded AA6061/10 wt% ZrB_2 aluminum matrix composites,” *Opt. laser technol.*, vol. 140, p. 107084, Aug. 2021, doi: 10.1016/j.optlastec.2021.107084.

[36] Q. Ming, L. C. Lim, and Z. D. Chen, “Laser cladding of nickel-based hardfacing alloys,” *Surf. coatings technol.*, vol. 106, no. 2–3, pp. 174–182, Aug. 1998, doi: 10.1016/S0257-8972(98)00524-6.

[37] K. Feng *et al.*, “Improved high-temperature hardness and wear resistance of Inconel 625 coatings fabricated by laser cladding,” *J. mater. process. technol.*, vol. 243, pp. 82–91, May 2017, doi: 10.1016/j.jmatprotec.2016.12.001.

[38] D. H. Doan, T. Q. Bui, I. Satoh, and K. Fushinobu, “Phase-field model for laser induced thermal crack propagation,” 2015.

[39] J. C. Ion, *Laser processing of engineering materials*. Biddles Ltd., Norfolk, 2005.

[40] W. Fang, J. Zhang, T. Yu, and T. Q. Bui, “Analysis of thermal effect on buckling of imperfect FG composite plates by adaptive XIGA,” *Compos. struct.*, vol. 275, p. 114450, Nov. 2021, doi: 10.1016/j.compstruct.2021.114450.

[41] J. Davis and R. Joseph, *Surface engineering for corrosion and wear resistance. ASM International*. 2001.

[42] T. Burakowki and T. Wierzchon, *Surface engineering of metals*, 1st ed. CRC Press LLC, 1999.

[43] D. Gupta, P. M. Bhovi, A. K. Sharma, and S. Dutta, “Development and characterization of microwave composite cladding,” *J. manuf. process.*, vol. 14, no. 3, pp. 243–249, Aug. 2012, doi: 10.1016/j.jmapro.2012.05.007.

[44] S. Zafar and A. K. Sharma, “Prediction of tribological behaviour of wc-12co nanostructured microwave clad through ANN,” *Tribol. online*, vol. 11, no. 2, pp. 333–340, 2016, doi: 10.2474/trol.11.333.

[45] A. M. Hebbale and M. S. Srinath, “Microstructural investigation of Ni based cladding developed on austenitic SS-304 through microwave irradiation,” *J. mater. res. technol.*, vol. 5, no. 4, pp. 293–301, Oct. 2016, doi: 10.1016/j.jmrt.2016.01.002.

[46] S. Kaushal, D. Singh, D. Gupta, and V. Jain, “Processing of Ni–WC–Cr_3C_2 -based metal matrix composite cladding on SS-316L substrate through microwave irradiation,” *J.compos.mater.*,vol.53,no.8,pp.1023–1032,Apr.2019, doi:10.1177/0021998318794846.

[47] T. P. Naik, R. S. Rana, I. Singh, and A. K. Sharma, “Microwave processing of polymer matrix composites: review of the understanding and future opportunities,” 2021, pp. 517–529.

[48] A. Atul Mali, A. K. Sharma, and I. Singh, “Microwave curing of natural fiber and synthetic fiber reinforced polymer matrix composites,” *i-manager’s J. mater. sci.*, vol. 1, no. 1, pp. 8–14, Jun. 2013, doi: 10.26634/jms.1.1.2279.

[49] M. Oghbaei and O. Mirzaee, “Microwave versus conventional sintering: A review of fundamentals, advantages and applications,” *J. alloys compd.*, vol. 494, no. 1–2, pp. 175–189, Apr. 2010, doi: 10.1016/j.jallcom.2010.01.068.

[50] D. Keyson *et al.*, “Domestic microwave oven adapted for fast heat treatment of Ba0.5Sr0.5(Ti0.8Sn0.2) O3 powders,” *J. mater. process. technol.*, vol. 189, no. 1–3, pp. 316–319, Jul. 2007, doi: 10.1016/j.jmatprotec.2007.02.001.

[51] E. T. Thostenson and T.-W. Chou, “Microwave processing: fundamentals and applications,” *Compos. part A appl. sci. manuf.*, vol. 30, no. 9, pp. 1055–1071, Sep. 1999, doi: 10.1016/S1359-835X (99)00020-2.

[52] P. L. Spencer, “Method of treating foodstuffs,” 620,919, 1945.

[53] P. K. Bajpai, I. Singh, and J. Madaan, “Joining of natural fiber reinforced composites using microwave energy: Experimental and finite element study,” *Mater. des.*, vol. 35, pp. 596–602, Mar. 2012, doi: 10.1016/j.matdes.2011.10.007.

[54] J. A. Menéndez *et al.*, “Microwave heating processes involving carbon materials,” *Fuel process. technol.*, vol. 91, no. 1, pp. 1–8, Jan. 2010, doi: 10.1016/j.fuproc.2009.08.021.

[55] D. Agrawal, “Latest global developments in microwave materials processing,” *Mater. res.innov.*,vol.14, no. 1, pp. 3–8, Feb. 2010, doi: 10.1179/143307510X1599329342926.

[56] S. Singh, D. Gupta, and V. Jain, “Recent applications of microwaves in materials joining and surface coatings,” *Proc. inst. mech. eng. part B j. eng. manuf.*, vol. 230, no. 4, pp. 603–617, Apr. 2016, doi: 10.1177/0954405414560778.

[57] A. Borrell and M. D. Salvador, “Advanced ceramic materials sintered by microwave technology,” in *Sintering technology - method and application*, InTech, 2018.

[58] D. E. Clark and W. H. Sutton, “Microwave processing of materials,” *Annu. rev. mater. sci.*, vol.26, no. 1, pp. 299–331, Aug. 1996, doi: 10.1146/annurev.ms.26.080196.001503.

[59] R. R. Mishra and A. K. Sharma, “Microwave–material interaction phenomena: Heating mechanisms, challenges and opportunities in material processing,” *Compos. part A appl.sci. manuf.*, vol. 81, pp. 78–97, Feb. 2016, doi: 10.1016/j.compositesa.2015.10.035.

[60] A. J. Moulson and J. M. Herbert, *Electroceramics : materials, properties, applications*, 2nd ed. Wiley, 2003.

[61] A. C. Metaxas and R. J. Meredith, *Industrial microwave heating*. London, UK : P. Peregrinus on behalf of the Institution of Electrical Engineers, 1993.

[62] D. M. Pozar, *Microwave engineering*, 2nd ed. Toronto: John Wiley and Sons, 2001.

[63] M. Sparks, *Ferromagnetic-relaxation theory*. McGraw-Hill, New York, 1964.

[64] S. Singh, D. Gupta, V. Jain, and A. K. Sharma, “Microwave processing of materials and applications in manufacturing industries: a review,” *Mater. manuf. process.*, vol. 30, no. 1, pp. 1–29, Jan. 2015, doi: 10.1080/10426914.2014.952028.

[65] M. Thumm, *Applications of high-power*. Generation and application of high power microwaves, 2020.

[66] R. Roy, D. Agrawal, J. Cheng, and S. Gedevanishvili, “Erratum: Full sintering of powdered-metal bodies in a microwave field,” *Nature*, vol. 401, no. 6750, pp. 304–304, Sep. 1999, doi: 10.1038/45853.

[67] G. Sethi, A. Upadhyaya, and D. Agrawal, “Microwave and conventional sintering of premixed and prealloyed Cu-12Sn bronze,” *Sci. sinter.*, vol. 35, no. 2, pp. 49–65, 2003, doi: 10.2298/SOS0302049S.

[68] W. L. E Wong and M. Gupta, “Simultaneously improving strength and ductility of magnesium using nano-size SiC particulates and microwaves,” *Adv. eng. mater.*, vol. 8, no. 8, pp. 735–740, Aug. 2006, doi: 10.1002/adem.200500209.

[69] K. Ishizaki, K. Nagata, and T. Hayashi, “Production of pig iron from magnetite ore–coal composite pellets by microwave heating,” *ISIJ int.*, vol. 46, no. 10, pp. 1403–1409, 2006, doi: 10.2355/isijinternational.46.1403.

[70] M. S. Srinath, A. K. Sharma, and P. Kumar, “A new approach to joining of bulk copper using microwave energy,” *Mater. des.*, vol. 32, no. 5, pp. 2685–2694, May 2011, doi: 10.1016/j.matdes.2011.01.023.

[71] D. Gupta and A. K. Sharma, “A method of cladding/coating metallic powder on metallic substrate by microwave irradiation,” Indian Patent No. 306568, 2010.

[72] S. Kaushal, D. Gupta, and H. Bhowmick, “Corrigendum: On processing of Ni-Cr_3C_2 based functionally graded clads through microwave heating (2018 Mater. res. express 5 066405),” *Mater. res. express*, vol. 6, no. 10, p. 109501, Aug. 2019, doi: 10.1088/2053-1591/ab3747.

[73] S. Kaushal, D. Gupta, and H. Bhowmick, “On processing and flexural behaviour of functionally graded clads developed through microwave irradiation,” *Mater. res. express*, vol. 6, no. 7, p. 076405, Apr. 2019, doi: 10.1088/2053-1591/ab11ea.

[74] S. Kaushal, D. Gupta, and H. Bhowmick, “On processing of Ni-Cr_3C_2 based functionally graded clads through microwave heating,” *Mater. res. express*, vol. 5, no. 6, p. 066405, Jun. 2018, doi: 10.1088/2053-1591/aac805.

[75] A. K. Sharma and R. Krishnamurthy, “Microwave processing of sprayed alumina composite for enhanced performance,” *J. eur. ceram. soc.*, vol. 22, no. 16, pp. 2849–2860, 2002, doi: 10.1016/S0955-2219(02)00051-1.

[76] M. S. Spotz, D. J. Skamser, and D. L. Johnson, “Thermal stability of ceramic materials in microwave heating,” *J. am. ceram. soc.*, vol. 78, no. 4, pp. 1041–1048, Apr. 1995, doi: 10.1111/j.1151-2916. 1995.tb08434. x.

[77] J. Lasri, P. D. Ramesh, and L. Schächter, “Energy conversion during microwave sintering of a multiphase ceramic surrounded by a susceptor,” *J. am. ceram. soc.*, vol. 83, no. 6, pp. 1465–1468, Jun. 2000, doi: 10.1111/j.1151-2916. 2000.tb01411. x.

[78] “India replaces Japan as second top steel producer: worldsteel,” 2019. https://economictimes.indiatimes.com/industry/indl-goods/svs/steel/india-replaces-japan-as-second-top-steel-producer-worldsteel/articleshow/67721395.cms?utm_source=contentofinterest&utm_medium=text&utm_campaign=cppst.

[79] M. Liljas and A. Sheffield, “Development of superaustenitic stainless steels,” *Avesta sheff. corros. manag. appl. eng.*, vol. ACOM No. 2, no. 95, pp. 1–7, 1995.

[80] ASTM International, “A276-04 - Standard specification for stainless steel bars and shapes,” *ASTM int.*, pp. 1–7, 2010.

[81] R. Singh, S. K. Tiwari, and S. K. Mishra, “Cavitation erosion in hydraulic turbine components and mitigation by coatings: current status and future needs,” *J. mater. eng. perform.*, vol. 21, no. 7, pp. 1539–1551, Jul. 2012, doi: 10.1007/s11665-011-0051-9.

[82] T. Bell, “Surface engineering of austenitic stainless steel,” *Surf. eng.*, vol. 18, no. 6, pp. 415–422, Dec. 2002, doi: 10.1179/026708402225006268.

[83] J. Lin, S. Hong, Y. Zheng, W. Sun, M. Kang, and X. Fu, “Cavitation erosion resistance in NaCl medium of HVOF sprayed WC-based cermet coatings at various flow velocities: A comparative study on the effect of Ni and CoCr binder phases,” *Int. J. refract. met. hard mater.*, vol. 94, no. August 2020, p. 105407, Jan. 2021, doi: 10.1016/j.ijrmhm.2020.105407.

[84] S. Hong *et al.*, “Microstructure and cavitation erosion behavior of HVOF sprayed ceramic-metal composite coatings for application in hydro-turbines,” *Renew. energy*, vol. 164, pp. 1089–1099, Feb. 2021, doi: 10.1016/j.renene.2020.08.099.

[85] S. Hong *et al.*, “Cavitation erosion characteristics at various flow velocities in NaCl medium of carbide-based cermet coatings prepared by HVOF spraying,” *Ceram. int.*, vol. 47, no. 2, pp. 1929–1939, Jan. 2021, doi: 10.1016/j.ceramint.2020.09.022.

[86] X. Ding, D. Ke, C. Yuan, Z. Ding, and X. Cheng, “Microstructure and cavitation erosion resistance of HVOF deposited WC-Co coatings with different sized WC,” *Coatings*, vol. 8, no. 9, p. 307, Aug. 2018, doi: 10.3390/coatings8090307.

[87] J. Basumatary and R. J. K. Wood, “Synergistic effects of cavitation erosion and corrosion for nickel aluminium bronze with oxide film in 3.5% NaCl solution,” *Wear*, vol. 376–377, pp. 1286–1297, Apr. 2017, doi: 10.1016/j.wear.2017.01.047.

[88] L. Qiao, Y. Wu, S. Hong, J. Zhang, W. Shi, and Y. Zheng, “Relationships between spray parameters, microstructures and ultrasonic cavitation erosion behavior of HVOF sprayed Fe-based amorphous/nanocrystalline coatings,” *Ultrason. sonochem.*, vol. 39, no. April, pp. 39–46, Nov. 2017, doi: 10.1016/j.ultsonch.2017.04.011.

[89] S. Lavigne, F. Pougoum, S. Savoie, L. Martinu, J. E. Klemberg-Sapieha, and R. Schulz, “Cavitation erosion behavior of HVOF caviTec coatings,” *Wear*, vol. 386–387, no. June, pp. 90–98, Sep. 2017, doi: 10.1016/j.wear.2017.06.003.

[90] P. Xu, C. Zhang, W. Wang, and L. Liu, “Pitting mechanism in a stainless steel-reinforced Fe-based amorphous coating,” *Electrochim. acta*, vol. 206, pp. 61–69, Jul. 2016, doi: 10.1016/j.electacta.2016.04.130.

[91] R. K. Kumar, M. Kamaraj, S. Seetharamu, T. Pramod, and P. Sampathkumaran, “Effect of spray particle velocity on cavitation erosion resistance characteristics of HVOF and HVAF processed 86WC-10Co4Cr hydro turbine coatings,” *J. therm. spray technol.*, vol. 25, no. 6, pp. 1217–1230, Aug. 2016, doi: 10.1007/s11666-016-0427-3.

[92] S. Hong, Y. Wu, J. Zhang, Y. Zheng, Y. Zheng, and J. Lin, “Synergistic effect of ultrasonic cavitation erosion and corrosion of WC–CoCr and FeCrSiBMn coatings prepared by HVOF spraying,” *Ultrason. sonochem.*, vol. 31, pp. 563–569, Jul. 2016, doi: 10.1016/j.ultsonch.2016.02.011.

[93] S. Hong, Y. Wu, J. Zhang, Y. Zheng, Y. Qin, and J. Lin, “Ultrasonic cavitation erosion of high-velocity oxygen-fuel (HVOF) sprayed near-nanostructured WC–10Co–4Cr coating in NaCl solution,” *Ultrason. sonochem.*, vol. 26, pp. 87–92, Sep. 2015, doi: 10.1016/j.ultsonch.2015.01.012.

[94] Q. Zhang *et al.*, “Correlation between microstructural characteristics and cavitation resistance of Stellite-6 coatings on 17-4 PH stainless steel prepared with supersonic laser deposition and laser cladding,” *J. alloys compd.*, vol. 860, p. 158417, Apr. 2021, doi: 10.1016/j.jallcom.2020.158417.

[95] M. E, H. X. Hu, X. M. Guo, and Y. G. Zheng, “Comparison of the cavitation erosion and slurry erosion behavior of cobalt-based and nickel-based coatings,” *Wear*, vol. 428–429, pp. 246–257, Jun. 2019, doi: 10.1016/j.wear.2019.03.022.

[96] C. Hardes, F. Pöhl, A. Röttger, M. Thiele, W. Theisen, and C. Esen, “Cavitation erosion resistance of 316L austenitic steel processed by selective laser melting (SLM),” *Addit. manuf.*, vol. 29, p. 100786, Oct. 2019, doi: 10.1016/j.addma.2019.100786.

[97] L. Girelli, M. Tocci, L. Montesano, M. Gelfi, and A. Pola, “Investigation of cavitation erosion resistance of AlSi10Mg alloy for additive manufacturing,” *Wear*, vol. 402–403, pp. 124–136, May 2018, doi: 10.1016/j.wear.2018.02.018.

[98] C. L. Wu, S. Zhang, C. H. Zhang, H. Zhang, and S. Y. Dong, “Phase evolution and cavitation erosion-corrosion behavior of FeCoCrAlNiTi x high entropy alloy coatings on 304 stainless steel by laser surface alloying,” *J. alloys compd.*, vol. 698, pp. 761–770, Mar. 2017, doi: 10.1016/j.jallcom.2016.12.196.

[99] C.-H. Zhang *et al.*, “Laser cladding of NiCrSiB on Monel 400 to enhance cavitation erosion and corrosion resistance,” *Rare met.*, Dec. 2016, doi: 10.1007/s12598-016-0814-4.

[100] R. Singh, D. Kumar, S. K. Mishra, and S. K. Tiwari, “Laser cladding of Stellite 6 on stainless steel to enhance solid particle erosion and cavitation resistance,” *Surf. coatings technol.*, vol. 251, pp. 87–97, Jul. 2014, doi: 10.1016/j.surfcoat.2014.04.008.

[101] C. P. Paul, B. K. Gandhi, P. Bhargava, D. K. Dwivedi, and L. M. Kukreja, “Cobalt-free laser cladding on AISI type 316L stainless steel for improved cavitation and slurry erosion wear behavior,” *J. mater. eng. perform.*, vol. 23, no. 12, pp. 4463–4471, Dec. 2014, doi: 10.1007/s11665-014-1244-9.

[102] G. Link, L. Feher, M. Thumm, H.-J. Ritzhaupt-Kleissl, R. Bohme, and A. Weisenburger, “Sintering of advanced ceramics using a 30-GHz, 10-kW, CW industrial gyrotron,” *IEEE trans. plasma sci.*, vol. 27, no. 2, pp. 547–554, Apr. 1999, doi: 10.1109/27.772284.

[103] A. K. Sharma, S. Aravindhan, and R. Krishnamurthy, “Microwave glazing of alumina–titania ceramic composite coatings,” *Mater. lett.*, vol. 50, no. 5–6, pp. 295–301, Sep. 2001, doi: 10.1016/S0167-577X(01)00243-9.

[104] J. W. Walkiewicz, G. Kazonich, and S. L. McGill, “Microwave heating characteristics of selected minerals and compounds,” *Mining, metall. explor.*, vol. 5, pp. 39–42, 1988, doi: https://doi.org/10.1007/BF03449501.

[105] K. S. V. L. Narasimhan, J. Arvidsson, H. G. Rutz, and W. J. Porter, “Methods and apparatus for heating metal powders,” US Patent No. US5397530 A, 1995.

[106] Y. Cheng, “Preparation and properties of diamond-CuTi composite sintered by microwave sintering,” *J. mater. sci. lett.*, vol. 18, pp. 1933–1935, 1999.

[107] C. Honnaiah, M. Amaresh, A. P. S L, and M. S. Srinath, “Tribological characterization of microwave processed Al-SIC metal matrix composites,” *Int. j. res. aeronaut. mech. eng.*, pp. 246–255, 2017.

[108] P. Ashwath,. J. Joel, M. Anthony Xavior, and H. G. Prashantha Kumar, “Effect of SiC and Al_2O_3 particles addition to AA 2900 and AA 2024 MMC’s synthesized through microwave sintering,” *Mater. today proc.*, vol. 5, no. 2, pp. 7329–7336, 2018, doi: 10.1016/j.matpr.2017.11.402.

[109] M. A. Himyan, M. Penchal Reddy, F. Ubaid, R. A. Shakoor, and A. M. A. Mohamed, "Scanning electron microscopic studies of microwave sintered Al-SiC nanocomposites and their properties," *Scanning*, vol. 2018, pp. 1–8, 2018, doi: 10.1155/2018/7546573.
[110] R. Rumman, L. C. Chuan, J. S. Quinton, and R. Ghomashchi, "Understanding the potential of microwave sintering on WC - Co," *Int. j. refract. met. hard mater.*, vol. 81, pp. 7–14, Jun. 2019, doi: 10.1016/j.ijrmhm.2019.02.007.
[111] C. Prakash *et al.*, "Processing of Ti50Nb50−xHAx composites by rapid microwave sintering technique for biomedical applications," *J. mater. res. technol.*, vol. 9, no. 1, pp. 242–252, Jan. 2020, doi: 10.1016/j.jmrt.2019.10.051.
[112] A. Kumar and P. M. Pandey, "Study of the influence of microwave sintering parameters on the mechanical behaviour of magnesium-based metal matrix composite," *Proc. inst. mech. eng. part C j. mech. eng. sci.*, vol. 235, no. 13, pp. 2416–2425, Jul. 2021, doi: 10.1177/0954406220951236.
[113] R. Kumar, H. Bhowmick, D. Gupta, and S. Bansal, "Development and characterization of multiwalled carbon nanotube-reinforced microwave sintered hybrid aluminum metal matrix composites: An experimental investigation on mechanical and tribological performances," *Proc. inst. mech. eng. part L j. mater. des. appl.*, vol. 235, no. 10, pp. 2310–2323, Oct. 2021, doi: 10.1177/14644207211028969.
[114] E. Siores and D. Do Rego, "Microwave applications in materials joining," *J. mater. process. technol.*, vol. 48, no. 1–4, pp. 619–625, Jan. 1995, doi: 10.1016/0924-0136(94)01701-2.
[115] M. S. Srinath, A. K. Sharma, and P. Kumar, "A novel route for joining of austenitic stainless steel (SS-316) using microwave energy," *Proc. inst. mech. eng. part B j. eng. manuf.*, vol. 225, no. 7, pp. 1083–1091, Jul. 2011, doi: 10.1177/2041297510393451.
[116] M. S. Srinath, A. K. Sharma, and P. Kumar, "Investigation on microstructural and mechanical properties of microwave processed dissimilar joints," *J. manuf. process.*, vol. 13, no. 2, pp. 141–146, Aug. 2011, doi: 10.1016/j.jmapro.2011.03.001.
[117] A. Bansal, A. K. Sharma, and S. Das, "Metallurgical and mechanical characterization of mild steel-mild steel joint formed by microwave hybrid heating process," *Sadhana*, vol. 38, no. 4, pp. 679–686, Aug. 2013, doi: 10.1007/s12046-013-0142-4.
[118] D. Gupta, S. Singh, V. Jain, and R. Kumar, "Joining of bulk cast iron through microwave energy," *Int. j. technol. res. eng.*, vol. 2, no. 7, pp. 1079–1084, 2015.
[119] D. Gamit, R. R. Mishra, and A. K. Sharma, "Joining of mild steel pipes using microwave hybrid heating at 2.45 GHz and joint characterization," *J. manuf. process.*, vol. 27, pp. 158–168, Jun. 2017, doi: 10.1016/j.jmapro.2017.04.028.
[120] S. Singh, R. Singh, D. Gupta, and V. Jain, "Preliminary metallurgical and mechanical investigations of microwave processed hastelloy joints," *J. manuf. sci. eng.*, vol. 139, no. 6, Jun. 2017, doi: 10.1115/1.4035370.
[121] A. Bansal, H. Vasudev, A. K. Sharma, and P. Kumar, "Investigation on the effect of post weld heat treatment on microwave joining of the Alloy-718 weldment," *Mater. res. express*, vol. 6, no. 8, p. 086554, May 2019, doi: 10.1088/2053-1591/ab1d9a.
[122] M. Pal, V. Kumar, S. Sehgal, H. Kumar, K. K. Saxena, and A. K. Bagha, "Microwave hybrid heating based optimized joining of SS304/SS316," *Mater. manuf. process.*, vol. 36, no. 13, pp. 1554–1560, Oct. 2021, doi: 10.1080/10426914.2020.1854469.

[123] R. Samyal, A. K. Bagha, and R. Bedi, “Evaluation of modal characteristics of SS202-SS202 lap joint produced using selective microwave hybrid heating,” *J. manuf. process.*, vol. 68, pp. 1–13, Aug. 2021, doi: 10.1016/j.jmapro.2021.07.018.

[124] S. Singh, D. Gupta, and V. Jain, “Novel microwave composite casting process: theory, feasibility and characterization,” *Mater. des.*, vol. 111, pp. 51–59, Dec. 2016, doi: 10.1016/j.matdes.2016.08.071.

[125] S. Singh, D. Gupta, and V. Jain, “Microwave melting and processing of metal–ceramic composite castings,” *Proc. inst. mech. eng. part B j. eng. manuf.*, vol. 232, no. 7, pp. 1–9, May 2016, doi: 10.1177/0954405416666900.

[126] T. R. Gouthama, G. Harisha, Y. R. Manjunatha, S. M. M. Kumara, M. S. Srinath, and M. S. Lingappa, “Melting of tin using muffle furnace and microwave energy and its characterization,” *IOP conf. ser. mater. sci. eng.*, vol. 149, p. 012100, Sep. 2016, doi: 10.1088/1757-899X/149/1/012100.

[127] R. R. Mishra and A. K. Sharma, “Microwave heating characteristics of bulk metallic materials and role of oxides,” *J. mater. sci.*, vol. 53, no. 24, pp. 16567–16584, Dec. 2018, doi: 10.1007/s10853-018-2771-9.

[128] R. R. Mishra and A. K. Sharma, “Multi-physics simulation of in situ microwave casting of 7039 Al alloy inside different applicators and cast microstructure,” *Proc. inst. mech. eng. part E j. process mech. eng.*, vol. 233, no. 3, pp. 617–629, Jun. 2019, doi: 10.1177/0954408918781479.

[129] S. Singh, D. Gupta, and V. Jain, “Microwave processing and characterization of nickel powder based metal matrix composite castings,” *Mater. res. express*, vol. 6, no. 8, p. 0865b1, Aug. 2019, doi: 10.1088/2053-1591/ab2138.

[130] S. Singh, D. Gupta, and S. Kaushal, “Dry sliding wear performance of Ni–SiC composites developed through an in situ microwave casting process,” *J. tribol.*, vol. 1V. Gangwar,

[131] S. Kumar, V. Singh, and H. Singh, “Effect of process parameters on hardness of AA-6063 in-situ microwave casting by using Taguchi method,” *IOP conf. ser. mater. sci. eng.*, vol. 804, no. 1, p. 012019, Apr. 2020, doi: 10.1088/1757-899X/804/1/012019.

[132] D. Gupta and A. K. Sharma, “A method of cladding-coating of mettalic and non-metallic powders on metallic substarte by microwave irradiation,” Patent application 527/Del, India, 2010.

[133] D. Gupta and A. K. Sharma, “Copper coating on austenitic stainless steel using microwave hybrid heating,” *Proc. inst. mech. eng. part E j. process mech. eng.*, vol. 226, no. 2, pp. 132–141, May 2012, doi: 10.1177/0954408911414652.

[134] S. Zafar, A. K. Sharma, and N. Arora, “Development and microstructural characterisation of inconel cladding on stainless steel through microwave irradiation,” *i-manager’s J. mech. eng.*, vol. 3, no. 1, pp. 9–16, Jan. 2013, doi: 10.26634/jme.3.1.2155.

[135] D. Gupta and A. K. Sharma, “Microstructural characterization of cermet cladding developed through microwave irradiation,” *J. mater. eng. perform.*, vol. 21, no. 10, pp. 2165–2172, Oct. 2012, doi: 10.1007/s11665-012-0142-2.

[136] S. Kaushal, D. Gupta, and H. Bhowmick, “Investigation of dry sliding wear behavior of Ni–SiC microwave cladding,” *J. tribol.*, vol. 139, no. 4, Jul. 2017, doi: 10.1115/1.4035147.

[137] B. Singh, S. Kaushal, D. Gupta, and H. Bhowmick, “On development and dry sliding wear behavior of microwave processed Ni/Al_2O_3 composite clad,” *J. tribol.*, vol. 140, no. 6, Nov. 2018, doi: 10.1115/1.4039996.

[138] J. Mago, S. Bansal, D. Gupta, and V. Jain, “Investigation of microwave processing parameters on development of Ni-40Cr_3C_2 composite clad and their characterization,” *Metall. mater. trans. A*, vol. 51, no. 8, pp. 4288–4300, Aug. 2020, doi: 10.1007/s11661-020-05832-y.

[139] D. Gupta and A. K. Sharma, “Investigation on sliding wear performance of WC10Co2Ni cladding developed through microwave irradiation,” *Wear*, vol. 271, no. 9–10, pp. 1642–1650, Jul. 2011, doi: 10.1016/j.wear.2010.12.037.

[140] S. Zafar, A. Bansal, A. K. Sharma, N. Arora, and C. S. Ramesh, “Dry erosion wear performance of Inconel 718 microwave clad,” *Surf. eng.*, vol. 30, no. 11, pp. 852–859, Nov. 2014, doi: 10.1179/1743294414Y.0000000359.

[141] S. Zafar, A. K. Sharma, and C. S. Ramesh, “Abrasive wear behaviour of Inconel 718 microwave clad,” in *National tribology conference- 2014*, 2014, pp. 255–263, doi: 10.13140/RG.2.1.4451.8564.

[142] A. Bansal, S. Zafar, and A. K. Sharma, “Microstructure and abrasive wear performance of Ni-WC composite microwave clad,” *J. mater. eng. perform.*, vol. 24, no. 10, pp. 3708–3716, Oct. 2015, doi: 10.1007/s11665-015-1657-0.

[143] S. Zafar and A. K. Sharma, “Dry sliding wear performance of nanostructured WC–12Co deposited through microwave cladding,” *Tribol. int.*, vol. 91, pp. 14–22, Nov. 2015, doi: 10.1016/j.triboint.2015.06.023.

[144] S. Zafar and A. K. Sharma, “On friction and wear behavior of WC-12Co microwave clad,” *Tribol. trans.*, vol. 58, no. 4, pp. 584–591, Jul. 2015, doi: 10.1080/10402004.2014.996310.

[145] A. M. Hebbale and M. S. Srinath, “Microstructure and experimental design analysis of nickel based clad developed through microwave energy,” *Perspect. sci.*, vol. 8, pp. 257–259, Sep. 2016, doi: 10.1016/j.pisc.2016.04.044.

[146] A. M. Hebbale and M. S. Srinath, “Taguchi analysis on erosive wear behavior of cobalt based microwave cladding on stainless steel AISI-420,” *Measurement*, vol. 99, pp. 98–107, Mar. 2017, doi: 10.1016/j.measurement.2016.12.024.

[147] M. Srinath and A. M. Hebbale, “Fuzzy prediction of slurry erosive behavior of cobalt based clad developed through microwave energy,” *Mater. today proc.*, vol. 4, no. 2, pp. 1804–1811, 2017, doi: 10.1016/j.matpr.2017.02.023.

[148] S. Kaushal, D. Gupta, and H. Bhowmick, “On microstructure and wear behavior of microwave processed composite clad,” *J. tribol.*, vol. 139, no. 6, Nov. 2017, doi: 10.1115/1.4035844.

[149] S. Kaushal, D. Gupta, and H. Bhowmick, “On surface modification of austenitic stainless steel using microwave processed Ni/Cr_3C_2 composite cladding,” *Surf. eng.*, vol. 34, no. 11, pp. 809–817, Nov. 2018, doi: 10.1080/02670844.2017.1362808.

[150] M. K. Akshata, A. M. Hebbale, and M. S. Srinath, “Sliding wear studies of microwave clad versus unclad surface of stainless steel 304,” *MATEC web conf.*, vol. 144, p. 02010, Jan. 2018, doi: 10.1051/matecconf/201814402010.

[151] K. Rajkumar and S. Aravindan, “Tribological behavior of microwave processed copper–nanographite composites,” *Tribol. int.*, vol. 57, pp. 282–296, Jan. 2013, doi: 10.1016/j.triboint.2012.06.023.

[152] M. Rani, G. Perumal, M. Roy, H. S. Grewal, H. Singh, and H. S. Arora, "Post-processing of Ni-Cr-Al_2O_3 thermal spray coatings through friction stir processing for enhanced erosion–corrosion performance," *J. therm. spray technol.*, vol. 28, no. 7, pp. 1466–1477, Oct. 2019, doi: 10.1007/s11666-019-00891-z.

[153] S. M. Lingappa, M. S. Srinath, and H. J. Amarendra, "An experimental investigation to find the critical (coupling) temperature in microwave hybrid heating of bulk metallic materials," *Mater. res. express*, vol. 4, no. 10, p. 106521, Oct. 2017, doi: 10.1088/2053-1591/aa931e.

[154] R. B. Bhagat, "Cavitation erosion of composites — a materials perspective," *J. mater. sci. lett.*, vol. 6, no. 12, pp. 1473–1475, Dec. 1987, doi: 10.1007/BF01689327.

[155] Z. B. Zheng, Y. G. Zheng, W. H. Sun, and J. Q. Wang, "Effect of heat treatment on the structure, cavitation erosion and erosion–corrosion behavior of Fe-based amorphous coatings,"*Tribol.int.*,vol.90,pp.393–403,Oct.2015, doi: 10.1016/j.triboint.2015.04.039.

[156] E. Sadeghimeresht, N. Markocsan, and P. Nylén, "Microstructural characteristics and corrosion behavior of HVAF- and HVOF-sprayed Fe-based coatings," *Surf. coatings technol.*, vol. 318, pp. 365–373, May 2017, doi: 10.1016/j.surfcoat.2016.11.088.

[157] B. K. Sreedhar, S. K. Albert, and A. B. Pandit, "Improving cavitation erosion resistance of austenitic stainless steel in liquid sodium by hardfacing – comparison of Ni and Co based deposits,"*Wear*, vol.342–343, pp.92–99, Nov.2015, doi: 10.1016/j.wear.2015.08.009.

[158] M. Muzyk, Z. Pakieła, and K. J. Kurzydłowski, "Generalized stacking fault energies of aluminum alloys–density functional theory calculations," *Metals (Basel).*, vol. 8, no. 10, p. 823, Oct. 2018, doi: 10.3390/met8100823.

[159] H. O. Pierson, "Carbides of group IV," in *Handbook of refractory carbides and nitrides*, Elsevier, 1996, pp. 55–80.

[160] C. Y. Ho and T. K. Chu, "Electrical resistivity and thermal conductivity of nine selected AISI stainless steels - Center for information and numerical data analysis and synthesis," *Distribution*, p. 15, 1977.

[161] A. K. Sharma and D. Gupta, "On microstructure and flexural strength of metal–ceramic composite cladding developed through microwave heating," *Appl. surf. sci.*, vol. 258, no. 15, pp. 5583–5592, May 2012, doi: 10.1016/j.apsusc.2012.02.019.

[162] W. D. Callister, "Materials science and engineering: An introduction (2nd edition)," *Mater. des.*, vol. 12, no. 1, p. 59, Feb. 1991, doi: 10.1016/0261-3069(91)90101-9.

[163] "AZoM.com. (2019). Properties: Stainless Steel - Grade 316 (UNS S31600).," 2019.

[164] P. E. Carrion, A. Soltani-Tehrani, N. Phan, and N. Shamsaei, "Powder recycling effects on the tensile and fatigue behavior of additively manufactured Ti-6Al-4V parts," *JOM*, vol. 71, no. 3, pp. 963–973, Mar. 2019, doi: 10.1007/s11837-018-3248-7.

[165] J. Mago, S. Bansal, D. Gupta, and V. Jain, "Investigation of erosion and pressure for direct and indirect acoustic cavitation testing," *J. emerg. technol. innov. res.*, vol. 6, no. july, pp. 468–476, 2019, doi: doi.one/10.1729/Journal.23133.

[166] K. N. Ballantyne, R. A. van Oorschot, and R. J. Mitchell, "Reduce optimisation time and effort: Taguchi experimental design methods," *Forensic sci. int. genet. suppl. ser.*, vol. 1, no. 1, pp. 7–8, Aug. 2008, doi: 10.1016/j.fsigss.2007.10.050.

[167] S. Singh, A. Singh, I. Singh, and A. Dvivedi, "Optimization of the process parameters for drilling of metal matrix composites (MMC) using Taguchi analysis," *Adv. mater. res.*,vol. 410, pp. 249–252, Nov. 2011, doi: 10.4028/www.scientific.net/AMR.410.249.

[168] P. Antil, S. Singh, and P. J. Singh, "Taguchi's methodology based electrochemical discharge machining of polymer matrix composites," *Procedia manuf.*, vol. 26, pp. 469–473, 2018, doi: 10.1016/j.promfg.2018.07.055.
[169] K. Kikuchi and F. G. Hammit, "Effect of separation distance on cavitation erosion of vibratory and stationary specimens: in a vibratory facility," *Wear*, vol. 102, pp. 211–225, 1985.
[170] D. Gupta and A. K. Sharma, "Development and microstructural characterization of microwave cladding on austenitic stainless steel," *Surf. coatings technol.*, vol. 205, no. 21–22, pp. 5147–5155, Aug. 2011, doi: 10.1016/j.surfcoat.2011.05.018.
[171] S. N. Aqida, M. I. Ghazali, and J. Hashim, "Effect of porosity on mechanical properties of metal matrix composite: an overview," *J. teknol.*, vol. 40, no. 1, pp. 17–32, Jun. 2013, doi: 10.11113/jt. v40.395.
[172] A. Mondal, A. Shukla, A. Upadhyaya, and D. Agrawal, "Effect of porosity and particle size on microwave heating of copper," *Sci. sinter.*, vol. 42, no. 2, pp. 169–182, 2010, doi: 10.2298/SOS1002169M.
[173] T. Pramod, R. K. Kumar, S. Seetharamu, and M. Kamaraj, "Effect of porosity on cavitation erosion resistance of HVOF processed tungsten carbide coatings," *Int. j. adv. mech. eng.*, vol. 4, no. 3, pp. 307–314, 2014.
[174] O. Knotek, R. Elsing, and H. -R. Heintz, "On plasma sprayed WSi_2 and Cr_3C_2 –Ni coatings," *J. vac. sci. technol. a vacuum, surfaces, film.*, vol. 3, no. 6, pp. 2490–2493, Nov. 1985, doi: 10.1116/1.572864.
[175] J. F. Santa, L. A. Espitia, J. A. Blanco, S. A. Romo, and A. Toro, "Slurry and cavitation erosion resistance of thermal spray coatings," *Wear*, vol. 267, no. 1–4, pp. 160–167, Jun. 2009, doi: 10.1016/j.wear.2009.01.018.
[176] C. P. Paul, H. Alemohammad, E. Toyserkani, A. Khajepour, and S. Corbin, "Cladding of WC–12Co on low carbon steel using a pulsed Nd:YAG laser," *Mater. sci. eng. A*, vol. 464, no. 1–2, pp. 170–176, Aug. 2007, doi: 10.1016/j.msea.2007.01.132.
[177] N. M. Parikh and M. Humenik, "Cermets: II, wettability and microstructure studies in liquid-phase sintering," *J. am. ceram. soc.*, vol. 40, no. 9, pp. 315–320, Sep. 1957, doi: 10.1111/j.1151-2916. 1957.tb12628. x.
[178] W. J. Boettinger *et al.*, "Solidification microstructures: recent developments, future directions," *Acta mater.*, vol. 48, no. 1, pp. 43–70, Jan. 2000, doi: 10.1016/S1359-6454(99)00287-6.
[179] M. K. Singh and S. Zafar, "Abrasive wear mechanism of microwave-assisted compression molded Kenaf/HDPE composite," *J. tribol.*, vol. 142, no. 10, pp. 1–23, Oct. 2020, doi: 10.1115/1.4046858.
[180] D. Demirskyi, D. Agrawal, and A. Ragulya, "Densification kinetics of powdered copper under single-mode and multimode microwave sintering," *Mater. lett.*, vol. 64, no. 13, pp. 1433–1436, Jul. 2010, doi: 10.1016/j.matlet.2010.03.047.
[181] A. Mondal, A. Upadhyaya, and D. Agrawal, "Effect of heating mode and copper content on the densification of W-Cu alloys," *Indian j. mater. sci.*, vol. 2013, pp. 1–7, 2013, doi: 10.1155/2013/603791.
[182] B. Singh and S. Zafar, "Effect of microwave exposure time on microstructure and slurry erosion behavior of Ni +20%Cr_7C_3 composite clads," *Wear*, vol. 426–427, pp. 491–500, Apr. 2019, doi: 10.1016/j.wear.2018.12.016.

[183] N. M. Alford and S. J. Penn, “Sintered alumina with low dielectric loss,” *J. appl. phys.*, vol. 80, no. 10, pp. 5895–5898, Nov. 1996, doi: 10.1063/1.363584.
[184] S. N. Ahmad, J. Hashim, and M. I. Ghazali, “The effects of porosity on mechanical properties of cast discontinuous reinforced metal–matrix composite,” *J. compos. mater.*, vol. 39, no. 5, pp. 451–466, Mar. 2005, doi: 10.1177/0021998305047096.
[185] P. R. Birkin, D. G. Offin, C. J. B. Vian, and T. G. Leighton, “Multiple observations of cavitation cluster dynamics close to an ultrasonic horn tip,” *J. acoust. soc. am.*, vol. 130, no. 5, pp. 3379–3388, Nov. 2011, doi: 10.1121/1.3650536.
[186] K. Kikuchi and F. G. Hammitt, “Effect of separation distance on cavitation erosion of vibratory and stationary specimens in a vibratory facility,” *Wear*, vol. 102, no. 3, pp. 211–225, Apr. 1985, doi: 10.1016/0043-1648(85)90219-4.

VISIBLE RESEARCH OUTPUT

International Journals

i. **Bansal S,** Gupta D, Jain V. Analysis of susceptor temperature during microwave heating and characterization of Ni-30Cr_3C_2 clads. Proceedings of the Institution of Mechanical Engineers, Part L: Journal of Materials: Design and Applications. Status: **Published Online**, Publisher: SAGE, (Impact Factor: 2.311, Category: SCI).

ii. **Bansal S,** Gupta D, Jain V. Surface Modification of SS-316 to Enhance Cavitation Resistance Through Composite Microwave Clads. Surface Review and Letters. Status: **Published Online**, Publisher: World Scientific, (Impact Factor: 1.152, Category: SCI).

iii. **Bansal S,** Mago J, Gupta D, Jain V. Parametric optimization and analysis of cavitation erosion behaviour of Ni-based+10WC microwave processed composite clad using Taguchi approach. Surface Topography: Metrology and Properties Status: **Published Online**, Publisher: IOP, (Impact Factor: 2.038, Category: SCI).

iv. **Bansal S,** Mago J, Gupta D, Jain V. Microwave cladding of NiCrSiC-5Al_2O_3 on austenitic stainless steel to improve cavitation erosion resistance. Surface Topography: Metrology and Properties. **Published Online**, Publisher: IOP, (Impact Factor: 2.038, Category: SCI).

v. Mago J, **Bansal S,** Gupta D, Jain V. Cavitation erosion behavior of microwave-processed Ni–40Cr_3C_2 composite clads: A parametric investigation using ultrasonic apparatus. Proceedings of the Institution of Mechanical Engineers, Part L: Journal of Materials: Design and Applications. Status: **Published Online**, Publisher: SAGE, (Impact Factor: 2.311, Category: SCI).

vi. Mago J, **Bansal S,** Gupta D, Jain V. Influence of microwave heating on metallurgical and mechanical properties of Ni-40Cr_3C_2 composite clads in the context of cavitation erosion resistance characteristics. Proceedings of the Institution of Mechanical Engineers, Part C: Journal of Mechanical Engineering Science Status: **Published Online**, Publisher: SAGE, (Impact Factor: 1.762, Category: SCI).

vii. Mago J, **Bansal S**, Gupta D, Jain V. Investigation of microwave processing parameters on development of Ni-40Cr_3C_2 composite clad and their characterization, Metallurgical and Materials Transactions A. Status: **Published Online**, Publisher: SPRINGER, (Impact Factor: 2.556, Category: SCI)

International Conferences

i. TIME-2021: Technological Innovations in Mechanical Engineering. 2021. Noida, INDIA

ii. International Conference on Smart and Sustainable developments in Materials, Manufacturing and Energy.2019. Udupi, INDIA

APPENDIX-A

Figure A-1: Scanning Electron Microscopy (Make: Oxford Instruments, Model: JEOL 8600M, Photo Courtesy: SAI Labs, TIET, Patiala)

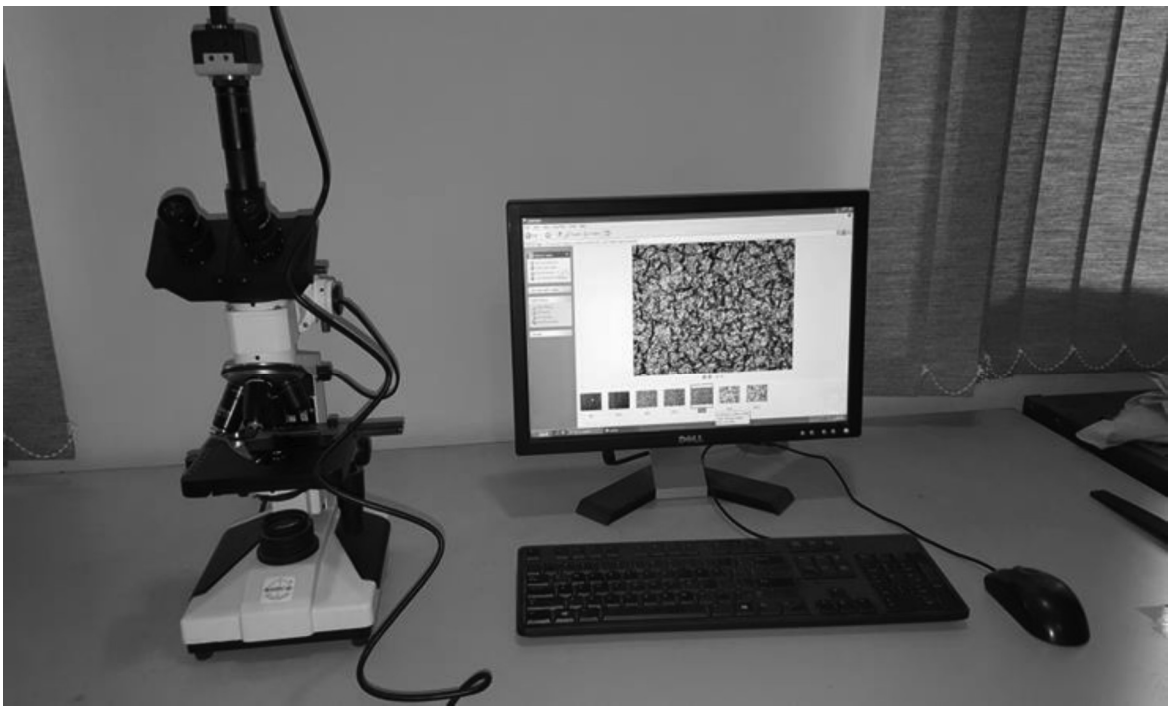

Figure A-2: Optical Microscopy (Make: Radical Scientific Equipment, Model: RMM-8T, Photo Courtesy: Surface Engineering and Tribology Research Lab, Mechanical Engineering Department, TIET, Patiala)

Figure A-3: X-Ray Diffractometer (XRD) (Make: PANalytical, Almelo, Model: X'Pert PRO, Photo Courtesy: SAI Labs, Thapar Institute of Engineering & Technology)

Figure A-4: Vickers Micro-Hardness Tester (Make: Meta-Tech, Model: MVH1) Photo Courtesy: A.M. Lab, Thapar Institute of Engineering & Technology)

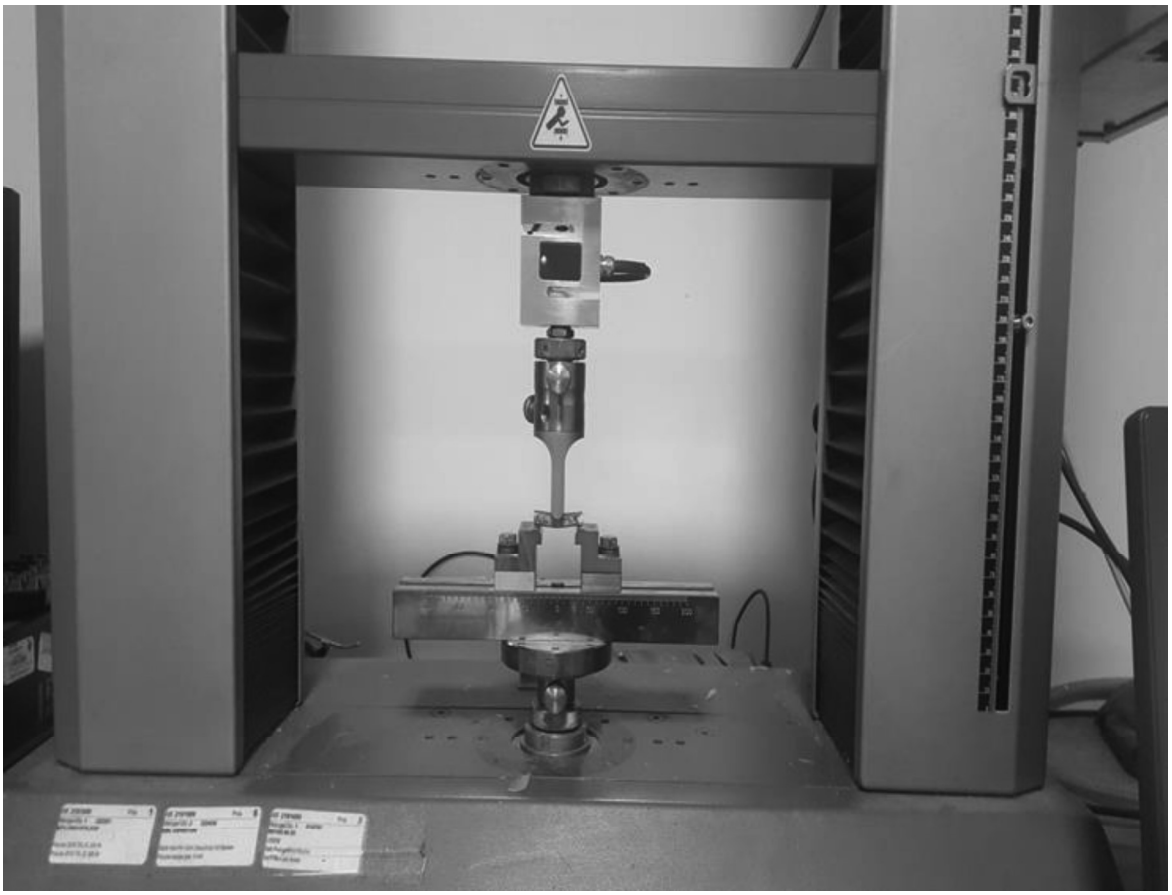

Figure A-5: Universal Testing Machine (Make: Zwick/Roell, Model: Z010, Photo Courtesy: Chemical Engineering Department, Thapar Institute of Engineering & Technology)

Figure A-6: Cavitation Probe Sonicator (Make: Kamtronics Technology Pvt. Ltd., Model: Samkoon, Photo Courtesy: Surface Engineering and Tribology Research Lab, Mechanical Engineering Department, TIET, Patiala)

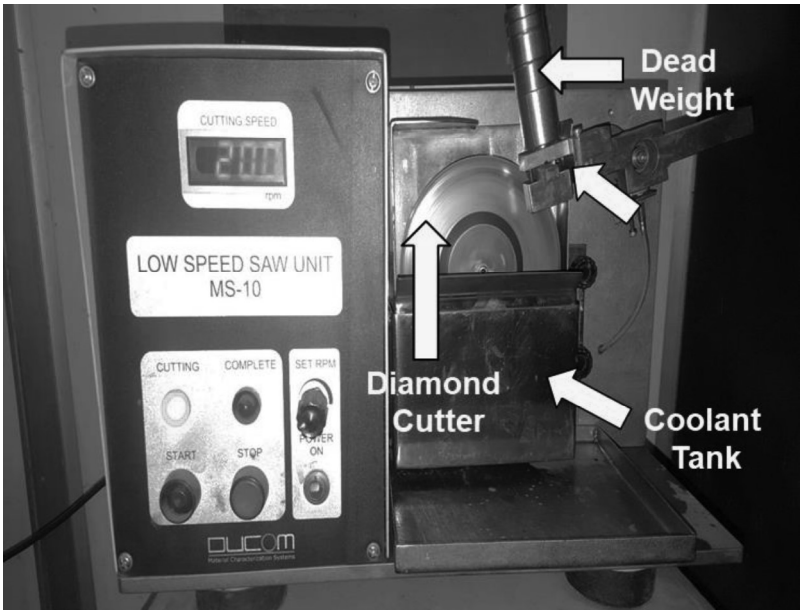

Figure A-7: Low Speed Diamond Cutter (Make: DUCOM, Model: MS-10, Photo Courtesy: Surface Engineering and Tribology Research Lab, Mechanical Engineering Department, TIET, Patiala)

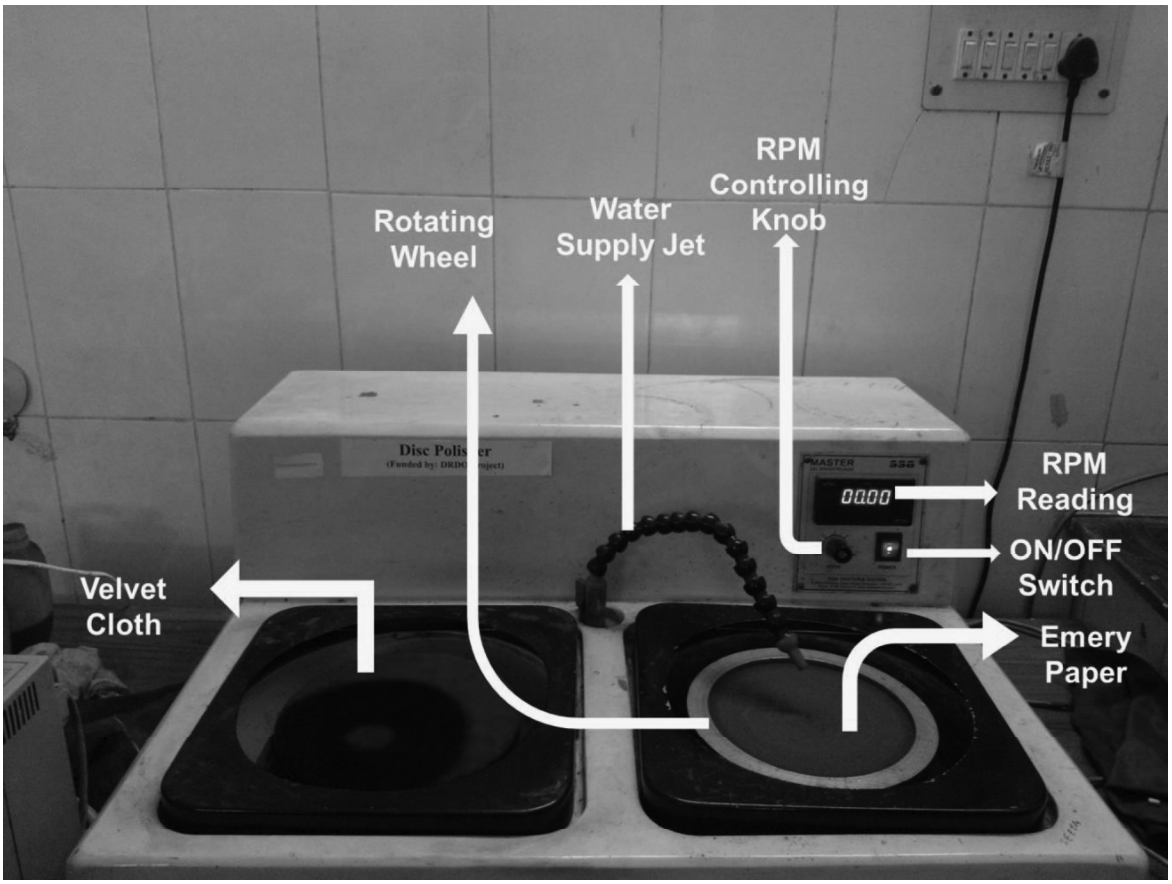

Figure A-8: Disc Polisher (Photo Courtesy: Surface Engineering and Tribology Research Lab, Mechanical Engineering Department, TIET, Patiala)